MULTIDISCIPLINARY CENTER FOR EARTHQUAKE ENGINEERING RESEARCH
A National Center of Excellence in Advanced Technology Applications

ISSN 1520-295X

Development of Seismic Strengthening and Retrofit Strategies for Critical Facilities Using Engineered Cementitious Composite Materials

by

Keith Kesner and Sarah L. Billington
Cornell University
Department of Civil and Environmental Engineering
Ithaca, New York 14853

Technical Report MCEER-05-0007

August 29, 2005

This research was conducted at Cornell University and was supported primarily by the Earthquake Engineering Research Centers Program of the National Science Foundation under award number EEC-9701471.

NOTICE

This report was prepared by Cornell University as a result of research sponsored by the Multidisciplinary Center for Earthquake Engineering Research (MCEER) through a grant from the Earthquake Engineering Research Centers Program of the National Science Foundation under NSF award number EEC-9701471 and other sponsors. Neither MCEER, associates of MCEER, its sponsors, Cornell University, nor any person acting on their behalf:

a. makes any warranty, express or implied, with respect to the use of any information, apparatus, method, or process disclosed in this report or that such use may not infringe upon privately owned rights; or

b. assumes any liabilities of whatsoever kind with respect to the use of, or the damage resulting from the use of, any information, apparatus, method, or process disclosed in this report.

Any opinions, findings, and conclusions or recommendations expressed in this publication are those of the author(s) and do not necessarily reflect the views of MCEER, the National Science Foundation, or other sponsors.

MULTIDISCIPLINARY CENTER FOR EARTHQUAKE ENGINEERING RESEARCH
A National Center of Excellence in Advanced Technology Applications

Development of Seismic Strengthening and Retrofit Strategies for Critical Facilities Using Engineered Cementitious Composite Materials

by

Keith Kesner[1] and Sarah L. Billington[2]

Publication Date: August 29, 2005
Submittal Date: August 7, 2003

Technical Report MCEER-05-0007

NSF Master Contract Number EEC-9701471

1 Project Director, Thornton Tomasetti Group, New York, New York; former Graduate Student, School of Civil and Environmental Engineering, Cornell University
2 Assistant Professor, Department of Civil and Environmental Engineering, Stanford University; former Assistant Professor, School of Civil and Environmental Engineering, Cornell University

MULTIDISCIPLINARY CENTER FOR EARTHQUAKE ENGINEERING RESEARCH
University at Buffalo, State University of New York
Red Jacket Quadrangle, Buffalo, NY 14261

Preface

The Multidisciplinary Center for Earthquake Engineering Research (MCEER) is a national center of excellence in advanced technology applications that is dedicated to the reduction of earthquake losses nationwide. Headquartered at the University at Buffalo, State University of New York, the Center was originally established by the National Science Foundation in 1986, as the National Center for Earthquake Engineering Research (NCEER).

Comprising a consortium of researchers from numerous disciplines and institutions throughout the United States, the Center's mission is to reduce earthquake losses through research and the application of advanced technologies that improve engineering, pre-earthquake planning and post-earthquake recovery strategies. Toward this end, the Center coordinates a nationwide program of multidisciplinary team research, education and outreach activities.

MCEER's research is conducted under the sponsorship of two major federal agencies: the National Science Foundation (NSF) and the Federal Highway Administration (FHWA), and the State of New York. Significant support is derived from the Federal Emergency Management Agency (FEMA), other state governments, academic institutions, foreign governments and private industry.

MCEER's NSF-sponsored research objectives are twofold: to increase resilience by developing seismic evaluation and rehabilitation strategies for the post-disaster facilities and systems (hospitals, electrical and water lifelines, and bridges and highways) that society expects to be operational following an earthquake; and to further enhance resilience by developing improved emergency management capabilities to ensure an effective response and recovery following the earthquake (see the figure below).

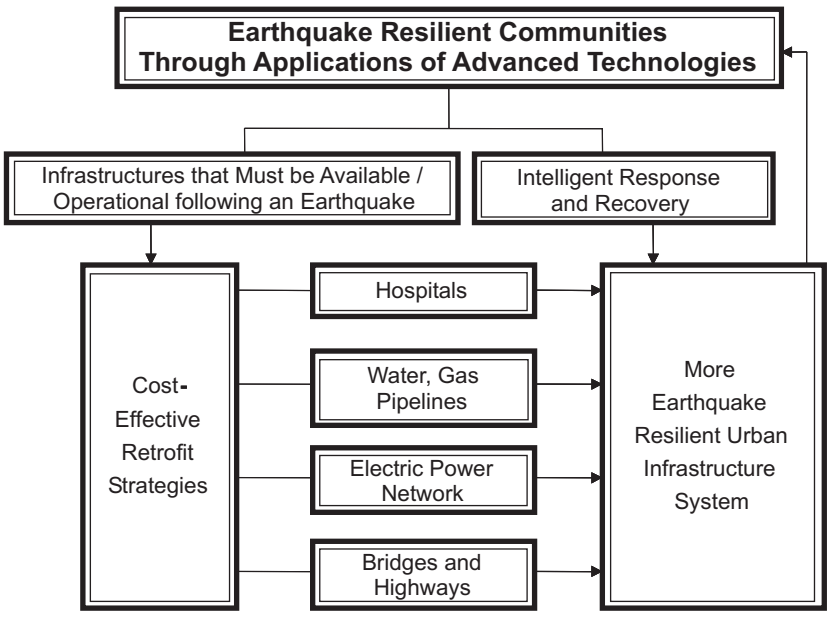

A cross-program activity focuses on the establishment of an effective experimental and analytical network to facilitate the exchange of information between researchers located in various institutions across the country. These are complemented by, and integrated with, other MCEER activities in education, outreach, technology transfer, and industry partnerships.

This research describes the development of a seismic retrofit system for critical facilities that uses steel reinforced engineered cementitious composite (ECC) materials. Specifically, an infill system made up of portable, precast panels was developed that uses the damage-tolerant and strain hardening properties of ECC materials. The research consisted of a combination of laboratory and numerical studies.

Structural-scale laboratory tests were used to test the strength of pre-tensioned bolted connections between panel members, and to evaluate the response of the infill panels made with various ECC materials, reinforcement layouts and panel geometries. The connection test results showed the viability of the proposed pre-tensioned bolted connections. The panel test results indicated the different levels of panel strength, stiffness and energy dissipation that can be achieved. The panel tests also demonstrated a significant increase in strength and energy dissipation possible when ECC is used in lieu of traditional concrete. These results serve as benchmark studies for further development of the infill system.

To examine the infill panel concept further, additional simulations were performed using a material model for the ECC developed from reversed cyclic tests on material specimens. The simulations offered insight into local connection behavior and demonstrated the ability of the proposed ECC infill system to strengthen, stiffen and increase the energy dissipation of a single bay frame from a prototype structure, without causing premature damage to the frame when compared to an unretrofitted frame.

ABSTRACT

The research presented herein describes the development of a seismic retrofit system for critical facilities that uses engineered cementitious composite (ECC) materials in lieu of traditional materials. Specifically an infill panel system was developed that utilizes the pseudo-strain hardening properties of the ECC materials. The research consisted of a combination of laboratory and numerical studies.

The infill panel system, which consists of precast ECC panels with bolted connections, was developed for use as a retrofit strategy in critical facilities. Based upon finite-element simulations, a beam-type infill system was found to be effective in increasing the strength, stiffness and energy dissipation of a steel frame without yielding of the bare frame at drift levels up to 0.75%.

Structural-scale laboratory tests were used to test the strength of the proposed bolted connections between panel members, and to evaluate the response of ECC infill panels made with various ECC materials, reinforcements and panel geometries. The connection tests results showed the viability of the pretensioned bolted connections. The panel test results indicated the different levels of panel strength, stiffness and energy dissipation that can be achieved. These results serve as benchmark studies for further development of the infill system.

To examine the infill panel concept further, additional simulations were performed using a material model for the ECC developed from reversed cyclic tests. The simulations demonstrated the ability of the proposed ECC infill system to strengthen, stiffen and increase the energy dissipation of steel frames, without causing damage in the frames.

TABLE OF CONTENTS

TABLE OF CONTENTS (cont'd)

TABLE OF CONTENTS (cont'd)

LIST OF ILLUSTRATIONS

LIST OF ILLUSTRATIONS (cont'd)

LIST OF ILLUSTRATIONS (cont'd)

LIST OF ILLUSTRATIONS (cont'd)

LIST OF ILLUSTRATIONS (cont'd)

LIST OF ILLUSTRATIONS (cont'd)

LIST OF TABLES

Section 1
Introduction and Overview

1.0 Introduction

The research presented herein focused on the development of an innovative method for seismic strengthening and rehabilitation applications using a new composite material. Specifically, engineered cementitious composite (ECC) materials, which exhibit multiple, fine cracking and a pseudo strain-hardening response in tension were evaluated and found to have excellent potential for use in strengthening and rehabilitation applications. Continued development of these materials will give engineers greater flexibility to design and rehabilitate structures to withstand seismic and other types of loading. The following chapters describe how applications that utilize these materials are developed for seismic strengthening and retrofit applications.

The development of seismic strengthening and retrofit applications using the ECC materials required the combination of several types of research. These included the use of small-scale laboratory testing both to evaluate the ECC material properties, specifically the response to reversed cyclic loadings, and to verify the micromechanical assumptions used in the development of the materials. These results are presented in Kesner and Billington (2004). Numerical, finite element-based simulations were performed using a material model developed from the cyclic laboratory test results. These simulations were used to model the performance of the ECC materials in structural retrofit applications. The numerical simulations were supported by large-scale laboratory tests that demonstrated the performance of the elements of the proposed retrofit.

The primary goal of the research was the development of seismic retrofit strategies to improve the performance of structures during earthquakes. Within the broad concept of developing seismic retrofit strategies, there were two unique focus areas providing practical bounds to the research:

1. Utilize the unique properties of ECC materials in structural retrofit applications

   The pseudo-strain hardening nature of the ECC materials, in combination with reinforcing steel, results in a material with the ability to both maintain structural capacity and integrity at higher tensile strain levels than traditional materials (Fisher and Li, 2001). The ability of the materials to maintain both capacity and integrity under load was used in the retrofit development.

2. Develop retrofit strategies for critical structures such as hospitals

   The development of retrofit strategies for critical structures addresses some of the needs of the MCEER research program (Program 2), which sponsored this research (MCEER, 2000). A primary thrust of the MCEER research project was the development of retrofit strategies for critical facilities, such as hospitals and emergency response centers. In particular, the MCEER program focused on the development of strategies to protect both structural and nonstructural components. The focus on protection of nonstructural components arose after

extensive damage was observed in nonstructural components of hospitals during the Northridge earthquake (OSHPD, 1995).

1.1 Overview

In Section 2 previous research on the use of infill walls for seismic strengthening is reviewed. Infill walls are commonly used for strengthening of both steel and concrete framed structures. The review of previous infill wall research was used to guide the development of retrofit strategies, which will use the ECC materials. The results of previous research were then combined with the specific needs of critical facilities resulting in the development of a new type of infill panel system, also described in Section 2. The system performance was then examined with a series of finite element-based analyses (Sections 2.3 to 2.5)

To verify the performance of infill system components a series of structural-scale laboratory tests were performed. Results from these tests are presented in Sections 3 and 4. The results from numerical simulations of the laboratory tests are presented in Section 5. These results utilize the material model that was developed from test results presented in Kesner and Billington (2004). In the simulation studies the effectiveness of the infill panel system in protecting critical structures during seismic events is evaluated.

A summary of the research program and conclusions are presented in Section 6. Several suggestions for future research are included; these are intended to expand upon the research presented in this report.

Section 2
Evaluation of Infilled Wall Systems

2.0 Introduction

In many parts of the Unites States and around the world, structures have been designed and constructed solely for gravity loads (gravity load design, GLD). Increasing knowledge of the susceptibility of these structures to catastrophic failures under seismic loadings has necessitated the development of strategies to increase the lateral strength of these structures (El Borgi et al., 1993). The addition of infill walls to a bare frame (illustrated in figure 2-1) is an accepted method to strengthen and stiffen structures that do not have adequate capacity to carry lateral loads (FEMA-276, 1999). Typical materials for infill wall construction include reinforced concrete, brick masonry and concrete masonry units (CMU). The basic effect of the infill wall addition is to provide an alternate load path for lateral loads from seismic loadings. Infill wall additions thus serve to limit the loads carried in the columns and joint regions, which are not adequately detailed for lateral loads. Section 2.1 briefly describes some of the previous research into the use of infill wall systems for strengthening of both concrete and steel framed structures.

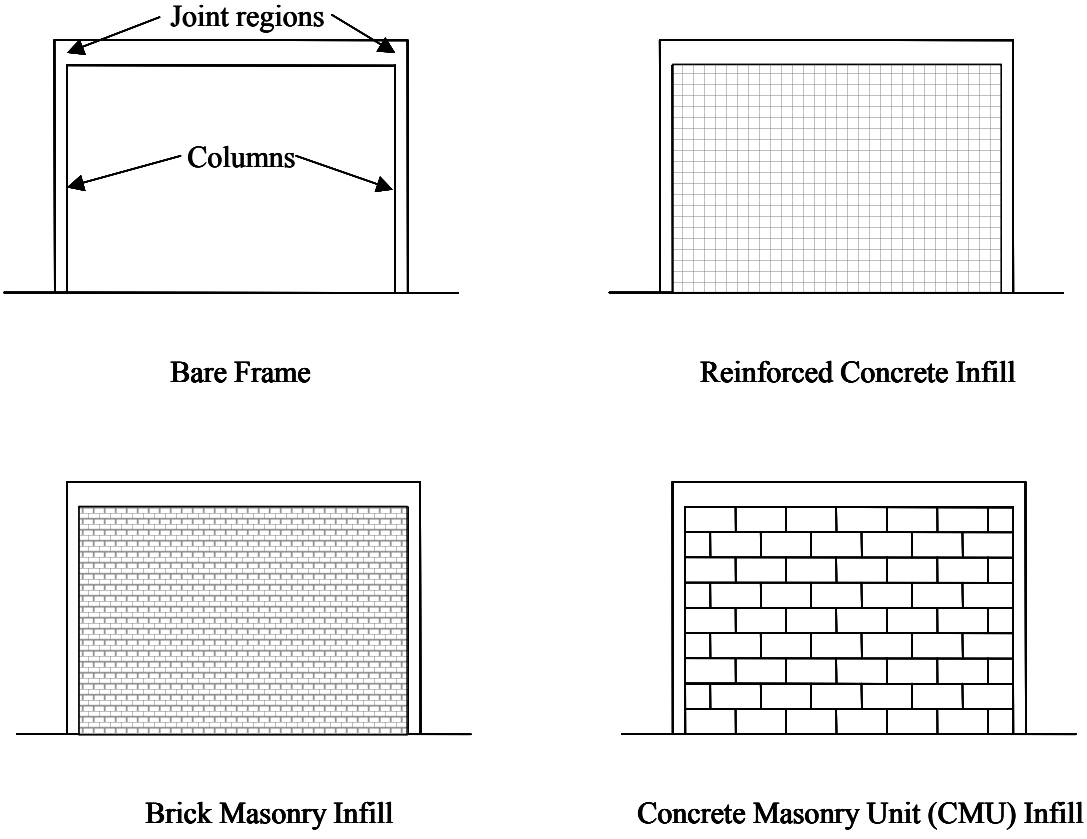

Figure 2-1. Schematic representation of infill walls in building frame.

The research presented herein focuses on the development of an infill system for retrofit of critical facilities that uses ECC materials in lieu of traditional concrete or masonry materials.

Due to the pseudo-strain hardening behavior of ECC materials, it is believed that the ECC materials will have significant advantages over traditional concrete or masonry materials. ECC materials, as shown in Kesner and Billington (2004), have high strain capacities and an inherent ability to absorb energy under seismic loadings. Furthermore, ECC materials maintain their integrity to high strain levels without spalling (Billington and Yoon, 2004).

In Section 2.2 the specific requirements for the retrofit of critical facilities are presented. The development of retrofit strategies for critical facilities satisfied the requirements of the research sponsor (MCEER, 2000). Two types of ECC infill system concepts were developed to satisfy these requirements. The ECC systems are presented in Section 2.3.

To examine the performance of the proposed infill systems, preliminary finite element studies were performed. The results of the analyses are presented in Sections 2.4 and 2.5. The finite element studies were used to examine the potential of the proposed systems to satisfy the performance requirements of the critical facilities. The studies were also used to identify options for laboratory testing of infill components.

2.1 Previous Related Research

The behavior of infill walls in structural frames has been extensively researched since the 1950s. Prior to this time, infill walls were commonly used both to stiffen and/or strengthen buildings. However the effects of the retrofits were not easily quantified. In general, simple static analysis methods were used to evaluate the infill effects.

Previous research into the behavior of infill wall systems is summarized in this section. The literature review is divided into two sections: laboratory evaluations and analytical evaluations. The review of both experimental and analytical research was needed, as both will be used in the current research. The reviews focus on examining research related to retrofit infill systems for critical facilities.

2.1.1 Laboratory Evaluations

One of the first efforts to develop an understanding of the effect of infill wall additions on frame capacity was performed by Benjamin and Williams (1957 and 1958). In the research, the effect of integrally cast concrete infill panels within a reinforced concrete frame was evaluated experimentally. The goal of the research was the development of expressions that predict the shear capacity of a single-story infilled frame. The empirical methods presented in the paper determined the ultimate strength and deflections as a function of the wall geometry and reinforcement. The research did not consider the effect of cyclic loads or loading rates in the prediction.

Holmes (1961 and 1963) presented the concept of the lateral load being carried through an "equivalent strut" through an infill panel as illustrated in figure 2-2. The "equivalent strut" concept was based upon an evaluation of test results on infilled steel frames. The capacity of the strut was reached when the axial strain in the strut reaches the failure strain of the material. The length of the frame diagonal and the infill thickness determines the strut area. This method

allowed for a simple prediction of the lateral load capacity and deflection of infilled frames at failure. Comparison of laboratory and analytical results obtained using the "equivalent strut" concept showed good agreement.

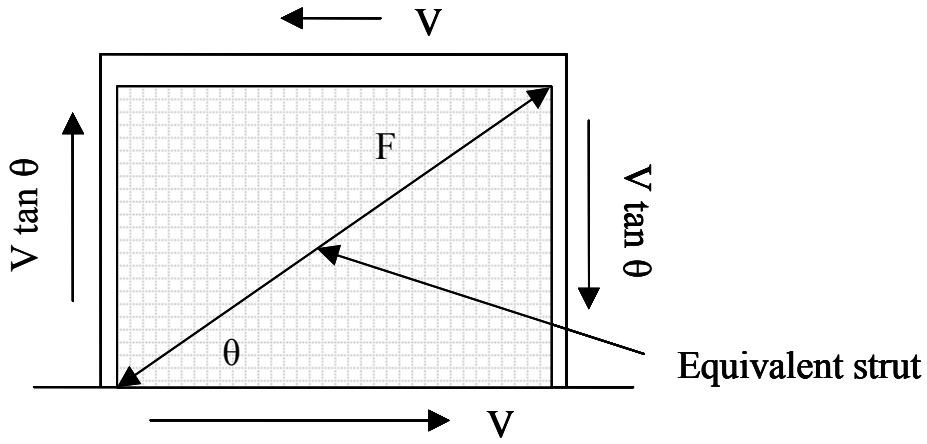

Figure 2-2. Concept of lateral load carried by "equivalent strut" in an infill panel.

Stafford Smith (1962 and 1965) further investigated the use of the equivalent strut approach. In this study small-scale tests were performed on infilled steel frames with varying height-to-width ratios. The results indicated that the equivalent strut method could be used to predict the wall capacity, provided the strut width is adjusted proportional to the height-to-width ratio of the frame. When the stiffness of the frame was increased, an increase in effective strut width was observed, which resulted in greater contact area of the strut at the frame corners. The calculation of deflections using this method was found to be complicated due to the potential for poor initial fit between the infill and frame.

In a further study of infilled frames Stafford Smith (1966) examined the behavior of square infilled frames. In the study, a series of experiments were performed on small-scale model structures with solid mortar infills. The study focused on the length of contact between the infill and frame, and on the effect of the relative stiffness between the infill and frame. This evaluation led to the development of a method that allowed prediction of the infilled frame stiffness based upon the evaluation of a frame using equivalent struts to represent the infill.

Kahn and Hanson (1979) performed a series of experiments on the behavior of different types of infill systems. In the study, the performance of a monolithically cast concrete wall was compared to the performance of a solid precast concrete wall system, a retrofit cast-in-place concrete solid wall, and a precast concrete panel system comprised of six panels spanning across the frame. All of the wall systems were tested within identical reinforced concrete frames. The failure mode of the monolithically cast concrete wall was similar to that of a low-rise concrete shear wall. Both the solid precast concrete shear wall and the cast-in-place concrete shear wall failed at the connections to the frame. The precast panels acted as a series of deep beams, and failed when adjacent panels came into contact. The monolithic shear wall was found to have the highest strength in the testing.

In a series of papers, Dawe and associates experimentally evaluated the behavior of CMU infilled steel frames (Dawe and Seah, 1989 and Dawe et al., 1989). The research involved

testing of 28 infilled frames. The parameters investigated included the effect of lateral wall ties, frame joint rigidity, gaps at the infill-frame intersection and the effect of wall reinforcement. The test results further confirmed the validity of the equivalent strut concept, as the test specimens with conditions that disrupted the compressive diagonal were observed to have lower strength. Packing of mortar to prevent gaps between the infill and frame was found to increase the initial stiffness of the system, but not the ultimate strength. Panel-to-column connection ties were not observed to increase either the strength or stiffness of the infilled frame. The use of bond beams (fully grouted and reinforced CMU sections) and other infill reinforcement was found to increase both the stiffness and strength of the infill frames.

Several researchers at Cornell University have investigated the behavior of masonry infilled frames (Buonopane and White, 1999, Mosalam et al., 1997, Beres et al., 1992, and Gergely et al., 1993). The research involved experimental and analytical studies of concrete and steel infilled frames with and without openings. The initial research focused on the evaluation of gravity-load designed (GLD) concrete frames under seismic conditions (Beres et al., 1992 and Gergely et al., 1993). Later research evaluated the capacity and energy dissipation of infilled concrete and steel frames (Buonopane and White, 1999 and Mosalam et al., 1997). Research results were used to develop analytical models for the energy dissipation and cracking response of infilled frames.

Frosch et al. (1996) developed a retrofit infill system for non-ductile concrete frames. Their work built upon the previous research of Kahn and Hanson (1979). Specifically, a retrofit system was developed for low rise, 2 to 5 story GLD concrete frames. In the system, precast concrete panels with reinforced shear key mortar joints between panels were used to increase the shear capacity and stiffness of the frame. Vertical, external post-tensioning was added to increase the overturning capacity of the retrofitted frames, and to increase the tensile capacity of the concrete columns. The panel system was developed to allow for simple installation in retrofit applications, which resulted in limitations on the panel size and weight. The resulting infill system was found to behave similarly to a monolithically cast concrete wall system, with the external post-tensioning capable of preventing failure of the columns.

Taghdi et al. (2000) evaluated the concept of strengthening existing infill walls via the application of bolted steel straps. The use of steel straps was evaluated both as a retrofit strategy and a strategy for the repair of damaged walls. Steel straps were found to be an effective strategy for retrofitting infill walls. Simple strut-and-tie models were developed to evaluate the retrofitted wall's capacity.

Related to ECC materials, Kanda et al. (1998) examined the experimental behavior of ECC shear panels joined using pre-tensioned bolted connections. A similar type of connection is proposed for the infill system investigated herein.

2.1.2 Analytical Developments

Parallel with experimental studies related to infill additions for improving lateral capacity of frames, analytical tools have been developed to predict the response of infilled frames. The overview here will primarily focus on the development of finite element-based methods due to

their preponderance in modern structural engineering. The finite element method is also used in the research presented herein.

In a series of papers, Mallick and associates demonstrated the applicability of the finite element method for evaluation of solid infill wall systems in multi-story, multi-bay frames. (Mallick and Severn, 1967, Mallick and Severn, 1968, and Mallick and Garg, 1971).

Kost et al., (1974), examined the effect of gaps between a frame and its infill panels using the finite element method. The gaps occur due to incomplete filling of the frame during construction, and due to time dependent shrinkage of the infill material. To evaluate the effect of the gaps between the infill and frame, gap elements were used. During the cyclic displacement analysis, when the gaps were determined to have closed, a rigid link was inserted at the gap element location. This resulted in a non-linear structural response during analysis. The research concluded that pre-existing gaps between the infill and masonry have a significant effect on the dynamic response of the infilled system.

Mosalam (1996) examined the use interface elements to represent the mortar joints in an infilled frame, with plane stress elements used for the CMU blocks. The interface elements were used to account for the nonlinearities associated with the cracking and slipping of the mortar joints. In the same work, a smeared cracking formulation was used to represent the infill. A smeared cracking approach will also be used in the current research.

Analytical research involving the use of ECC infill panels has been conducted. Kabele et al. (1999) and Horii et al. (1998) examined the concept of ECC infill panels through a simulation-based study of panel behavior. The results indicated that an unreinforced ECC panel would provide higher shear strength and ductility when compared to a steel fiber reinforced concrete panel.

2.1.3 Summary of Previous Related Research

Selected previous research into the behavior of infilled frames was reviewed. Several ideas from the previous research can be incorporated into the development of retrofit infill systems for critical facilities. These ideas include the following:

1. The use of modular infills (Kahn and Hanson, 1979, Frosch et al., 1996, Kabele et al., 1999 and Horii et al., 1998) can be beneficial in retrofit applications.
2. The impact of initial gaps (Kost, 1974, Dawe and Seah, 1989 and Dawe et al., 1989) between the infill and existing frames will need to be minimized if a complete infill is the desired strategy.
3. Pretensioned bolted connections are a viable option for ECC infill panel connections.

2.2 ECC Infill System Development

In the current research, a new type of infill system is developed that builds upon the previous research and also addresses the specific needs of critical facilities. The following sections highlight specific features of the new infill panel system.

2.2.1 Critical Facilities

One of the thrust areas of the MCEER research project (MCEER, 2000) is the development of retrofit strategies to improve the seismic performance of critical facilities such as hospitals and emergency response structures. The retrofit of critical facilities is significantly more complicated than the retrofit of traditional structures for several reasons. These include:

1. Critical facilities generally cannot be taken out of service for extended periods during retrofit installation.
2. Critical facilities, especially hospital structures, will generally have larger and more complex secondary systems, such as oversized elevators and medical equipment, compared to traditional structures.
3. Secondary systems in critical facilities must be sufficiently protected during earthquakes to allow immediate use after the earthquake.
4. Frequent changes in use in critical facilities (such as modifications due to technology upgrades) require adaptable retrofit strategies.

2.2.2 System Considerations

The infill system under development is specifically intended for use as a retrofit system within a critical facility. Installation as a retrofit system is considerably more demanding than infill systems that are purely intended to stiffen/strengthen existing structures. The following items are some of the overall system considerations that were incorporated into the system under development.

1. Minimize the retrofit construction time and impact on facility use.
2. Incorporate the ability to accommodate existing and new secondary systems.
3. Provide a system that is quickly replaceable in the event of severe damage during an earthquake.
4. Provide a flexible/relocatable system to accommodate potential changes in facility use.

2.2.3 Performance Guidelines

Performance guidelines for critical facilities can be found in the NEHRP Guidelines for Seismic Rehabilitation of Buildings. (FEMA 273, 1999) The guidelines describe specific performance requirements for both structural and non-structural (secondary) systems. Performance guidelines are specific criteria, which a component (structural or nonstructural) must satisfy, such as limitations on structural drift during earthquakes.

The performance guidelines for both structural and nonstructural building components are combined into the building performance level. The critical facilities under consideration in the present research need to satisfy the requirements of building performance level Operational Level 1-A. This level is a combination of the Structural Immediate Occupancy level (S-1) for structural components, and the Operation N-A level for nonstructural components.

Structures in the Operation Level 1-A are expected to be immediately available for use after an earthquake with only minor limitations in use. The performance level is intended only for structures that house critical services. Some specific requirements of this level (taken from FEMA 273) are summarized below:

Building Element	**Required Performance**
Overall damage	Very light damage, no permanent drift, structure retains original strength and stiffness. All systems important to normal operation are functional
Nonstructural components	Negligible damage occurs
Steel moment frames	Minor local yielding at a few places. No fractures, buckling or permanent distortion of members
Drift	0.7% transient[1], negligible permanent.

These performance criteria were used to help guide the development of the retrofit strategies proposed herein. However, considering the readily replaceable nature of the infill panel system under development, damage to the panels requiring replacement after an earthquake is considered acceptable.

2.2.4 ECC Infill Panel Systems

To accommodate the requirements discussed in the preceding sections, two infill systems using precast ECC panels with pre-tensioned bolted connections were considered for further investigation and development. The infill concepts are shown in figure 2.3, with the connections shown in figure 2.4. In both systems the panels contain steel reinforcing bars or welded wire mesh.

The full frame infill system (figure 2.3a) is conceptually similar to a traditional infill wall system, such as a CMU or concrete infill. The full frame infill system is expected to behave as a shear wall and builds upon the previous work by Kahn and Hanson (1979), and Frosch et al. (1996). In the system, the ECC materials are expected to be advantageous over traditional materials due to their high compressive and tensile strain capacities, and their ability to maintain integrity without spalling.

In figure 2.3b a beam-type infill system is shown. In this concept, the infill panels act as flexural elements, with the individual beam-type infill sections acting as fixed-fixed beams. Thus, the ECC is used with tensile reinforcing steel to help carry the flexural and shear stresses in the beam elements. The beam-type infill system builds on research by Fischer and Li (2002), where

[1] Drift level is not intended to be used as an acceptance criterion, rather the level is indicative of the drift that typical structures may undergo when satisfying the performance limits. (FEMA-273, 1999)

the combination of reinforcing steel and ECC materials in tension was shown to have significant advantages over traditional reinforced concrete. The combination allows for greater spreading of yielding in the reinforcing steel and increased energy dissipation than traditional materials.

Both of the proposed panel systems specifically address the performance requirements presented in Section 2.2.3. Specific features of the systems include:

1. Limited panel size minimizes construction time, and allows for installation using simple tools.
2. Simple bolted connections allow for ease of panel relocation and removal if damaged after an earthquake. The use of bolted connections can (potentially) eliminate problems associated with gaps between a full infill and the existing structure
3. Partial infill additions can be used to accommodate existing secondary systems in the structure.

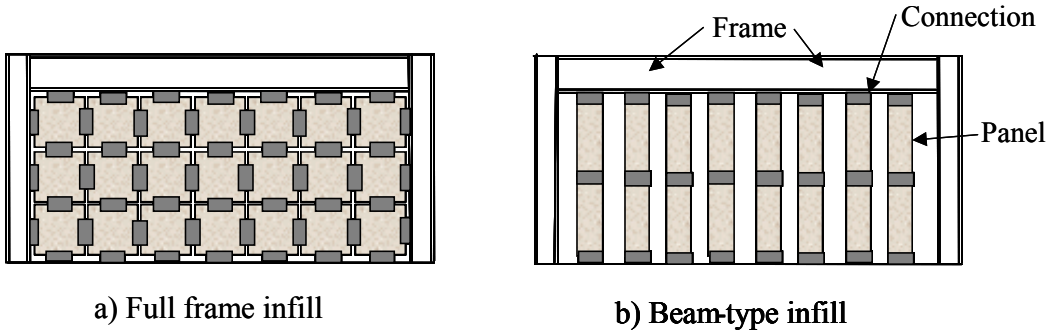

Figure 2-3. Panel infill systems considered.

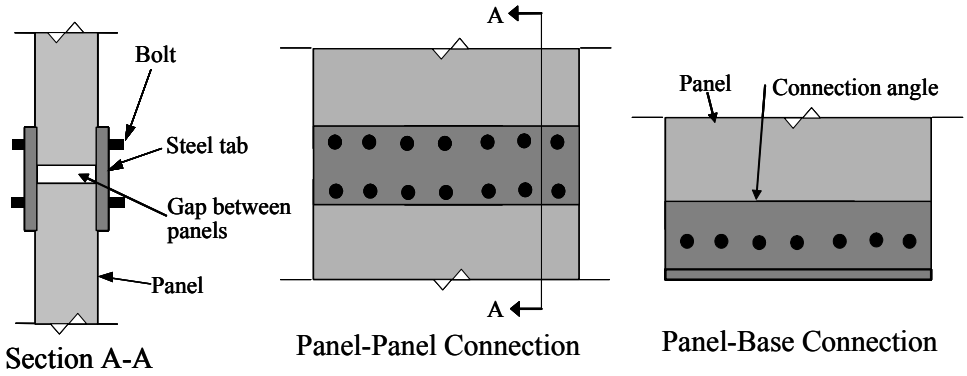

Figure 2-4. Example of connection between ECC infill panels.

2.3 Infill System Analysis

To examine the effect of the infill panel systems on a structure, a series of analyses were performed. The goals of the analyses were to:

1. Determine how the addition of the infill panels affects the response of a structure (in this case a steel frame) to an imposed lateral load.
2. Examine advantages and disadvantages of various infill systems.
3. Examine the optimal size, shape and thickness of the infill panels.
4. Determine the optimal use of ECC in the infill systems considering the results of the cyclic ECC material testing.
5. Use the results from the preliminary analyses to guide the development of laboratory tests to develop further the infill panel system.

These goals were common to the evaluation of both the full frame and beam-type infill systems.

2.3.1 Analysis Method

The finite element method was used to simulate the response of the different infill panel systems using the commercial software program DIANA (TNO 1998a and 1998b). The DIANA program was selected because it has numerous material models for brittle materials such as concrete, as well as readily available features such as embedded reinforcement. All of the analyses are two dimensional (2D), with all of the models comprised of combinations of plane stress and beam elements. To evaluate the effect of the infill system, a finite element model was created of a single bay of a steel frame with infill panels added. The specific properties of the elements and materials used in the analyses will be presented when the models are discussed.

The analyses were all displacement-controlled simulations of both bare frame and ECC infilled frame behavior. The regular Newton-Raphson iteration method was used for the non-linear analyses using an energy norm as the convergence criteria. A convergence criterion of 0.5% was used in the analyses. The size of the displacement steps varied and was selected to provide a balance between achieving numerical stability at each displacement step and minimizing the computation time.

The following sections describe the analyses performed on the full frame and beam-type infill systems.

2.4 Full Frame Infill Evaluation

The initial studies of the infill wall system examined the response of a full frame infill, specifically, the effect of different panel geometries. Results from preliminary studies of the full frame infill were shown in Kesner and Billington (2001). The full frame infill was selected because it represented an outgrowth of the full frame infill systems that were discussed in Section 2.1. To simplify the analysis, a single story, single bay frame was examined. The steel frame used in the analysis was taken from an MCEER project hospital (Yuan and Whitaker, 2002). Fixed column and panel bases were assumed in the simulations.

2.4.1 Full Frame Infill Models

To examine the response of the full frame infill a series of four models were created with different infill panel geometries. The frame members were comprised of 2-noded beam elements. The infill panels and connection tab members were modeled with 4-noded plane stress elements. Table 2-1 shows the frame member properties. Figure 2-5 shows the frame with the four different panel geometries examined in the study, with the panel dimensions given in Table 2-2. A spacing of 100 mm was used between all of the panels and at the connections to the frames.

In the some of the simulations 0.5% (by area) of steel reinforcement in each direction was added to the panels. The reinforcement was similar to the addition of welded wire fabric (WWF) to the panels. The reinforcement was modeled as embedded reinforcement. The concept of embedded reinforcement assumes that perfect bond exists between the plane stress elements of the panels and the reinforcement.

The four different infill panel geometries were examined to study the variation in load distribution through different panel geometries. The simplest geometry was a square panel, which was sized to allow for three panels to span from the base of the frame to the bottom of the beam. Two different rectangular panel geometries were examined. The rectangular panels have the advantage of needing fewer panels to fill the frame, which reduces the number of panel connections. Finally, an octagonal panel geometry was created by removing the corner sections from the square panel. It was believed that the octagonal panel geometry would allow for a more efficient infill panel system, by removing the unused material at the corners of the square panels. Secondary systems could also potentially be located in the holes between octagonal panels.

In the models, the connection tabs between panels were located at the center of the panels with the tab width equal to one half of the panel side length. To represent the connection of the connection tab members to the frames, multi-point constraints were used between the beam elements and the connection tabs (TNO 1998a). The constraints link the nodal displacement of the beam elements (at the centerline of the beam elements) with the nodal displacement at the edge of the tab elements. The use of multi-point constraints allows for a more accurate geometrical representation of the infill panels and connection tabs.

Table 2-1 – Frame member properties for full infill panel system analyses

Member	Moment of Inertia	Area	Depth
	mm^4	mm^2	mm
Top Beam	561,912,000	10,500	600
Columns	222,268,000	16,700	275

Table 2-2 – Panel geometries examined

Panel Type	Length	Height	Thickness
	mm	mm	mm
Square	1,670	1,670	100
Octagon[1]	835	835	100
Narrow Rectangle	787	1,700	100
Wide Rectangle	1,930	1,016	100

1. Dimensions given are tab dimensions. Panel has same length and height as square panel

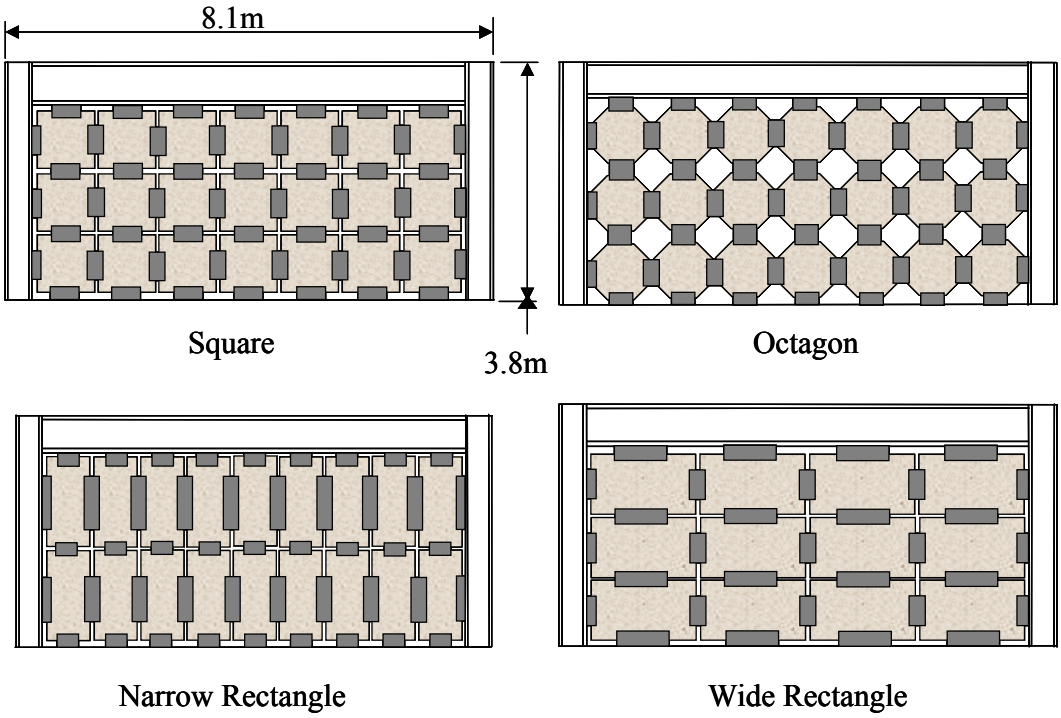

Figure 2-5. Infill panel geometries examined. All frames have the same dimensions.

2.4.2 Full Frame Infill Materials

The ECC model used in the analysis was based on a total strain based fixed-crack model (Feenstra et al., 1998). In tension, for the ECC material a multilinear stress-strain curve was used to represent the strain-hardening portion of the model, followed by linear softening after the peak tensile strain (strain at peak tensile strength) was exceeded. The transition points on the tensile stress-strain diagram were obtained from uniaxial tension tests as described in Kesner and

Billington (2004). In compression the ECC was modeled as elastic-perfectly plastic with a compressive strength of 70 MPa. Softening of the ECC, beyond the peak compressive strength was not considered. The ECC material model used secant unloading and reloading in both tension and compression, which compared to the cyclic testing results discussed in Kesner and Billington (2004), was a significant simplification of the unloading and reloading behavior of the materials.

Figure 2-6 shows representations of the material models used for the steel (figure 2.6a) and ECC (figure 2.6b). An elastoplastic material model with isotropic hardening was used for the steel frame, the panel connection (tab) members and the reinforcing steel (when used). The Bauschinger effect was not captured in the steel model used.

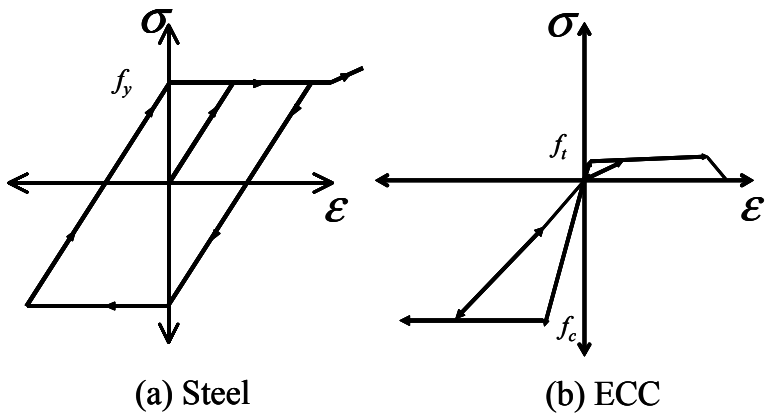

Figure 2-6. Representation of material models used in preliminary analysis for (a) steel and (b) ECC

To represent the stiffness of the panel material in the connection region, the modulus of elasticity in the connection region was increased based upon a strain capability analysis of the different materials and thicknesses used in the connection region. The analysis resulted in a composite modulus of 63.8 GPa for the material in the connection region. Because of the pre-compression (from the pretensioned bolts) in the connection region, damage was not expected inside the connection regions, thus the material in the connection region was assumed to remain elastic in the analysis. These assumptions will be evaluated in the laboratory tests presented in Sections 3 and 4.

Figure 2-7 shows a schematic representation of a square panel at the joint region with the different materials used in the analyses. Table 2-3 shows a summary of the material properties used in the analyses.

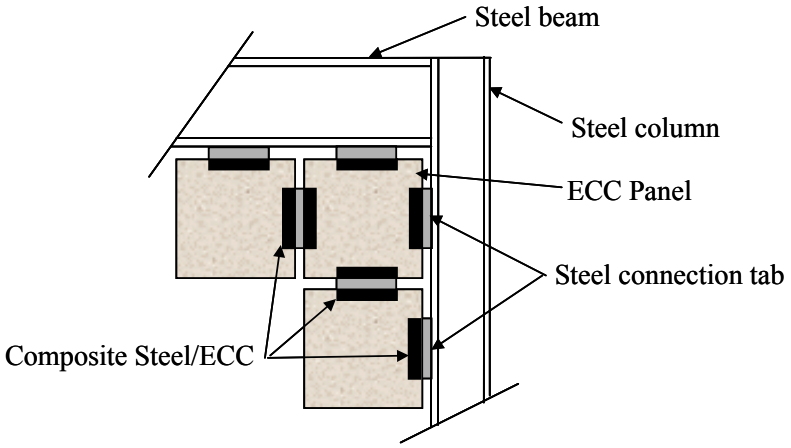

Figure 2-7. Schematic showing different materials used in analysis

Table 2-3 – Material properties used in preliminary analyses

Material	Elastic Mod.	Yield/ Cracking Strain	Yield/ Cracking Stress	Peak Comp. Strain	Peak Tens. Strain	Peak Stress
	GPa	%	MPa	%	%	MPa
Steel – Frame / Tab	200	0.17	345 (f_y)	0.10	10	552
Steel – Reinf.	200	0.207	414	0.10	10	552
ECC	13.8	0.015	2.0 (f_t)	0.005	3	3.0 / 70[1]
Comp. Steel/ECC[2]	63.8	-	-	-	-	-

1. Peak tensile strength / peak compressive strength
2. Composite Steel/ECC assumed to be linear elastic

To evaluate the response of both the bare and infilled frames, a cyclic displacement was simulated to three drift levels (+/-0.25%, +/-0.50%, and +/-1%). The displacement was applied in equal displacement steps of 0.35 mm. The drift was determined by dividing the top displacement by the frame height. Thus, each displacement step represented 0.01% drift.

2.4.3 Full Frame Infill Analysis Results

Figure 2-8 shows the load-drift response obtained from the simulations. These results were obtained from the simulations without reinforcement in the panels. In the simulation results, the bare frame had a peak capacity of 430 kN (at 1% drift). The infilled frames had significant increases in capacity compared to the bare frame. The increase in capacity (at 1% drift) ranged from 590% (2251 kN) for the narrow rectangular panels to 860% (3684 kN) for the square panels.

Figure 2-9 shows the results obtained from simulations of the square and octagonal panels with 0.5% (by area) of reinforcement added to the panels. The addition of the reinforcing to the square and octagonal panels resulted in further increases (27% greater capacity compared to unreinforced panels) in the infilled frame capacity.

Figures 2.10 and 2.11 show the principle tensile strain contours obtained from the simulations at 0.25% drift from the frame infilled with reinforced and unreinforced square panels, respectively. The upper limit in the tensile strain contours was 0.0017, which represents the yield strain of the steel frame members. Yielding of the bare frame was observed at a drift level of 0.8%. The infilled frame members began yielding at the beam-column joint at drift levels as low as 0.25% in the case of reinforced square panel infills. The onset of yielding can be seen in the left beam-column joint in figure 2-11.

Figures 2.12 and 2.13 show the principle compressive strain contours at 1% drift obtained from the frame infilled with the unreinforced and reinforced square panels, respectively. In the results shown, the upper limit on the compressive strain contour was -0.005, which represents the strain at the peak compressive stress in the ECC material.

Figures 2.14 and 2.15 show the principle tensile strain contours at 1% drift obtained from the frame infilled with the unreinforced and reinforced square panels, respectively. The upper limit on the tensile strain contour in these figures is 0.03, which represents the strain level at the onset of softening in the ECC material.

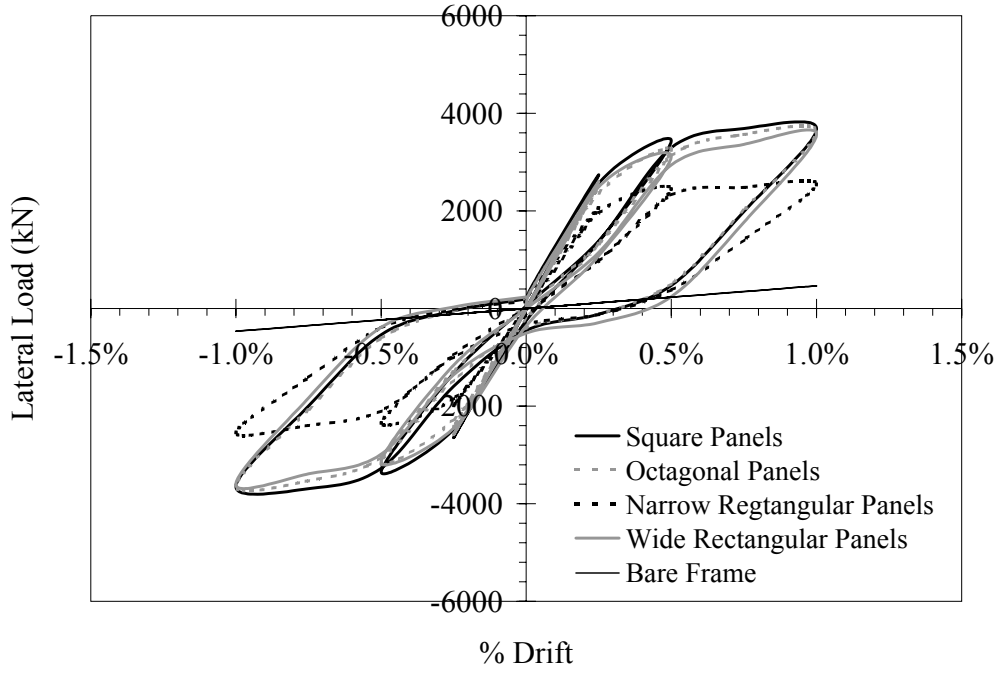

Figure 2-8. Load-drift response of infilled frame

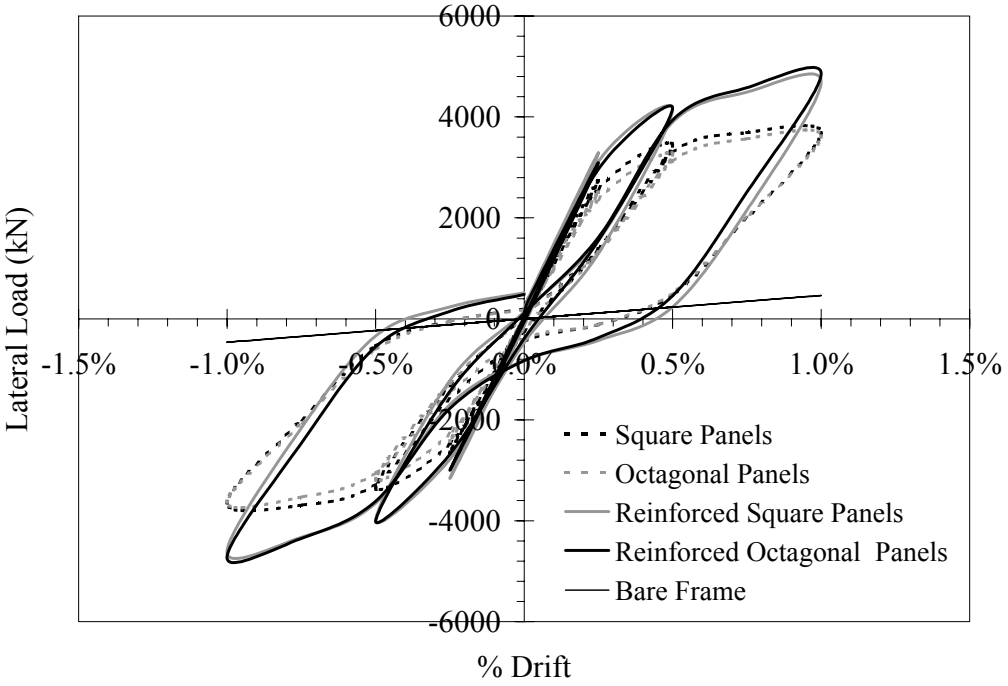

Figure 2-9. Load-drift response of reinforced infill panels

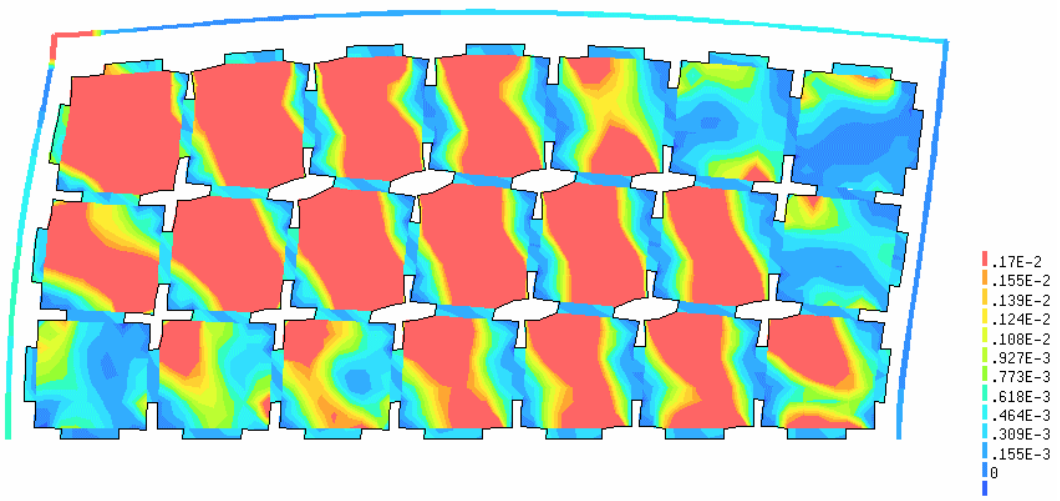

Figure 2-10. Principle tensile strains in frame infilled with unreinforced square panels at 0.25% drift

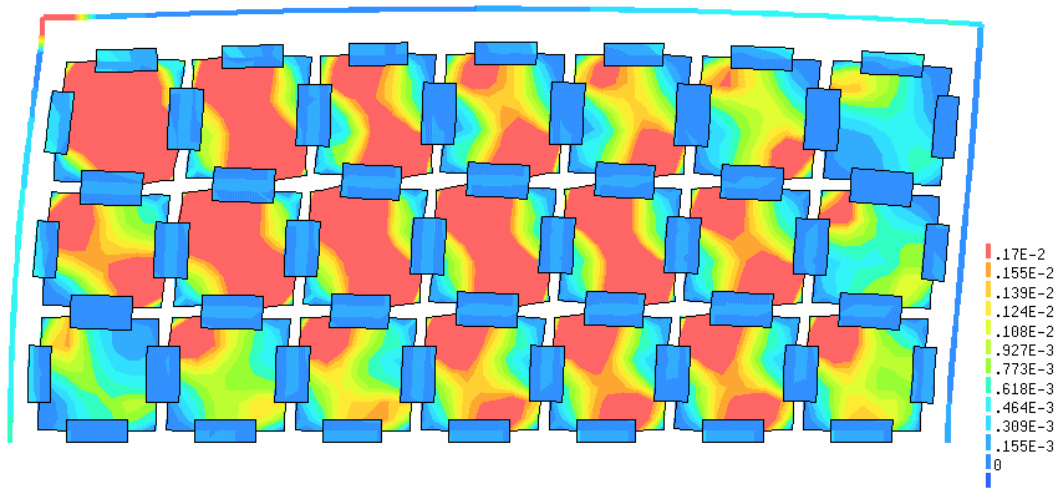

Figure 2-11. Principle tensile strains in frame infilled with reinforced square panels at 0.25% drift

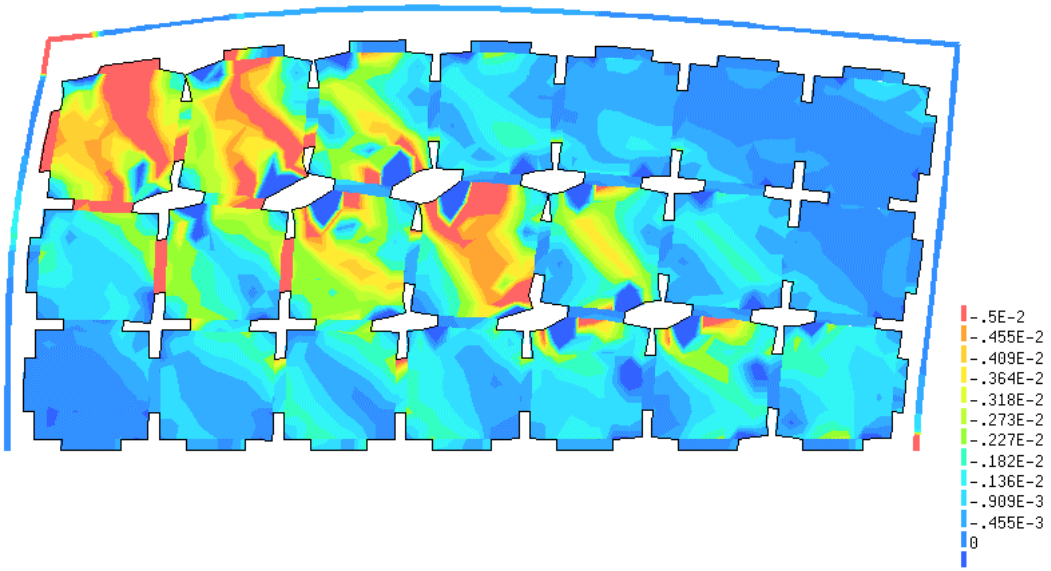

Figure 2-12. Principle compressive strains in frame infilled with unreinforced square panels at 1% drift

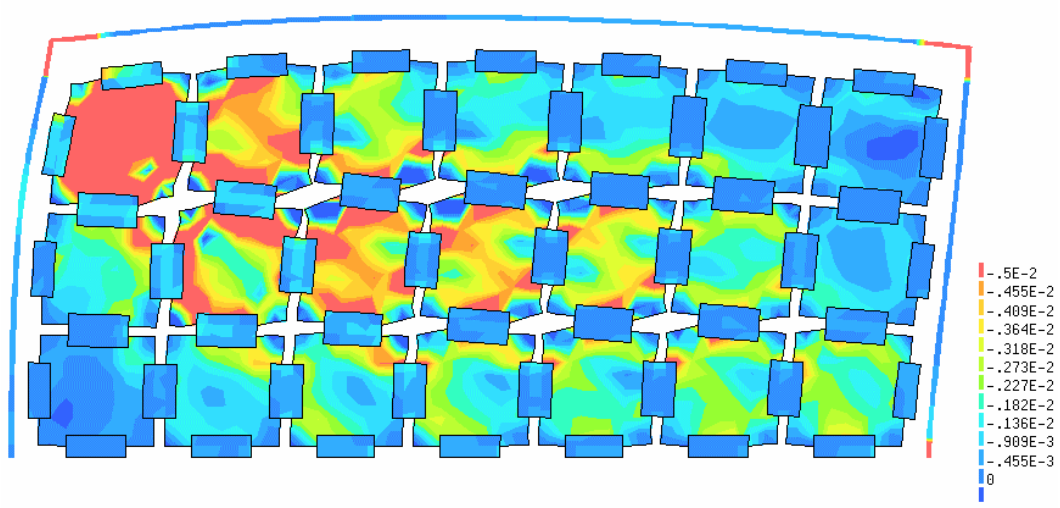

Figure 2-13. Principle compressive strains in frame infilled with reinforced square panels at 1% drift

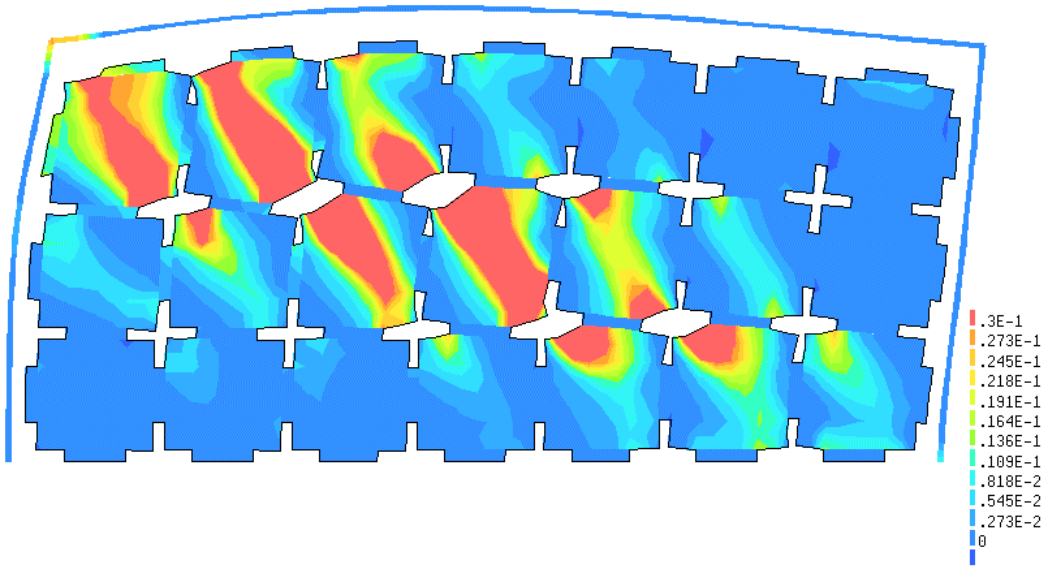

Figure 2-14. Principle tensile strains in frame infilled with reinforced square panels at 1% drift

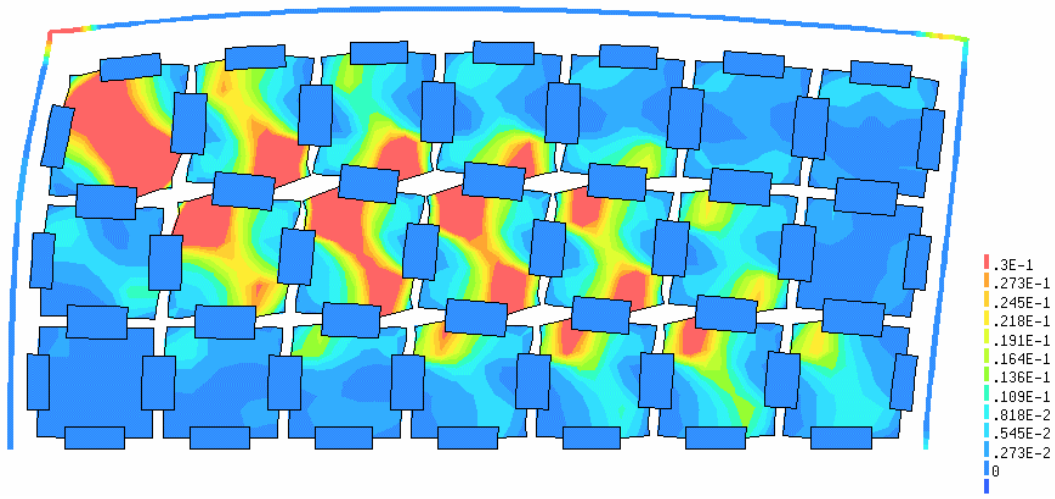

Figure 2-15. Principle tensile strains in frame infilled with reinforced square panels at 1% drift

2.4.4 Discussion of Full Frame Infill Analysis

The similarity in load-drift response exhibited by the square, octagonal and wide rectangle geometries can be explained by examining the infill frame geometries shown in figure 2-5, and the principle compressive strain contours at 1% drift shown in figures 2.12 to 2.13. In the square, octagonal, and wide rectangular panel a straight compressive strut can be seen as a direct load path to the base of the model. The compressive strut was not as direct in the narrow rectangular system, due to the narrower width of the panels. The compressive strut is conceptually similar to the compressive strut shown in figure 2-2, with the added complication of the load being transferred through the connection tabs before entering the panels and frame.

The addition of the reinforcing steel to the panels resulted in an increase in capacity, and energy dissipation (figure 2-9). The reinforcing steel did not appreciably change the load distribution through the panels as observed by the lack of significant differences in the strain contours.

The infilled frames had substantial increases in energy dissipation compared to the bare frame. The area enclosed by the load vs. displacement response can be used to represent the hysteretic energy dissipated. The bare frame, which yielded at 0.8% drift, had virtually no energy dissipation, whereas the infill additions resulted in large amounts of energy dissipation. The energy was dissipated by the steel reinforcement in the panels (when used), by the ECC, and from yielding of the steel frame and connection tab members.

The substantial increase in the load carrying capacity and energy dissipation in the frame due to the infills was accompanied by yielding of the members in the frame at the beam-column joint at low drift levels, which is inconsistent with the objectives of the retrofit installation, as discussed in Section 2.2. Yielding was observed in the simulations at a drift level as low as 0.25% (figure 2-11). Frame yielding at low drift levels is a disadvantage of the full frame infill.

A second disadvantage of the full frame infill panel system is the method in which the ECC material was used. The results from reversed cyclic tests on ECC materials shown in Kesner and Billington (2004) indicated that when the peak compressive strength in the material was exceeded; the tensile strain capacity of the ECC will be reduced. Thus, the high compressive strains in the ECC panels expected with the full frame infill will limit the tensile strain capacity in the infill panels.

More specifically, the simulation results indicated that the peak compressive stress of the ECC was exceeded at 1% drift in portions of the infill panels (in the upper left corner), as seen in figures 2.12 and 2.13. In subsequent loadings, these areas of the panels will have a reduced tensile strain capacity. These panels also have tensile strains that exceed the peak strain capacity of the ECC material at 1% drift (figures 2.14 and 2.15). Thus, the panels in these locations will have extensive compressive and tensile damage, which was not desirable. Additionally, the panels in the lower corners of the frames are only lightly loaded as will be the case under reversed loading as well, which is an indication of an inefficient system.

The results indicate that the panels in upper corners of the infill sections will be severely damaged under cyclic loadings. The extent of damage cannot be readily assessed because the material model used in these analyses did not capture the reduction in tensile strain capacity when the compressive strength of the material was exceeded.

2.4.5 Summary of Full Frame Infill Analysis

The full frame infill additions resulted in substantial increases in strength and stiffness, when compared to results from a bare frame. Reinforcement of the panels resulted in small increases in the capacity of the frames, and increases in energy dissipation. The addition of reinforcement strengthened the panels, but did not significantly affect the distribution of the load through the panels as seen in figures 2.10 to 2.15.

The addition of the infill panels resulted in a significant decrease in the drift capacity before the onset of frame yielding, from 0.8% drift for the bare frame, to as low as 0.25% for the frame with reinforced square panels. Yielding of the frame at low drift levels is inconsistent with the goals of the retrofit installation discussed in Section 2.2.

The simulation results also indicated that the peak compressive strength of the infill panels would be easily exceeded. The ECC tensile capacity will be reduced in these areas. The high damage to the panels in these areas suggests an alternate method to strengthen the frame will be desirable. The inability of the selected material model to capture the reduction in tensile capacity in these areas limits the accuracy of the simulation results.

2.5 Beam-Type Infill Evaluation

To address some of the limitations of the full frame infill system, a beam-type infill system was developed. Figure 2-3b shows the beam-type infill concept. In the beam-type system, the infill elements under lateral load act as fixed-fixed beams in flexure and shear. When the panels are steel reinforced, this arrangement can more effectively use the desirable tensile properties of the ECC material than the full frame system.

To examine the response of the beam-type infill system, a series of finite element studies were performed. In particular, these analyses were conducted to examine the effect of the infill addition on the strength/stiffness of the frame, examine the load distribution through the panels, and determine the effectiveness of the infill addition in satisfying the requirements presented in Section 2.2.3. An additional goal of the evaluation of beam-type infills was to determine if the panel geometry can be optimized to minimize infill system cost.

2.5.1 Beam-Type Infill Models

The initial analysis of the beam-type infill system involved the simulation of a frame with six beam-type infills added. The finite-element models used the features discussed in Section 2.4.2. For simplicity, and to allow for comparisons with the previous analyses, the frame from Section 2.4 was used in these analyses. The frame properties are given in Table 2-1.

The materials properties used in the simulations are given in Table 2-3. The ECC material used in the current simulations was modified to allow for parabolic softening of the material in compression. Figure 2-16 shows a schematic representation of the ECC material model used. The compressive fracture energy (G) of the ECC was assumed to be 2.5 MPa-mm.

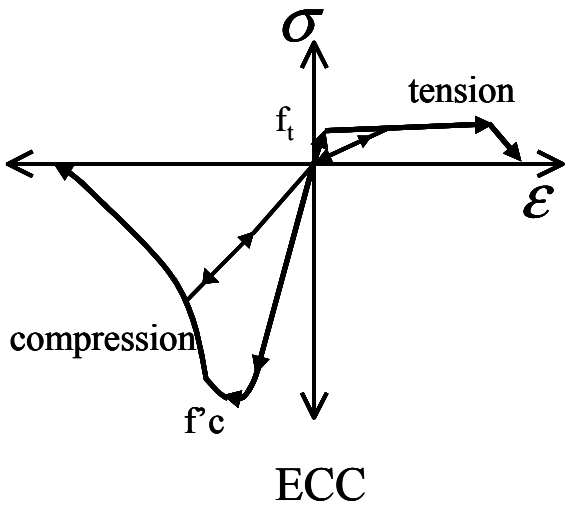

Figure 2-16. Schematic representation of ECC material model used in beam-type infill evaluation

In the simulations 0.5% (by area) of steel reinforcement (welded wire fabric (WWF)) in each direction was added in all of the panels. In addition to the WWF reinforcement, a 9.5 mm perimeter bar was added to the panels. Figure 2-17 shows a schematic representation of a single ECC infill panel. The panel shown in figure 2-17 represents one-half of a beam-type infill section. The reinforcement of the panels is intended to help the beam-type infill sections act as flexural members and provide the advantages of steel reinforced ECC (Fischer and Li, 2002).

Figure 2-18 shows a schematic of the beam-type infill system. The beam-type infills were placed with the centerline of the panel group at the midpoint of the beam span. The location was selected to correspond with the inflection point of the beam where the beam bending moment will be zero. The grouping of the panels near the inflection point was expected to result in a shear displacement applied to the panels, and minimize the bending moment applied to the panels by the beam.

The beam-type infills were comprised of two panel sections 762 mm in width by 1524 mm tall with a thickness of 100 mm, resulting in an approximate panel aspect ratio of 4:1 (height/width). A 50 mm gap was used at mid-height between the panels, with a 25 mm gap used at the top and bottom of the infill elements. The connection tab extended 125 mm onto the top and bottom of the panel to form the connection region. A spacing of 50 mm was used between the beam-type infills. This infill arrangement resulted in a gap of approximately 700 mm between the infill panels and the columns on the left and right sides of the model.

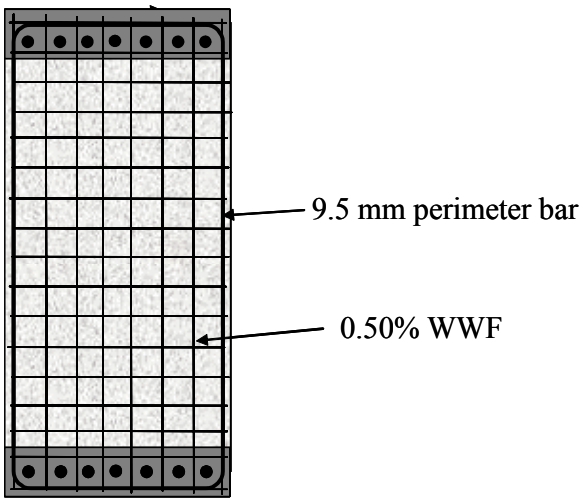

Figure 2-17. Beam type infill panel with reinforcement

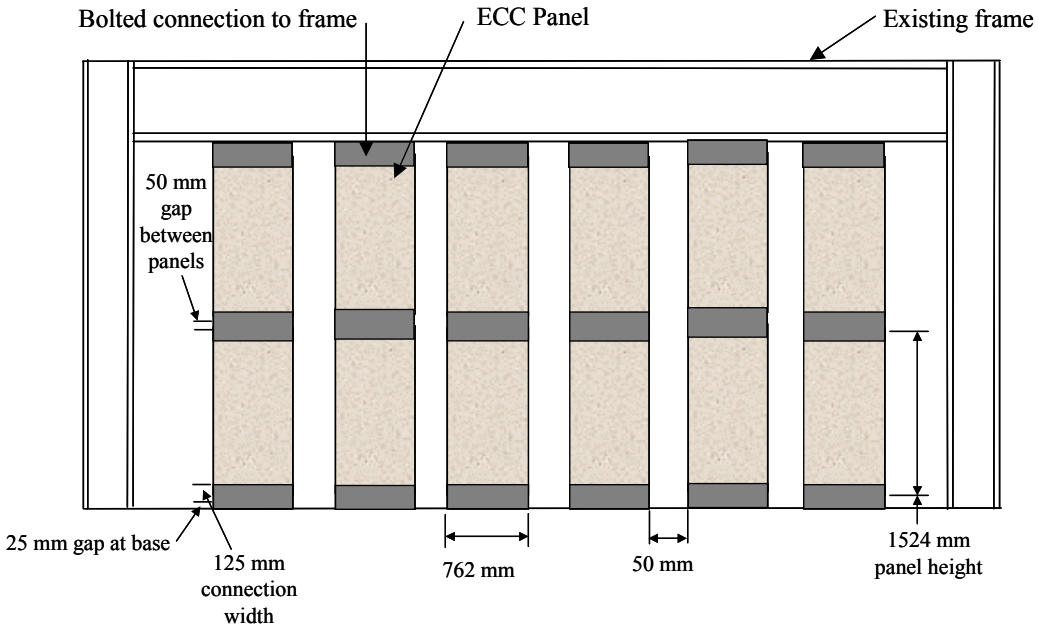

Figure 2-18. Schematic of frame with 6 beam-type infill sections added (*not to scale*)

Two additional beam-type infill models were created by removing pairs of beam-type infill sections from the model shown in figure 2-18. The pairs of infill sections were removed from the outside edge of the models resulting in models with 4 and 2 beam-type infill sections as shown in figures 2.19 and 2.20, respectively. The models with the reduced number of infill additions were examined to determine how the beam-type infill system could be tailored to provide different amounts of strengthening and stiffening to a frame.

To evaluate the response of these configurations, a cyclic displacement was applied to the models to five drift levels (+/-0.10%, +/-0.25%, +/-0.50%, +/-0.75%, and +/-1%). The displacement step size was identical to that in the analyses of the full frame infill.

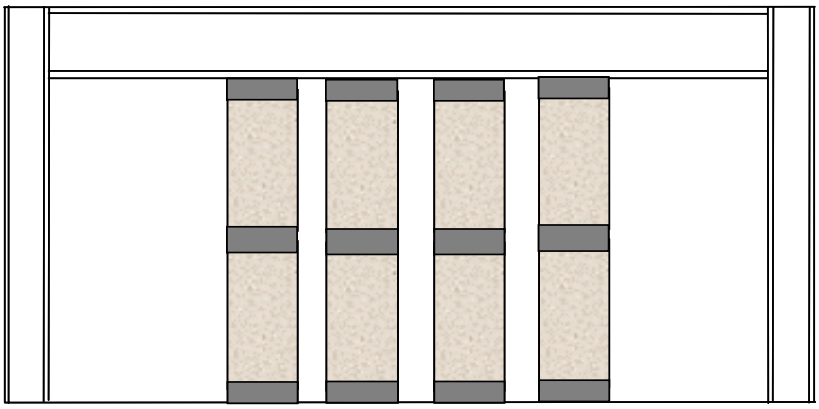

Figure 2-19. Schematic of frame with 4 beam-type infill sections added (*not to scale*)

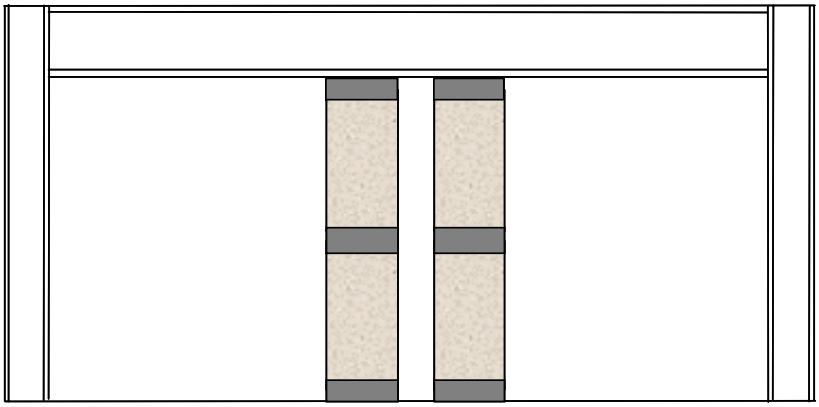

Figure 2-20. Schematic of frame with 2 beam-type infill sections added (*not to scale*)

2.5.2 Beam-Type Infill - Initial Results

Figure 2-21 shows the load-drift results obtained from the simulation of the cyclic displacement of the frame with 6 beam-type infill sections added. The results from the bare frame simulation are also shown. Figure 2-22 shows the load-drift response obtained from the simulations with 2, 4, and 6 beam-type infill section additions as well as the bare frame.

Figures 2.23 and 2.24 show the principle tensile strain contours obtained from the model with 6 beam-type infill sections at 1% drift. In figure 2-23, the upper limit of the tensile strain contour is 0.0017, which represents the yield strain of the frame members. In figure 2-24, the upper limit of the tensile strain contour is 0.03, which represents the strain level at the onset of softening in

the ECC material. Figure 2-25 shows the principle compressive strain contours from the same simulation. The lower limit in the compressive strain contour was –0.005, which is the strain level at the onset of compressive softening of ECC. Similar tensile and compressive strain contours were obtained from the simulations with 2 and 4 beam-type infill section additions and are not shown here.

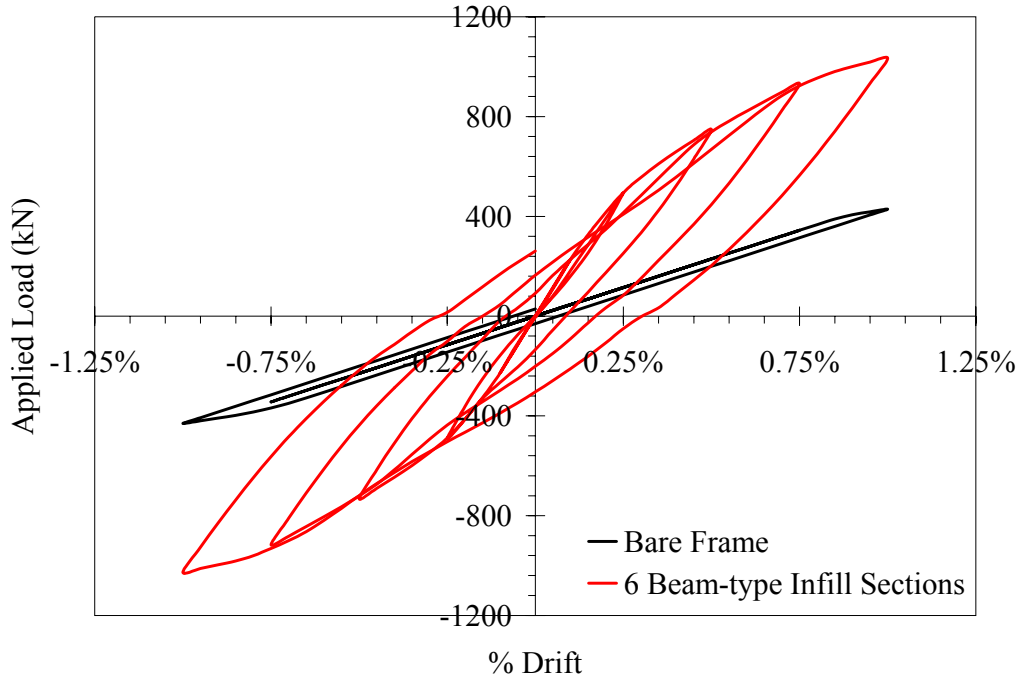

Figure 2-21. Load-drift response from frame with 6 beam type infills compared to results from bare frame

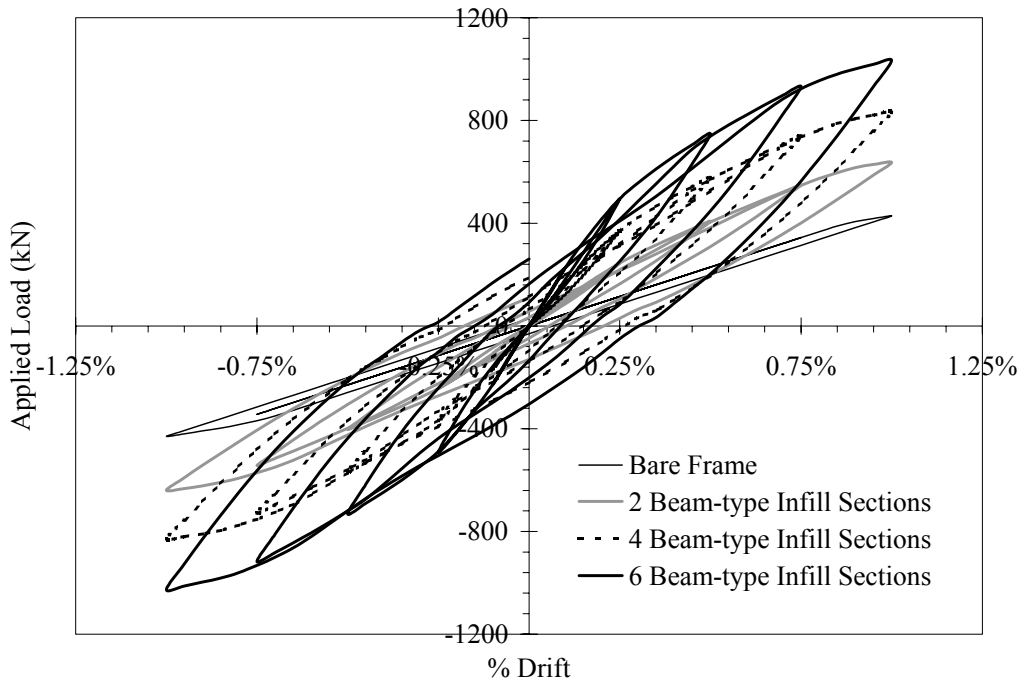

Figure 2-22. Load-drift response from frame with 2, 4 and 6 beam type infill sections compared to results from bare frame

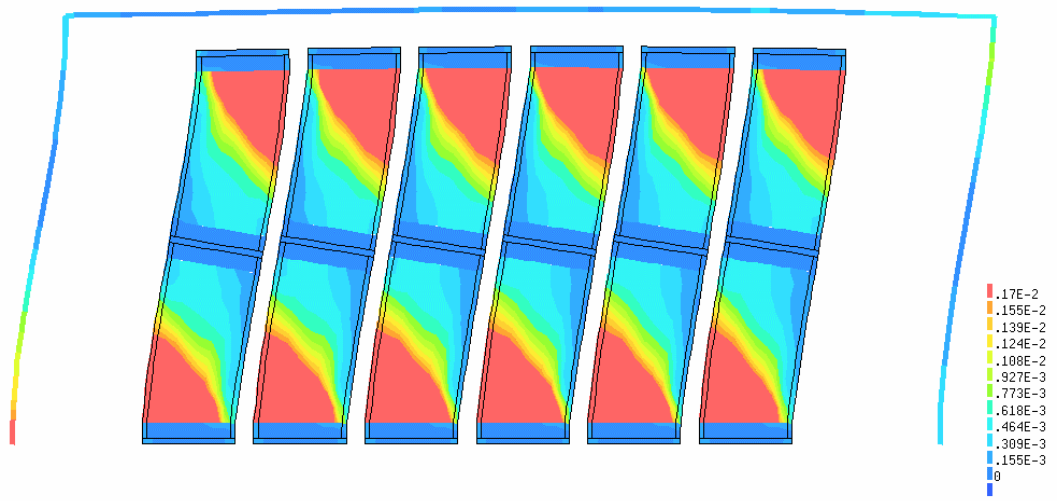

Figure 2-23. Principle tensile strain contour from simulation with 6 beam-type infill sections added at 1% drift

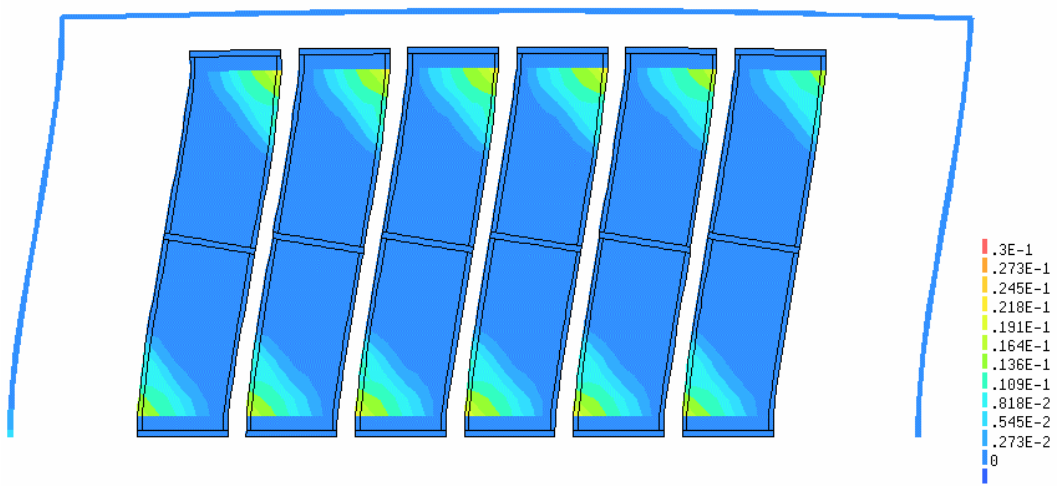

Figure 2-24. Principle tensile strain contour from simulation with 6 beam-type infill sections added at 1% drift

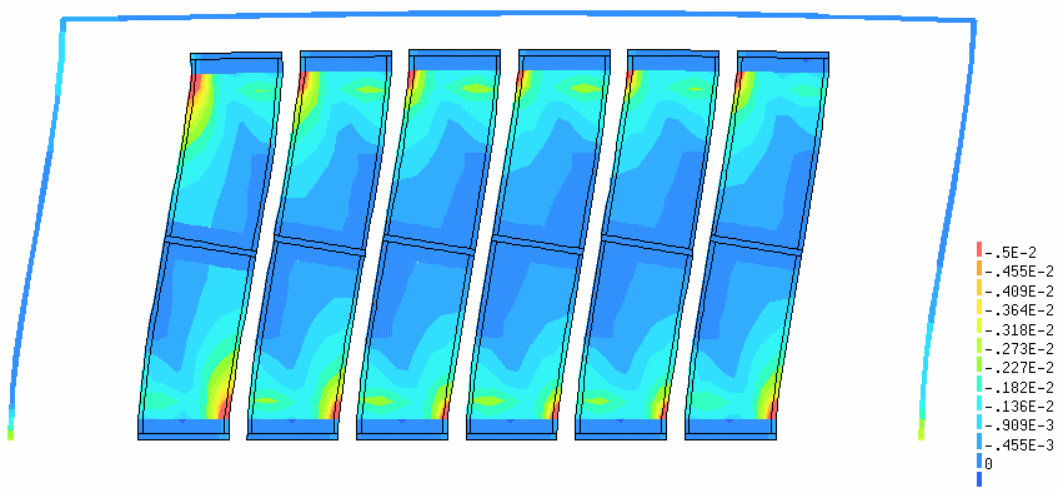

Figure 2-25. Principle compressive strain contour from simulation with 6 beam-type infill sections added at 1% drift

The results of the analysis indicate that the addition of 6 beam-type infill sections will increase the strength of the bare frame. At 1% drift the load in the infilled frame was 1034 kN compared to 430 kN in the bare frame. As expected, the addition of 2 and 4 beam-type infill sections resulted in smaller increases in load at 1% drift (637 kN and 832 kN, respectively) when compared to the 6 beam-type infill section additions.

Yielding of the frame members was apparent at 1% drift in the simulation results with 6 infill sections added, as seen in figure 2-23. The bare frame began to yield at a drift level of 0.80%. The onset of yielding in the infilled frames (2, 4 and 6 infill section additions) was observed to begin at a drift level of 0.75%. Yielding of the frame can be seen in figure 2-26 (upper tensile strain limit of 0.0017), which shows a principle strain contour at 0.75% drift from the simulation with 6 beam-type infill sections added.

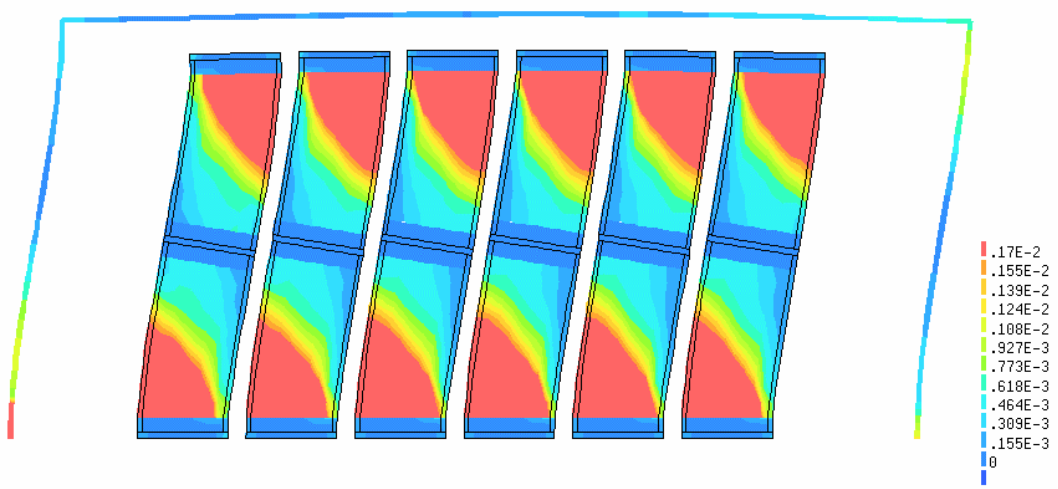

Figure 2-26. Principle tensile strain contour from simulation with 6 beam-type infill sections added at 0.75% drift

2.5.3 Discussion of Initial Beam-Type Infill Results

The results shown in the previous section indicate that the beam-type infill sections can significantly increase the stiffness of the frame, as well as the hysteretic energy dissipation during cyclic loading. The nonlinear load-drift response shown in figures 2.21 and 2.22 was due to the strain hardening behavior of the ECC coupled with the plastic deformation of the reinforcement in the panel. At drift levels above 0.75%, the yielding of the frame contributed to the nonlinear load-drift response.

The energy dissipation in the frames with the beam-type infill additions was attributed to energy dissipated by the reinforced ECC at drift levels below 0.75%. The energy dissipation by the reinforced ECC occurs primarily due to the yielding of the panel reinforcement, with a small contribution from cracking of the ECC material. At higher drift levels the yielding of the frame will also contribute to the energy dissipation. The energy dissipation by the frame was not a desirable result.

The beam-type infill additions appear to represent an efficient use of the ECC material as can be seen in figures 2.24 and 2.25. At 1% drift, the tensile strains (figure 2-24) in the panel sections were below the strain level at the onset of softening (0.03) of ECC. Similarly, only very small sections of the infill panel have exceeded the compressive strain (–0.005) by 1% drift. Thus, the ECC material in the infill sections at 1% drift (the peak drift) has approached failure, but has not

failed. Similar results were obtained from the simulations with 2 and 4 beam-type infill section additions. Additionally, as seen in figure 2-23, the tensile strain (and thus cracking) in the panels has spread over a large portion of the panel indicating that the majority of the panels was being used.

In the analysis of the bare frame, yielding was observed at the base of the columns at approximately 0.80% drift. Yielding was apparent as the load-drift response from the bare frame deviated from a linear response (figure 2-21). In the infilled frame with 6 infill sections, yielding was observed at a drift level of 0.75%, which was very close to the bare frame result. The similarity in drift level at the onset of frame yielding indicates the beam-type infill additions can in this case maintain roughly the same frame response while increasing the strength and energy dissipation of the system.

These results demonstrate the variation in strength and stiffness increase that can be achieved with different levels of beam-type infill addition.

2.5.4 Examination of Infill Section Aspect Ratio

In Section 2.5.2, the addition of beam-type infills sections with a constant aspect ratio of approximately 4:1 was examined. In this section, the effect of different infill section aspect ratios is examined.

Simulations were performed using different infill section aspect ratios (height/depth). The simulations were performed using the load-drift history used in Section 2.5.1. In the simulations, the number of infill sections was varied such that 33 to 46% of frame area was infilled with reinforced ECC panels. These simulations used the same spacing between infill sections, and the same panel thickness as in the analyses presented in Section 2.5.1. However, the infill sections only contained 0.5% WWF reinforcement with no perimeter bar. Table 2-4 summarizes the different infill section geometries examined. Figures 2.27 to 2.29 show the finite-element meshes used in the simulations.

Table 2-4 – Panel geometries examined in study of different panel aspect ratios

Aspect Ratio[1]	Infill Section Depth (mm)	Infill Section Height (mm)	Number of infill sections added	% Infill Area[2]
2:1	1,752	3,505	2	44%
2.75:1	1,219	3,505	3	46%
5:1	660	3,505	4	33%

1. Approximate aspect ratio
2. Percentage of area inside frame occupied by infill sections

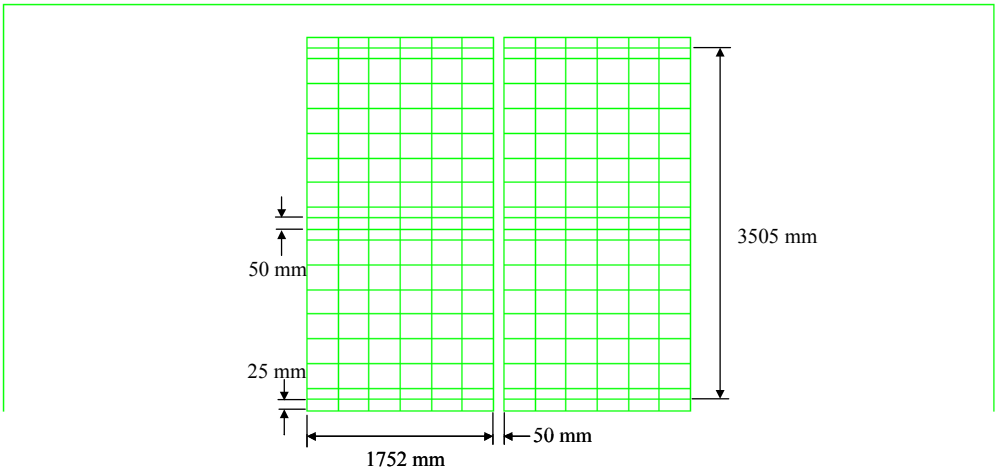

Figure 2-27. 2 panels with 2:1 aspect ratio

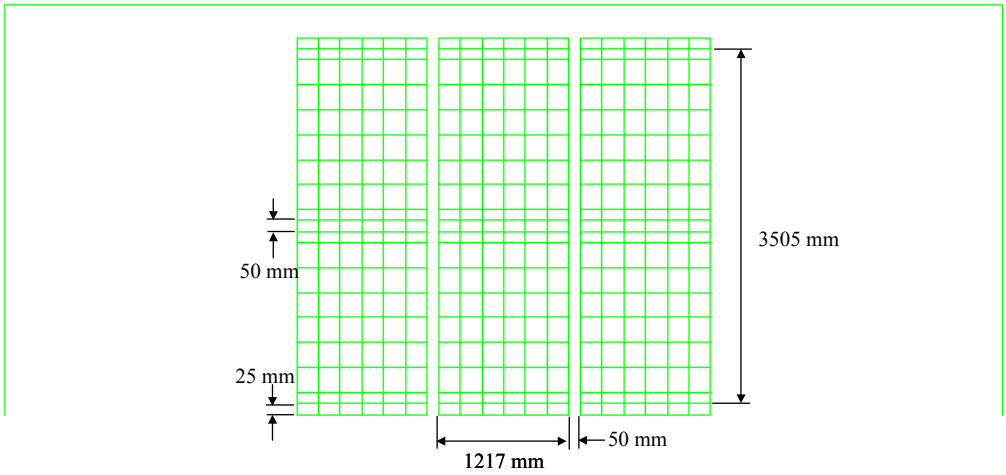

Figure 2-28. 3 infill sections with 2.75:1 aspect ratio

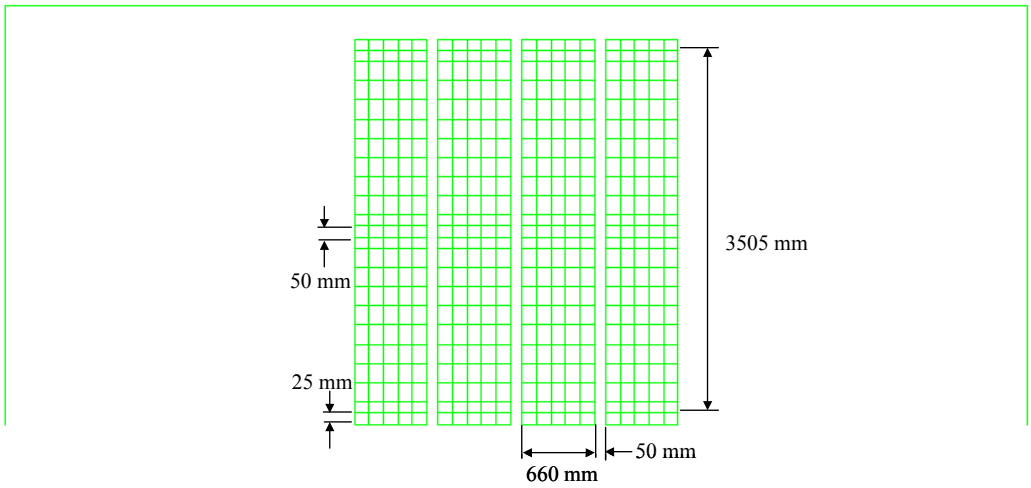

Figure 2-29. 4 infill sections with 5:1 aspect ratio

Figure 2-30 shows the load-drift response from the simulations, along with the result obtained from the simulation of the bare frame. The results indicate that the aspect ratio of the infill sections will have a significant effect on the load-drift response of the infilled frame. At 1% drift, the 2 infill sections with the 2:1 aspect ratio panels had the highest capacity (1484 kN), followed by the 3 infill sections with the 2.75:1 aspect ratio (933 kN). The lowest capacity (736 kN) at 1% drift came from the 4 infill sections with the 5:1 aspect ratio. All of the infilled frames had significant increases in strength compared to the bare frame.

The results shown in figure 2-30 indicate that the addition of two infill sections with a 2:1 aspect ratio resulted in a higher stiffness and capacity than three infill sections with a 2.75:1 aspect ratio despite filling a lower percentage (46 versus 44%) of the frame area. The difference in stiffness can be explained by considering the moment of inertia of the infill sections. Calculations show that the two infill sections with the 2:1 aspect ratio have a 50% higher moment of inertia than the three panels with the higher aspect ratio. The greater moment of inertia results in the greater stiffness. The higher capacity is a consequence of the greater section depth with increases the flexural and shear capacity of the panels.

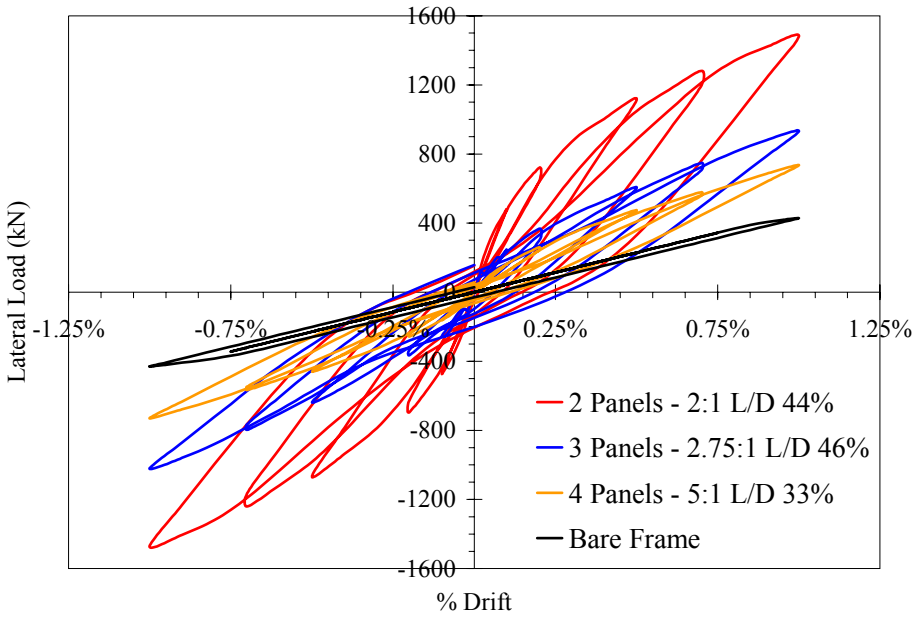

Figure 2-30. Load-drift response from frame with different aspect ratio beam-type infill sections

Similar to the results shown in Section 2.5.2, yielding of the frame was observed at drift levels of 0.75% in the simulations with the variable aspect ratio infill sections. Yielding of the bare frame occurred at 0.8% drift.

Figures 2.31 and 2.32 show principle tensile strain contours from the simulations with the two 2:1 aspect ratio infill sections and the four 5:1 aspect ratio infill sections at 1% drift. In both figures, the upper limit on the tensile strain was 0.03 (onset of softening in the ECC). The results show the strain in the majority of the panels was well below the peak strain in the panel. A more effective geometry for the beam-type infill sections, one that uses more of the panels in tension, will be discussed in the following sections.

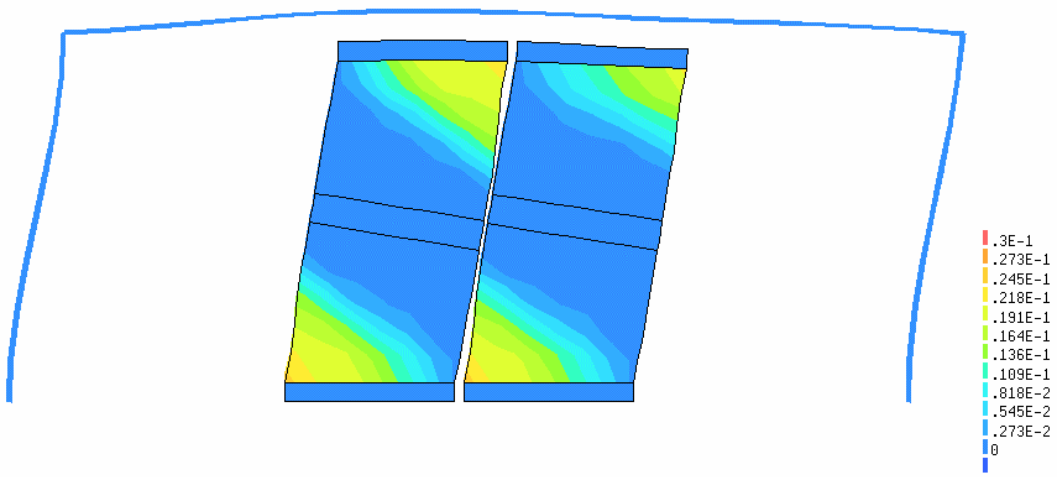

Figure 2-31. Principle tensile strain contour from simulation with 2 panels with 2:1 aspect ratio at 1% drift

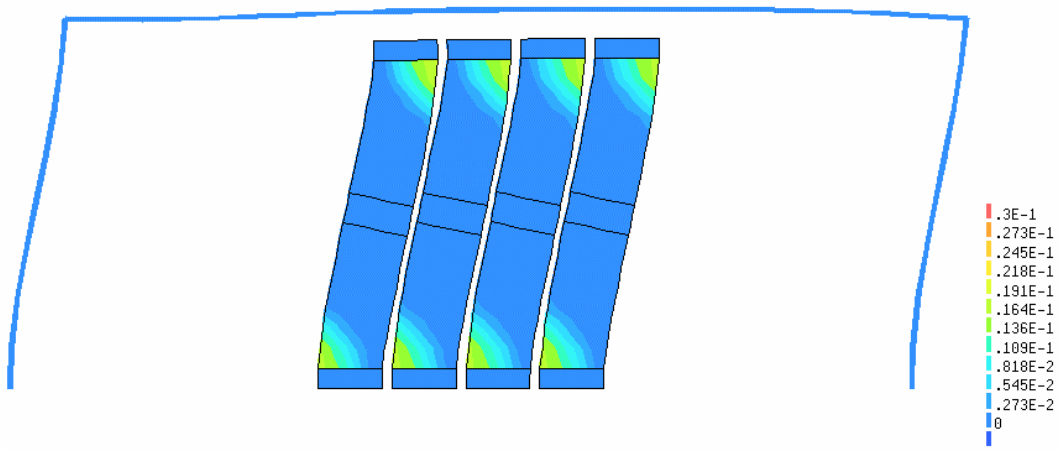

Figure 2-32. Principle tensile strain contour from simulation with 4 panels with 5:1 aspect ratio at 1% drift

2.5.5 Examination of Tapered Panel Geometries

In figures 2.24, 2.31 and 2.32, principle tensile strain contours at 1% drift from simulation results of various infill geometries were presented. In the figures, the highest strains in the panels were concentrated in the maximum moment region of the panel at the top and bottom of the panels, with very low strains near the middle of the infill sections (point of inflection). To use the ECC material more effectively, an alternate geometry that more uniformly distributes the strains in the panel was needed.

To use the ECC material more efficiently, the middle portion of the infill section was tapered to produce an infill section with an hourglass shape. A linear taper was used to correspond with the shape of the moment diagram in the infill section. Figure 2-33 shows six different taper geometries that were studied, with the relative dimensions of the panels shown. The different

geometries were based upon a 4:1 rectangular aspect ratio to allow for direct comparisons with the results presented in Section 2.5.2. Both the width of the top portion of the panels and the height of the rectangular base section were varied.

The panel geometries shown in figure 2-33 were analyzed to determine the optimal geometry of the tapered infill section. In the simulations, only the portion shown in figure 2-33 was considered, which represented one half of an infill section. Figure 2-34 shows a typical finite element mesh from the tapered panels simulations (geometry F) with the boundary and loading conditions indicated. The models used the material models described in Section 2.4.2, and contained 0.5% by area of steel reinforcement in the vertical and horizontal direction. The loading in the analysis consisted of a simple displacement (push over analysis) of the top of the panel section. Displacements were increased until a drop in capacity was observed.

Figure 2-35 shows the pushover analysis results. The drift levels in figure 2-35 were determined by dividing the top panel displacement by the panel height. The load-drift results indicated four of the taper geometries (C-F) had similar capacities at drift levels of 2% drift. Figure 2-36 shows the principle tensile strain contour at 1% drift with the maximum strain limited to 0.03 (onset of softening in the ECC) for each panel. The load on the panel represents the panel capacity at 1% drift. Based upon the results, taper geometry "D" was selected as it provided the best distribution of strains through the height of the panel.

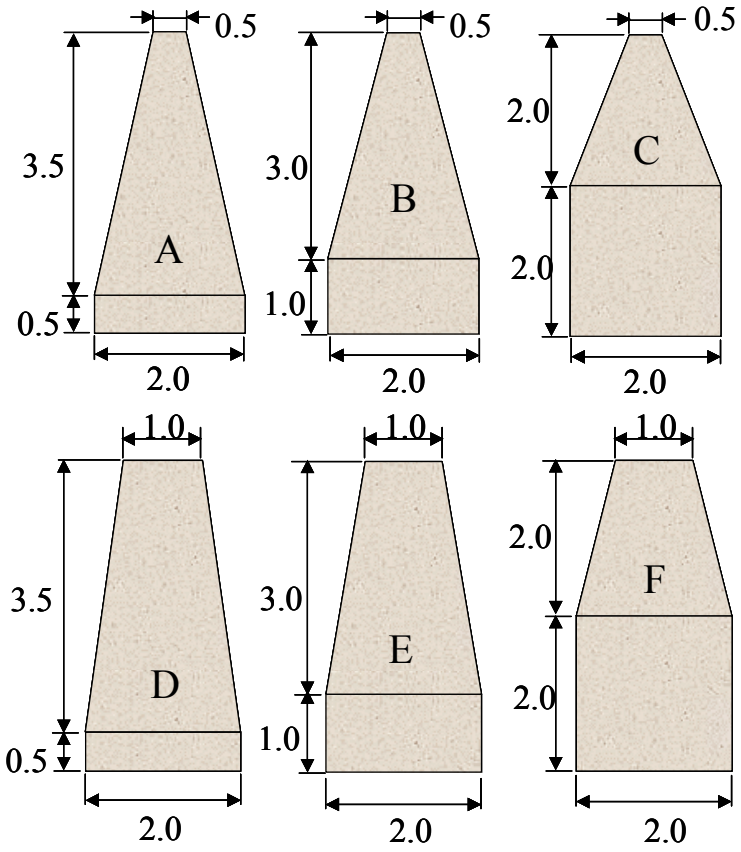

Figure 2-33. Tapered panel geometries examined with relative dimensions shown. All panels have fixed base condition.

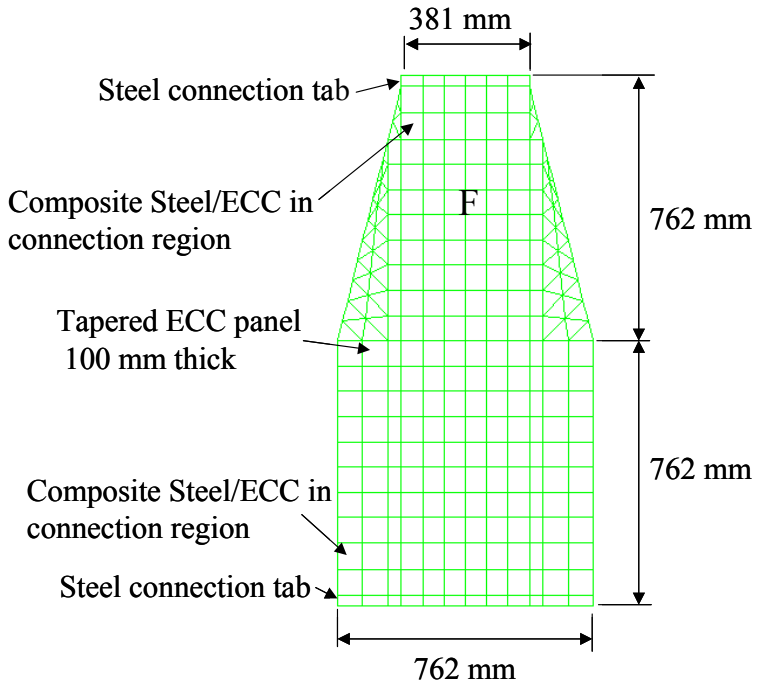

Figure 2-34. Finite element mesh from simulation of geometry F (figure 2-33). Panel has fixed base condition.

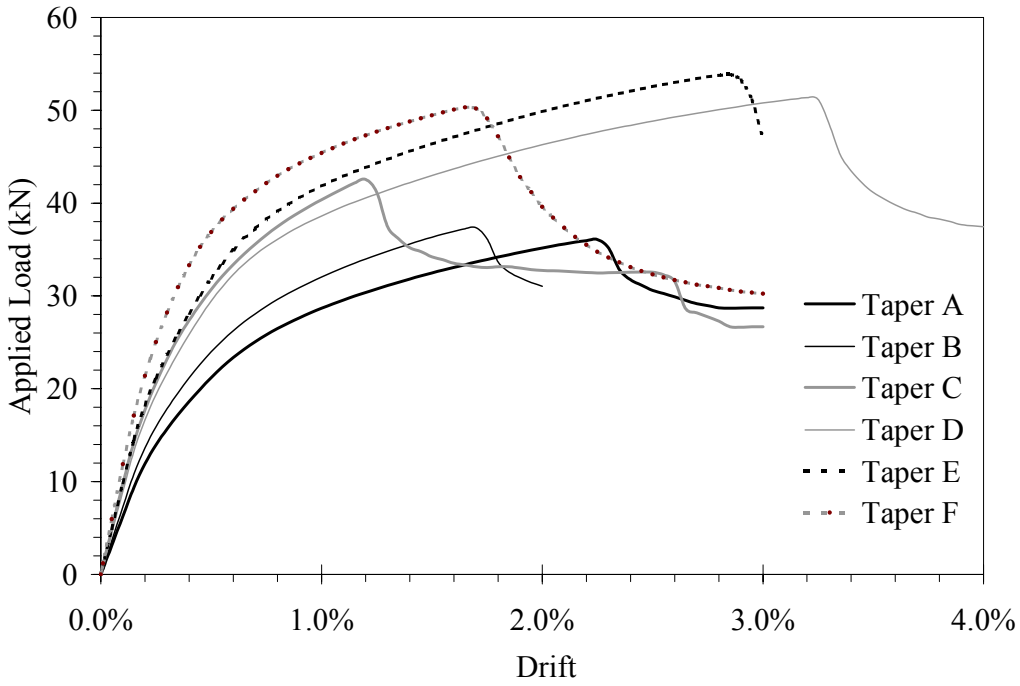

Figure 2-35. Load-drift results from pushover analysis of tapered panels

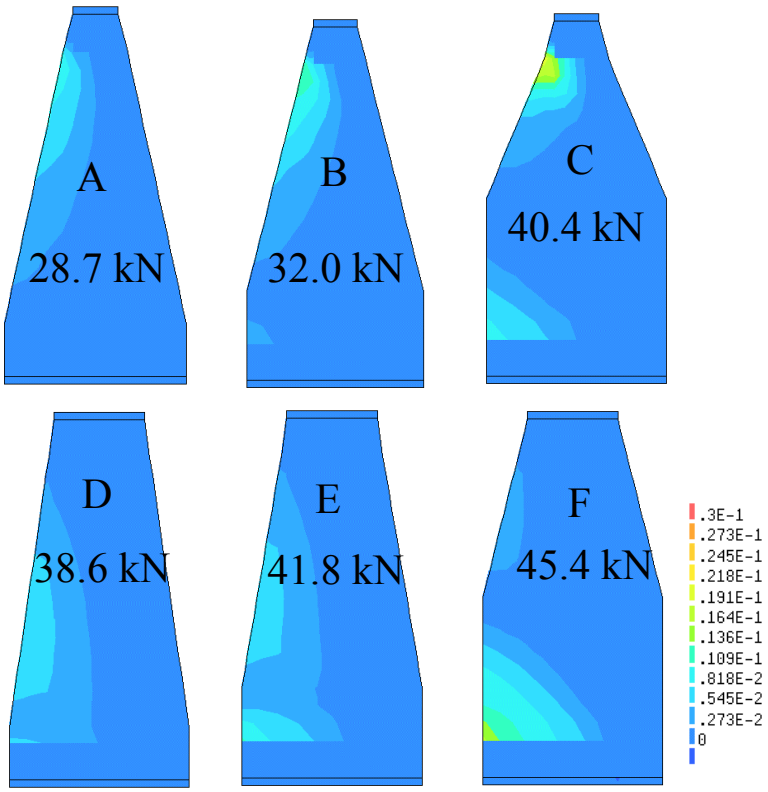

Figure 2-36. Principle strain contour at 1% drift from simulations of tapered geometries

2.5.6 Examination of Tapered Panels in Frames

To examine the response of the tapered panel geometry selected in Section 2.5.5, the analyses presented in Section 2.5.2 were repeated. In the analyses, the addition of 6, 4 and 2 tapered infill sections was performed using taper geometry "D" from figure 2-36. The panel spacing and reinforcement discussed in Section 2.5.1 were used in the analysis. Figure 2-37 shows the finite-element mesh with 6 tapered infill sections. The base of the panels and frame columns were fixed and the loading was applied at the top of the columns. The models with 4 and 2 taped infill sections were created by removing the outer panels from the model, in the same manner as shown in Figures 2.19 and 2.20.

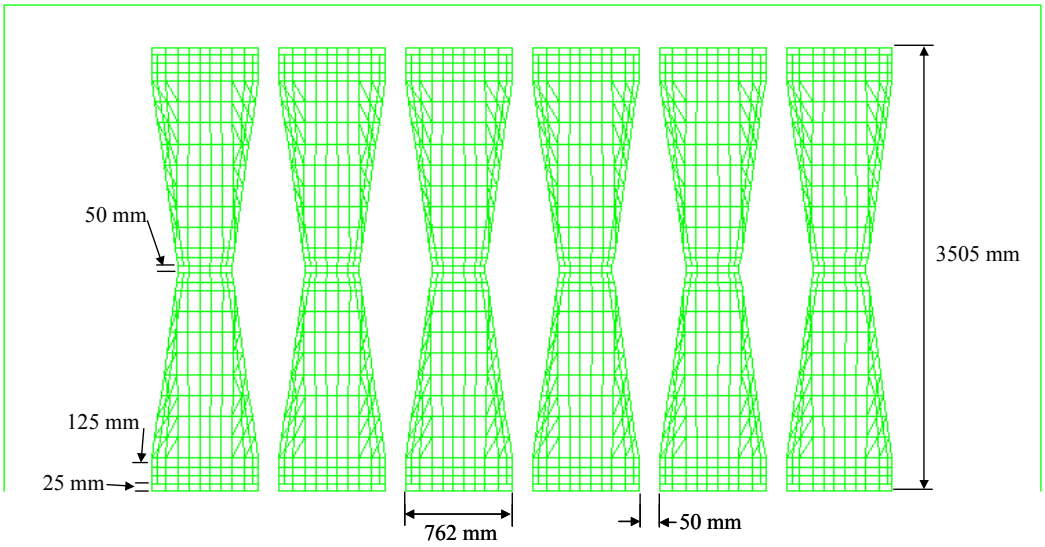

Figure 2-37. Finite-element model from simulation of 6 tapered infill sections added to bare frame

Figure 2-38 shows the load-drift results of the simulations with 6 tapered infill sections added to the frame. For comparison purposes the results of the simulations of the 6 rectangular beam-type infills (figure 2-18) are also shown. Figure 2-39 shows the load-drift results from the simulations with 2 and 6 tapered infill sections compared with the results from the simulation with 2 and 6 rectangular infill sections and the bare frame.

The load-drift results show that the tapered infill sections provide a very similar response to the rectangular infill sections. There were two major differences in the load-drift responses between the tapered and rectangular infill sections; the tapered infill sections had lower capacities at each drift level, and they had smaller residual displacements when unloaded. The capacity of the tapered infill sections decreased by 7% for the 6-infill section addition and 8% for the 2-infill section addition. The residual displacements were observed to decrease by 5% in results from both the 6- and 2-infill section additions.

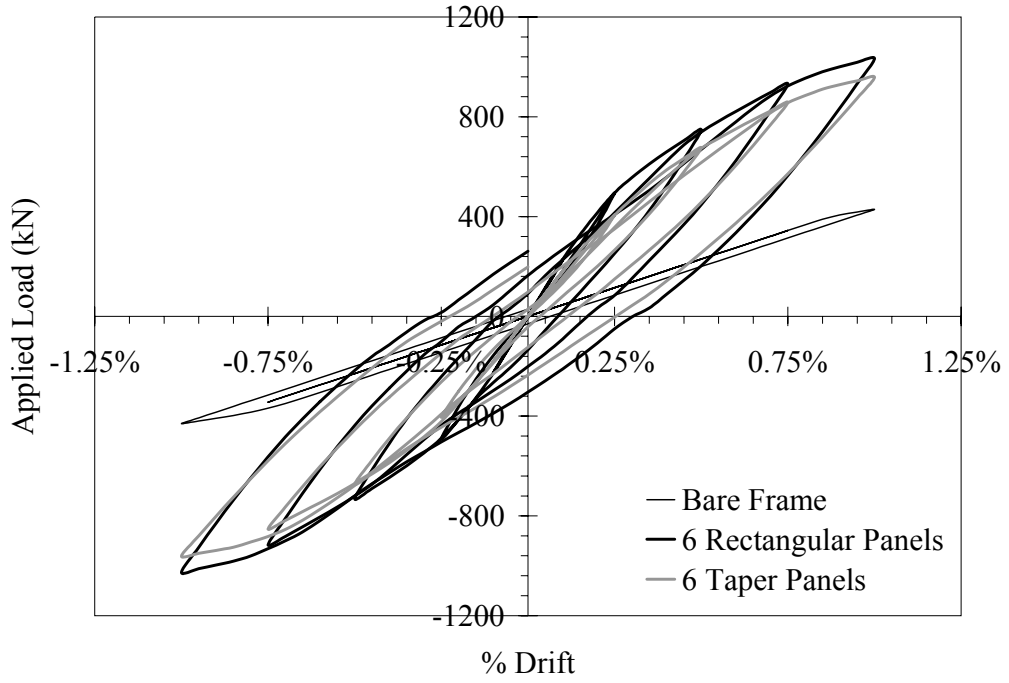

Figure 2-38. Load-drift response from frame with 6 taper infills compared to results from bare frame and results with 6 rectangular panels

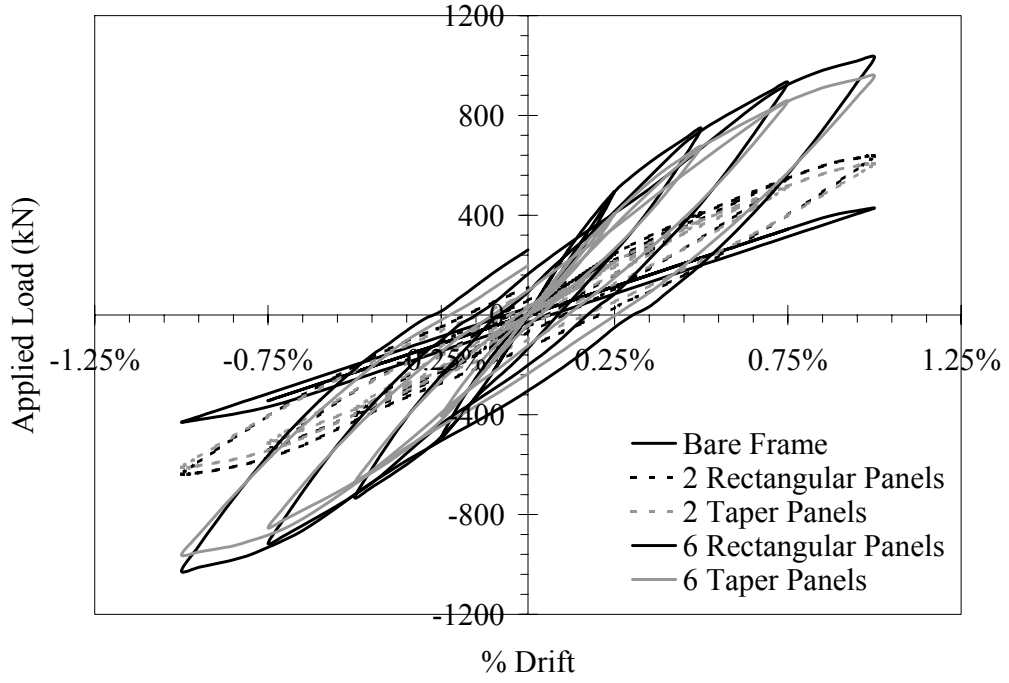

Figure 2-39. Load-drift response from frame with tapered and rectangular infills

The lower capacity at any given drift level resulted from the lower stiffness of the tapered infill sections relative to the rectangular infill sections. The decrease in amount of steel yielding will result in less permanent deformation in the steel, and hence produce smaller residual displacements for the panels.

In the tapered infill section simulations, yielding of the steel frame began at a drift level of 0.75%, which was similar to the results from the rectangular infill section (0.75%) and the bare frame (0.80%). The onset of yielding in the frame with 6 tapered infill sections can be seen in Figure 2-40, which shows a principle tensile strain contour at 0.75% drift. The upper strain limit in the contour was 0.0017, which represents the yield strain in the frame steel. Figure 2-41 shows the same information at 1% drift. In the figure, the yielding of the frame members can be seen at the column base. The results from the simulations with 2 and 4 tapered infill sections were similar to the 6 tapered infill section results.

Figures 2.42 and 2.43 show tensile and compressive strain contours, respectively, at 1% drift obtained from the simulations with 6 tapered infill sections added. The upper limit in the tensile strain contour (figure 2-42) was 0.03 (onset of softening the in the ECC) and -0.05 (onset of compressive softening) in the compressive strain contour (figure 2-43). The strain contours show the ability of the tapered geometry to use the ECC material effectively. In the tensile contour, the strains were distributed along the panel height instead of being concentrated at the base of the panel as was observed in the rectangular infill section simulation results (figure 2-24). The compressive strain contour shows that only very small sections of the panels have began to soften in compression, as was also seen in the rectangular panels (figure 2-25). The spreading of tensile strains in the tapered panel geometry demonstrates how the tapered geometry can use the ECC material more efficiently than the rectangular geometry.

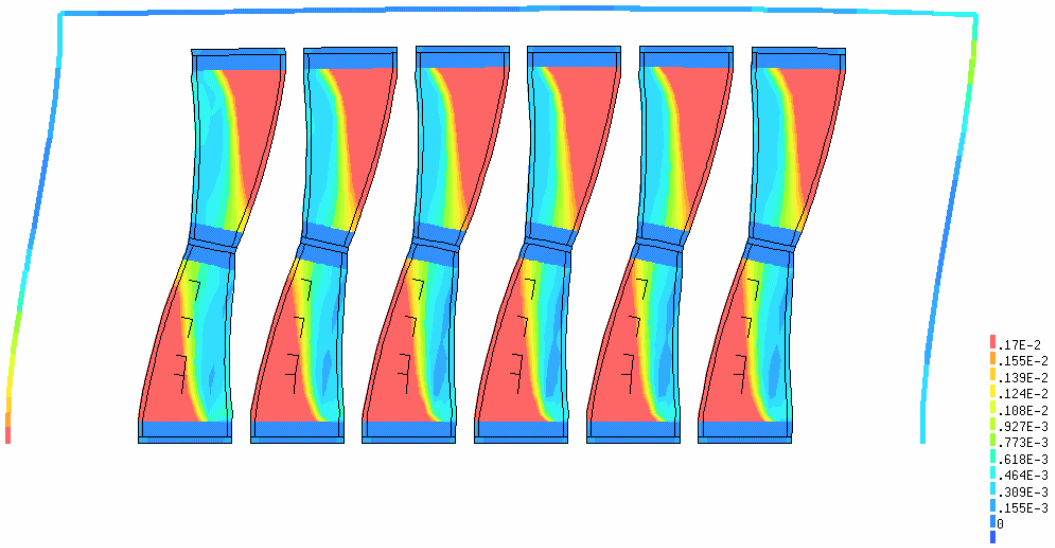

Figure 2-40. Principle tensile strain contour at 0.75% drift from simulation with 6 tapered infill sections added

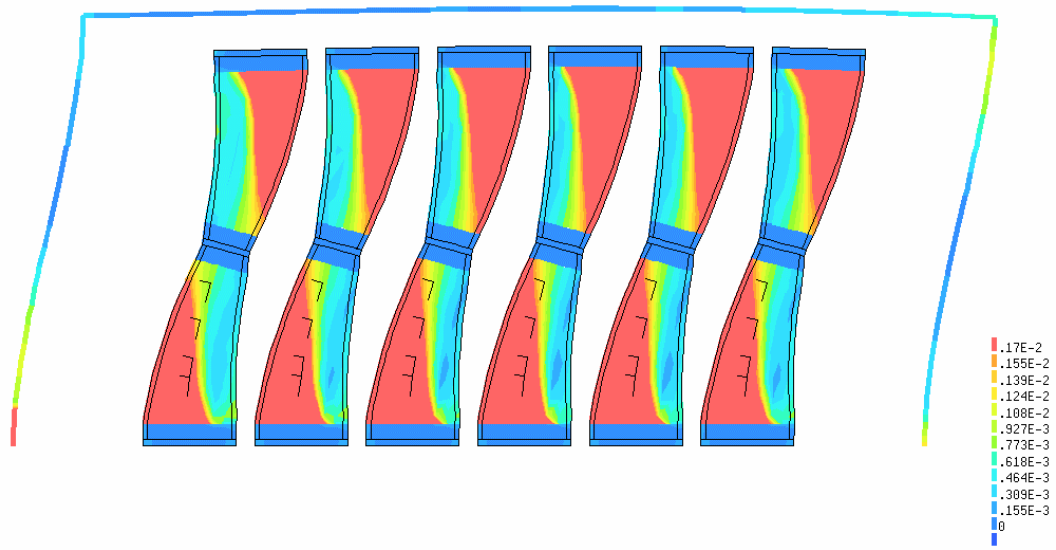

Figure 2-41. Principle tensile strain contour at 1% drift from simulation with 6 tapered infill sections added

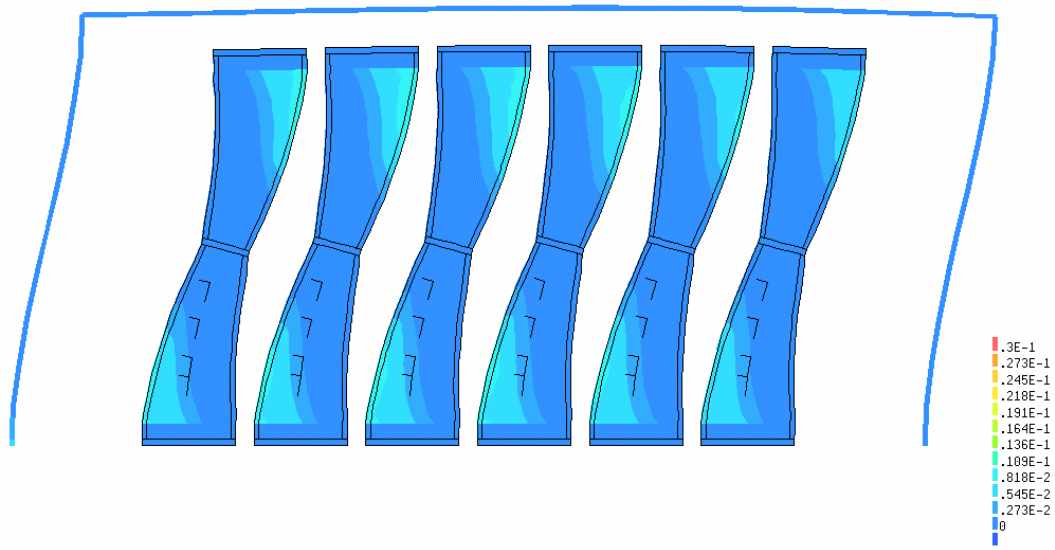

Figure 2-42. Principle tensile strain contour at 1% drift from simulation with 6 tapered infill sections added

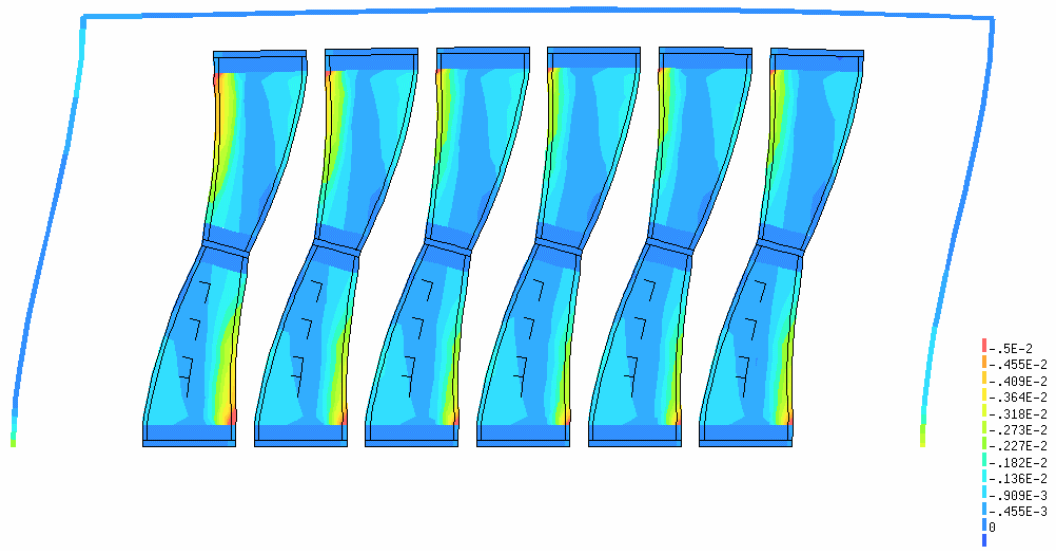

Figure 2-43. Principle tensile strain contour at 1% drift from simulation with 6 tapered infill sections added

2.5.7 Beam-Type Infill Panel Reactions

The simulation results shown in Sections 2.5.2 to 2.5.4 demonstrate the potential for the beam-type infill system to increase the capacity and stiffness of a bare steel frame. For the infill sections to strengthen a structure the loads from the infill system will need to be transferred from the infill member into the structure. The simulation results in Sections 2.5.5 to 2.5.6 can be used to determine the loads to be transferred through the connection regions. The required number of bolts to transfer the panel loads is then obtained by dividing the connection load by the bolt capacity.

Table 2-5 shows a summary of the base reactions from individual beam-type infill sections obtained from the simulations. For simplicity, only the results at 1% drift are shown. The loads shown in the table include the distributed shear load at the panel base, and the compressive and tensile loads that occur in the connection region due to flexure in the panel.

Table 2-5 – Summary of reactions[1] obtained from beam-type infill simulations

Panel Geometry	Number of Panels	Aspect Ratio	Lateral Shear Load[2] (kN)	Tensile Load[2,3] (kN)
Rectangular	2	2:1	484	789
Rectangular	3	2.75:1	216	531
Rectangular	2	4:1	106	330
Rectangular	4	4:1	102	320
Rectangular	6	4:1	106	321
Rectangular	4	5:1	61	254
Taper	2	4:1	92	282
Taper	4	4:1	89	275
Taper	6	4:1	89	280

1. Reactions per beam-type infill at 1% drift.
2. Loads are an average of the loads on each panel
3. Compressive loads have same magnitude with opposite sign

The loads shown in table 2-5 would need to be transferred through pre-tensioned bolted connections to the frame members. The load transfer mechanism can be conceptually identical to slip critical connections in steel structures. The procedures in the AISC manual (1988) for slip critical connections can be used to estimate of the number and size of connection bolts. However, experimental tests will be needed to verify the connection capacity (presented in Section 3).

2.5.8 Discussion of Beam-Type Infill Simulation Results

The performance of the beam-type infill system in terms of increasing the strength, stiffness and energy dissipation of a steel frame was analyzed using finite element-based simulations. The frames with the beam-type infill sections were found to yield at similar drift levels as the bare frame. Therefore the frames can be strengthened by the infill installation without causing damage in the frames at low drift levels (less than 0.75%).

At drift levels below yielding of the frame, the reinforced ECC infill sections examined in the current study dissipate energy through yielding of the steel reinforcement and through the formation of multiple cracks in the ECC material. The results indicated that the energy dissipation was occurring without exceeding the tensile or compressive strain limits (strain levels at the onset of tensile or compressive softening) in the ECC materials. At drift levels above 0.75%, the yielding of the steel frame will contribute to the observed energy dissipation.

Comparison of the load-drift results shown in figures 2.22, 2.30 and 2.39 show the different levels of strength and stiffness that can be achieved by the addition of various amounts of beam-type infill sections. The ability to produce varying levels of strength and stiffness allows the strengthening measures to be tailored to the demand placed on the structure.

The reactions at the base of the beam-type infill sections were summarized in table 2-5. These forces need to be transferred via the pretensioned bolted connections into the existing frame. Experimental testing was needed to verify the performance of the proposed connections.

To verify the performance of the proposed beam-type infill system, experimental testing was required. Specifically, the ability of the proposed connections to transfer loads and the overall response and failure modes of the panels with different geometries, and types of reinforcement needed to be investigated.

The ability of the beam type infill sections to partially infill a frame is an important aspect of the retrofit system. Existing secondary systems in buildings can be located in the gaps between panels and or an unfilled portion of the frame. The ability to minimize the impact of the retrofit installation on existing systems is consistent with the overall retrofit goals presented in Section 2.2.

2.6 SUMMARY

In this chapter several important areas related to the development of seismic retrofit strategies for critical facilities were addressed. Section 2.1 summarized past research related to the testing and evaluation of infilled walled systems in structures. The review facilitated incorporating previously developed retrofit concepts into the current work. The previous research was reviewed to examine how the desirable properties of the ECC materials can be incorporated into the infill systems under development.

The current research focuses on the development of retrofit strategies for critical facilities. To guide the research, a series of requirements for the retrofit of critical facilities were presented. The requirements include minimizing construction time, accommodating existing secondary systems, and development of a replaceable system in the event of severe damage. Seismic retrofit guidelines (FEMA 273, 1999) were also reviewed to evaluate performance guidelines for the retrofit development.

Two infill concepts were developed that build upon previous related research, and that satisfy constraints of critical facilities. To examine the infill concepts a series of finite element-based simulations were performed. The goal of the simulations was to examine how the infill additions affected the strength, stiffness and energy dissipation of a steel frame. The simulations were also used to examine if the infill systems can satisfy critical facility performance requirements, in particular limit yielding of the frame members.

The results from simulations of the full frame system were presented in Section 2.4. The addition of full frame infills resulted in substantial increases in both the strength and stiffness of the infilled frame. Substantial increases in energy dissipation were also observed.

Two disadvantages were observed in the full frame results. Yielding of the frame members was observed at drift levels as low as 0.25%, which was lower than the results obtained from the bare frame (0.8%). The second disadvantage of the full frame infill system was in the use of the ECC materials. The peak compressive and tensile strains were exceeded at drifts greater than 0.25% which indicates both compressive and tensile softening of the ECC was occurring. These two factors indicate that the full frame infill system will not satisfy the requirements for the retrofit of critical facilities at high drift levels.

In Section 2.5 the results from simulations using the beam-type infill system were presented. The results indicated that the beam type infill system was desirable in terms of the ability of the system to increase the strength, stiffness, and energy dissipation of the frame without exceeding the peak strains in the ECC. Yielding of the frames with the beam-type infill systems was observed to occur at similar drift levels as the bare frame.

The simulation results also indicated that different levels of strength and stiffness can be achieved by varying the size (aspect ratio) or the number of beam-type infills added to the frame. These results point to the ability of the infill additions to be tailored to provide the desired level of strength or stiffness for a given facility.

To develop an efficient beam-type infill system further, tapered panel geometries were evaluated and presented in Sections 2.5.5 and 2.5.6. The tapered panel geometry removes ECC material from the middle of the infill sections, resulting in an infill section with an hourglass shape. The load-drift response of a frame with tapered infill sections behaved in a similar manner as the rectangular infill sections. The tapered panel geometry resulted in a more efficient use of the ECC material than the rectangular panels.

The preliminary analyses of the infill systems suggest several areas for laboratory testing to develop the infill panel concepts presented here. Testing to verify the ability of the pretensioned connections to safely transmit the loads shown in Table 2-5 is needed. Testing is also needed to verify infill panel construction methods, as well as the strength, stiffness and energy dissipation in the panels. Finally, infill panel testing is needed to examine the response of larger-scale ECC elements.

Section 3
Laboratory Testing of Infill System Connections

3.0 Introduction

In the preceding chapter an infill panel concept was presented which used pretensioned bolted connections both between panels and at the connection of the panels to a steel frame. In this chapter the strength of the pretensioned connections for the ECC infill panels, and long-term connection performance will be evaluated. Specific goals of the testing included:

1. Examination of connection strength under various load orientations
2. Examination of the time-dependent losses in bolt tension
3. Examination of the confined and composite properties of the material in the connection region

The laboratory connection test results will be used to design the connections for the panel tests and to provide data for further studies of pretensioned bolted connections between ECC sections.

3.1 Connection Strength Tests

The infill panel concept being developed uses pre-tensioned bolted connections both between the panels and at the connection of the panels to the frame. Figure 3-1 shows a schematic representation of the proposed connections. In this application the behavior of the bolted connections is conceptually similar to slip-critical connections in steel structures. Slip critical connections are commonly used in structures where reversals in load or significant vibrations are expected (Salmon and Johnson, 1990). As discussed in Section 2.1, Kanda et al., (1998) first investigated the concept of using pre-tensioned bolted connections between ECC panels. The geometry of their tested specimens resulted in a compression failure of the specimens outside of the connection region. In their testing, no attempts were made to enhance the friction between the ECC segment and the steel members.

In this research, both the capacity and long-term performance of the proposed connections was evaluated. The composite behavior of the ECC material confined in the connection area was also examined. Results of these tests were then used to determine the number and size of the bolts needed for laboratory tests of infill panels (described in Section 4). The connection test results in combination with the infill test results can later be used later to design various infill schemes in steel framed structures.

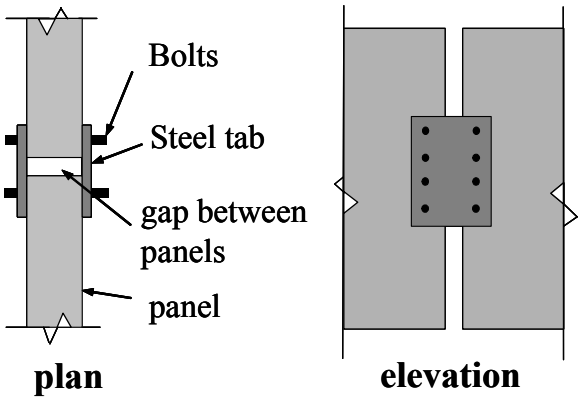

Figure 3-1. Concept of pre-tensioned bolted connection between panels

3.1.1 Test Series

To evaluate the connection region of precast panel segments using pre-tensioned bolted connections a series of laboratory tests were developed. The goals of the tests were to evaluate the following variables:

1. The effect of interface roughness between the ECC and the steel members
2. The effect of load orientation with respect to the bolt line axis

Table 3-1 shows a summary of the three series of tests. In the first test series the specimens are oriented to simulate a compressive (vertical load in figure 3-1) loading on the connection. These tests served as a baseline for comparisons with the second and third test series. In the second series the effect of surface roughness was investigated. In the third series, the effect of load orientation with respect to the load axis was evaluated by simulating a shear (lateral load in figure 3-1) loading on the connection. An additional set of tests (presented in Section 3.2) was performed to examine the loss of bolt tension with time due to creep and shrinkage of the ECC and relaxation of the steel bolts.

Table 3-1 - Summary of connection test variables

Test Series	# Specimens	Parameter of Interest	Surface	Bolt Orientation
1	3	Strength	Plain-formed	Horizontal
2	3	Strength	Sandblasted	Horizontal
3	3	Strength	Sandblasted	Vertical

Intentional roughening by sandblasting or other means was expected to increase the amount of friction between the ECC and steel element. Connections with the sandblasted surfaces were expected to have a higher load capacity prior to slippage than connections with plain-formed surfaces. Test series 1 and 2 were designed to test this hypothesis. In the tests both the ECC

specimen and the steel angles were sandblasted. Sandblasting was selected for surface enhancement due to its ease of use, and common use in the precast concrete industry. Figure 3-2 shows a comparison of the relatively smooth formed surface and rougher sandblasted surface.

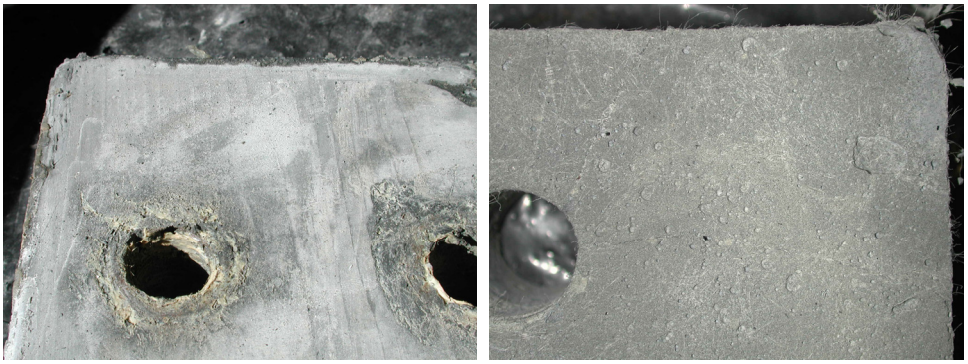

(a) plain-formed (b) sandblasted

Figure 3-2. Comparison of tested ECC block surfaces

To examine the effect of load orientation with respect to bolt orientation results from test series 1 (or 2) and 3 will be compared. The comparison was necessary to examine the effect of compression or shear loading on the infill panels. Bolt orientation was not expected to have a significant effect on the peak load capacity of the joints. In the design of slip critical steel connections, load orientation does not influence the connection strength when standard and oversized holes are used in the connections (Salmon and Johnson, 1990).

All of the ECC specimens used in the evaluation were cast using the SP mix design, shown in table 4-1. All of the ECC specimens were wet cured for 28 days and allowed to dry for at least 14 days prior to testing. The curing and drying period was selected to optimize the performance of the ECC materials.

3.1.2 Connection Test Setup

Figure 3-3 shows the geometry of test series 1 and 2. This geometry represents the compression capacity in a connection such as shown in figure 3-1. The bolt size and location in the specimen was designed based on the panel reactions obtained in the analyses presented in Section 2.5. The ECC block (representing a panel segment) was sized to prevent a compression failure of the block outside of the connection area prior to connection slippage. In test series 3 the bolt orientation was rotated 90 degrees, as shown in figure 3-4. Again, this specimen orientation simulated a shear loading on the connection.

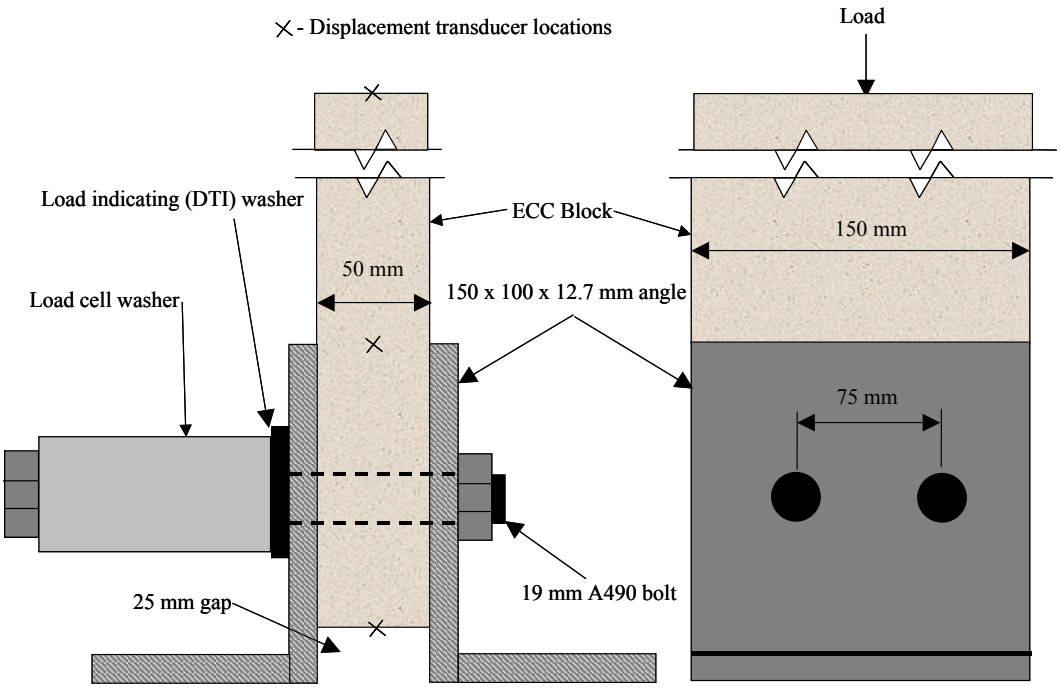

Figure 3-3. Connection test setup with load oriented perpendicular to axis of bolts

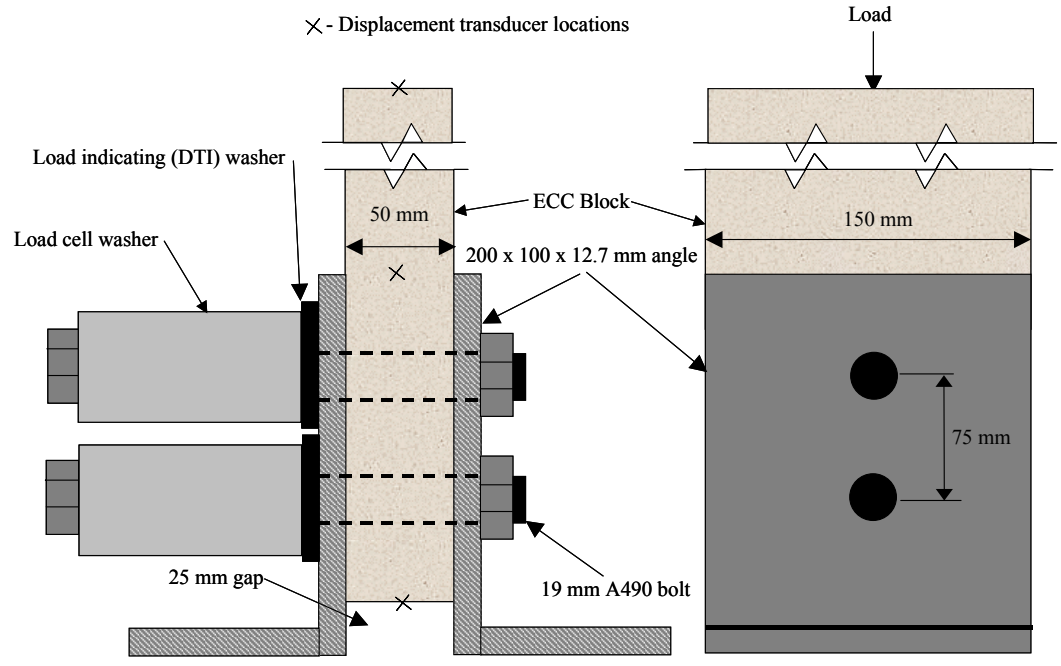

Figure 3-4. Connection test setup with load oriented parallel to axis of bolts

The bolts used in the connections were 19 mm ASTM A490 high strength bolts with a pretensioning load of 133 kN per bolt, which is slightly below the AISC (1988) specified load of

156 kN for 19mm bolts in slip critical connections. The pretensioning load was selected to be slightly lower than the AISC specified load so as to limit the compressive stresses within the connection region and therefore prevent localized crushing during bolt tensioning. To provide additional space for alignment of the connections, the bolt holes in both the steel angles and ECC blocks were 22 mm in diameter, which was 1.4 mm larger than AISC (1988) specifications.

The pre-tensioning load in the bolts was monitored using load cell washers, which allowed the variation in bolt load to be recorded during testing. In addition to the load cell washers, direct tension indicator (DTI) washers were used. These washers have raised sections that compress at the AISC specified loads for pretensioned connections. The purpose of the DTI washers was to examine their acceptability in lieu of load cells washers in larger test specimens and in full-scale installations.

Prior to testing, the bolts were loaded to the desired pre-tensioning levels using a long handled torque wrench. During tightening, the bolt load versus applied torque data was recorded. This information was used to evaluate the use of torque wrenches as a method of evaluating bolt tension in larger specimens. Testing of the specimens started a minimum of 4 hours after completion of the initial bolt tensioning. The bolt tension levels were reset to the desired values immediately prior to testing to eliminate early age bolt tension loss due to ECC creep and shrinkage. The loss in bolt tension prior to testing was less than 5 kN.

The testing was performed in a displacement-controlled, 2670 kN MTS test frame at an approximate displacement rate of 4 mm per minute. To ensure uniform bearing on the loaded face of the specimen, a hydrostone layer was placed on top of the ECC block prior to testing. During testing 6 displacement transducers (3 per side) (LVDTs) were used to monitor the deformation and slip of the specimen. The location of the transducers is shown in figures 3.3 and 3.4. Figure 3-5 shows a test specimen in the test frame prior to testing.

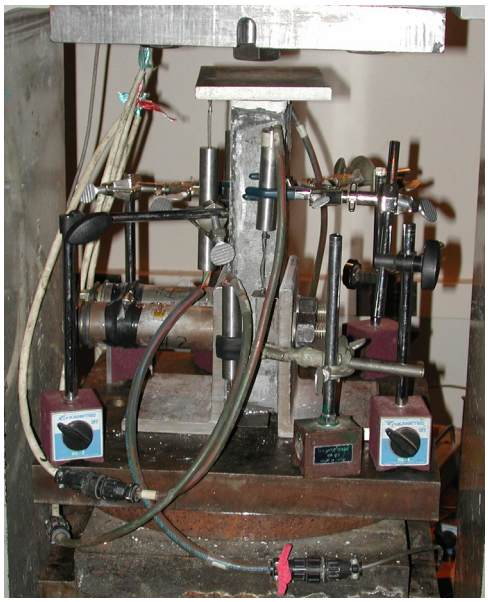

Figure 3-5. ECC connection specimen in test frame with LVDTs prior to testing

3.1.3 Connection Test Results

Figure 3-6 shows the load-displacement response from the 3 test specimens with a plain-formed ECC surface with the load oriented perpendicular to the axis of the bolts (Test series 1, Table 3-1). In the figure, the displacements recorded at the top of the specimen, at the top of the angle section (dashed line) and bottom of the specimen are plotted versus the applied load. The specimens began to slip at an average load of approximately 300 kN. Slippage of the specimen was considered to occur when a significant change in the load-displacement plot occurred, as indicated in figure 3-6. After the specimen began to slip, the load gradually increased until a compressive failure occurred in the top section. The compressive failure initiated as the ECC began bearing on the bolts in the connection region.

In all three specimens the displacements recorded by the LVDTs followed similar trends before the onset of ECC block slippage. The top displacement was the largest in all tests; this was expected as it includes both the elastic deformation of the unconfined section of the ECC block and the deformation in the confined region. The bottom LVDT recorded the smallest displacement in all three specimens. The deflection of the bottom LVDT represents the displacement of the ECC block relative to the steel angles. Slippage of the ECC block relative to the angles was not expected to be significant due to the clamping force provided by the pretensioned bolts. Prior to the onset of slippage, there was only a small difference between the displacement at the bottom of the specimen and the displacement at the top of the angles. The difference in the amount of displacement between the bottom of the specimen and at the top of the angle (dashed) represents the displacement of the ECC confined within the connection region. The variability of the results before slippage can be attributed to differences in interfacial contact between the plain-formed surfaces and the steel angles.

In all three specimens slippage occurred at a load below the peak level. After the slippage occurred, the load increased to a peak value as the ECC block began to bear on the bolts. In specimens a and c, the slippage of the specimen is gradual and occurred without large changes in the applied load. In specimen b, large drops in load were observed. The large load drops occurred as a consequence of the displacement control of the tests. As the specimen began to slip, the load dropped to prevent the actuator from exceeding the desired displacement.

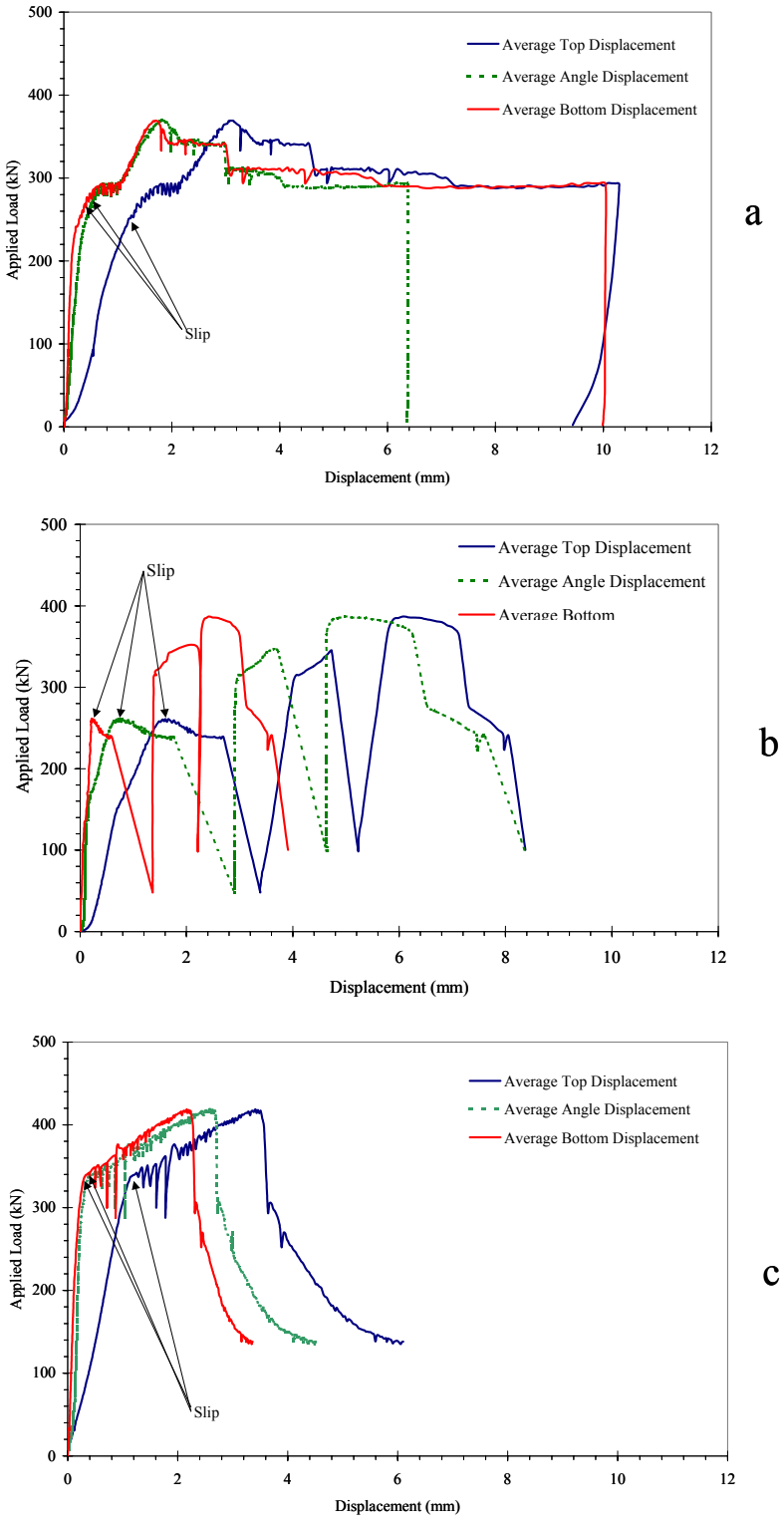

Figure 3-6. Results from connection test Series 1 (plain-formed surface and load perpendicular to axis of bolts)

Figure 3-7 shows the results from the specimens with sandblasted surfaces (Test series 2, Table 3-1). The sandblasted specimens had an average capacity of 480 kN at the onset of slippage which is significantly higher than the 300 kN average capacity of the plain-formed specimens. Sandblasting the surfaces increased the interfacial shear capacity of the connection region. The shape of the load displacement response was generally similar to the results from the formed surfaces, shown in figure 3-6. However, compared to the results shown in figure 3-6 there was little increase in load (i.e., hardening) after slippage began in the sandblasted specimens. The lack of a hardening region was due to the higher capacity of the sandblasted specimens prior to slippage, which approached the capacity of the ECC. There was no additional capacity for hardening to occur.

The effect of the sandblasted surfaces also can be seen in a comparison of the pre-slip response in figure 3-7 with the pre-slip response in figure 3-6. The sandblasted specimens show less variability in the pre-softening response, which indicates better interfacial contact between the ECC specimen and the steel angles.

Figure 3-8 shows a comparison of plain-formed (Series 1 a) and sandblasted (Series 2 b) specimens after completion of testing. Both of the specimens show large deformation of the material at the edges of the specimen near the bolt holes. This material spalled as the load began to drop. The portion of the specimens above the connection region remained largely intact throughout the tests until the final failure of the bolt holes. The large deformation capacity of the ECC material can be seen in figure 3-9, which shows a comparison of a bolt hole in a sandblasted specimen before and after testing.

Figure 3-10 shows the results from the tests with the load inline with the bolt axis (Test Series 3, Table 3-1). The specimens were sandblasted prior to testing to maximize the connection capacity as demonstrated in the previous test series. The average load in these tests at the onset of slippage was 445 kN and was similar in magnitude to the previous tests with sandblasted surfaces (Test Series 2, 480 kN). The pre-slip response of the Test Series 3 specimens was also similar to the results observed in Test Series 2 (figure 3-7).

The primary difference in the results from Test series 2 and 3 was in the slip and softening (dropping in load) region. The results from the inline bolt tests showed a rapid decrease in load after the onset of slip. This rapid decrease is caused by the confined area around the bolts acting to split the specimen (causing a shear failure) as the specimen began to bear on the bolts. As a result, cracks propagate into the unconfined portion of the ECC block specimen, splitting the specimen. The splitting of this region results in the rapid post-peak load softening seen in figure 3-10. This softening was in contrast to the less rapid softening typically seen in the previous test series, as shown in figures 3.6 and 3.7. The splitting of the specimen can be seen in figure 3-11, which shows two of the specimens after completion of testing.

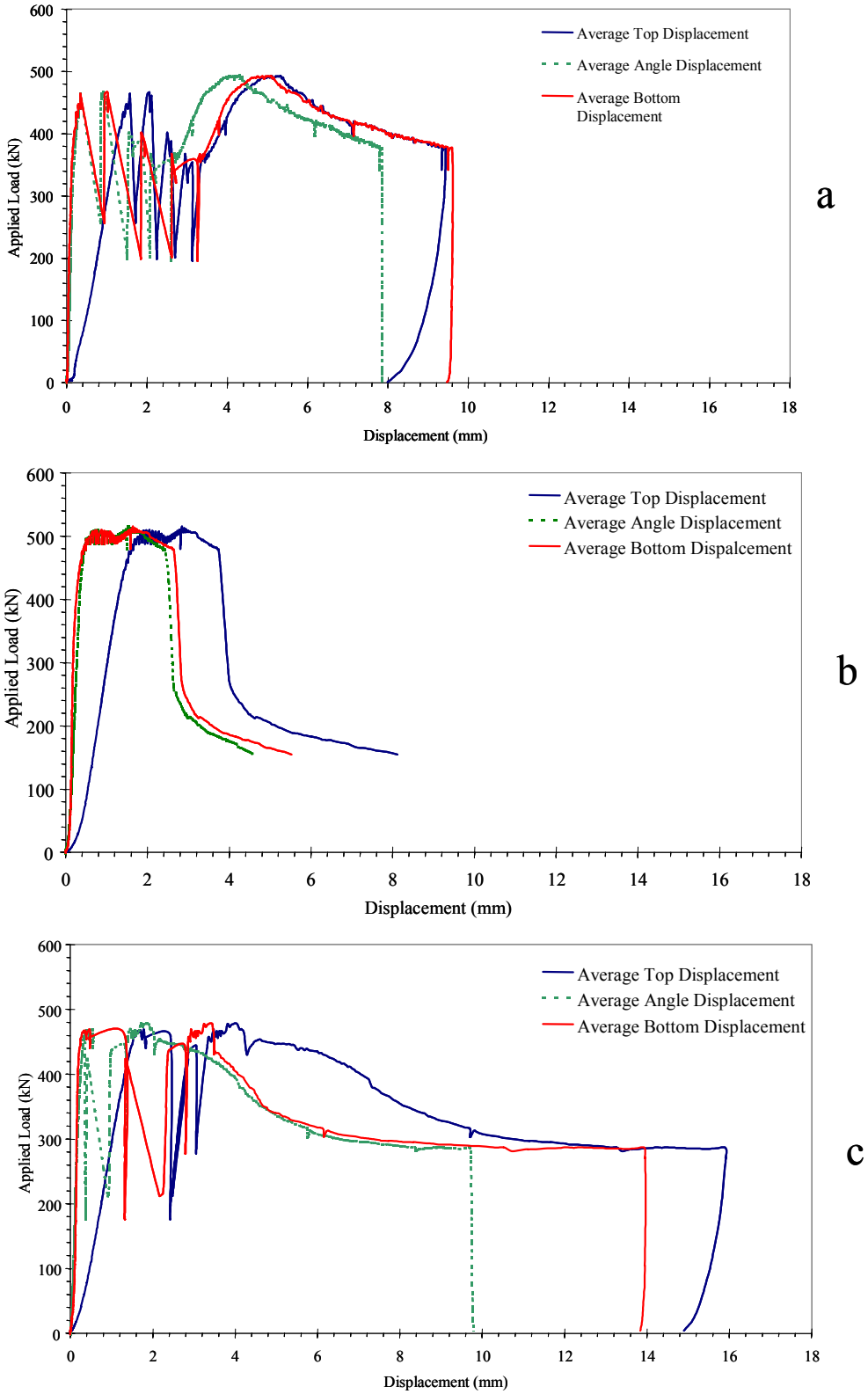

Figure 3-7. Results from connection tests with sandblasted surface and load perpendicular to axis of bolts

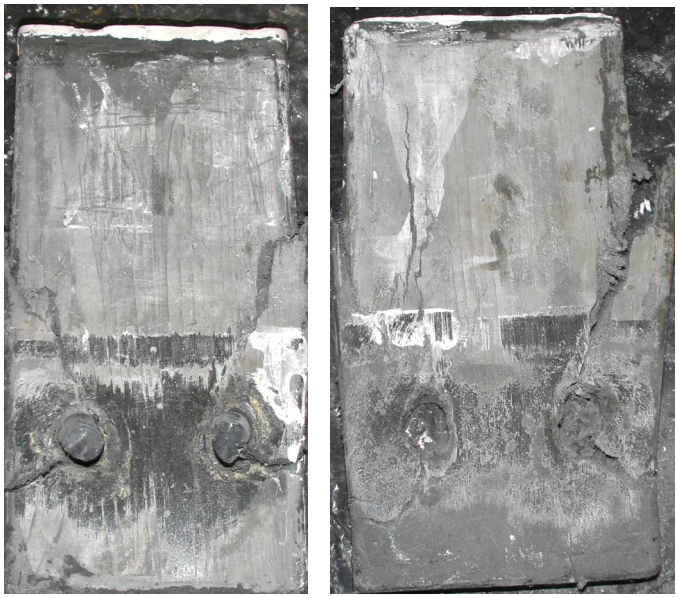

(a) plain-formed (Series 1 a) (b) sandblasted (Series 2 b)

Figure 3-8. Comparison of specimens (a) plain-formed and (b) sandblasted after completion of testing

(a) before test (b) after test (c) close-up

Figure 3-9. Comparison of bolt holes in sandblasted specimen

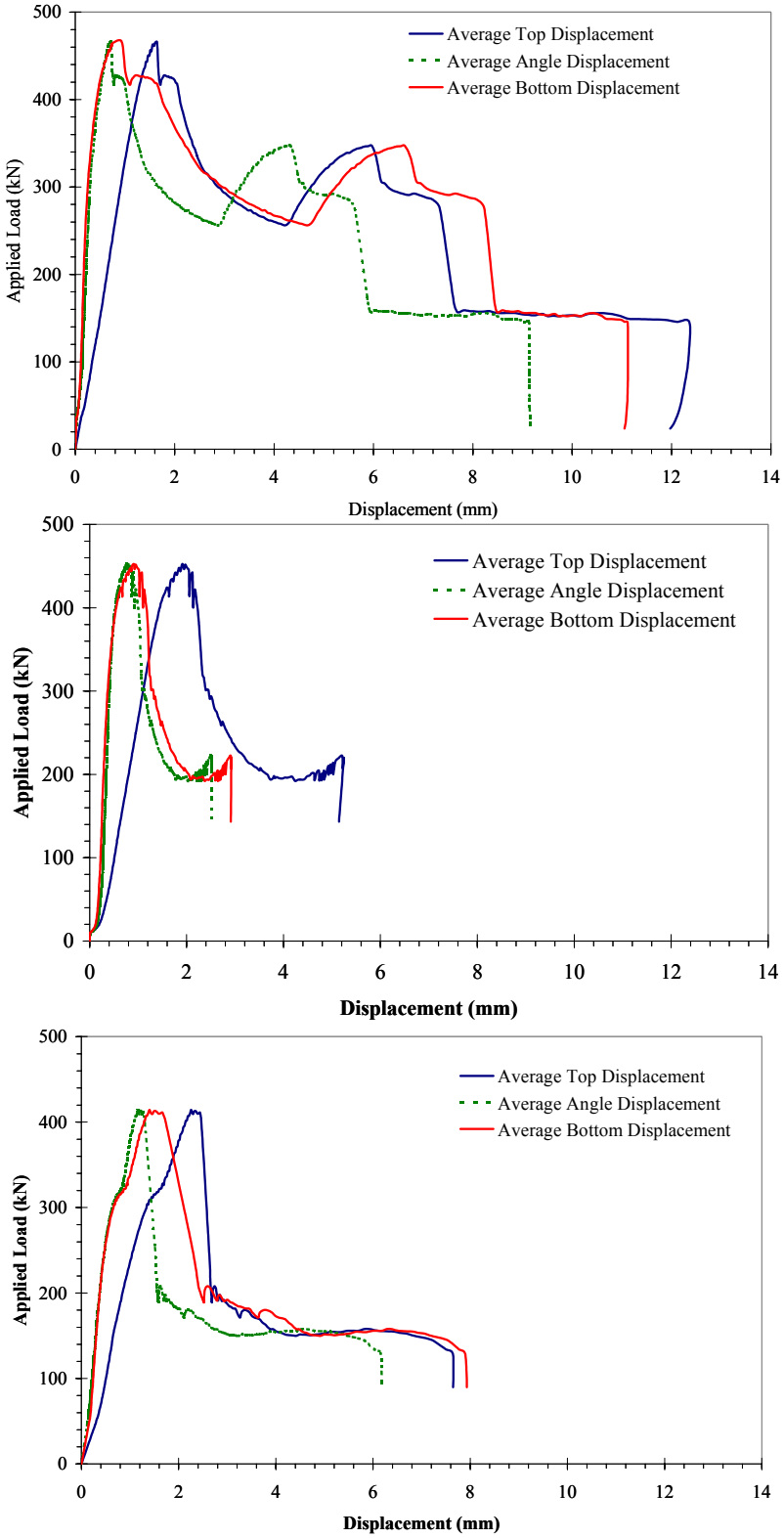

Figure 3-10. Results from connection tests with sandblasted surface and load parallel to axis of bolts

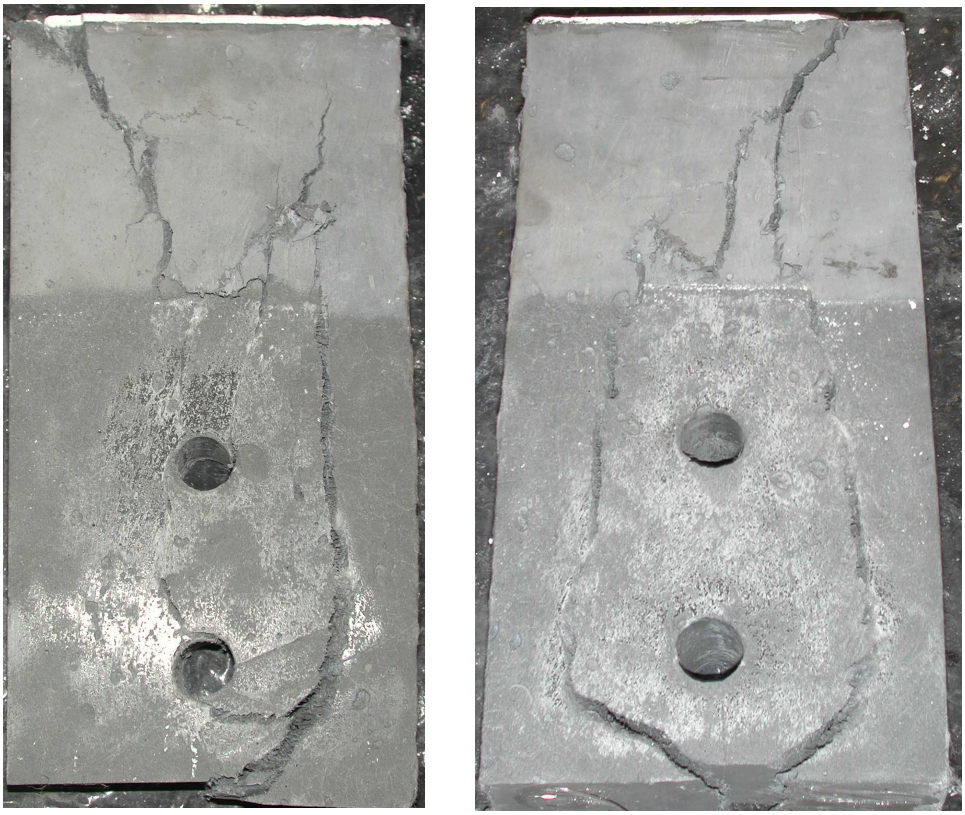

Series 3 a Series 3 b

Figure 3-11. Splitting of specimens after testing

Table 3-2 shows a summary of the bolted connection test results from both bolt orientations and interface conditions (Test Series 1-3, table 3-1). In table 3-2 the slip coefficient, k_s was calculated using (3-1), shown below, which was adopted from the AISC (1988) specifications for the use of high strength bolts.

$$k_s = \frac{sl}{2 \cdot cf} \tag{3-1}$$

where:

k_s = slip (interface friction) coefficient
cf = total bolt pretensioning force
sl = load at which the deformation rate increases

Table 3-2 - Summary of average panel connection strength tests

Test Series	Bolt Orientation[1]	Interface type	Clamping force (kN)	Average Slip load (kN)	Slip coefficient (k_s)
1	Perpendicular	Formed	267	301	0.56
2	Perpendicular	Sandblasted	267	480	0.90
3	Inline	Sandblasted	267	445	0.83

1. Orientation of the axis of the bolts relative to the applied load.

3.1.4 Discussion of Connection Test Results

The results shown in the Section 3.1.3 demonstrated the concept of using pretensioned bolted connection as a part of the infill wall system under development. The results indicated that sandblasting both the ECC and steel in the connection region will increase the capacity of the connections. The plain-formed specimens were observed to have a lower capacity at the onset of softening and more variability in the pre-slip region.

The orientation of the bolts with respect to the load was not found to have a significant effect on the capacity of the connection. The slip coefficient values obtained from the testing can be used to evaluate the size and number of bolts required between precast ECC panels and at the connections to steel frames.

During bolt tensioning, a calibrated torque wrench was used to tighten the bolts, with the loads recorded to establish a calibration curve for the torque wrench. Load-indicating (DTI) washers were also used to indicate the load in the bolts. It was found that both methods can be used to determine the appropriate load on the bolts during installation. However, the torque wrench would need to be calibrated to the specific procedure used in the installation.

3.2 Time-Dependent Loss of Bolt Tension

The loss of pretensioning force due to time dependent effects such as concrete creep, concrete shrinkage and steel relaxation can be a significant factor in prestressed concrete design. However losses in pretensioning force are not considered in the design of slip critical steel connections (Salmon and Johnson, 1990). This dichotomy, plus the high level of creep expected in the ECC material (Rouse, 2003) resulted in the decision to examine the loss of bolt tensioning force over time. Due to the behavioral similarity to prestressed concrete, some measure of bolt tensioning force is expected to be lost over time, primarily due to creep and shrinkage of the ECC material and possibly from relaxation of the high strength steel bolts.

3.2.1 Test Series

To evaluate time-dependent losses in bolt tension, a series of tests were performed using the test setup from test series 2 (table 3-1). Six ECC specimens were tested. To distinguish between losses in bolt tension force due to ECC creep and shrinkage and the losses due to relaxation of the steel bolts a companion steel specimen that would not exhibit creep or shrinkage strains was also tested. The companion steel specimen was made from a piece of cold rolled steel plate with the same geometry as the ECC specimens. Figure 3-12 shows a picture of the steel specimen and one of the six ECC specimens.

Figure 3-12. Steel and ECC specimens used to examine time dependent loss of bolt tension

In these tests, the load in the bolts was monitored using bolt load cells. Figure 3-13 shows a picture of a bolt load cell. The bolt load cells were made by installing strain gages in a full bridge orientation on high strength steel bolts (ASTM A-490, 2002) and calibrating the load cell's output with the applied loads. The bolt load cell connections to the data acquisition system are also visible in figures 3-12 and 3-13.

At the start of testing the bolts were tightened in the same manner as described in Section 3.1.2. To examine the effects of retensioning of the bolts, three of the six specimens were retensioned 28 days after initial loading. The load in the connection bolts was monitored for 140 days.

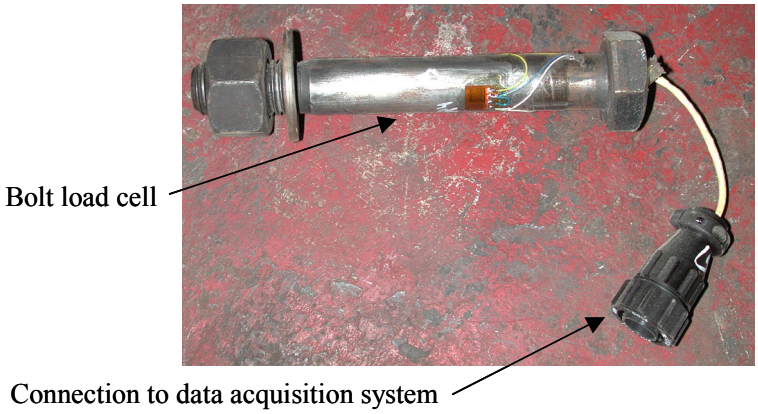

Figure 3-13. Bolt load cell used in testing

3.2.2 Test Results

Figures 3.14 and 3.15 show the testing results from the 6 ECC specimens. In each figure the results from 3 ECC specimens were shown, with the results obtained from each bolt (bolt a and b) plotted. The specimens shown in figure 3-14 were not retensioned during the testing period, while the specimens shown in figure 3-15 were retensioned after 28 days. Figure 3-16 shows the results obtained from the companion steel specimen. Table 3-3 gives a summary of the results obtained from all of the specimens at different times.

Table 3-3 - Summary of average[1] results from ECC specimens in bolt tension investigation

Specimens	Initial Force (kN)	Force at 28 days (kN)	Force at 135 days (kN)	% Loss in bolt tension at 135 days
ECC 1 to 3	130	99	86	35
ECC 4 to 6	130	98[2]	105	19
Steel	137	136	134	2

1. Average of two bolts on three specimens
2. Re-tensioned to 130 kN after measured at 98 kN

The results shown in figures 3.14 to 3.16 indicate that losses in bolt tension occur in the ECC specimens, while only negligible losses occur in the steel specimen. The ECC specimens with only an initial tensioning (figure 3-14) lost an average of 35% of the initial bolt tension force, compared to 19% for the retensioned specimens. The all steel specimen only lost 2% of the initial bolt tension force. Based upon these results, the loss in bolt tension can be attributed to primarily to creep and shrinkage of the ECC materials.

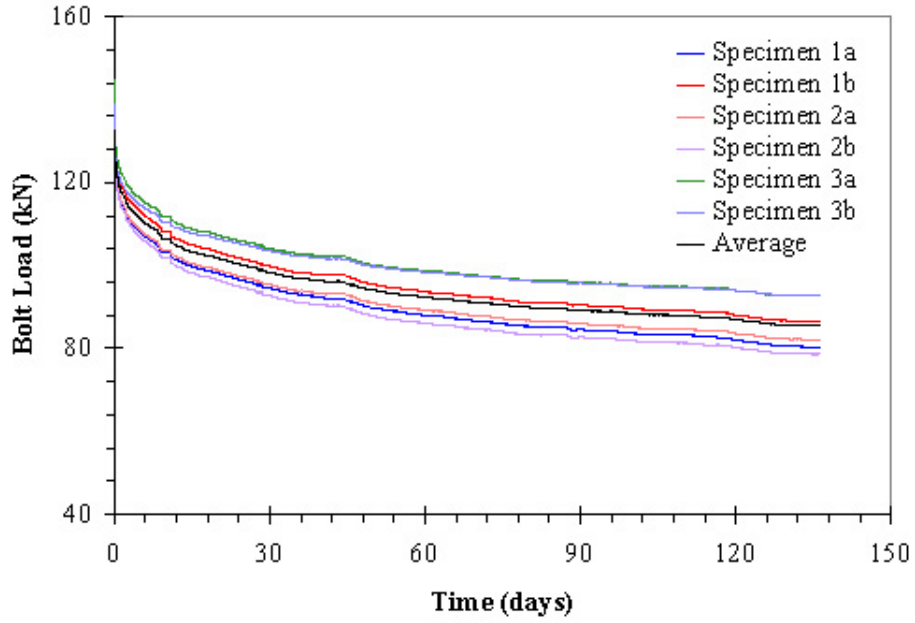

Figure 3-14. Loss in bolt tension over time in ECC specimens

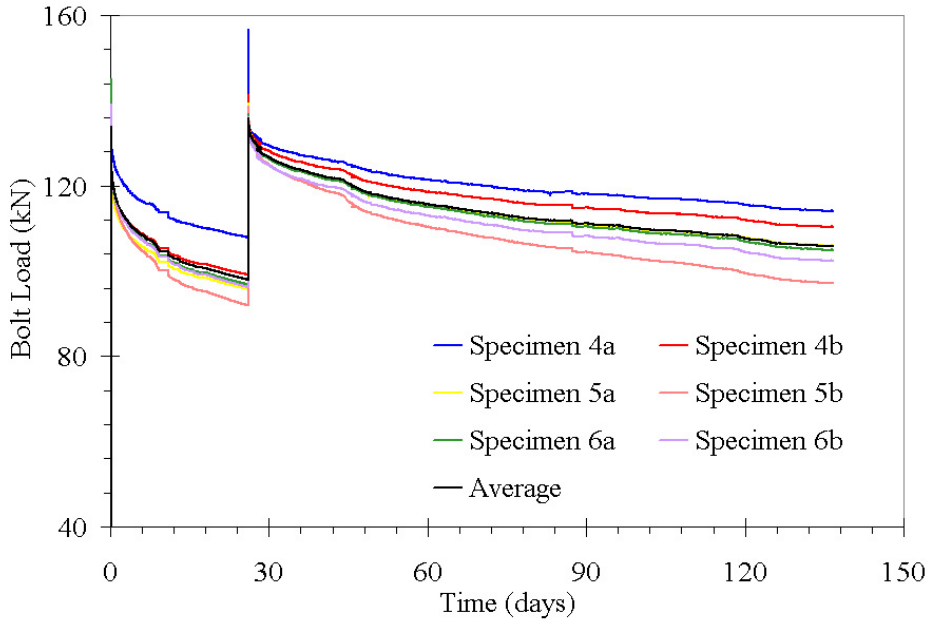

Figure 3-15. Loss in bolt tension over time in ECC specimens with bolts retensioned after 28 days

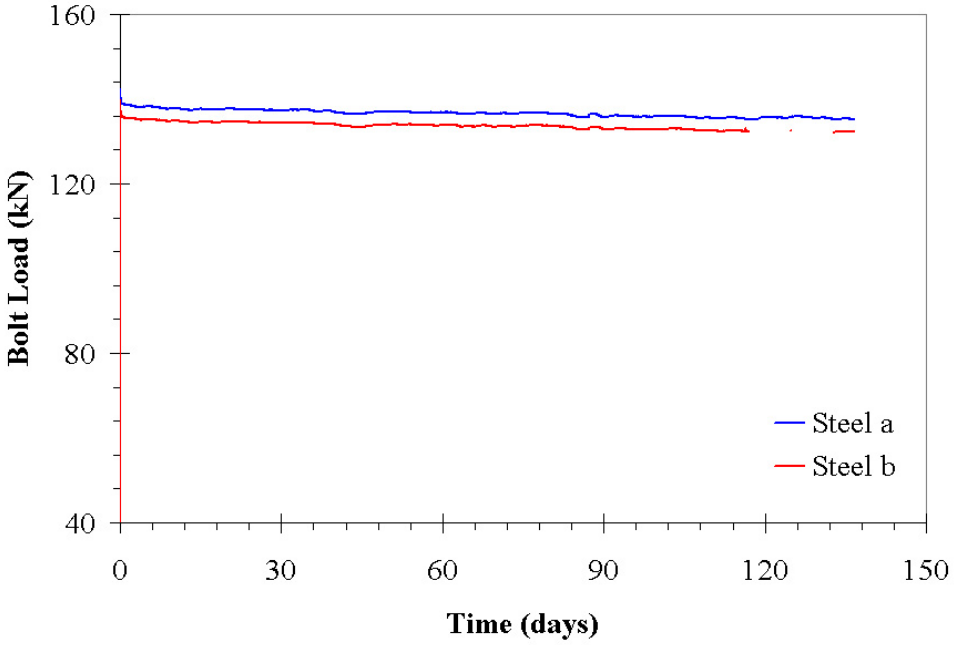

Figure 3-16. Loss in bolt tension over time in steel specimens

Creep and shrinkage of the ECC will result in significant losses in bolt tension and will need to be addressed in ECC infill panel connection design. Retensioning of the bolts can be used to mitigate the effects of creep and shrinkage, as seen in figure 3-15. While losses in bolt tension continued to occur after retensioning (as expected). However, the final bolt tension was higher at 135 days.

Several strategies are available to mitigate the effect of bolt tension losses, these include use of fine aggregates in the ECC to reduce the creep and shrinkage in the material (Rouse, 2003), retensioning of the bolts (as shown above), and sufficiently over-tensioning the bolts to allow for the desired level of bolt tension to be achieved after losses have occurred.

Prediction of the magnitude of the losses will be difficult. There is considerable variation in the creep and shrinkage of cementitious materials due to factors such as the age at initial loading, curing time, and ambient conditions (Mehta, 1986 and Rouse, 2003). The confined geometry and variable stress condition in the connection region will also complicate predictions of the magnitude of bolt tensioning losses. Additional research on the behavior of the ECC under constant load, with multi-axial confining boundary conditions will be needed to accurately predict the loss of bolt tension in the connection region.

3.3 Evaluation of Confined Material

The load-displacement results from the connection tests can be used to evaluate the modulus of elasticity of the ECC material inside the connection region. As discussed in Section 2.4.2, an accurate assessment of the material properties in the connection region is needed for accurate simulation results. In Section 2.4.2, a composite modulus, determined from a strain compatibility analysis, was used to represent the stiffness of both the steel tab and ECC in the

connection regions. In the strain compatibility analysis, the modulus of elasticity of the ECC materials was based upon the results from unconfined compression tests. To accurately assess the stiffness of the ECC, the effect of the lateral confinement by the bolts is determined here.

3.3.1 Confined Material Evaluation and Results

To examine the confined modulus of the ECC within the connection region, the results from the LVDTs and the applied loads can be used. The orientation of the connection region is shown in figure 3-17. To determine the confined modulus the strain in the confined material can be determined using Hooke's Law as shown below:

$$\varepsilon_x = \frac{1}{E}\left(\sigma_x - \upsilon\left(\sigma_y + \sigma_z\right)\right) \tag{3-2}$$

where: $\varepsilon_x = \varepsilon_c$ = the average vertical strain in the confined material
E = modulus of elasticity of unconfined ECC
σ_x = applied stress in the confined material
ν = Poisson's ratio of the confined material (assumed to be 0.18)
σ_z = measured lateral stress on confined ECC from pretensioned bolts.
$\sigma_y = 0$

The modulus of elasticity of the unconfined ECC material was calculated from the displacement of the ECC section above the angles, prior to slip of the block. The average modulus of the 6 specimens was 10.2 GPa. The value for the unconfined modulus of elasticity was similar (though lower) to the value measured in compression testing on cylinders of mix design SP (Table 4-3). The confined modulus of the ECC was then determined as:

$$E_c = \frac{\sigma_x}{\varepsilon_c} \tag{3-3}$$

where: E_c = confined modulus of ECC
ε_c = strain in confined ECC calculated using (3-2)
σ_x = applied stress in the x-direction on the confined material

Table 3-4 summarizes of the confined modulus values for the ECC calculated from the test results. The unconfined modulus results are also shown. The results shown in table 3-4 were obtained from specimens with the bolts oriented perpendicular with respect to the applied load (Test Series 2) because the horizontal orientation of the bolts was expected to provide a more uniform distribution of stress across the specimen at the bolt level than in the specimens with the load oriented inline with the axis of the bolts (Test Series 3).

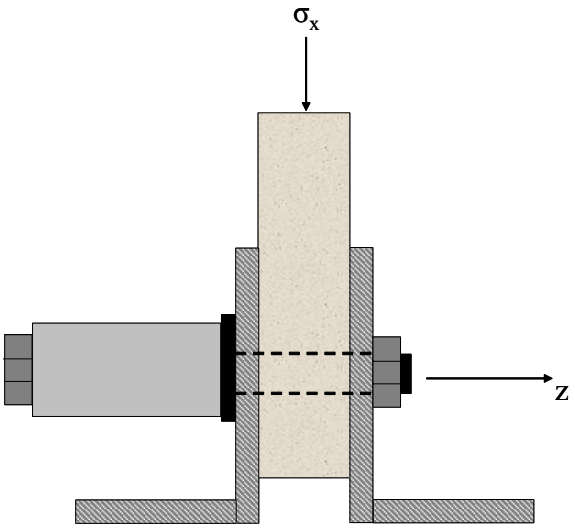

Figure 3-17. Orientation of stresses in confined region

The confined modulus of elasticity of the ECC can then be used in the strain compatibility analysis to determine the composite modulus of the connection region. The values obtained for the composite steel ECC region from the strain compatibility analysis with the confined ECC are shown in table 3-4. Note that in the analysis presented in Sections 2.3 to 2.5, the composite modulus of the ECC was based upon an assumed ECC modulus of elasticity of 13.8 GPa, which resulted in a composite modulus of 114 GPa in the connection for the geometry used in the connection tests. The values obtained from the strain compatibility analysis with the confined ECC are shown in table 3-4.

Table 3-4 - Summary of average[1] results of confined modulus evaluation

Bolt Orientation[2]	**Surface Condition**	**Measured Unconfined Modulus (GPa)**	**Measured Confined Modulus (GPa)**	**Computed Composite Steel/Confined ECC modulus (GPa)**
Perpendicular	Plain-formed	10.2	11.3	111
Perpendicular	Sandblasted	10.2	13.8	114

1. Average of three specimens
2. Bolt orientation with respect to applied load
3. ECC modulus of 13.8 GPa used in calculation

3.3.2. Discussion of Confined Material

The sandblasted specimens had a greater confined modulus due to reduced slip in the connection region. These values can be used in the strain compatibility analysis to determine the composite modulus of the connection regions of the ECC materials. The calculated confined modulus for the sandblasted specimens was identical to the value used in Chapter 2, (only because of the estimated value of the modulus of ECC used in the analysis). The use of the confined modulus will increase the composite modulus of the confined ECC. However, the test results will not be significantly impacted if the simple to determine unconfined modulus value is used for the ECC in the strain compatibility analysis.

3.4 Summary of Connection Test Results

The connection testing presented in Sections 3.1 to 3.2 demonstrated the viability of pretensioned bolted connections for ECC panels. The slip coefficient values obtained from the testing can be used to evaluate the size and number of bolts required between precast panels and at the connections to steel frames. The test results indicated that a single line of bolts is a viable strategy for the connection of ECC panels. The test results also indicate that connections can be designed with sufficient strength to prevent connection slippage and failure prior to failure in the panel.

To enhance the strength of the specimens, sandblasting of the connection region of the specimens is recommended. In the testing, sandblasted specimens had a 37% higher slip coefficient compared to the plain-formed specimens. Due to the common use of sandblasting in precast concrete, the additional step of sandblasting the connection region is unlikely to have a substantial impact on the overall cost of the panels.

The time-dependent tests indicated that some measure of bolt retensioning over time may be required for in-service infill panel installations. The loss of bolt tensioning force was significant and was related to the creep and shrinkage of the ECC material in the connection region. Prediction of the magnitude of losses will be difficult due to variations in the age at initial loading and the variable stress state in the connection region. Strategies to mitigate the effect of bolt tension losses include the use of bolt tension monitoring devices, establishment of bolt retensioning schedules and development of ECC materials that exhibit lower creep and shrinkage.

To determine a composite modulus for the ECC in the connection region the recorded displacements of the ECC in the confined region were evaluated along with the recorded variation in bolt force. The tests results were used to develop a composite modulus that represents the stiffness of the material in the connection region. These results will be used in the finite element models presented in Section 5.

Section 4
Laboratory Testing of Infill Panels

4.0 Introduction

In Section 2 an infill panel concept was presented which used steel reinforced ECC infill panel sections in lieu of traditional materials. In this chapter a series of laboratory tests are used to examine the response of infill panels to lateral loads. Specific goals of the testing included:

1. Examination of peak load and drift capacity of a variety of infill panel types
2. Examination of the shape of the load-drift response and energy dissipation of infill panels
3. Examination of infill panel failure mechanisms

The infill panel test results will be used to evaluate the material model discussed in Kesner and Billington (2004) for nonlinear finite element simulations. The infill panel tests will also provide benchmark data for future studies of the performance of ECC infilled frames.

4.1 Infill Panel Test Series and Setup

To evaluate the beam-type infill system developed in Section 2 a series of infill panels were tested. To simplify the testing a single panel test was developed as shown in figure 4-1. The tested panel represents one half of a beam-type infill section. The effect of different ECC mix designs, reinforcement details and panel shape were examined in the testing program. The performance of the infill panels was evaluated in terms of the goals shown above. The construction, instrumentation, installation procedures and loading scheme applied to the test panels are described here.

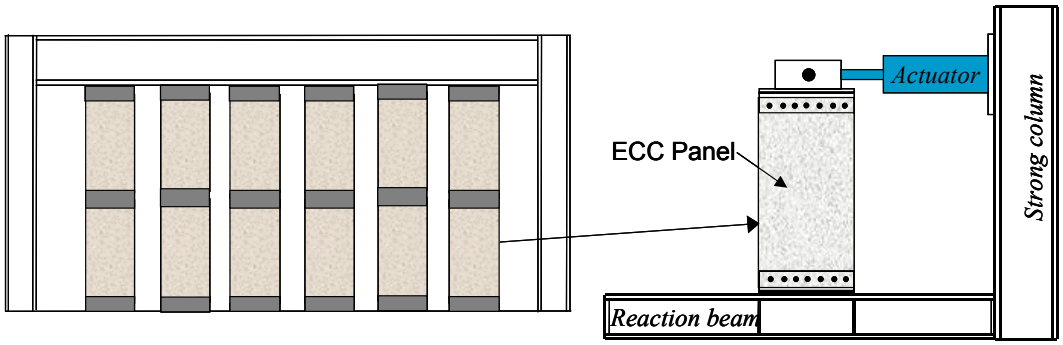

Figure 4-1. Single panel test setup for beam type infill

4.1.1 Test Series

Table 4-1 shows a summary of the panels tested in the program. The ECC mix designs used in the testing, shown in table 4-2, were adopted from the investigation of the cyclic response of ECC materials (Kesner and Billington, 2004). The concrete panel was tested for comparison

purposes using a mix design adopted from an investigation of ECC in precast bridge piers (Yoon, 2002). The materials used in the panels are further discussed in Section 4.1.3.

The basic panel geometry of 1220 mm tall by 610 mm wide by 75 mm thick was selected to represent an approximately ¾-scale panel in a typical hospital structure being investigated by MCEER (MCEER, 2000). The tapered panel has a reduced width (305 mm) at the top of the panel, with the tapered section starting 150 mm above the base of the panel. This geometry was selected to use the ECC material more effectively as discussed in Section 2.5.6.

All of the panels used a 150 mm tall connection angle at the top and bottom of the panel. The connection angle was located to allow 25 mm of clear space below panel bottom. The 25 mm space at the base of the panel resulted in 125 mm of the panel being confined by the steel connection angle. In actual structures, the connection angle will need to be sized to match the beam flange width. Figure 4-2 shows a schematic comparison of the different panel geometries.

Table 4-1 - Summary of Panel Specimens

Panel	Geometry	ECC Material	Reinforcement
1	Rectangular	SP	0.44% WWF[1]
2	Rectangular	SP	0.44% WWF with 9.5 mm perimeter bar
3	Rectangular	SP-A	0.44% WWF with 9.5 mm perimeter bar
4	Rectangular	RECS-A	0.44% WWF with 9.5 mm perimeter bar
5	Rectangular	Concrete	0.44% WWF with 9.5 mm perimeter bar
6	Taper	RECS-A	0.44% WWF with 9.5 mm perimeter bar

1. WWF = welded wire fabric (W4 wire 5.7mm diameter)

Table 4-2 – Mix designs used in the panel testing

Material	SP[1]	SP-A[1]	RECS-A[2,3]	Concrete
Water / cm[4]	0.35	0.35	0.39	0.35
Type I Portland Cement (kg/m^3)	1295	1016	733	493
Water (kg/m^3)	504	345	408	192
Silica Fume (SF) (kg/m^3)	144	113	0	54.8
SF/cm	0.10	0.10	0	0.10
Fly ash[5] (kg/m^3)	0	0	314	0
Fly ash[5] / cm	0	0	0.3	0
Fine Aggregate (kg/m^3)	0	565	523	664
Fine Aggregate / cm	0	0.5	0.5	1.21
Coarse Aggregate	0	0	0	1020
Coarse Aggregate / cm	0	0	0	1.86
Fiber (kg/m^3)	19.4	19.4	26.0	0
Fiber volume fraction	2%	2%	2%	0

1. Superplastizer (Daracem 100) added at 22mL per kg of cement
2. Superplastizer (Daracem ML 330) added at 3mL per kg of cement
3. Methylcellulose (Methocel 228 by Dow Corning) added as an admixture (0.1% by weight)
4. cm: cementitious materials
5. Class F Fly ash obtained from AES Cayuga, Lansing, NY.

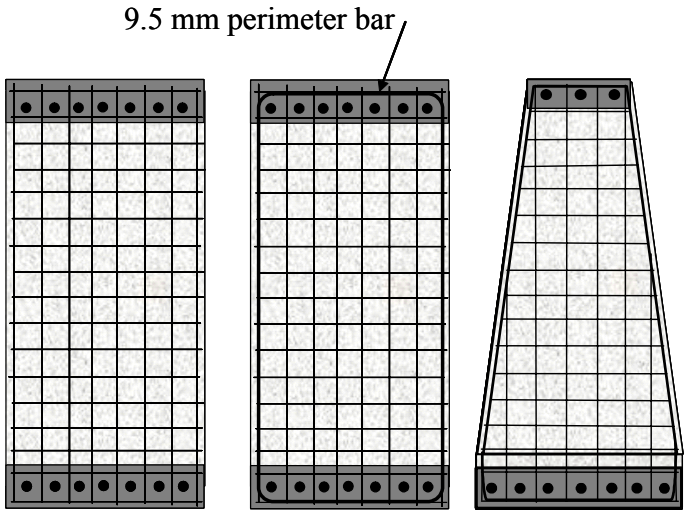

Figure 4-2. Configuration of test panels (a) panel with WWF, (b) panel with WWF and perimeter bar and (c) tapered panel

In all panels, a bolt spacing of 76 mm was used on the top and bottom of the panel, with the centerline of the bolts located 76 mm from the bottom and side edge of panels. This bolt spacing resulted in seven bolts being installed across of top and bottom of the rectangular panels. Three bolts were used at the top of the tapered panel. A bolt size of 19 mm was used in the panels, which, based upon the results of the connection tests and preliminary analysis (Sections 3.1 and 2.5, respectively), would provide ample capacity to the panel connections.

The basic reinforcement used in the panel was welded wire fabric (WWF), which was detailed to provide for 76 mm spacing between wires. The wire diameter was 5.7 mm. This wire spacing allowed for the reinforcement to be centered between the bolts. Figure 4-3 shows a schematic drawing of the reinforcement at the bottom edge of the panel. As seen in the figure, the spacing of the reinforcement and bolts results in approximately 38 mm of clear cover for the reinforcement. The WWF reinforcement used in the panel provided a 0.44% reinforcement area. In addition to the WWF reinforcement, a 9.5 mm reinforcing steel perimeter bar was used in the majority of the panels to provide additional tensile reinforcement. The combination of the perimeter bar and WWF provided sufficient distributed reinforcement in the panel, without creating consolidation problems due to reinforcement congestion. The ultimate strength (lateral load capacity) of the panels was estimated to be 44 kN for the panels with WWF, and 54 kN for the panels with both the WWF and the perimeter bar. The ultimate panel strength estimate included the tensile contribution of both the ECC and the mild reinforcing steel at ultimate strength.

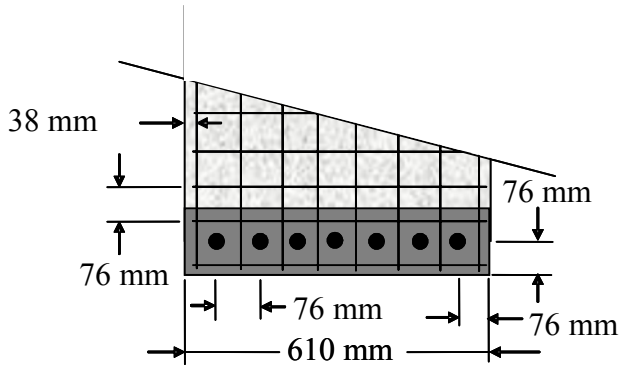

Figure 4-3. Panel and reinforcement spacing at base of panel

4.1.2 Panel Fabrication

The rectangular panels were cast on their sides (the tapered panel was cast flat) in clear Plexiglas forms stiffened with wood. Figure 4-4 shows the form at the start of casting. The Plexiglas forms were selected to help ensure consolidation by allowing the flow of the material to be seen during casting and to provide a smooth finished surface. After completion of casting the exposed panel surface was covered with wet burlap and plastic. Fans were used to dissipate the heat generated by the hydration of the cement. The panels were removed from the forms approximately 48 hours after casting, and were then wet cured under burlap and plastic until 28 days after casting. The panels were allowed to dry under laboratory conditions (roughly 21° C. and 50% RH) after the wet curing period and prior to testing to minimize the effects of drying shrinkage stresses as discussed in Kesner and Billington (2004).

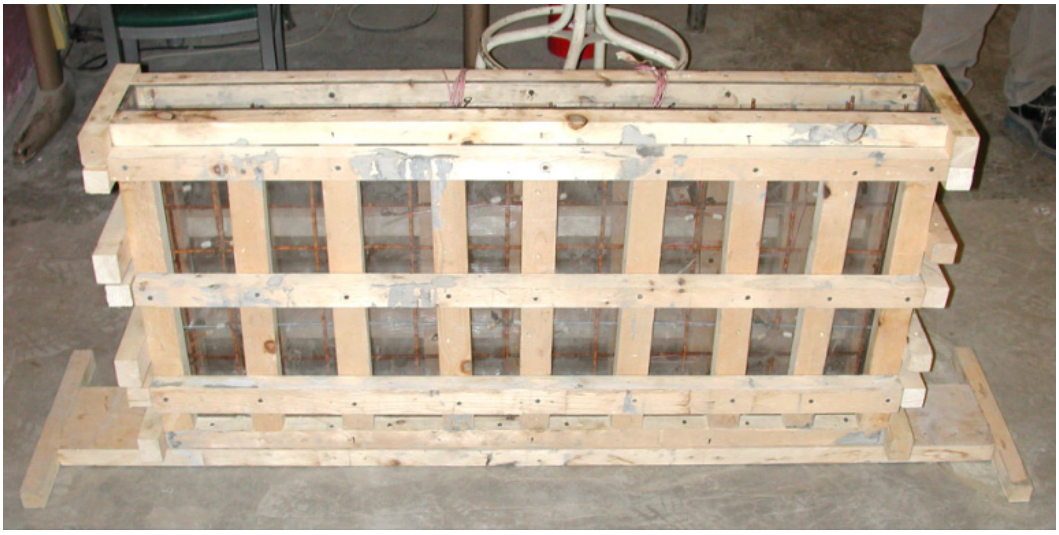

Figure 4-4. Panel form at the start of casting

Prior to testing, the boltholes were placed in the panels using a 22 mm diamond edged core drill. Similar to the panel connection tests (Section 3.1) the boltholes in the panels were slightly

oversized to provide room to accommodate construction variation. After coring, the connection regions were sandblasted to maximize the connection capacity. The surface was sandblasted to the same level of roughness as the ECC connection block specimens shown in figure 3.2b.

4.1.3 Material Properties

Material tests were performed to determine the properties of both the ECC and concrete materials and the reinforcing steel prior to panel testing. Table 4-3 shows a summary of pertinent properties for the ECC and concrete materials. The concrete properties shown in table 4-3 were obtained from testing 100 mm by 200 mm cylinders in accordance with standard test methods. Similar to the ECC specimens, the concrete cylinders were wet cured for 28 days after casting and then stored under laboratory conditions until testing.

Table 4-3 – Properties of Cementitious Materials Used in Panel Testing

Material	First Cracking Strength (MPa)	Ultimate Tensile Strength (MPa)	Tensile Strain Capacity[1] (%)	Compressive Strength (MPa)	Compressive Modulus (GPa)
SP[2]	1.2	1.5	2.3	63	13.8
SP-A[2]	1.2	1.4	0.8	38	11.2
RECS-A[2]	1.4	2.1	0.5	41	12.1
Concrete[3]	3.6[4]	-	-	36	28.6

1. Tensile strain capacity defined as strain capacity at the onset of softening
2. Properties of ECC materials obtained from cylindrical specimens (Kesner and Billington, 2004)
3. Compressive strength of concrete measured in accordance with ASTM C-39 (1995)
4. Splitting tensile strength of concrete measured in accordance with ASTM C-496 (1995)

The properties of the WWF and reinforcing steel were obtained from uniaxial tension tests on samples of the material, using bonded electrical strain gages to record the strains. A minimum of three samples of each material was tested, with the average test results summarized in table 4-4.

Table 4-4 – Properties of Reinforcing Materials Used in Panel Testing

Material	Yield Strength[1] (MPa)	Ultimate Tensile Strength[2] (MPa)	Ultimate Strain Capacity	Modulus of Elasticity (GPa)
9.5 mm bar	427	667	1.65%	200
W4 wire	500	640	1.75%	200

1. Stress at 0.2% strain
2. Determined at wire or bar fracture

4.1.4 Test Frame

The test frame was formed by anchoring a heavily stiffened beam to the floor in the George Winter Laboratory for Structural Engineering Research at Cornell University (as seen in figure 4-5). Above the reaction beam, a 222 kN actuator was installed on a strong column. The actuator had a maximum stroke of +/- 64 mm. To simplify installation of the panels, the actuator was mounted on a swivel, which allowed the actuator to be temporarily moved to ease panel installation. Two steel sections were anchored to the reaction beam to serve as mounting areas for the displacement transducers (LVDTs). Figure 4-5 shows the test frame prior to the installation of the panel. Angle sections (150 mm by 100 mm by 12.7 mm) were used to connect the panel to the reaction beam at the bottom of the panel and to the actuator at the top of the panel. A single 25 mm diameter pin was used to connect the actuator to the angle section, allowing for only lateral displacements (horizontal loading) to be transmitted to the panel. Figure 4-6 shows the pin connection in place on a panel prior to testing. The connection pin was located 75 mm above the top of the connection angle.

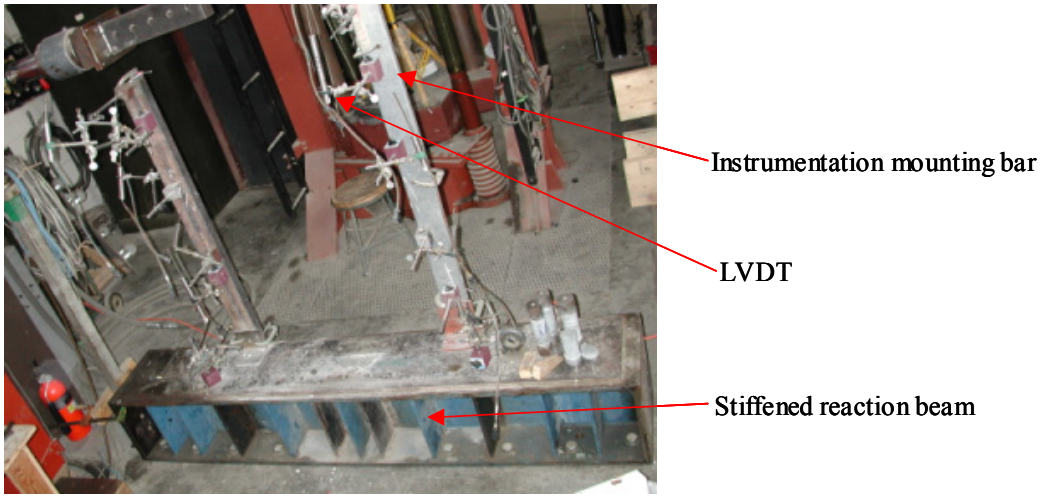

Figure 4-5. Test frame prior to installation of panel

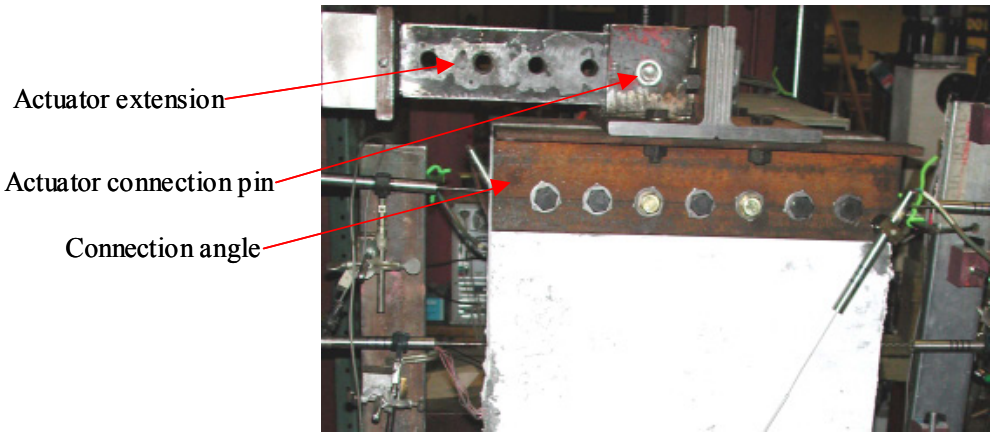

Figure 4-6 Connection of actuator to test panel

4.1.5 Panel Instrumentation

To evaluate the load-drift response of the infill panels, a variety of instrumentation devices were used. Prior to casting a series of bonded electrical strain gages were installed on both the WWF reinforcing and 9.5 mm perimeter bars (if used) in the panel. Figure 4-7 shows a schematic drawing of the strain gage locations on a rectangular panel with WWF reinforcing, while figure 4-8 shows the same information for a rectangular panel with both the WWF and the perimeter reinforcing bar. The gages on the tapered panel were installed in the same locations as on the rectangular panel as shown in figure 4-8. The gages were oriented to examine the distribution of the strains in the panel during testing. In addition to the strain distribution, the results from the strain gages can be used to locate areas where plastic deformation of the reinforcing steel occurred.

Sixteen LVDTs were used in each panel test. Ten are used to monitor the horizontal displacement profile of the panel. The remaining LVDTs are used to record the diagonal displacement, the slip of the panels at the base connections, and the out-of-plane displacement of the panels. Figure 4-9 shows the location of the horizontal LVDTs on a rectangular panel. The horizontal LVDTs were installed in the same location on the tapered panel.

Load cells were used to measure the actuator load applied to the panel and to monitor the load in the connection bolts. Four load cells were installed on the panels at the connection of the panel to the steel angles (ECC panel bolts), two at the top and two at the bottom as seen in figure 4-9. Twelve load cells were used to measure the load transferred from the base angles into the reaction beam. Figure 4-10 shows a plan view of the panel base with the panel connection load cells, with the cross-section of the base shown in figure 4-11. Figure 4-12 shows an instrumented panel prior to testing with the instrumentation devices in place.

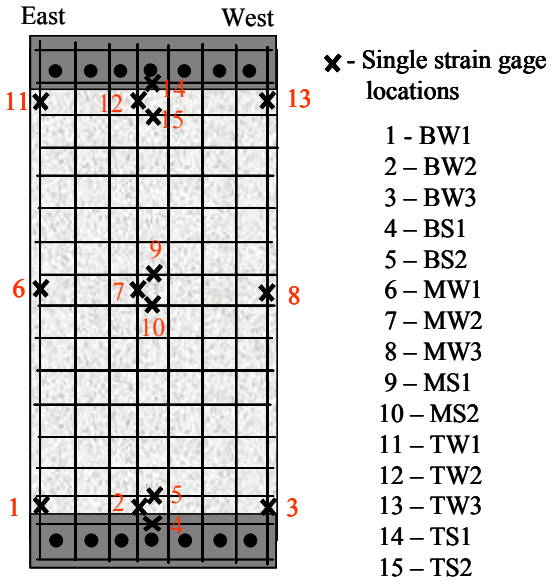

Figure 4-7. Location of strain gages on panel with WWF

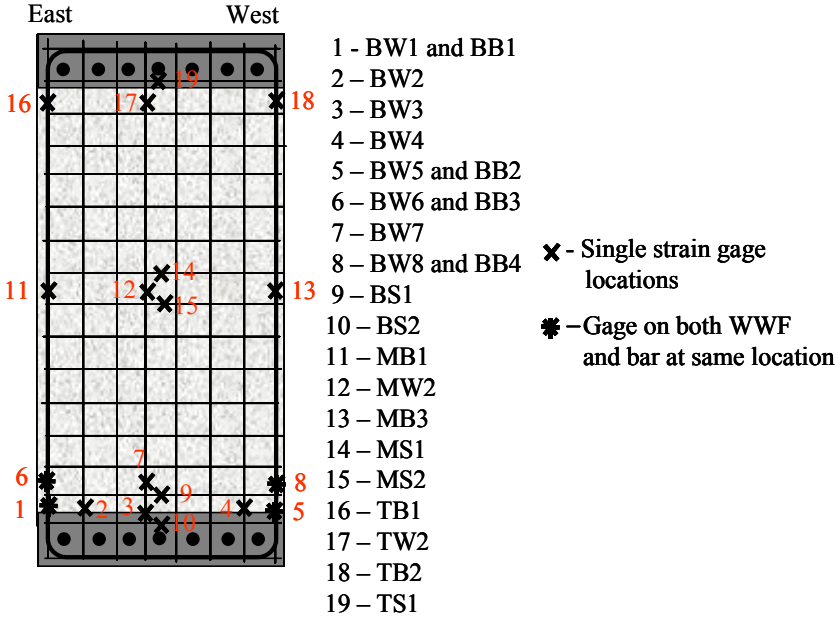

Figure 4-8. Location of strain gages on panel with WWF and perimeter reinforcing bar

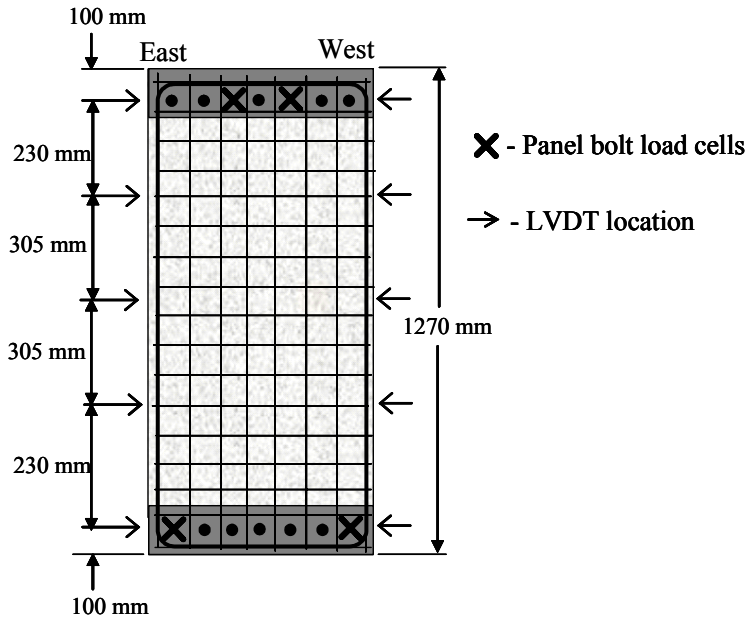

Figure 4-9. Location of horizontal LVDTs above stiffened reaction beam and panel bolt load cells

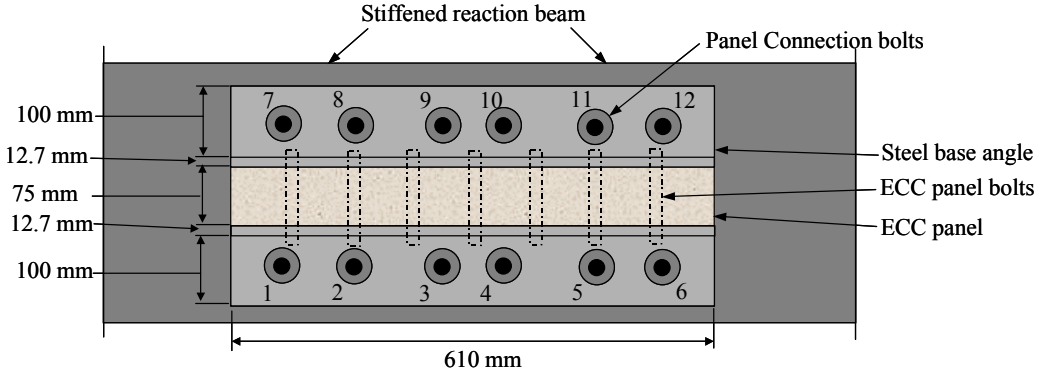

Figure 4-10. Plan view of panel base with location of panel connection bolts

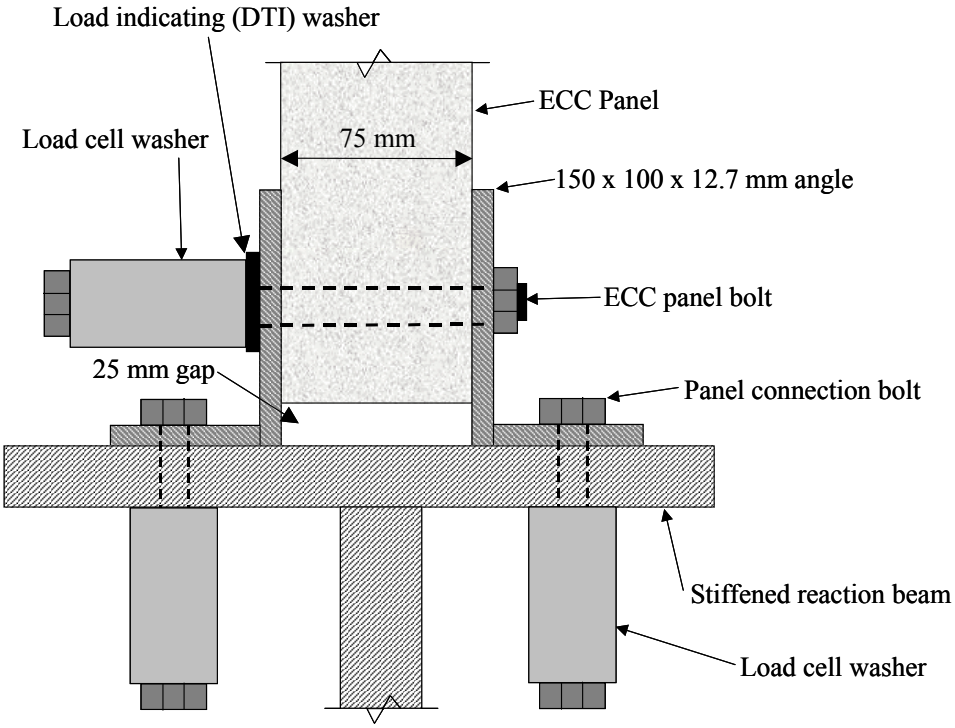

Figure 4-11. Cross-section of panel base. Reaction beam stiffeners not shown

Figure 4-12. Panel with instrumentation in place at start of testing

4.1.6 Panel Installation

The panel was moved into the test frame using an overhead crane. The panel was placed to allow a 25 mm clear space between the panel and the base reaction beam. After placing and plumbing the panel, the panel bolts at the base and top of the panel were torqued to provide a pretensioning load of 133 kN in each bolt. To limit non-uniform stresses being placed on the bottom of the panel, the panel bolts were tensioned in three stages, with approximately 45 kN applied in each stage. To mitigate the effects of bolt tension loss due to ECC creep and shrinkage, the bolts were tensioned approximately 24 hours prior to testing and were then retensioned immediately prior to the start of testing.

The panel connection bolts that connect the angles to the reaction beam were pre-tensioned after the installation of the ECC panel bolts. All of the panel connection bolts were tensioned to near identical values. However, in the tests, two different levels of pretensioning were used on the panel connection bolts. In Panels 1, 2, and 6 a pretensioning force of 67 kN was used, while on Panels 3, 4 and 5, a pretensioning force of 111 kN was used. The different loads were used to examine the impact of different clamping forces on the connections.

The LVDTs were installed and zeroed after completion of the panel connection bolt tensioning. The last step in the panel installation was the connection of the strain gages to the data acquisition system.

4.1.7 Panel Loading

To evaluate the load-drift response of the ECC panels each panel was subjected to a symmetric cyclic loading to various drift levels, with the panel displacement (the average reading of the two LVDTs located at the top of the panels) used as the control parameter. The loading scheme was similar to the loading used in the preliminary infill analysis (Section 2.5). However, more loading cycles at high drifts were applied in the testing to ensure complete failure of the panel. Figure 4-13 shows the drift history used in the panel tests. Beyond 3% drift, the panels exceeded the maximum stroke of the actuator. The panel drift (typically expressed as a percentage) was defined as:

$$\text{drift} = (\delta / h) \tag{4-1}$$

where: δ = average displacement measured at the level of the top bolts in the panel
h = panel height (1220mm)

The panel testing was controlled by a computerized data acquisition system, which both incremented the actuator displacement and recorded data from the measuring instruments. The control system was capable of providing a minimum displacement step size of 0.03 mm to the panel. At each step in the testing, the data acquisition system recorded data from each of the 51 measuring instruments used in the test. During each test, approximately 2,000 data readings were captured by the data acquisition with the data written to a computer hard drive. The testing was performed at a quasi-static rate, with each panel test requiring about 8 hours to complete (exclusive of panel installation time).

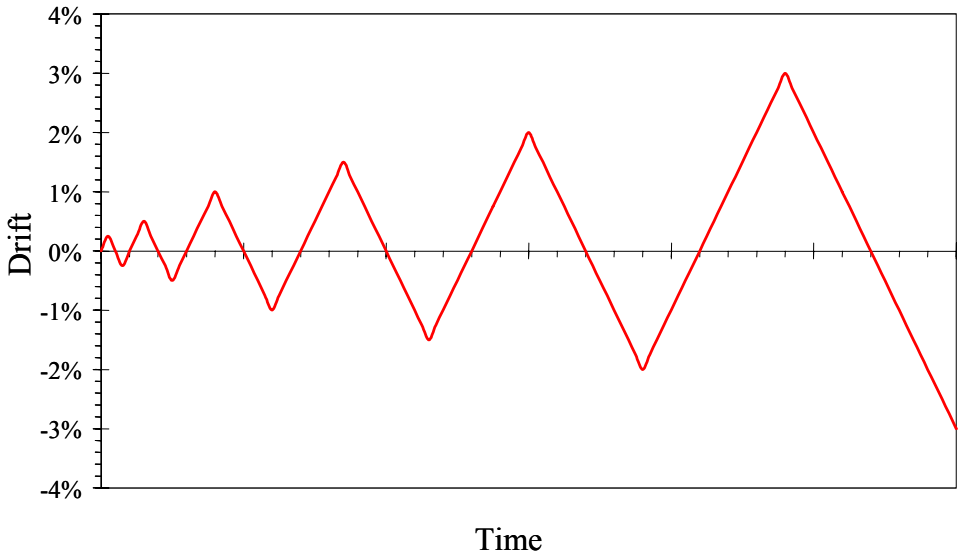

Figure 4-13. Drift history used in panel testing

As each drift level was reached the loading was temporarily paused to allow for cracks to be marked and photographs of the panel to be taken. Two different colors were used to mark the cracks, with the different colors corresponding to negative and positive drifts. Following the photographs, the loading direction was reversed until the next drift level was reached. The loading was continued until the panel failed (defined as a near complete loss of load carrying capacity) or until the displacement capacity of the actuator was reached.

4.2 Infill Panel Test Results

The following sections present the results obtained during the panel testing. The key parameters of interest in the panel tests were the peak load and drift capacity of the panel, the shape of the load-drift response, the amount of energy dissipation in the panels, and the panel failure mechanisms. Comparisons between results from different panels are presented in Section 4.3.

4.2.1 Load vs. Drift Response

The load vs. drift responses from the infill panels are shown in figures 4.14 to 4.19. Table 4-5 shows a summary of the peak load applied to the panel, the drift level at the onset of softening (defined as the drift level when noticeable drops in the panel capacity occur), the panel stiffness at 0.5% drift and the residual panel strength. The panel stiffness was determined by dividing the average load (load at positive and negative drift) in the panel at 0.5% drift by the panel displacement at 0.5% drift (6.1 mm). The residual strength is defined as the panel load at the maximum drift level prior to completion of testing.

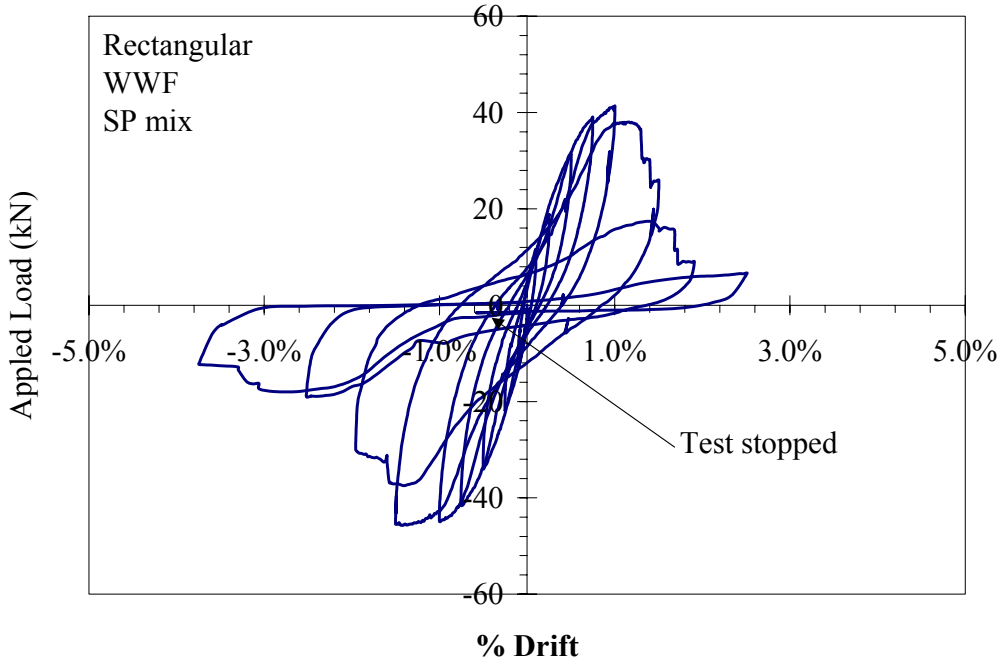

Figure 4-14. Load-drift response from Panel 1

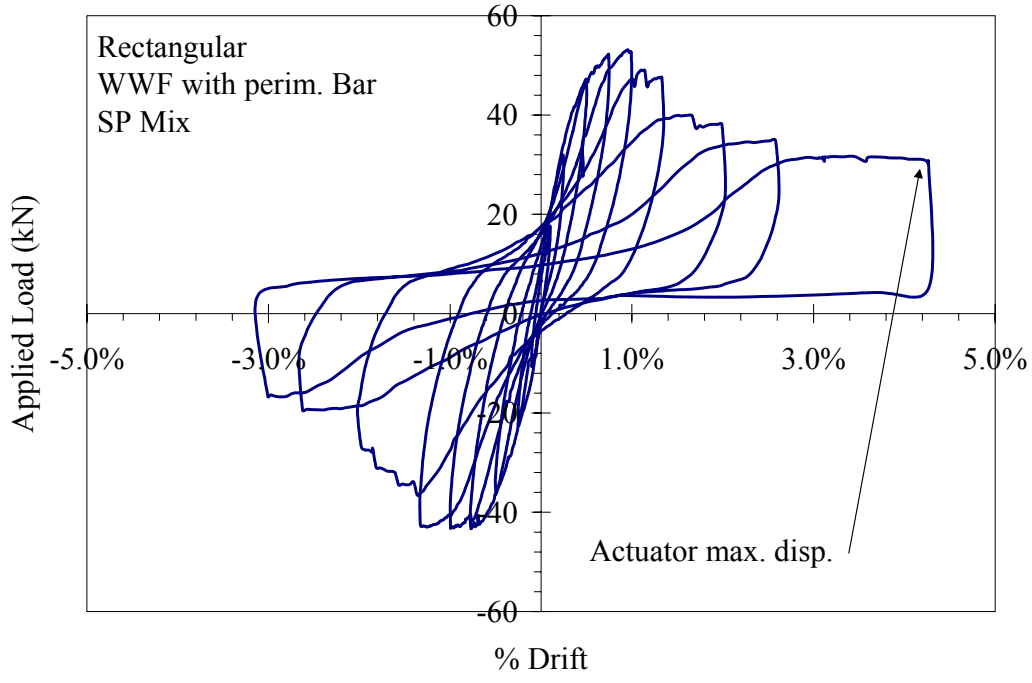

Figure 4-15. Load-drift response from Panel 2

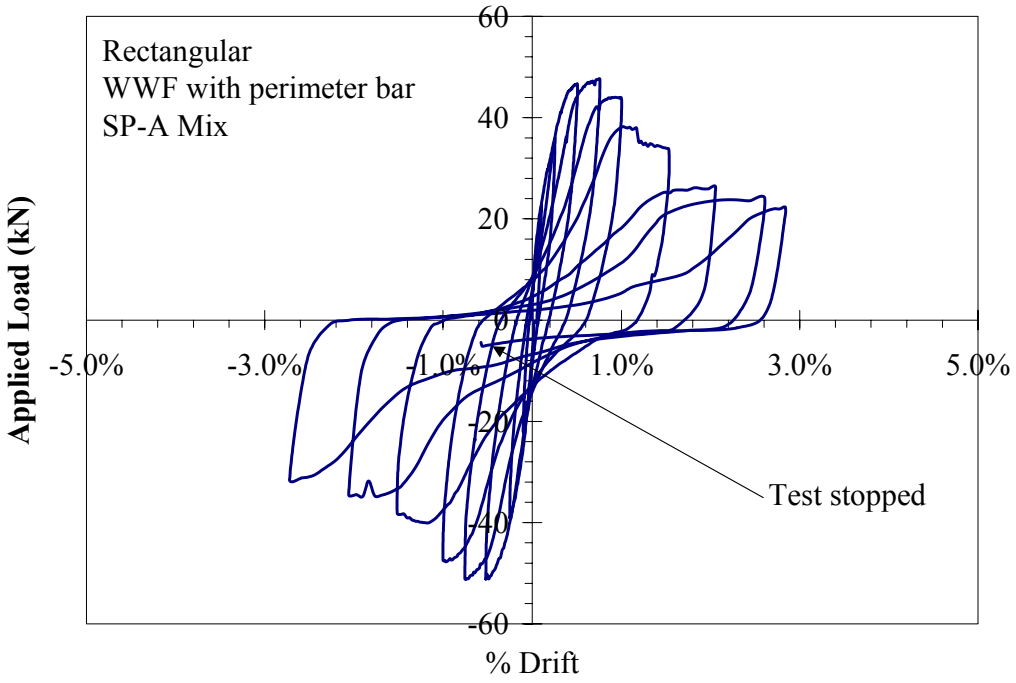

Figure 4-16. Load-drift response from Panel 3

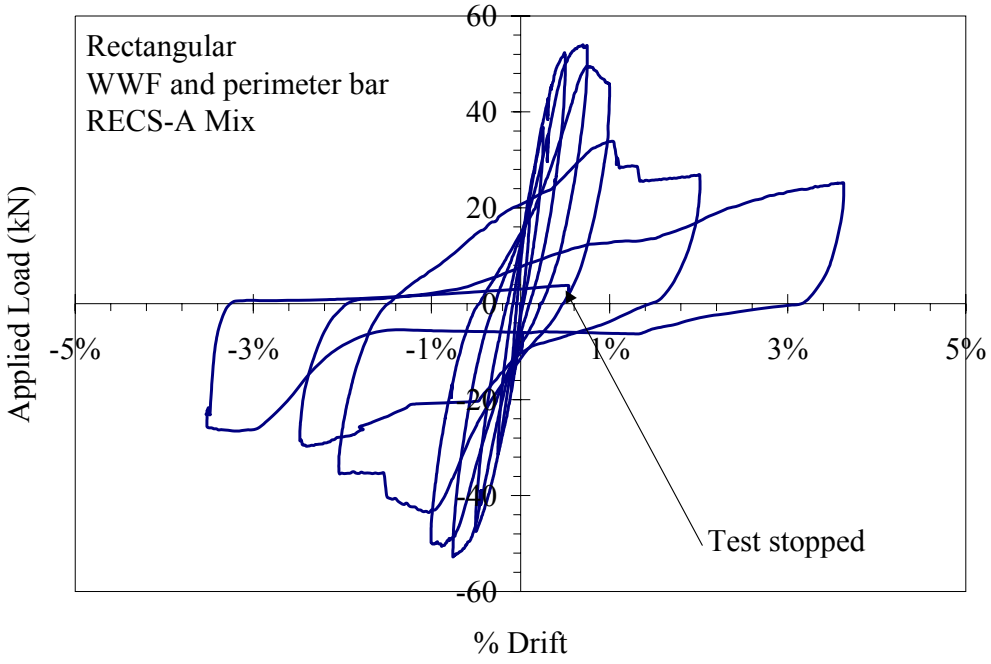

Figure 4-17. Load-drift response from Panel 4

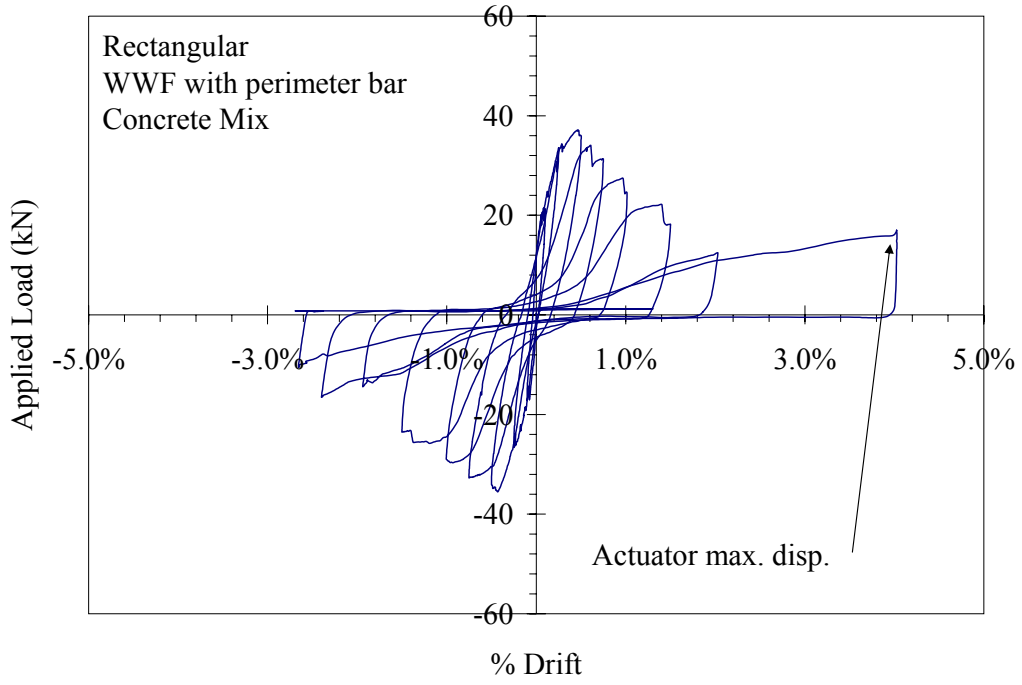

Figure 4-18. Load-drift response from Panel 5

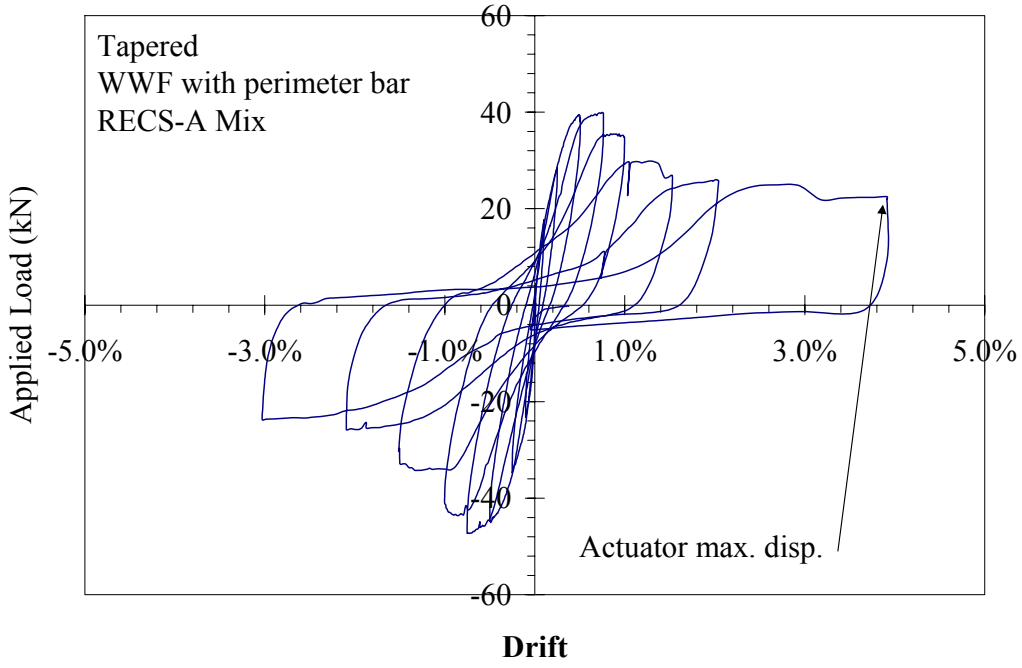

Figure 4-19. Load-drift response from Panel 6

Table 4-5 – Summary of Results from Infill Panel Tests

Panel	Peak Load (kN)	Drift at onset of softening	Average Stiffness at 0.5% drift[1] (kN/mm)	Residual Strength[2] (kN)
1	45	-1.5%	5.37	7
2	53	-1.33%	6.84	32
3	51	-0.75%	8.03	24
4	54	0.75%	8.15	25
5	37	0.5%	5.82	16
6	47	-0.75%	6.85	24

1. Using average load and average displacements at positive and negative 0.5% drift
2. Strength at maximum drift level prior to completion of test

The loading portion of the load vs. drift response was non-linear as a consequence of the cracking and strain hardening of the ECC and yielding of the reinforcing steel. The response was similar to that observed in the cyclic testing of the ECC materials, with the added effect of the reinforcing steel. As the ECC material was loaded, the cracks gradually open, and steel starts carrying load with the ECC. The portion of load carried by the reinforcing steel was a function of the amount and position of the reinforcing in the panel.

The unloading response was also related to the multiple cracking in the ECC material and the strain in the reinforcing steel. The initial unloading of the panel was elastic, which occurs primarily due to the elastic unloading of the reinforcing steel. As discussed in Kesner and Billington (2004), the ECC materials only have small amounts of elastic energy. After the removal of load, the pinching of the load-drift response occurs as the cracks in the ECC material were gradually closed. During the closure of cracks the ECC material has very little stiffness as discussed in Kesner and Billington (2004). The panel load increases as the cracks fully close and bear in compression.

During reloading, the load on the panel increases until the existing cracks are fully reopened. The increase in load capacity, above the capacity at the previous drift level, occurs as new cracks form in the ECC material resulting in additional pseudo-strain hardening of the ECC, and yielding of the reinforcing steel. The panel load increases until the peak strain capacity of the ECC is reached. After the peak strain capacity is reached, strength degradation occurs as load can no longer be carried by the ECC and is carried only by the steel reinforcement.

The variation in initial stiffness between the panels shown in table 4-5 is attributed to the difference in panel materials, reinforcement details, and panel geometry. The highest initial

stiffness was achieved with the rectangular panels that contained both the WWF and the perimeter bar, and ECC that contained aggregate.

In table 4-5, the average panel load at each drift level was used to calculate the panel stiffness because the load-drift response of the panels was not symmetric. The non-symmetry of the response was due to small amounts of slip of the panels in the connection, and from the cracking of the ECC. The slip of panels in the connection region is further discussed in Sections 4.2.5 and 4.3.6.

The residual strength in the panels varied from 7 to 32 kN. The high amount of variation in residual strength and the strength degradation of the panels will be further discussed in Section 4.2.3.

4.2.2 Cracking Response

The cracking response of the panels varied with the drift level in the panel, and with the various panel materials. As described in Section 4.1.7, during the testing as each drift level was reached the location of cracks was marked on the panels. Table 4-6 shows a summary of the cracking response of the panels. The crack distribution column in the table represents a relative visual assessment of the extent of distribution of cracking in the panel. An excellent crack distribution refers to a uniform spacing of cracks, without large caps between cracks. Good crack spacing has isolated gaps in the spacing of the cracks. Poor crack spacing was typified by a spacing between cracks of greater than 50 mm. In all of the panels, the crack formation was similar at both the positive and negative drift levels. The following paragraphs describe the cracking observed at various drift levels in the different panels. Due to the similarity in cracking response, the discussion of cracking at the positive and negative drift levels is combined.

Table 4-6 – Summary of Cracking Response in Infill Panels

Panel	Drift at 1st crack	Crack Distribution	Location of dominant crack
1	0.1%	Excellent	¼ of the way up panel
2	0.25%	Excellent	Panel base
3	0.1%	Good	Panel base
4	0.1%	Good	Panel base
5	0.1%	Poor	Panel base
6	0.1%	Good	Panel base

The initial crack formation in all but one of the panels (Panel 2) was observed at a drift of 0.1%, with the initial crack typically located in the bottom ¼ of the panel. In Panel 2 the first crack was observed at 0.25% drift. In Panel 1, the initial crack occurred at approximately ¼ of the panel height on the edge of the panel. The initial cracks in the other panels were observed on the panel faces. All of the initial cracks were fine cracks (less than 0.1 mm in width). Figure 4-20 shows the first cracks, which occurred in Panels 1, 3 and 6.

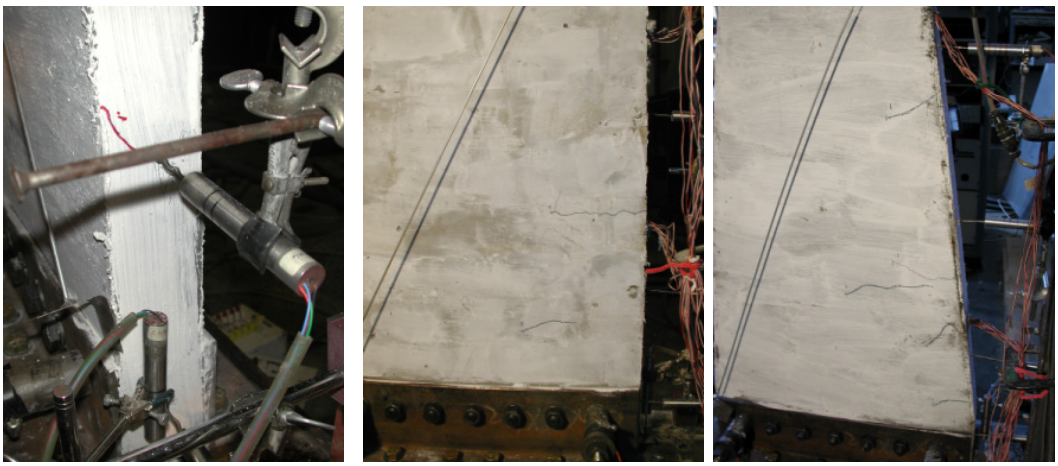

Panel 1 Panel 3 Panel 6

Figure 4-20. Initial crack on Panels 1, 3 and 6 at 0.1% drift

At 0.25% drift the formation of multiple cracks was seen in all of the panels. Figure 4-21 shows the cracking in Panels 2 and 4. The cracking in Panel 5 (concrete panel) was different from the remaining panels at this drift level. The cracks in Panel 5 extended nearly across the full panel width, as seen in figure 4-22. This was in contrast to the results obtained in the ECC panels (figure 4-21).

Panel 2 Panel 4

Figure 4-21. Cracks in Panels 2 and 4 at 0.25% drift

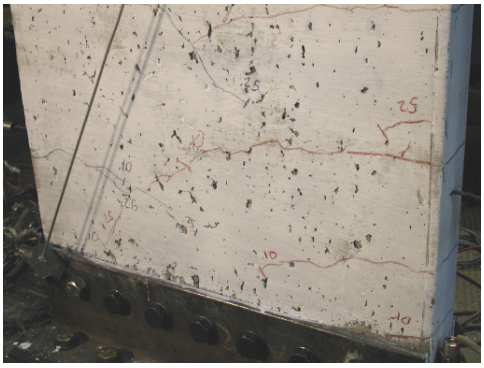

Panel 5

Figure 4-22. Cracks in Panel 5 at 0.25% drift

At 0.5% drift, the formation of a localized crack was observed across the base of Panel 5 (concrete). The crack at the panel edge can be seen in figure 4-23. The crack propagated immediately below the edge of the connection angle, which prevented good photographs from being taken. The ECC panels continued to form new cracks, with existing cracks propagating. At 0.5% drift, cracks from different panel sides were observed to have intersected with cracks from the other side. The cracks were well distributed along the panel height. Figure 4-24 shows typical cracking patterns in Panels 2 and 4 at 0.5% drift.

Panel 5

Figure 4-23. Localized crack at edge of Panel 5 (0.5% drift)

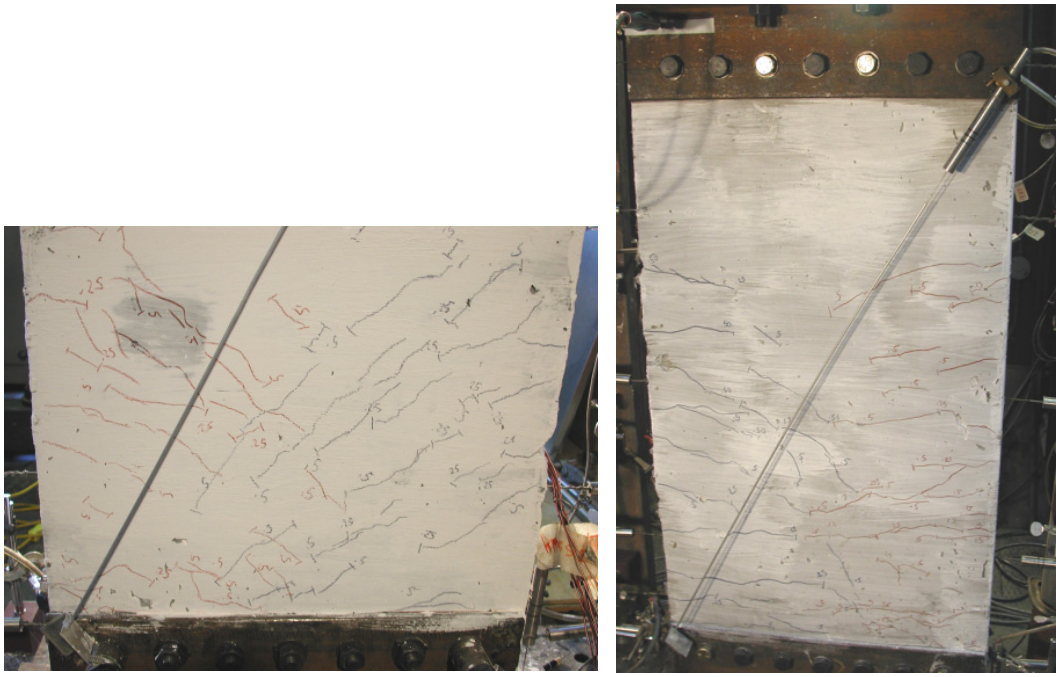

Panel 2 Panel 4

Figure 4-24. Cracks in Panels 2 and 4 at 0.5% drift

At 0.75%, localized cracks were observed to form in Panels 3, 4 and 6. Similar to Panel 5, the localized crack was difficult to photograph as it was obscured by the connection angle. Figure 4-25 shows the base of Panels 3 and 4. In the figures, the distribution of cracking in the panel at the onset of softening can be seen. Figure 4-26 shows the distribution in cracking in Panels 1 and 2 at 0.75% drift. In Panel 5, the localized crack could clearly be seen at 0.75% drift (figure 4-27).

Panel 3 Panel 4

Figure 4-25. Cracking in Panels 3 and 4 at 0.75% drift

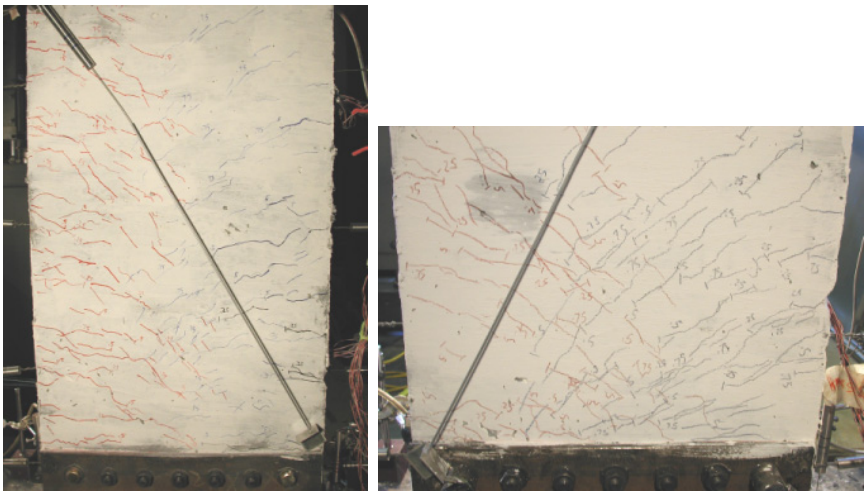

Panel 1 Panel 2

Figure 4-26. Cracking in Panels 1 and 2 at 0.75% drift

Panel 5 Panel 5

Figure 4-27. Localized crack in Panel 5 at 0.75% drift

At a drift level of 1.5%, localization of a crack occurred on Panels 1 and 2, as seen in figure 4-28. In Panel 1, the localization occurred approximately 230 mm above the base of the panel, and was the only panel to localize away from the panel base. In the other panels, the cracking became concentrated at the base. Figure 4-29 shows localized cracks in Panels 4 and 6, which were typical results at higher drift levels.

Panel 1 Panel 2

Figure 4-28. Localized cracks in Panels 1 and 2 at 1.5% drift

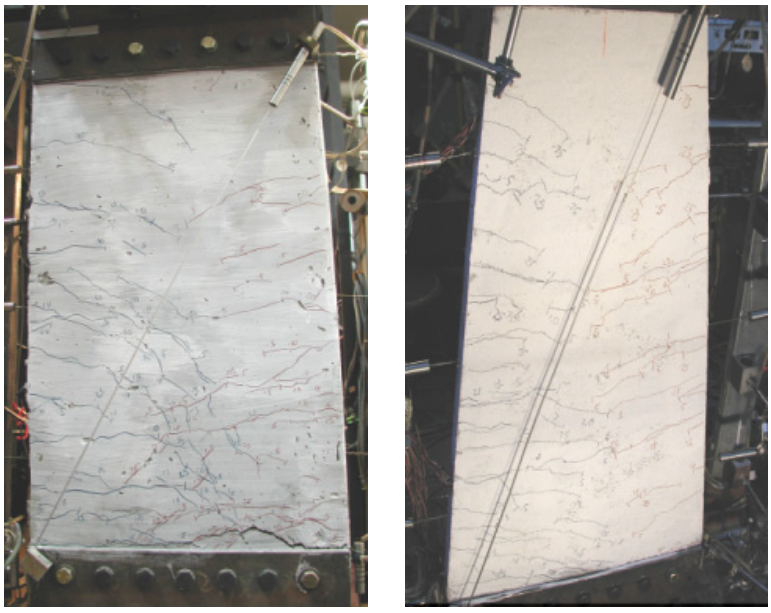

Panel 4 Panel 6

Figure 4-29. Localized cracks in Panels 4 and 6 at 1.5% drift

At higher drift levels, the localized cracks continued to grow larger until testing was stopped. The formation of new cracks was not observed after the localization of a crack near the panel base.

The greatest number of individual cracks was observed in the panels made with ECC mix SP (Panel 1 and 2). These panels also achieved the highest drift capacities before localization of a

crack. The greater number of individual cracks in Panels 1 and 2 compared to Panels 3 and 4 can be seen in a comparison of figures 4.25 and 4.26.

4.2.3 Failure Mechanisms

In table 4-5, the peak load and drift level at the onset of panel softening (drop in load carrying capacity) observed in the panel testing was presented. The softening of the panel was considered the onset of panel failure. In all of the panels made with an ECC material, the failure of the panels initiated with the softening of (i.e. localization of strain at a dominant crack in) the ECC material. However, the reinforcing details affected the failure shape. The following paragraphs discuss the failures observed in the individual panels. To avoid repetition, the panel results were grouped based upon the panel reinforcing. The concrete panel (Panel 5) was observed to have a slightly different failure mechanism than the ECC panels, and will be discussed separately.

In Panel 1 (which was reinforced with only WWF mesh), the onset of softening occurred at a drift level of 1.5%, as seen in figure 4-14. Fracture of some of the WWF reinforcing steel was observed. The sudden drops of load seen in figure 4-14 were the result of both fracture and development failure of the WWF. Figure 4-30 shows a fractured WWF wire (photograph taken after completion of testing). After the softening of the ECC, the load in the panel was carried solely by the remaining intact WWF. The small amount of intact reinforcement resulted in the low residual strength in Panel 1.

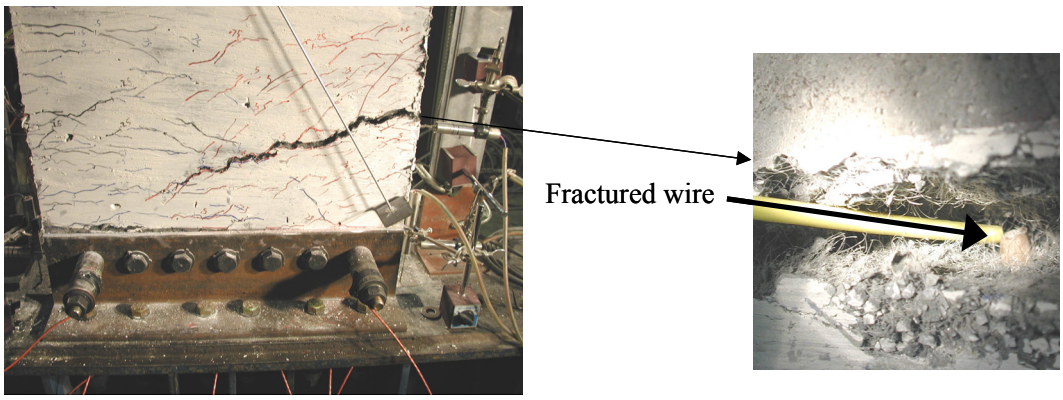

Figure 4-30 Fractured WWF at the base of Panel 1

Panels 2, 3, 4, and 6 used a combination of WWF reinforcement and a perimeter reinforcing bar for reinforcement. In all four of the panels the onset of softening occurred as the ECC material began to soften due to localization of strain at a single crack. As shown in table 4-5, and discussed in Section 4.3.2, the drift level at the onset of panel softening varied with the ECC material used in the panels. After localization of the ECC material occurred, some fracture or development failure of the WWF reinforcing steel occurred. Again, the sudden drops seen in the load-drift response of the panels indicated WWF failure.

The strain localization of the ECC material occurs at the base of the panel in the area immediately above the connection region. Figure 4-31 shows a photograph of localization in the ECC material in Panel 2. After the localization of the ECC material, the reinforcing steel holds the panel together, and the load carrying capacity of the panel is equivalent to the flexural capacity of the steel in tension and ECC in compression. Eventually, steel fractures in the WWF were observed. Fracture of the 9.5 mm reinforcing bar did not occur in any of the test panels.

In the base connection region, damage was only observed at the panel edges. The precompression of panel bolts held the material at the base of the panel intact. Figures 4.31and 4.32 show the intact portions of the connection region of Panels 2 and 6 after completion of testing. The intact material served to develop the perimeter reinforcing bar. The perimeter bar then served to provide the residual strength of Panels 2, 3, 4 and 6.

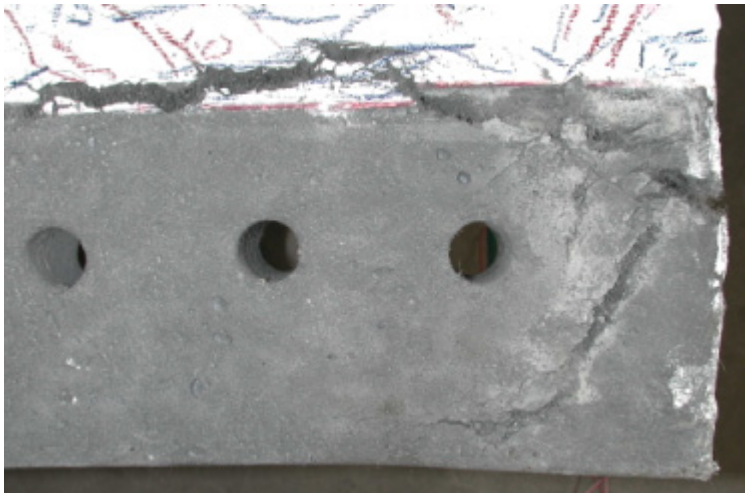

Figure 4-31. Connection region of Panel 2 after completion of testing

Figure 4-32. Connection region of Panel 6 after completion of testing

The failure of the concrete panel (Panel 5) was different in nature than that observed in the ECC panels. The low tensile strain capacity of the concrete resulted in the localization of a crack across the panel at low drift levels. After the localization of the concrete across the panel width, the reinforcing steel carried the panel load. Similar to the other panels, fracture and development failure of the WWF occurred during the testing. The low inherent toughness of the concrete, relative to the ECC, resulted in extensive spalling of the concrete in the connection region starting at approximately 1% drift; as is shown in figure 4-33. The spalling occurred as a consequence of the development failure of the perimeter bar at the base of the panel. Figure 4-34 shows the panel after completion of testing. Spalling of the concrete in the connect region resulted in the lower residual strength of Panel 5 relative to the ECC panels with similar reinforcement as the perimeter bar in Panel 5 was not fully developed.

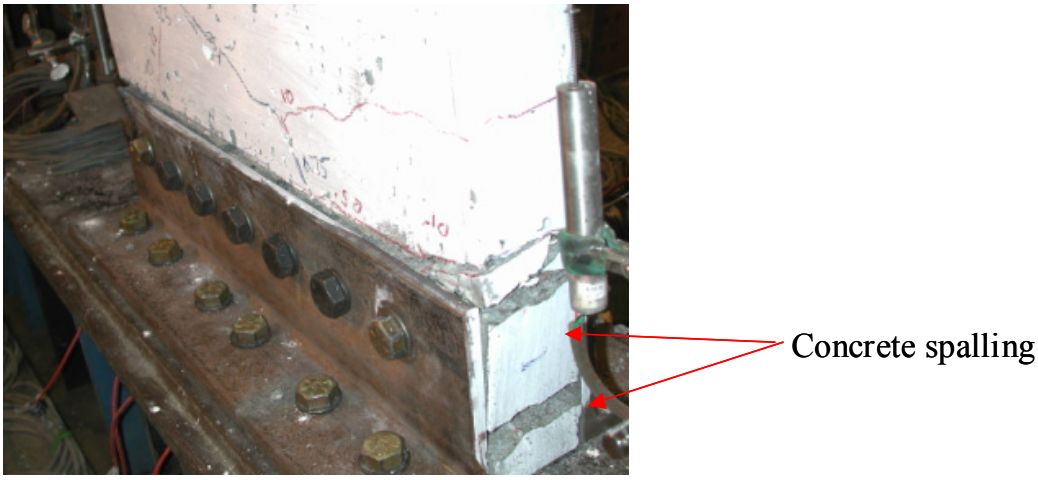

Figure 4-33. Spalling in connection region of Panel 5 at 1% drift

Figure 4-34. Connection region of Panel 5 after completion of testing

4.2.4 Panel Displaced Shape

The ten LVDTs installed on the panel sides allowed for the displaced shape of the panels to be examined. Figures 4.35 and 4.36 show typical load-displacement data obtained from the LVDTs from the east and west sides, respectively, of Panel 1.

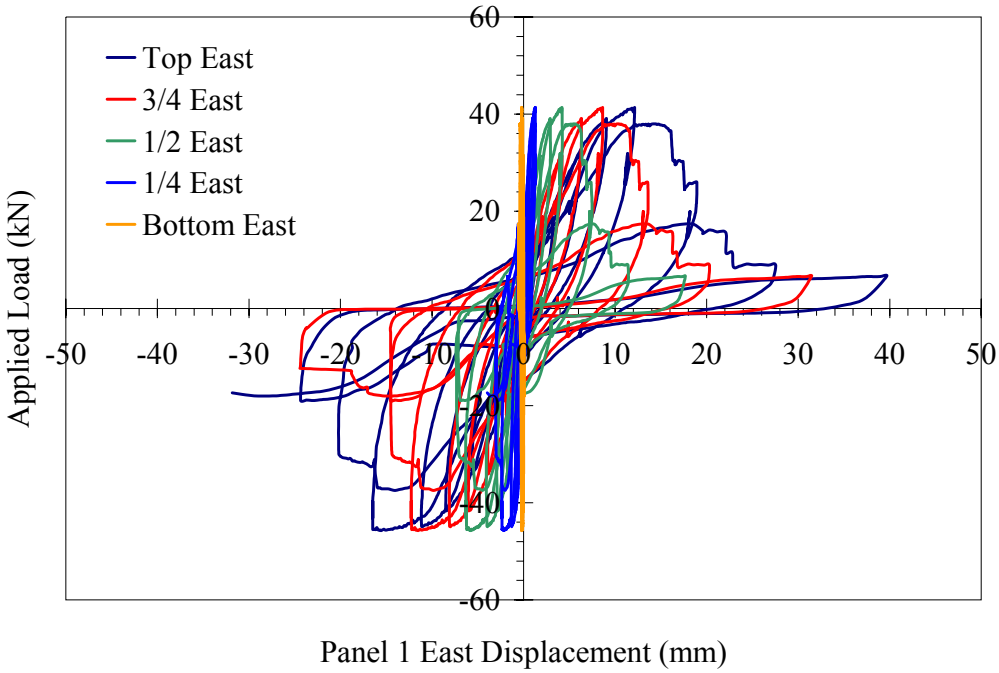

Figure 4-35. Panel displacement variation on east side of Panel 1

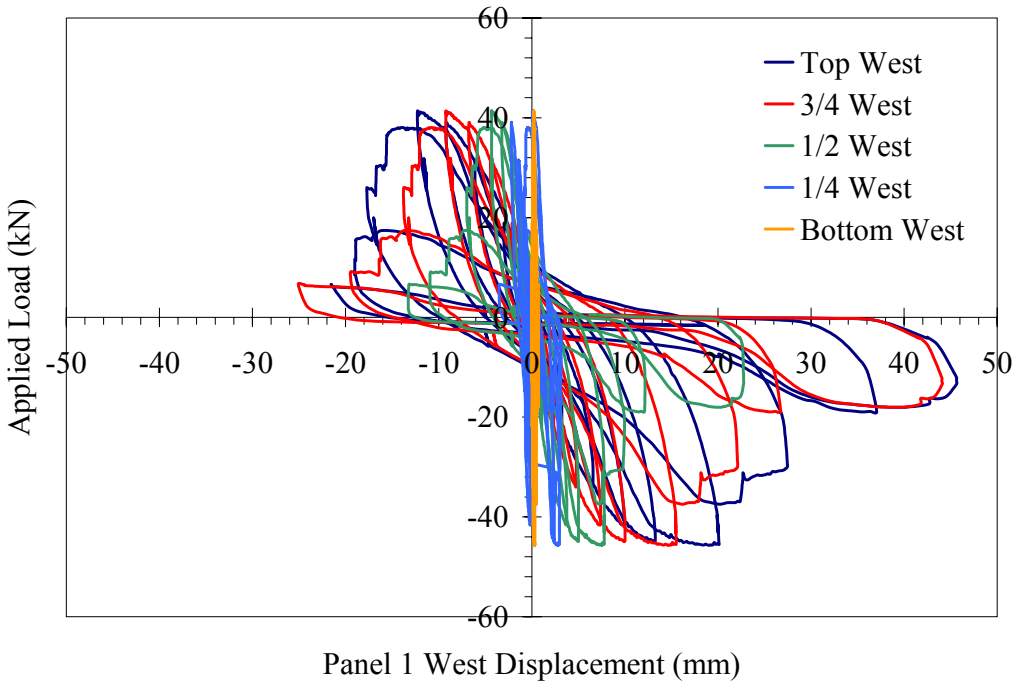

Figure 4-36. Panel displacement variation on west side of Panel 1

The displaced shape was investigated to try to observe flexural vs. shear deformation. To evaluate the panel displacements, the data shown in figures 4.35 and 4.36 was reduced to determine the displacement profiles at different drift levels. Figures 4.37 to 4.39 show typical displacement distributions, over the panel height, obtained from Panels 1, 3 and 6 at different drift levels. The displacements shown in the figures were obtained by averaging the recorded displacements on two panel edges.

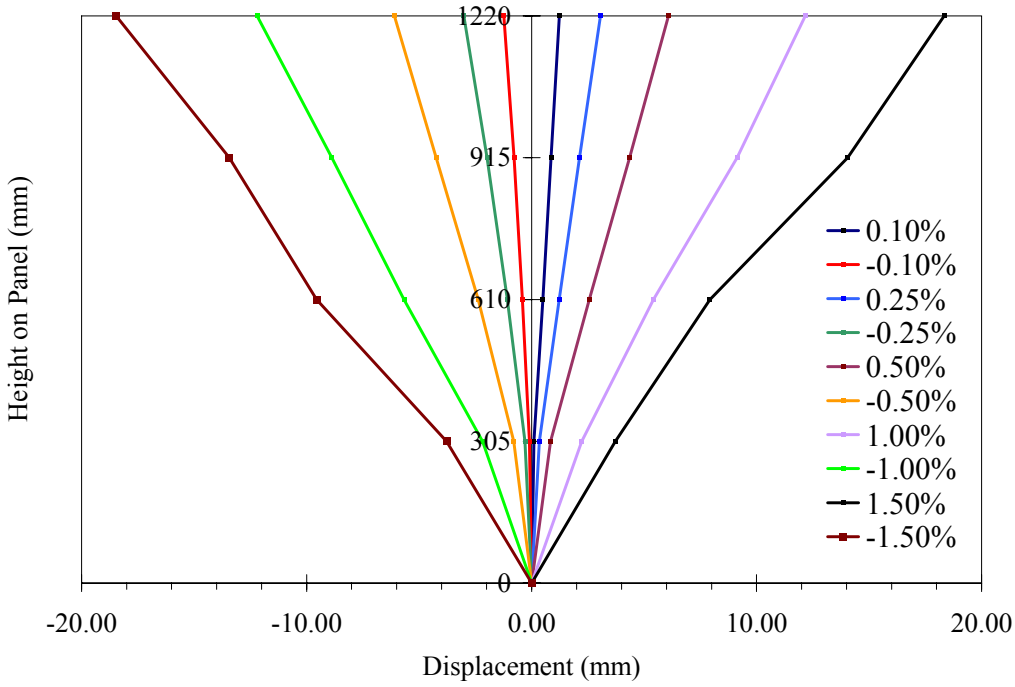

Figure 4-37. – Displacement profile across height of Panel 1

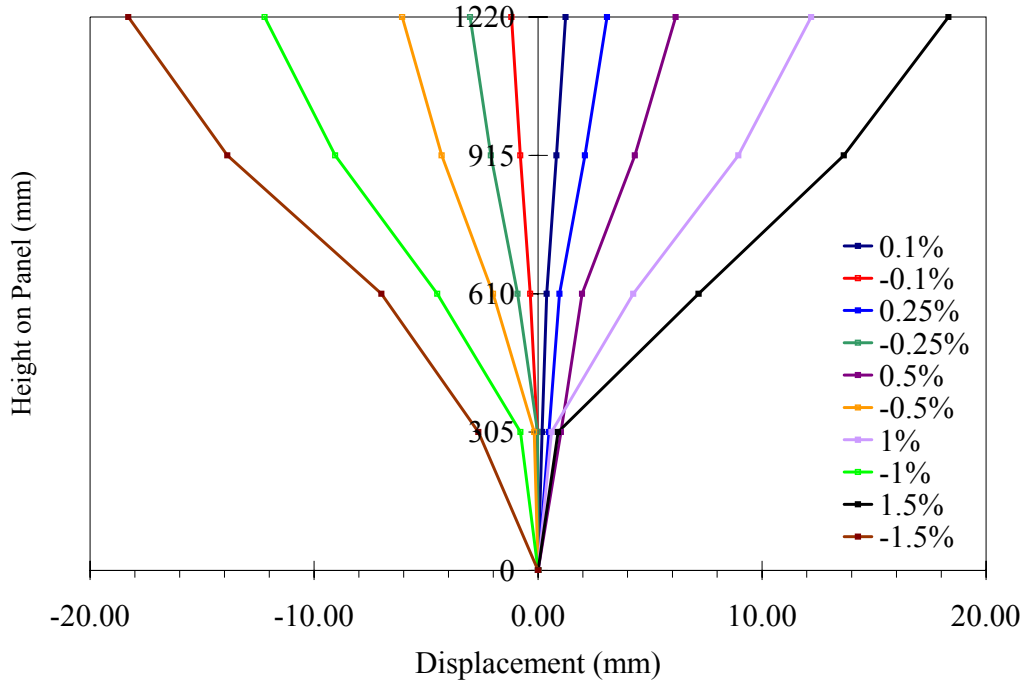

Figure 4-38. – Displacement profile across height of Panel 3

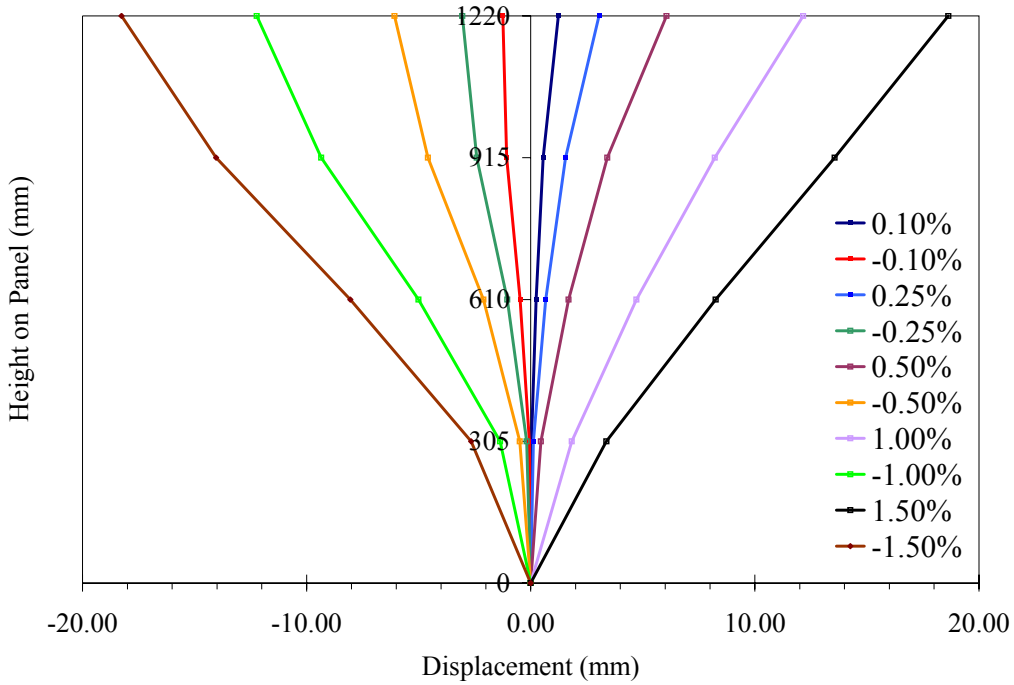

Figure 4-39. – Displacement profile across height of Panel 6

In the displacement profiles at drift levels before the onset of panel softening (mostly 0.75% to 1%), the response was indicative of predominantly flexural displacements. At higher drift levels, panel deformation was concentrated at the panel base causing the displacement profile to approach that of a rigid body.

4.2.5 Panel Slip

In the panel testing, two LVDTs were used to record the slip of the panels relative to the connection angles. To measure the slip, the LVDTs were installed at the base of the panels, with the rod of the LVDT attached to a tab, which was glued to the bottom of the panel. Figure 4-40 shows one of the LVDTs in place during testing on Panel 1.

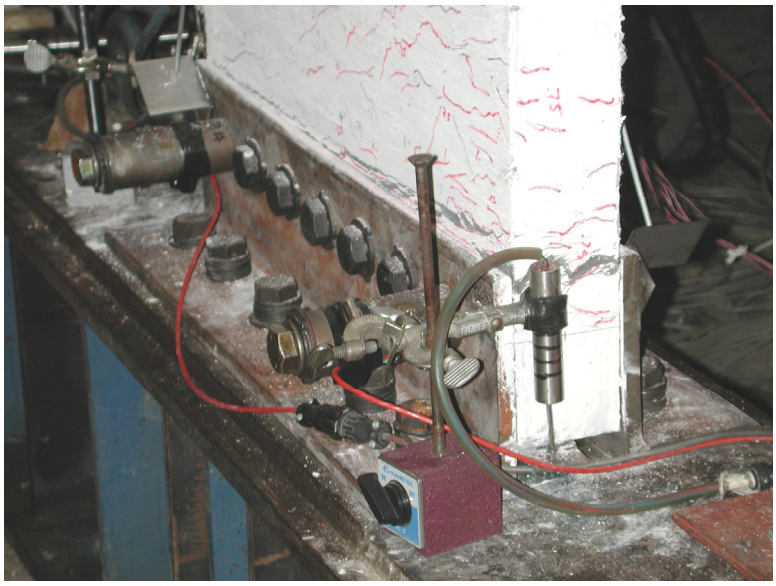

Figure 4-40. Panel slip LVDT in place

Slip of the panel base was not desirable because excessive slippage can result in the panel bearing on the connection bolts, which will decrease the capacity of the connections. Slip of the panel was also an indicator of rigid body motion of the panel. If excessive rigid body motion occurs the panel will not effectively dissipate energy by cracking of the ECC and yielding of the reinforcement. Figures 4.41 to 4.46 show the load versus slip displacement recorded during the tests on Panels 1 to 6. In the figures, increasing positive displacement indicates upward motion of the panel.

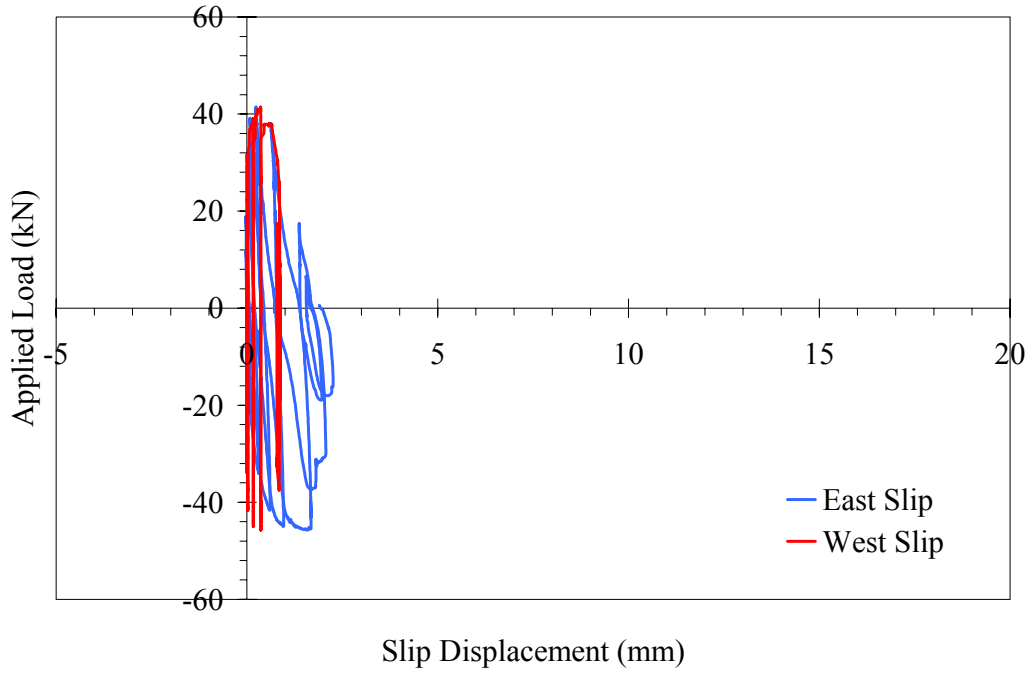

Figure 4-41. Slip at base of Panel 1

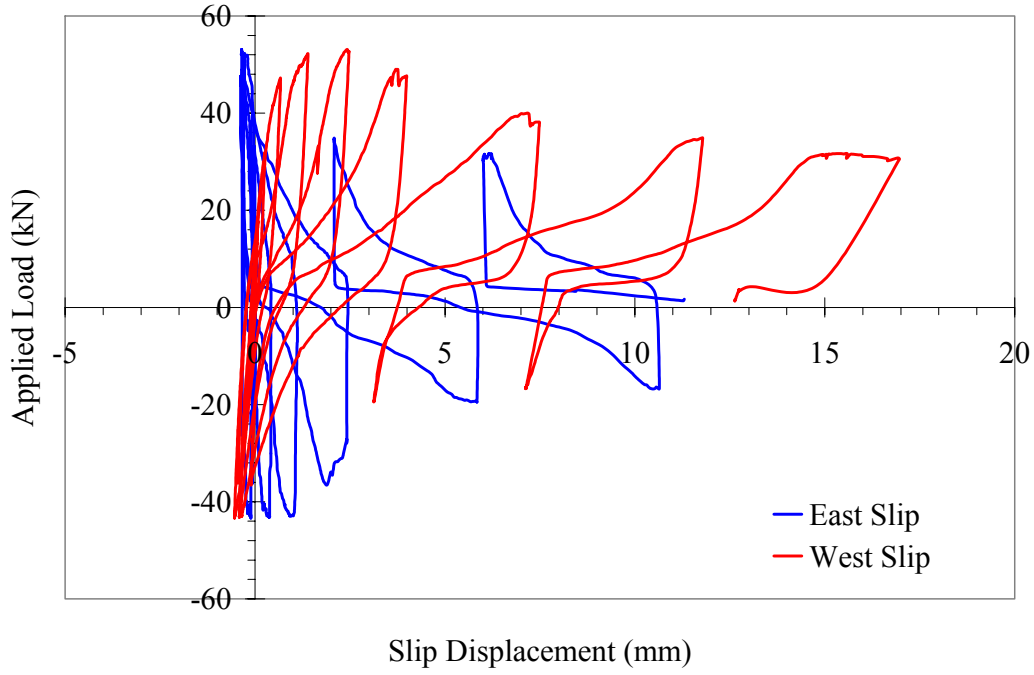

Figure 4-42. Slip at base of Panel 2

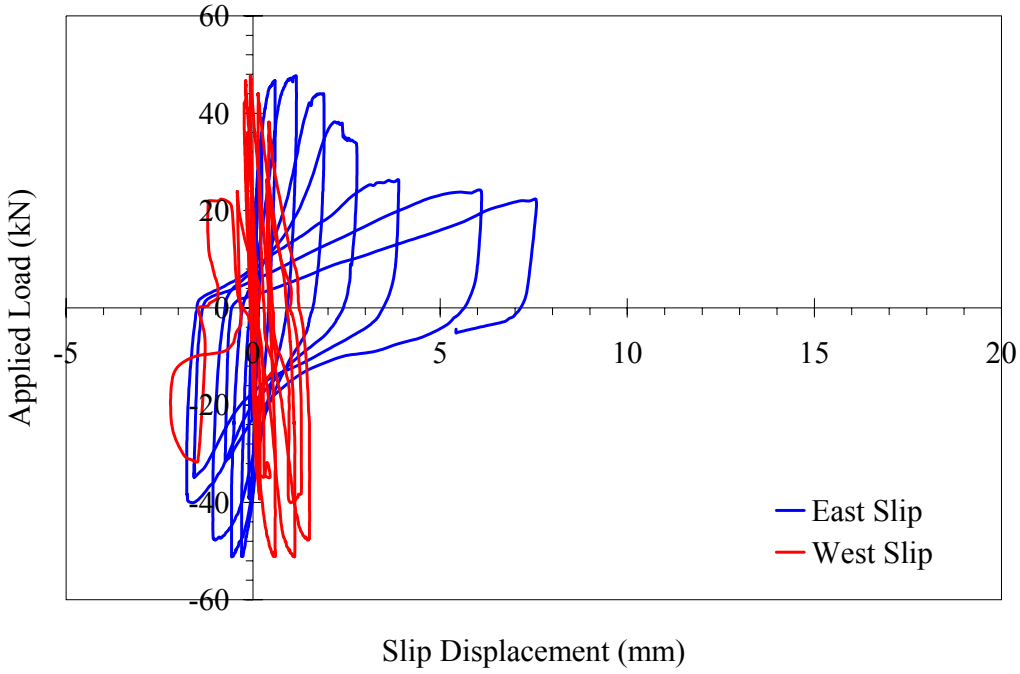

Figure 4-43. Slip at base of Panel 3

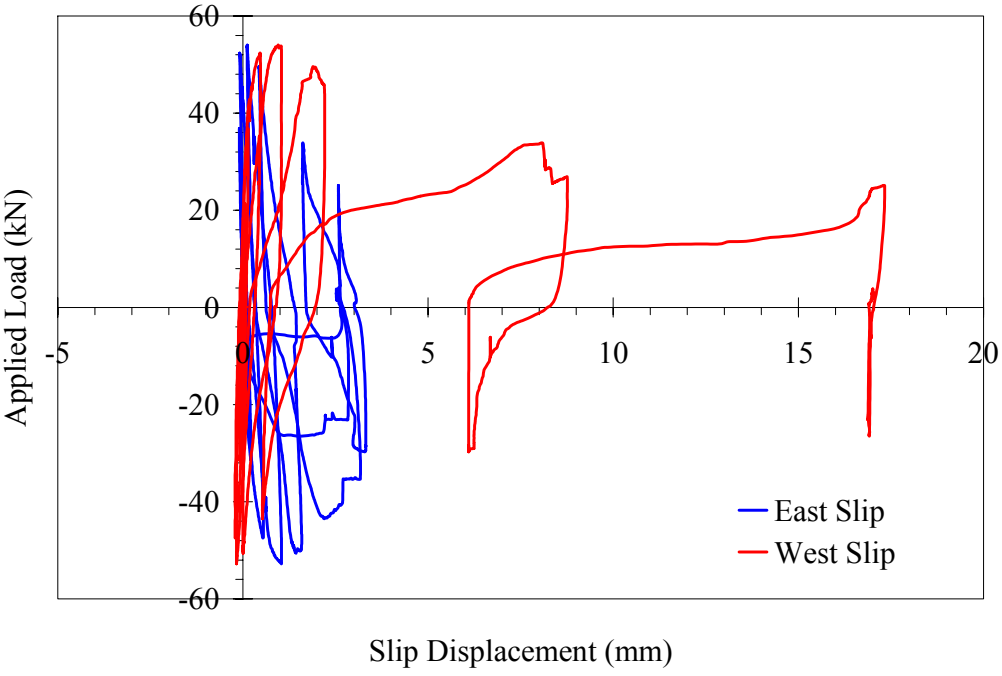

Figure 4-44. Slip at base of Panel 4

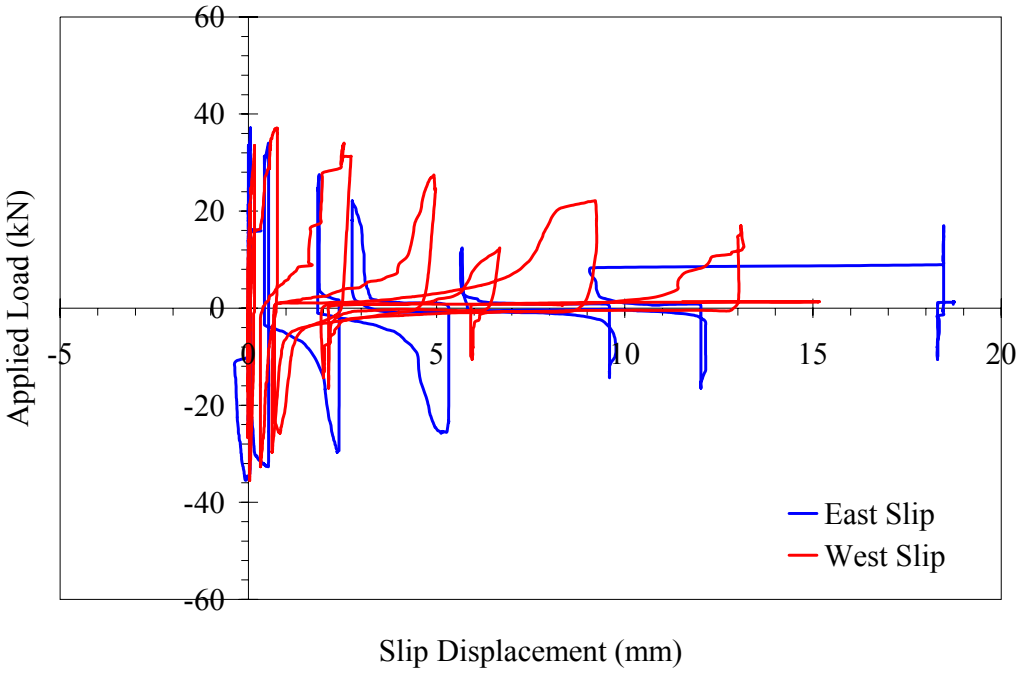

Figure 4-45. Slip at base of Panel 5

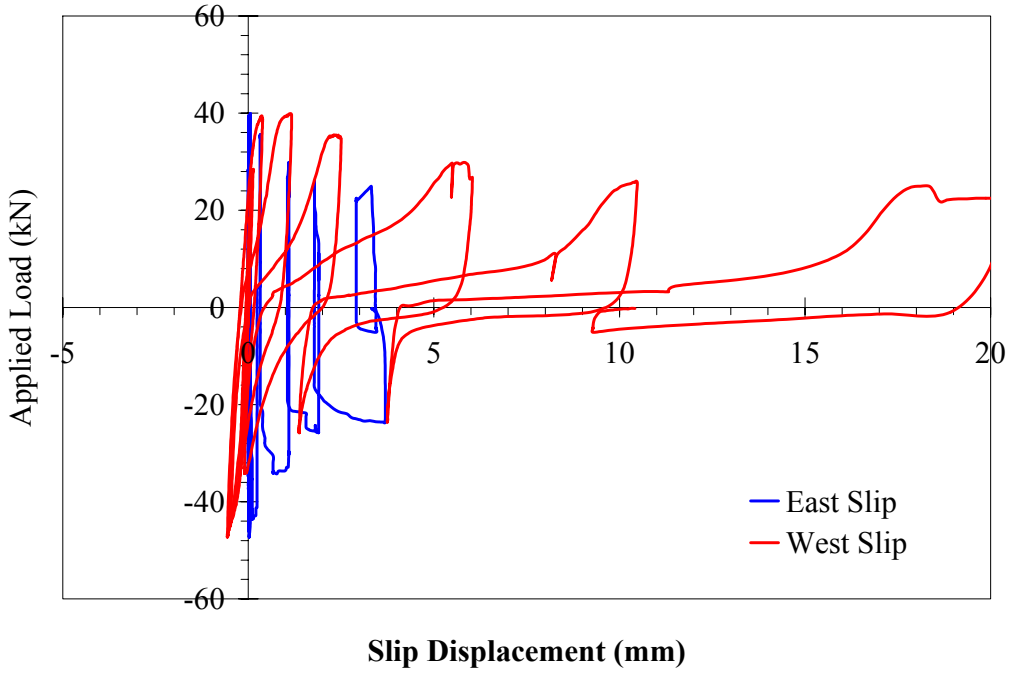

Figure 4-46. Slip at base of Panel 6

The results in figures 4.41 and 4.46 show the significant variation in slip observed in the testing results. The reason for the different magnitudes of panel slip was not apparent from the results. Panel 1 showed the lowest amount of panel slip (less than 2 mm) during the test. The remaining 5 panels showed larger amounts of slip on at least one side. In Panels 3, 4 and 6 the slip was not uniform, with one side showing significantly more slip, Panels 2 and 5 showed nearly even amounts of slip on both sides of the panel.

In general, the largest panel slip occurred after the onset of panel softening, with softening indicated by the drop in load capacity. The slip of the panels was also a contributing factor in the unsymmetrical load-drift response of the panels. For example, the results from Panel 2 show a relatively large slip occurred (approximately 2 mm) on the west side of the panel before the peak load was reached. The slippage of the panel was indicative of rigid body motion of the panel and contributed to the observed unsymmetrical load-drift response (see figure 4-15).

4.2.6 Out-of-plane Displacements

Out-of-plane displacement was measured to assess potential damage to the panels due to twisting. Out-of-plane displacements were recorded during all panel tests with the exception of Panel 1. Figure 4-47 shows an LVDT used to measure out-of-plane displacement during testing on Panel 4. The LVDTs were located on opposite corners at the top of the panel. The selected orientation of the LVDTs resulted in the LVDT displacement having the same sign when twisting of the panel occurs. Figure 4-48 shows typical output from the out-of-plane LVDTs from Panel 3.

Figure 4-47. LVDT used for measurement of out-of-plane panel displacement

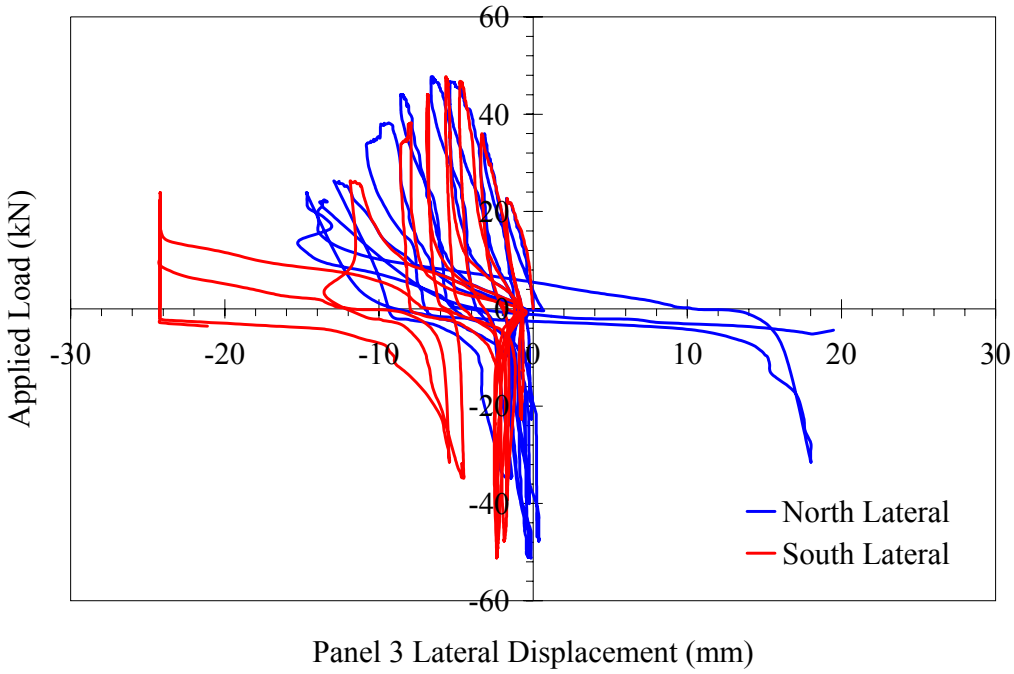

Figure 4-48. Out-of-plane displacements measured on Panel 3

The out-of-plane displacement of the panels was typically less than 5 mm (0.4%) before the onset of panel softening. Table 4-7 shows a summary of the measured out-of-plane displacements. The out-of-plane displacement of the panels was not found to have an impact on the peak strength of the panels or the drift at the onset of softening.

Table 4-7 – Summary of out-of-plane panel displacements

Panel[1]	Average Displacement at Peak Load (mm)	Average Displacement at ±1% Drift (mm)	Average Displacement at ±2% Drift (mm)
2	3.1	3.0 / 6.3	6.3 / 12
3	1.9	7.7 / 2.8	12 / 2.9
4	1.1	2.3 / 2.3	5.7 / 4.7
5	2.9	2.7 / 2.9	3.6 / 6.3
6	2.5	2.3 / 1.9	17 / 14

1. Out-of-plane displacements were not recorded on Panel 1

4.2.7 Steel Reinforcement Response

In the panel testing, bonded electrical strain gages were used to monitor the strain levels in the panel reinforcing steel. The location of the strain gages on the panels was shown in figures 4.7 (Panel 1) and 4.8 (Panels 2 to 6). Figures 4.49 to 4.52 show the applied load vs. measured strain from the strain gages on the reinforcing steel at the base of Panels 1 and 2. For simplicity the results were split into two groups representing the east (figures 4.49 and 4.51) and west (figures 4.50 and 4.52) sides of panels.

The results from the strain gages indicate the extent of yielding of the reinforcing steel. Yielding of the reinforcing steel occurred when the strain level exceeded approximately 0.00207 strain (2,070 microstrain), as determined from tension tests. Measured strains above this value indicate that energy dissipation due to plastic deformation of the steel has occurred.

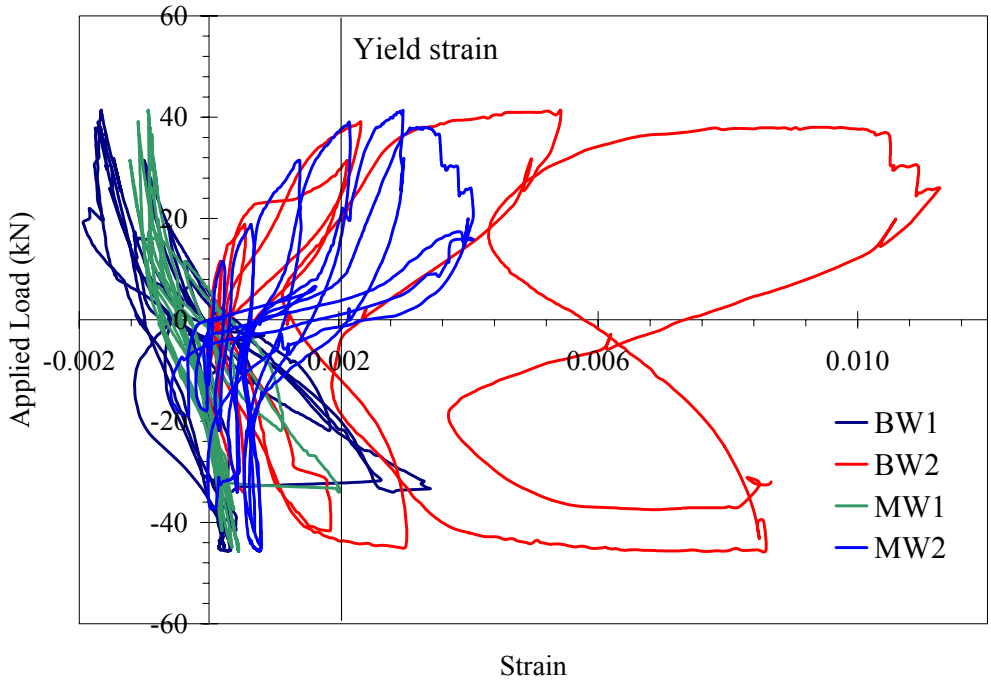

Figure 4-49. Strain gage results from base of Panel 1 (East side)

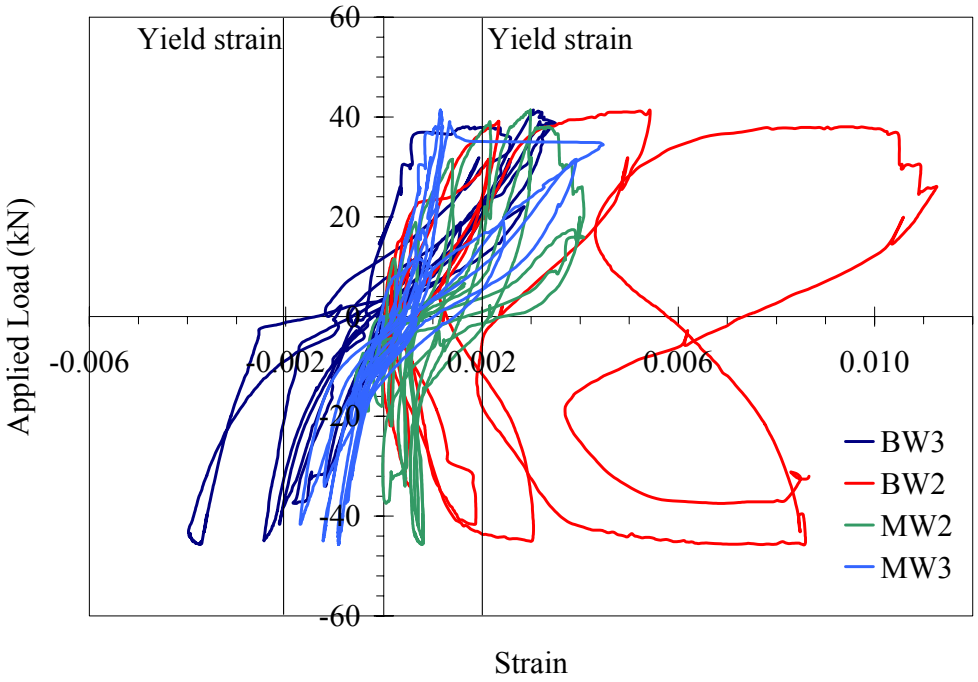

Figure 4-50. Strain gage results from base of Panel 1 (West side)

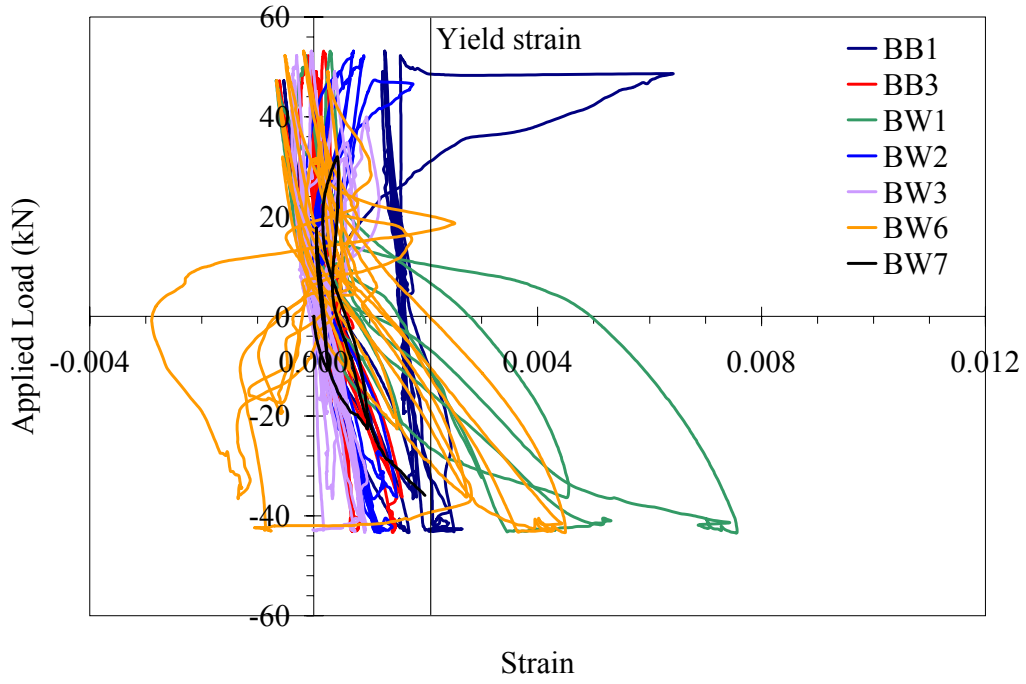

Figure 4-51. Strain gage results from base of Panel 2 (East side)

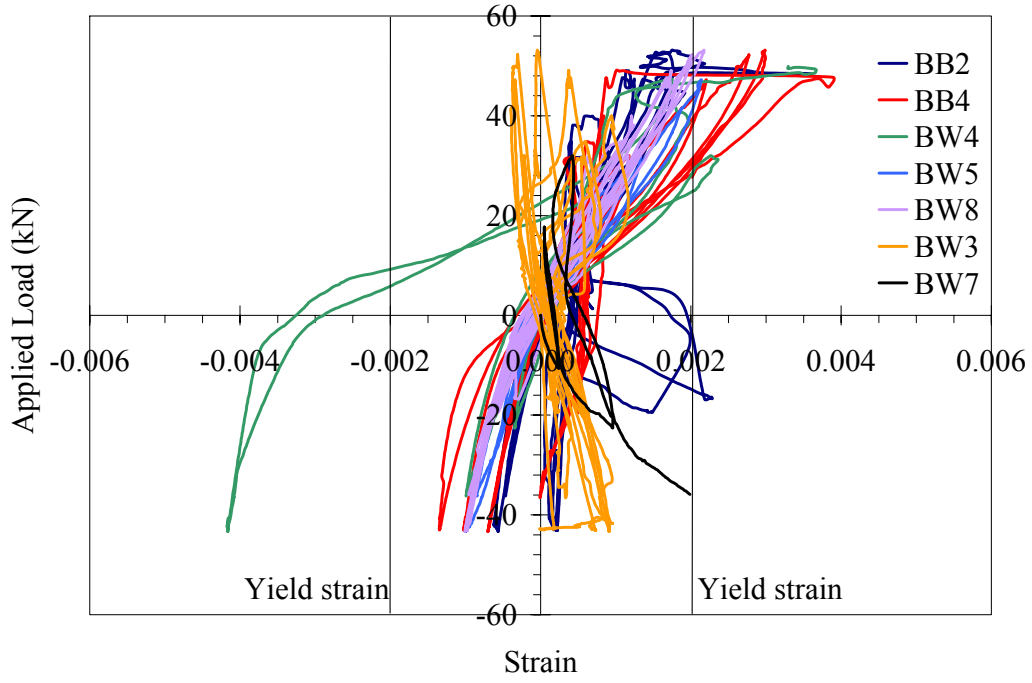

Figure 4-52. Strain gage results from base of Panel 2 (West side)

The results shown in figures 4.49 to 4.52 were representative of the results obtained from the strain gages. To simplify the examination of the strain gage results, tables 4-8 to 4-13 summarize the results from all of the panels. In the tables, data from strain gages from the panel base and middle of the panels at drift levels of +/-0.10%, +/- 0.25%, +/- 0.5% and +/- 1.0% are presented. These drift levels were selected to correspond to infill frame drift levels of interest as discussed in Section 4.5. The bold values in the tables were the measured strain values in excess of 2000 microstrain, which was the approximate yield strain in the reinforcing steel.

The results shown in tables 4-8 to 4-13 identify areas where the panel reinforcing steel has yielded. The use of strain gages to examine yielding of reinforcing steel was somewhat limited due to failure of some of the gages before and during testing. Furthermore, the yielding of the steel must occur at the location of the strain gage to be recorded. Yielding of the reinforcing steel away from the strain gages will not be captured by the strain gages.

Table 4-8 – Summary of strain[1] gage results from Panel 1

Strain	**Drift Level**			
gage	**+/- 0.10%**	**+/- 0.25%**	**+/- 0.50%**	**+/- 1%**
BW1	-347 / 644	-619 / 1834	-1001 / **2656**	-1662 / 227
BW2	131 / -75	534 / 134	**2130** / 538	**5423** / **3030**
BW3	757 / -422	1540 / -741	**2558** / -1178	**3041** / **2444**
MW1	-362 / 307	635 / 177	1385 / 436	-936 / 356
MW2	-10 / 204	1385 / 436	**2989** / 808	**2989** / 808
MW3	696 / -289	**2410** / -650	**3910** / -1215	1153 / -1327

1. All strain in microstrain

Table 4-9 – Summary of strain[1] gage results from Panel 2

Strain gage	Drift Level			
	+/- 0.10%	**+/- 0.25%**	**+/- 0.50%**	**+/- 1%**
BB1	-223 / 396	-427 / 1018	-534 / 1829	1280 / **2508**
BB2	350 / -221	1056 / -401	1395 / -468	1526 / 222
BB3	-261 / 400	-486 / 938	-611 / 1575	202 / 692
BB4	348 / -219	1177 / -457	**2202** / -606	**2973** / -1018
BW1	-222 / 496	-485 / 1502	-667 / **4463**	311 / **3449**
BW2	-10 / 110	377 / 436	1138 / 1486	686 / 1087
BW3	-128 / 232	-220 / 637	-340 / 852	-26 / 729
BW4	585 / -246	**2256** / -339	1689 / -990	*[2] / *
BW5	407 / -272	1330 / -506	**2134** / -842	* / *
BW6	-260 / 591	-556 / 1468	-662 / 2715	-174 / **3640**
BW7	49 / 224	426 / 942	* / *	* / *
BW8	416 / -339	1166 / -665	1823 / -910	**2166** / -980
MB1	-214 / 255	-500 / 765	-703 / 1533	-661 / 1364
MW2	-21 / 62	-2 / 173	474 / 1760	-225 / 1445
MB2	342 / -241	955 / -490	**2225** / -608	**3919** / -863

1. All strain in microstrain
2. * - Strain gage failed

Table 4-10 – Summary of strain[1] gage results from Panel 3

Strain gage	Drift Level			
	+/- 0.10%	**+/- 0.25%**	**+/- 0.50%**	**+/- 1%**
BB1	-287 / 946	-437 / 1992	-577 / **5301**	*[2] / *
BB2	341 / -268	**2816** / -487	**2598** / 861	* / *
BB3	-304 / 559	-495 / 1519	-645 / **2082**	-677 / **2048**
BB4	292 / -259	1519 / -460	1669 / -595	2142 / -445
BW1	* / *	* / *	* / *	* / *
BW2	-204 / 1010	-251 / 1229	-460 / 1348	-9 / 1544
BW3	221 / 421	-734 / 1108	* / *	* / *
BW4	773 / -173	824 / 97	462 / 122	1340 / 885
BW5	852 / -168	1944 / -305	**2584** / -147	**2000** / -119
BW6	-188 / 532	-146 / 1923	-75 / **3752**	-514 / **3269**
BW7	89 / 296	901 / 1127	1918 / **2237**	* / *
BW8	642 / -145	**2088** / -376	703 / -79	419 / -74
MB1	249 / -138	1020 / -232	1810 / -378	1932 / -240
MW2	37 / 89	234 / 279	967 / 1218	1554 / 1562
MB2	* / *	* / *	* / *	* / *

1. All strain in microstrain
2. * - Strain gage failed

Table 4-11 – Summary of strain[1] gage results from Panel 4

Strain gage	Drift Level			
	+/- 0.10%	**+/- 0.25%**	**+/- 0.50%**	**+/- 1%**
BB1	-83 / 90	-172 / 335	-225 / 590	*[2] / *
BB2	162 / -61	334 / -43	1401 / 157	1572 / -459
BB3	-218 / 658	-548 / 1714	-727 / **2701**	-1698 / **4334**
BB4	658 / -167	775 / -256	1147 / -378	1101 / -120
BW1	-252 / 323	-433 / 937	-660 / 1983	* / *
BW2	-56 / 454	-325 / 1839	-629 / 1826	-207 / 394
BW3	60 / 40	237 / 125	840 / 357	* / *
BW4	441 / -127	1126 / -235	* / *	* / *
BW5	852 / -275	-626 / -649	-14 / -615	-119 / -455
BW6	-175 / 396	-221 / 540	-185 / 586	-53 / 957
BW7	157 / 30	388 / 169	-364 / 536	1345 / 1222
BW8	165 / -92	85 / -128	68 / -202	38 / -321
MB1	-111 / 513	-330 / -1386	-500 / -**2423**	-438 / -**2760**
MW2	29 / 43	162 / 91	701 / 266	656 / 373
MB2	* / *	* / *	* / *	* / *

1. All strain in microstrain
2. * - Strain gage failed

Table 4-12 – Summary of strain[1] gage results from Panel 5

Strain gage	Drift Level			
	+/- 0.10%	**+/- 0.25%**	**+/- 0.50%**	**+/- 1%**
BB1	-64 / -33	-75 / -109	-91 / -236	-185 / -68
BB2	*[2] / *	* / *	* / *	* / *
BB3	-275 / 1230	-479 / 1977	-508 / **2734**	-632 / **2702**
BB4	-159 / -10	-97 / -12	-29 / 48	2 / 59
BW1	-117 / 47	-82 / 191	6 / 435	129 / **-2097**
BW2	-133 / -143	-80 / -148	4 / -133	7 / -5
BW3	89 / -7	264 / 309	374 / 784	146 / 861
BW4	102 / -117	129 / -371	* / *	* / *
BW5	852 / -275	-626 / -649	-14 / -615	-119 / -455
BW6	-175 / 396	-221 / 540	-185 / 586	-53 / 957
BW7	157 / 30	388 / 169	-364 / 536	1345 / 1222
BW8	165 / -92	85 / -128	68 / -202	38 / -321
MB1	-111 / 513	-330 / -1386	-500 / **-2423**	-438 / **-2760**
MW2	29 / 43	162 / 91	701 / 266	656 / 373
MB2	* / *	* / *	* / *	* / *

1. All strain in microstrain
2. * - Strain gage failed

Table 4-13 – Summary of strain[1] gage results from Panel 6

Strain gage	Drift Level			
	+/- 0.10%	**+/- 0.25%**	**+/- 0.50%**	**+/- 1%**
BB1	-53 / 167	-84 / 541	62 / 571	69 / 925
BB2	156 / -196	627 / -300	*[2] / *	/ *
BB3	-151 / 531	-285 / 1401	-429 / **2734**	-875 / **2915**
BB4	185 / -277	934 / -460	1997 / -536	**2257** / -730
BW1	-128 / 352	-228 / 1044	683 / -3399	930 / 1315
BW2	14 / 527	-27 / -1825	-451 / 1615	947 / 1091
BW3	20 / 193	-92 / 355	24 / 591	91 / 927
BW4	279 / -281	1317 / -425	7373 / -651	* / *
BW5	108 / -275	22 / -147	-78 / -302	120 / -112
BW6	-88 / -124	-39 / 1482	-370 / **2182**	-446 / **2135**
BW7	82 / 213	117 / 653	254 / 1006	556 / 1510
BW8	196 / -239	1055 / -290	1977 / -262	* / *
MB1	-226 / 552	-391 / 1456	-806 / **2700**	-768 / **2571**
MW2	42 / 227	767 / 1707	559 / 1579	473 / 888
MB2	310 / -380	1334 / -608	**2337** / -804	**2339** / -718

1. All strain in microstrain
3. * - Strain gage failed

All of the panels showed some amount of reinforcing steel yielding, with yielding typically observed to start at a drift of 0.25%. The extent of yielding varied in the tested panels. In Panel 1, yielding was observed in nearly all of the strain gages at 1% drift, including the gages located at mid-height of the panels. The extensive yielding of reinforcing in the panel was consistent with the large number of cracks observed in the ECC (figure 4-27). The strains at the panel bottom were observed to be generally symmetric, which was seen in comparisons of results from gages BW1 and BW3 (located on opposite sides of the panel) at all drift levels. The panel's load-drift response was also symmetric as seen in figure 4-14.

The results from Panel 2 were generally similar to Panel 1, with large amounts of reinforcing steel yielding in the panel. Below 0.5% drift, the strains at the panel base were symmetric

(comparison of gages BB1 and BB3 or BB2 and BB4). Above 0.5%, the strains become less symmetric.

In Panel 3, less yielding of the reinforcing steel occurred, compared to Panels 1 and 2. Yielding of the gages at mid-height was not observed in Panel 3. The results from Panel 3 were somewhat limited by the premature failure of three of the fifteen gages on the panel.

Panel 4 showed the lowest amount of yielding of the tested ECC panels, possibly due to the gages not being located at the crack locations. Yielding was observed in three of the strain gages in the panel. In addition to the low number of yielded gages, the gage readings were not symmetric in nature at low drift levels. The lack of symmetry in the results was not observed in the load-drift response or the cracking response.

The results from the concrete panel (Panel 5) were similar to those from Panel 4. Yielding of the reinforcing steel was observed in only two locations. The development failure or fracture of the reinforcing was apparent in the very low strains recorded by gages BB4, BW2 and BW8 at 1% drift. The low strain level in these gages was consistent with the low residual strength in the panel.

The tapered panel (Panel 6) showed extensive yielding of the reinforcing steel, beginning at 0.5% drift, in gages both at the panel base and at mid-height in the panel. At mid-height of the panel symmetric yielding of the reinforcing steel was observed. These results demonstrate the effectiveness of the tapered geometry in distributing strains in the panels.

4.2.8 Energy Dissipation

One of the primary motivations for the installation of the ECC infill retrofits is to increase the energy dissipation in a structure. The energy dissipation in the tested panels can be evaluated by calculating the area enclosed by the hysteretic loops (from load vs. displacement graphs) for each cycle during the test. To calculate the area, the trapezoidal rule can be used as shown in figure 4-53, using (4-3) for the calculation. The results of the energy dissipation calculations are summarized in table 4-14, and shown graphically in figure 4-54.

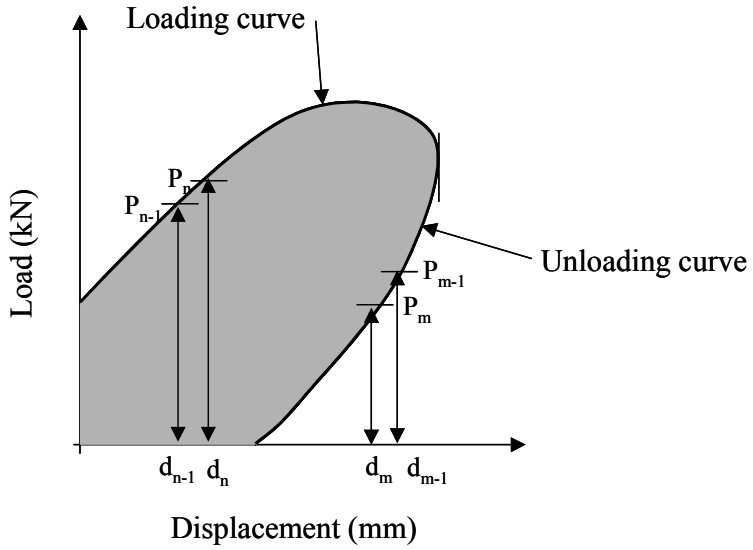

Figure 4-53. – Graphical explanation of trapezoidal rule to calculate energy dissipation from load-displacement results

$$E = A_{loading} - A_{unloading} = \sum_{n=1}^{p\_load} \frac{1}{2}(d_n - d_{n-1})(P_n + P_{n-1}) - \sum_{n=1}^{p\_unload} \frac{1}{2}(d_{m-1} - d_m)(P_m + P_{m-1}) \quad (4\text{-}3)$$

where:

E = Energy dissipated during hysteretic loop
$A_{loading}$ = Area under loading curve
$A_{unloading}$ = Area under unloading curve
p_load = number of points on loading curve
p_unload = number of points on unloading curve

Table 4-14 - Summary of Energy Dissipation in Tested Panels

Panel	Energy Dissipation (kN-m) at Different Panel Drift Levels						
	0.1%	**0.25%**	**0.5%**	**0.75%**	**1%**	**1.5%**	**2%**
1	0.0183	0.0762	0.238	0.533	1.01	2.01	2.96
2	0.0149	0.0794	0.273	0.680	1.25	2.11	3.44
3	0.0281	0.129	0.449	0.981	1.65	2.71	3.71
4	0.0229	0.105	0.353	0.836	1.55	-[1]	3.20
5	0.0259	0.102	0.324	0.669	1.04	1.53	1.83
6	0.0216	0.0963	0.323	0.750	1.32	2.21	3.10

1. Panel 4 was inadvertently not unloaded at 1.5% drift

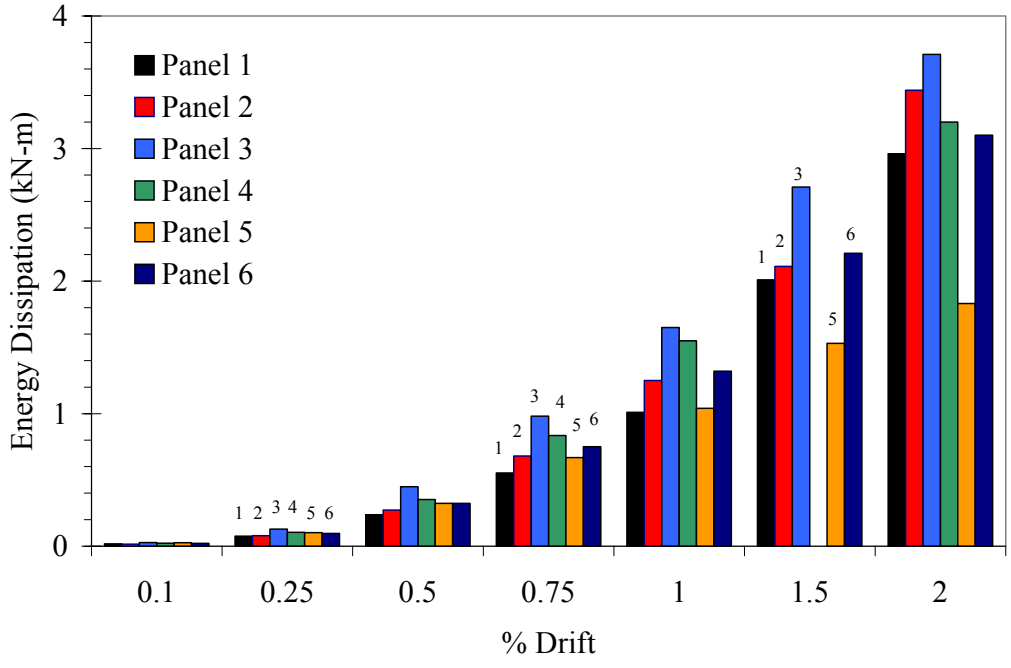

Figure 4-54. Comparison of energy dissipation at various drift levels

The energy dissipation in Panels 2, 3, 4 and 6 were generally similar, with Panel 3 having the highest energy dissipation at all drift levels. At low drift levels (less than 0.75%) Panel 1 had the lowest energy dissipation; while at higher drifts Panel 5 had the lowest energy dissipation.

The energy dissipation in the panels occurs as a consequence of the strain hardening of the ECC materials and plastic deformation of the reinforcing steel. The extent of reinforcing steel strain in an individual panel can be estimated using the results shown in tables 4-8 to 4-13.

The large amount of reinforcing steel yielding in Panel 6 (table 4-13) results in the large amount of energy dissipation the panel despite its lower stiffness and peak strength (table 4-5) when compared to Panels 2, 3 and 4. The tapered geometry of Panel 6 resulted in efficient spreading of cracking in the panel and allowed for significant yielding of the reinforcing steel. The energy dissipation observed in Panel 4 was inconsistent with the low amount of yielded reinforcing steel measured (table 4-11). The amount of energy dissipation in the panel suggests that yielding of the reinforcing steel in Panel 4 was not captured by the strain gages.

4.2.9 Panel Bolt Load Cells

During testing, four load cells were used to monitor the loads in the panel bolts. The location of the panel bolt load cells was shown in figure 4-9. The bolt forces measured during testing can be used to determine if significant losses in bolt tension, due to ECC creep and shrinkage, occur during the testing period. The load cells at the base of the panel also indicate damage in the connection region. Figures 4.55 and 4.56 show the measured bolt force versus panel drift results obtained from Panels 2 and 3, respectively. These results were selected as they represent typical test data.

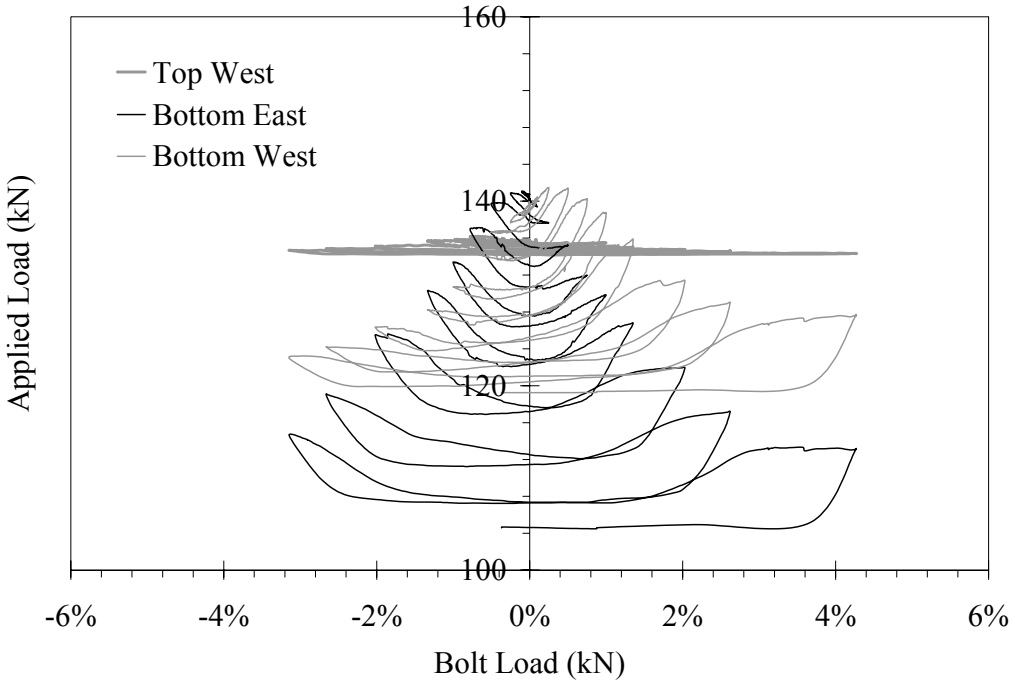

Figure 4-55. Variation of load in panel bolts versus drift in Panel 2

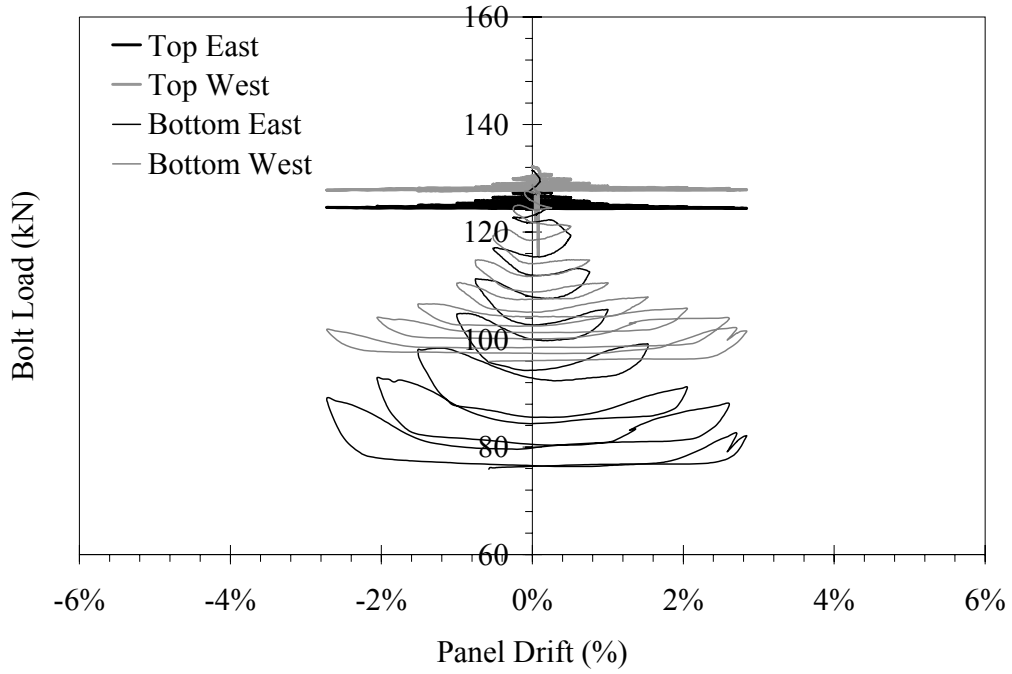

Figure 4-56. Variation of load in panel bolts versus drift in Panel 3

In the figures, the top panel bolts show very small changes in bolt force during the testing period. This indicates that losses in bolt tensioning force due to ECC creep and shrinkage during testing was not significant. Losses due to panel damage would not be expected at the top of the panel.

The results from the panel bolts at the base of the panel showed significant changes in bolt force during the testing. The decrease in bolt tension increased with increasing levels of drift. The loss of bolt tension was due to damage in the connection regions. The interaction of the variation in panel bolt tension force with the observed panel slip (discussed in Section 4.2.5) will be further examined in Section 4.3.

4.2.10 Panel Connection Bolts

The variation in the connection bolt loads (connecting the angles with the reaction beam) during testing partially represents the distribution of load across the base of the panel. The orientation of the connection bolts was shown in figure 4-10. To determine the distribution of load across the panel, the results from the bolts pairs (e.g., bolts 1 and 7) at the same distance from the panel edge were grouped. The relative change in bolt tension pairs during testing was evaluated by subtracting the initial load in the bolt from the measured bolt load. This information was used to examine the tensile load applied by the panel to the stiffened reaction beam.

Prior to examining the results of load distribution across the base, the drift in bolt tension was removed. The drift in bolt tension occurred due to small changes in the location of the panel during testing, such as movement caused by slip of the panels. The small changes resulted in changes in the location and relative orientation of the steel connection angles, and hence changes in measured connection bolt tension.

The drift was removed by locating the test points with zero load applied to the panels. The value of the bolt tension at these points was set to equal the initial bolt tension (removing the drift in bolt tension). The points in between the zero points were linearly adjusted, by applying a weighted average of the offset values applied at the zero points. Figure 4-57 shows the raw tension bolt data obtained from Panel 6, while figure 4-58 shows the same data with the drift removed.

The corrected change in connection bolt tension results for Panels 1-5 are shown in figures 4.59 to 4.63. In these figures, the x-axis represents the test step number. In figures 4.59 to 4.63 the positive values represent the increase in panel connection bolt tension due to applied tensile loads in the connections. The panel connection bolts provide the only means in the panel tests for the transfer of tensile loads. In contrast, bearing of the connection angles on the stiffened reaction beam carries the compressive loads. Because the compressive loads were carried in bearing, the decrease in bolt tension when the bolts are in a compression region cannot be analyzed to aid in the determination of load distribution in the connection region.

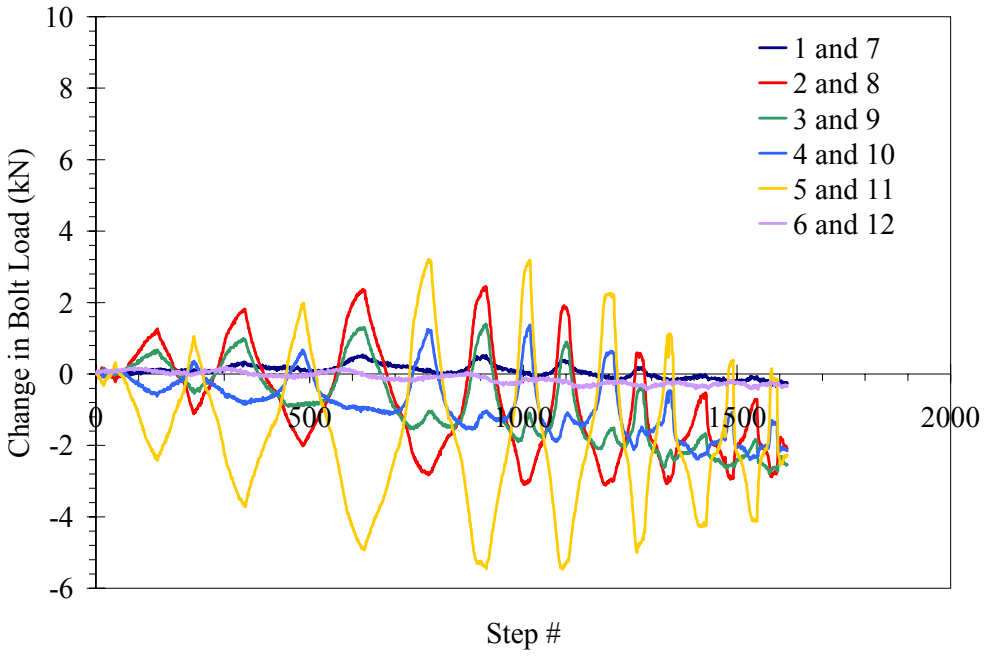

Figure 4-57. Raw data from Panel 6 connection bolts

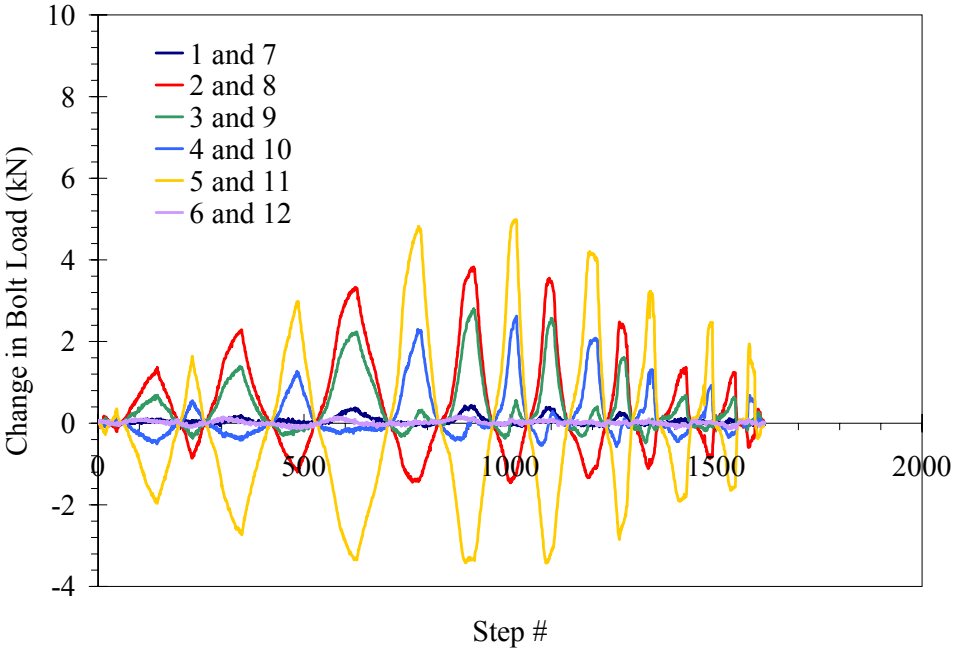

Figure 4-58. Results from Panel 6 connection bolts with drift removed

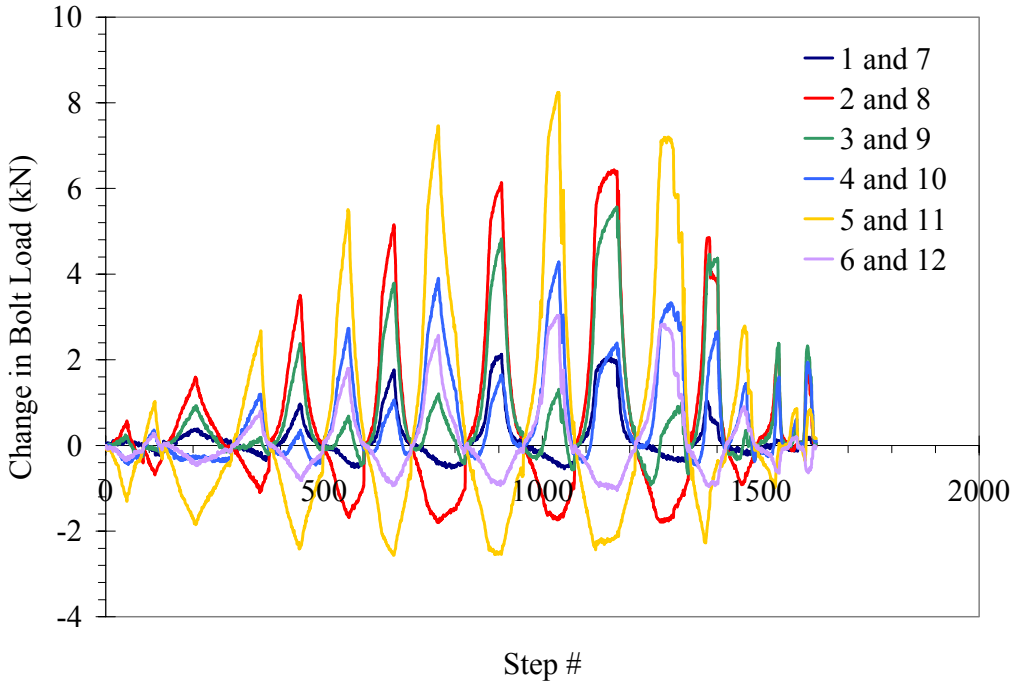

Figure 4-59. Results from Panel 1 connection bolts with drift removed

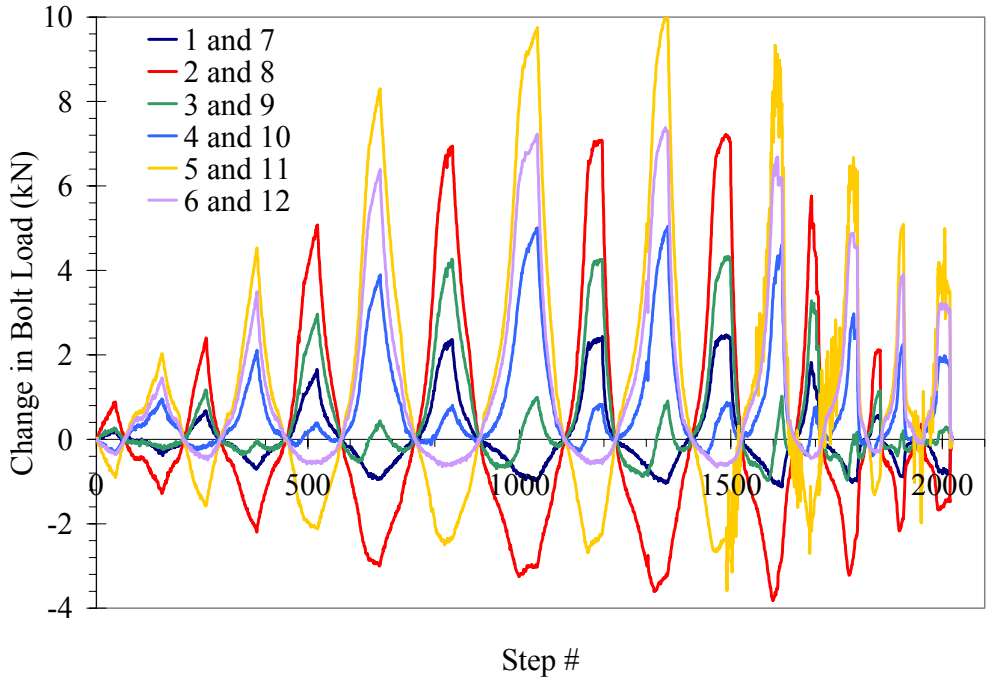

Figure 4-60. Results from Panel 2 connection bolts with drift removed

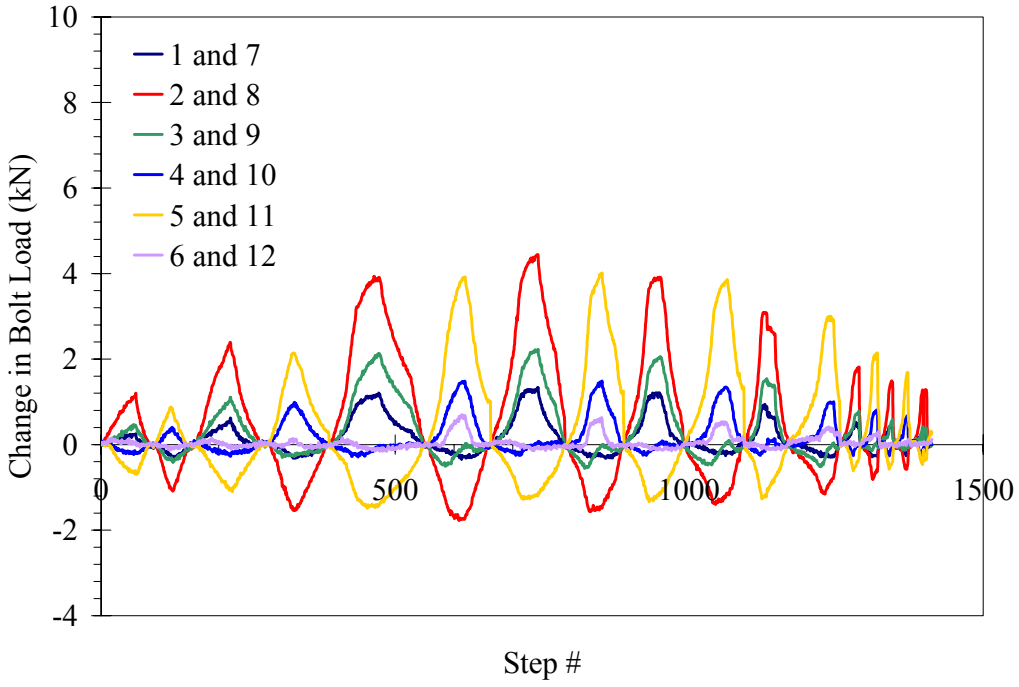

Figure 4-61. Results from Panel 3 connection bolts with drift removed

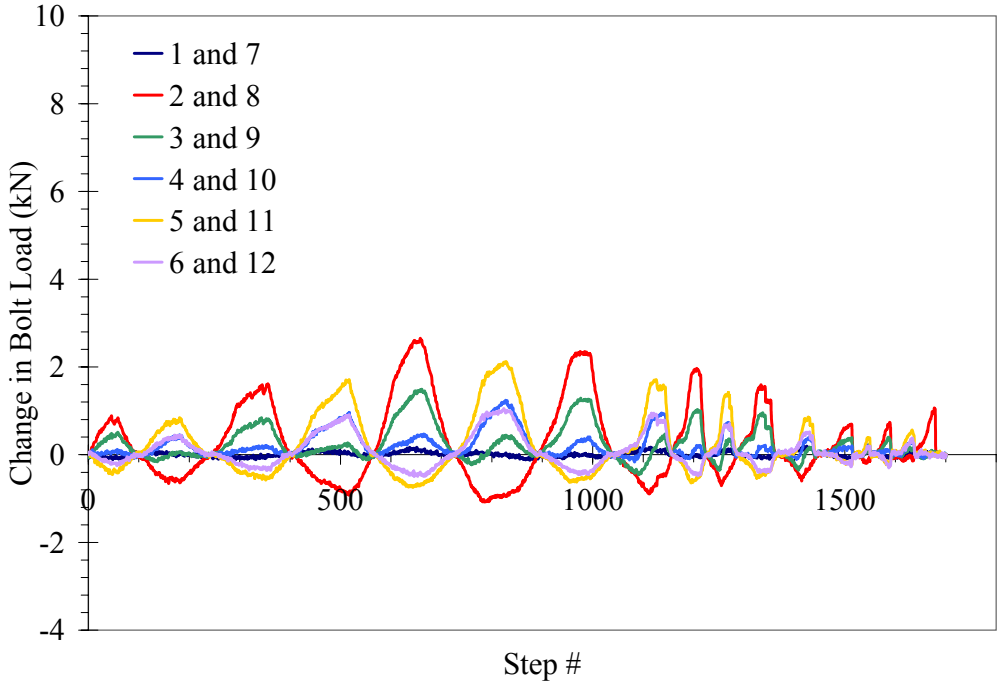

Figure 4-62. Results from Panel 4 connection bolts with drift removed

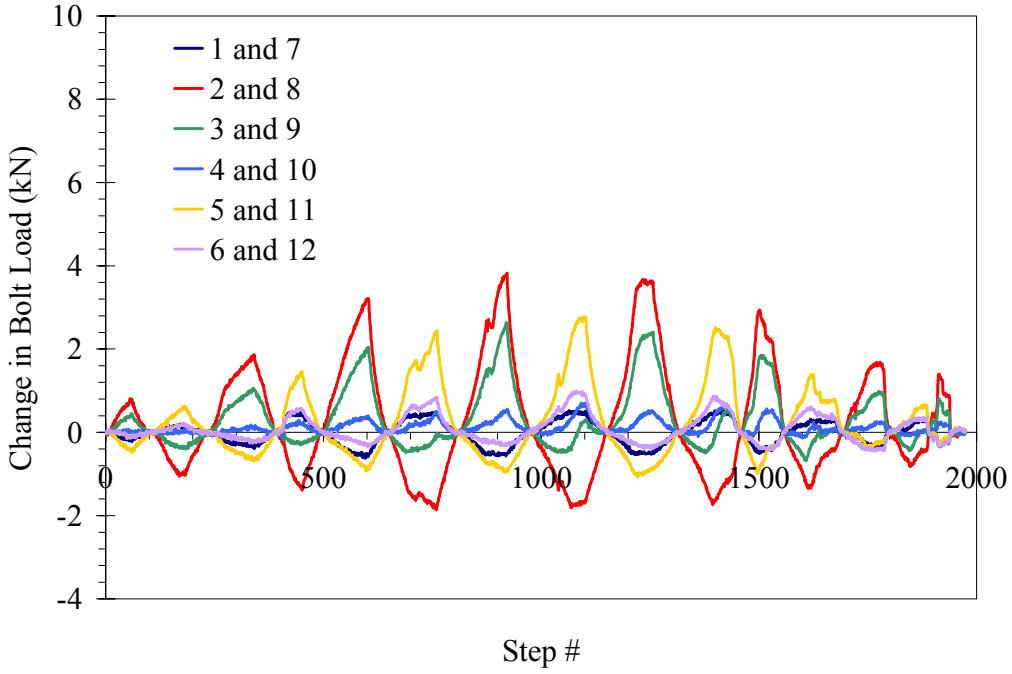

Figure 4-63. Results from Panel 5 connection bolts with drift removed

In all panel results, a greater change in load was observed in the second set of bolts from the panel edge (Pairs 2 and 8 or 5 and 11), than in the bolts closest to the edge. This observation will be addressed further in Section 5.2.5.

In the panel installation two different pretensioning values were used for the panel connection bolts (Section 4.1.6). The magnitude of change in bolt load shown in figures 4.58 to 4.63 was related to the magnitude of the pretensioning force. Panels 1, 2 and 6 used a pretensioning force of 67 kN on the bolts, and show greater changes in bolt tension that was observed in Panels 3, 4 and 5 which used a pretensioning force of 111 kN. The greater clamping force provided by the higher preload resulted in the smaller observed changes in bolt load during testing, i.e., the panel was better held in place by the bolts during testing. The results in figures 4-58 to 4.63 will be further analyzed in the Section 4.3.6 to evaluate the transfer of load in the connection region.

4.3 Evaluation of Infill Test Results

The infill panel tests were developed to examine the effect of different variables such as ECC mix designs, reinforcement details and panel shape on various measures of performance. The most important measures used to compare the different panel types were the load-drift response, peak load and drift capacity, energy dissipation and failure mechanisms. In this section, the effect of the different panel variables on these performance measures is examined. The results are further studied in Sections 4.3.6 to 4.3.8 to determine how the panel behavior and construction can be improved for future study.

4.3.1 Comparison of Panel Strength and Stiffness

The loads applied to the panels at various drift levels are summarized in tables 4-15 and 4-16. Table 4-17 shows the stiffness of the panels at each drift level. The stiffness was determined by dividing the average load (at positive and negative drift) by the displacement at each drift level. These results show the variation in strength and stiffness that can be achieved with the different reinforcement levels and materials used.

The highest strength was achieved in Panels 3 and 4, which were identically reinforced, and made with the SP-A and RECS-A material, respectively. The lowest peak strength was observed in Panel 1, which was cast without the 9.5 mm perimeter bar. However, Panel 1 was able to reach the highest drift level before a decrease in capacity occurred. Panel 6, which had a reduced cross-section, had similar strengths as Panels 2, 3, and 4. The panel stiffness variation follows the same trends as observed in the strength. The observed variations in strength and stiffness will be further discussed in Sections 4.3.2 to 4.3.4.

The peak strength of Panel 1 (45 kN) was nearly identical to its calculated ultimate strength of 44 kN. Similarly the ultimate strengths of Panels 2-4 (53, 51 and 54 kN) compared favorably with the calculated strength of 54 kN. The observed peak strength of the tapered panel (47 kN) was slightly lower than the expected 54 kN.

Table 4-15 - Summary of Panel Loads at Positive Drift Levels

Panel	Panel Load (kN) at various drifts						
	0.1%	**0.25%**	**0.5%**	**0.75%**	**1%**	**1.5%**	**2%**
1	12.9	21.9	34.0	41.7	45.0	45.5	29.9
2	17.6	32.0	47.2	52.3	52.7	47.6	38.1
3	22.7	35.9	46.7	47.7	44.0	33.9	26.3
4	21.3	36.8	51.8	53.8	45.9	40.2[1]	35.4
5	21.3	33.5	36.1	31.3	24.7	18.2	12.4
6	17.7	28.4	38.7	39.9	34.7	26.8	26.0

1. Panel 4 was inadvertently not unloaded at 1.5% drift, load shown was obtained on loading to 2% drift

Table 4-16 - Summary of Panel Loads at Negative Drift Levels

Panel	Panel Load (kN) at various drifts						
	-0.1%	**-0.25%**	**-0.5%**	**-0.75%**	**-1%**	**-1.5%**	**-2%**
1	11.5	18.8	31.4	39.1	41.4	26.	9.0
2	10.6	22.5	36.2	43.3	43.2	42.9	26.9
3	22.7	39.3	51.1	51.2	47.6	38.2	23.9
4	18.2	31.4	47.5	52.8	50.1	25.7[1]	26.9
5	17.2	26.6	34.8	32.7	29.1	23.5	13.6
6	23.2	34.7	44.7	47.3	41.2	32.8	25.8

1. Panel 4 was inadvertently not unloaded at 1.5% drift, load shown was obtained on loading to 2% drift

Table 4-17 - Summary of Panel Stiffness at Various Drift Levels

Panel	Panel Stiffness (kN / mm) at various drifts						
	0.1%	**0.25%**	**0.5%**	**0.75%**	**1%**	**1.5%**	**2%**
1	10.0	16.7	10.7	6.6	3.5	2.0	0.8
2	11.6	22.3	13.7	7.8	3.9	2.5	1.3
3	18.6	30.8	16.0	8.1	3.8	2.0	1.0
4	16.2	28.0	16.3	8.7	3.9	1.8	1.3
5	15.8	24.6	11.6	5.2	2.2	1.1	0.5
6	16.8	25.9	13.7	7.1	3.1	1.6	1.1

4.3.2 Effect of Reinforcing Type

Two different reinforcement types were used in the panel construction. Panel 1 had 0.44% WWF (by area), while the remaining panels were reinforced with the same amount of WWF and an additional 9.5 mm perimeter bar. Figure 4-64 shows a comparison of the load-drift response from Panels 1 and 2, which are both made with the SP material. The comparison in figure 4-64 as well as tables 4-15 to 4-17, show that the perimeter bar increase the strength by 5 kN (10%) and stiffness by 11% at 1% drift. Energy dissipation was increased by 25% due to yielding of the perimeter bar. The perimeter bar also increased the residual strength of the panels, as seen in Table 4-5.

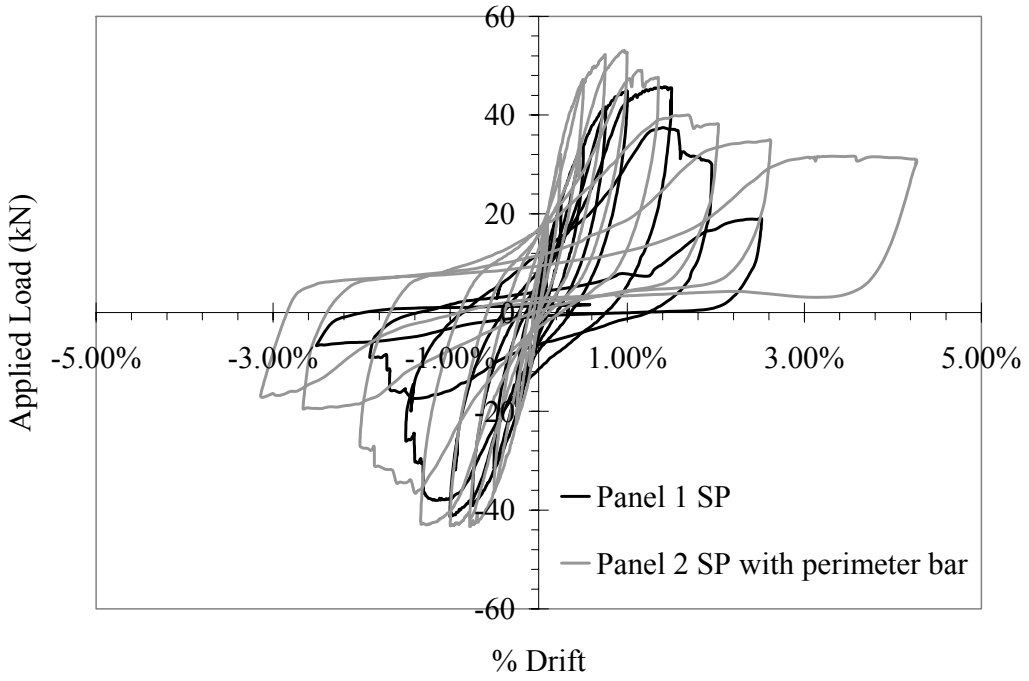

Figure 4-64. – Comparison of load vs. drift response from Panels 1 and 2

4.3.3 Effect of Panel Material

Panels 2, 3, 4 and 5 were constructed with identical reinforcement, using three different ECC materials and a regular concrete. The three identically reinforced ECC panels had similar strength and stiffness as seen in Table 4-15 to 4-17. The concrete panel (Panel 5) had a lower peak strength and stiffness. Figure 4-65 shows a comparison of the load-drift response from the Panels 2, 3 and 4. Panels 3 and 4 (both made from ECC with aggregate) were found to have similar load-drift responses. Both panels began to lose capacity at a lower drift level (0.75%) compared to Panel 2 (1.33%). The ECC in Panels 3 and 4 (SP-A and RECS-A) localized and lost strength at a lower strain level compared to the material without aggregate (SP) (See Kesner and Billington, 2004).

Figure 4-66 shows the load-drift response of Panels 2, 4 and 5. The concrete panel (Panel 5) showed lower peak strength, lower drift level at peak strength, and lower energy dissipation compared to the other panels, due to the near immediate softening of the concrete as it cracked. The concrete panel failed due to a combination of fracture and development failure of the WWF and development failure of the perimeter bar from the connection region. Because Panels 2-5 were identically reinforced, the difference in response between Panel 5, and Panels 2, 3, and 4 can be attributed to the ability of the ECC to strain harden and deform compatibly with the yielding steel, which was consistent with the observations of Fischer and Li (2002).

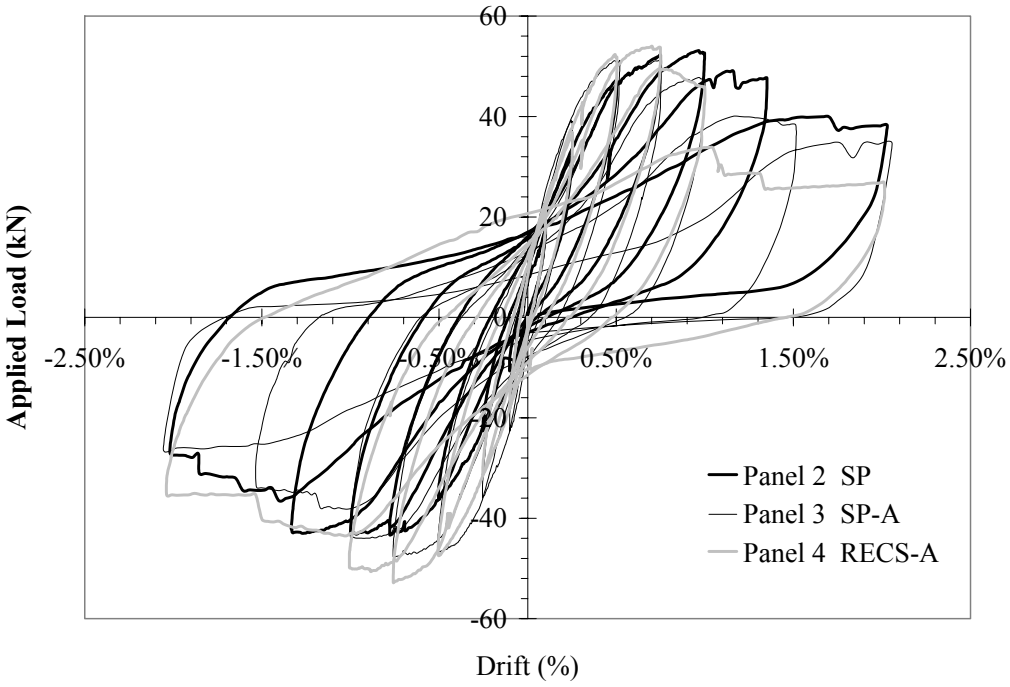

Figure 4-65. Comparison of load-drift response from Panels 2, 3 and 4

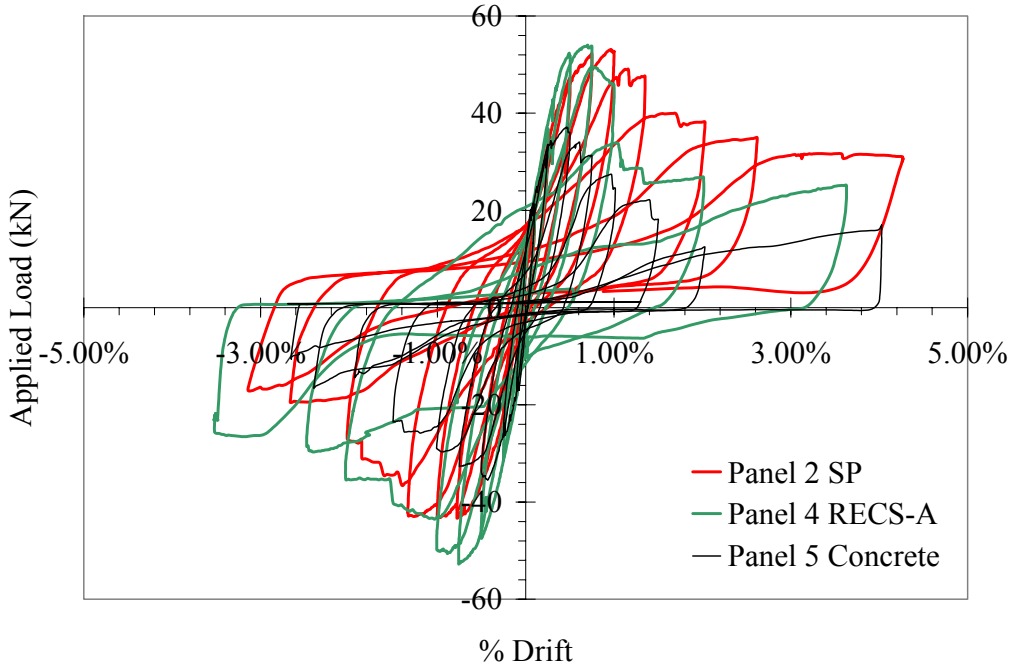

Figure 4-66. Comparison of load-drift response from Panels 2, 4 and 5

4.3.4 Effect of Panel Shape

Panel 6 had a tapered cross-section that was designed to utilize the ECC material more efficiently by reducing the stress concentration at the base of the panel (Section 2.5.5). Figure 4-67 shows a comparison of the load-drift response of Panels 4 and 6, which were constructed with identical materials (RECS-A). As expected the tapered panel reaches slightly lower loads than the rectangular panel at similar drift levels due to lower panel stiffness. However, as seen in Table 4-14, and figure 4-54, the tapered panel has comparable (slightly lower) levels of energy dissipation as the full rectangular panels. These results confirm the viability of the modified geometry as an efficient retrofit option.

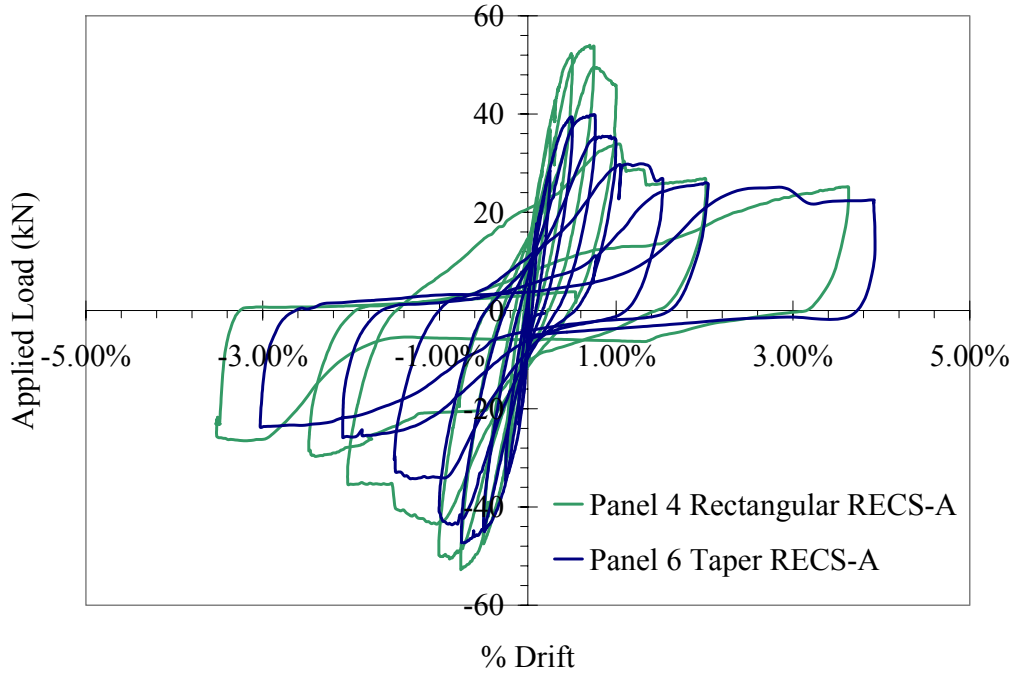

Figure 4-67. Comparison of load-drift response from Panels 4 and 6

4.3.5 Examination of Load Distribution at Panel Base

The analyses shown in Sections 2.4 and 2.5 examined the effect of an infill panel installation on the global load-drift response of an infilled frame. To investigate if the infill addition has any adverse effects on the frame, the local effect of the infill addition was examined. The load distribution across the base of the panel is a critical factor in evaluating the local impact the retrofit installation on an existing structure. Loads transferred from the panel connection bolts to a frame beam flange will have to be then transferred from the beam flange through the beam. Depending upon the magnitude of load transferred from the panel connection bolts and the size of the beam flange, localized damage to the beam could possibly occur when the load is transferred.

The infill panel test setup used pretensioned bolted connections to connect the angles at the base of the panels to the stiffened reaction beam. No other method was provided to transfer the panel

tension loads to the stiffened reaction beam. As discussed in Section 4.2.10, load cells were used to monitor the load in the panel connection bolts during testing. Results from the panel connection bolts can only provide direct information about the tensile load and not the compressive load at the panel base. The angles, which bear on the stiffened reaction beams, will transfer the compressive load from the panel and cause a loss of tension in the bolts.

The measured variation in the tensile load in the panel connection bolts was used to evaluate the load distribution across the connection. Due to the pretensioning of the connections, the applied load at the connection was not equal to the change in panel connection bolt load. The load transferred in the connection region was higher than the change in panel connection bolt load because the connection region has a greater stiffness than the pretensioned bolt (Bickford, 1995).

To determine the load transferred through the connection region, the following equation, which relates the change in panel connection bolt tension to the connection region load, was used (Bickford, 1995):

$$\Delta P_b = \left(\frac{K_b}{K_b + K_j}\right) F_a \tag{4-4}$$

where:

ΔP_b = Measured load change in pretensioned bolt
K_b = Stiffness of bolt
K_j = Stiffness of connection region
F_a = Load applied the region

The stiffness of the bolt and connection region was evaluated using the following equations:

$$K_b = \frac{A_b E_b}{L_b} \tag{4-5}$$

$$K_j = \left(\frac{A_{lc} E_{lc}}{L_{lc}}\right) + \left(\frac{A_j E_j}{L_j}\right) \tag{4-6}$$

where:

A_b = Bolt area
L_b = Bolt length
E_b = Bolt modulus of elasticity
A_{lc} = Load cell area
L_{lc} = Load cell length
E_{lc} = Load cell modulus of elasticity
A_j = Connection area
L_j = Connection length = depth of stiffened reaction beam and connection angle
E_j = Connection modulus of elasticity

Equations (4-5) and (4-6) were used to evaluate the stiffness of the joint and bolt. The connection stiffness, K_j, includes the effect of the load cell at the bolt. The connection area (A_j) takes into account the effect of the precompression in the circumferential area around the load cell in connection region. The area was estimated based upon suggestions in Bickford (1995) and from finite-element simulations. After determining the relative stiffness of the connection members, (4-4) was then used to determine the load applied by the panel connection bolts to the joint. Table 4-18 shows a summary of the values used in (4-5) and (4-6).

Table 4-18 – Summary of Values Used in Equations 4-5 and 4-6

Bolt Pretension (kN)	**Modulus of Elasticity[1] (GPa)**	**A_b (mm^2)**	**L_b (mm)**	**A_{lc} (mm^2)**	**L_{lc} (mm)**	**A_j (mm^2)**	**L_j (mm)**
67	200	284	178	1,219	146	161	44.5
111	200	284	178	1,219	146	1,262	44.5

1. Steel modulus used for all materials

The change in connection bolt tension (F_a) results were shown in figures 4.58 to 4.63. These results were analyzed using equation (4-4) to determine the loads transferred through the connection region (Figures 4.68 to 4.73). These results will be further compared with results from finite element-based simulations in Section 5, where the effect of these loads on hospital frame members is evaluated.

The results in figures 4.68 to 4.73 represent the load transferred by the bolt pairs at the base of the panel. The positive (tensile) loads shown in the figures represent the tension force transferred at the base of the panel. The negative values have no meaning as the compressive load in the connections was transferred through bearing of the connection angles on the reaction beam.

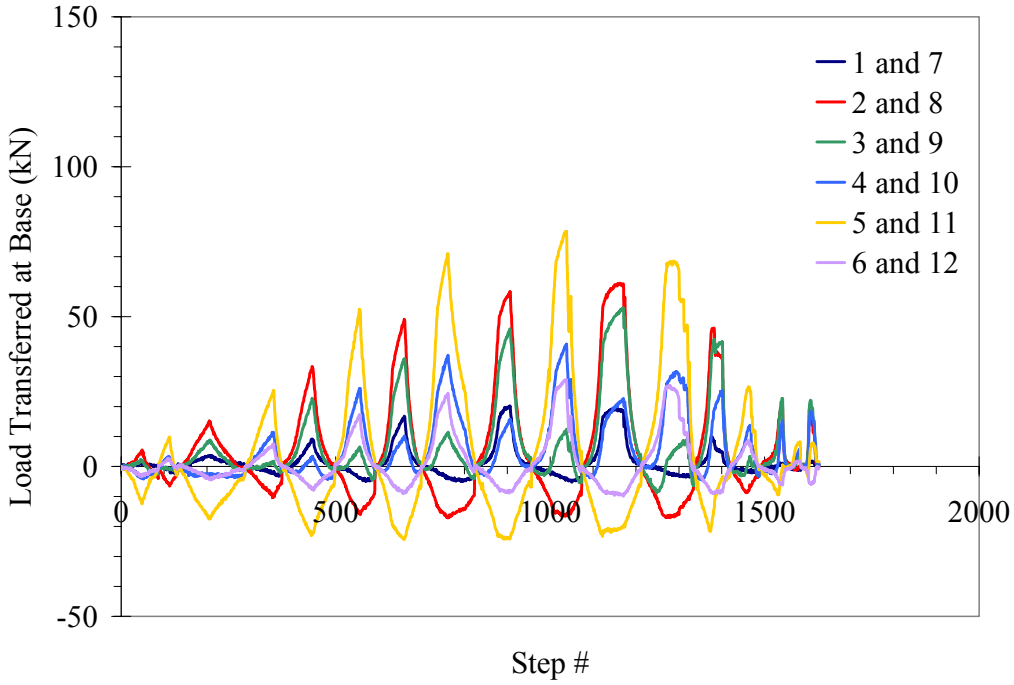

Figure 4-68. Load transferred at base of Panel 1

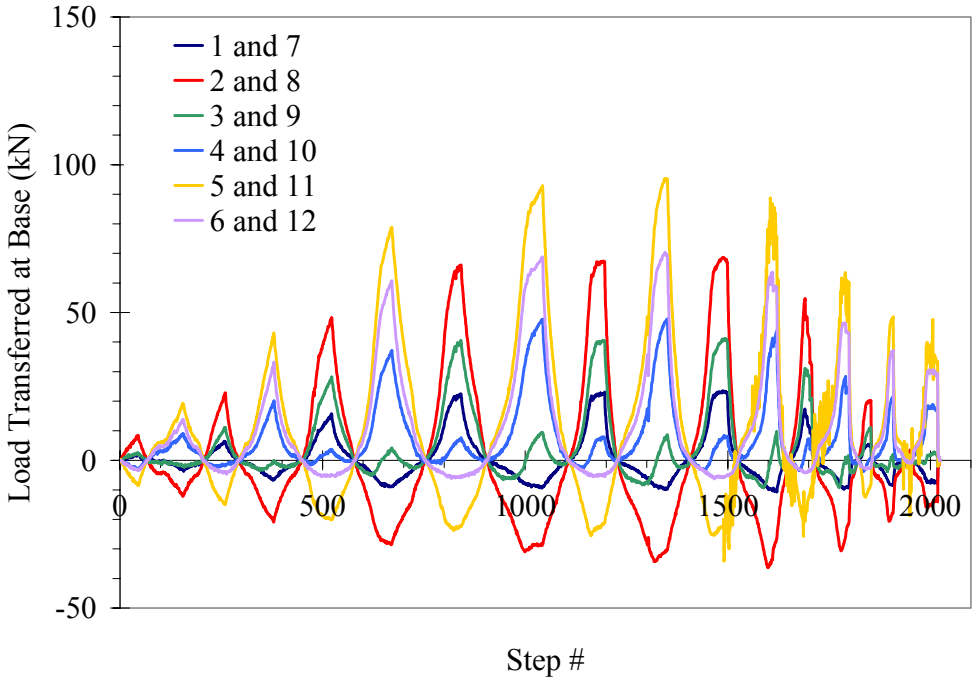

Figure 4-69. Load transferred at base of Panel 2

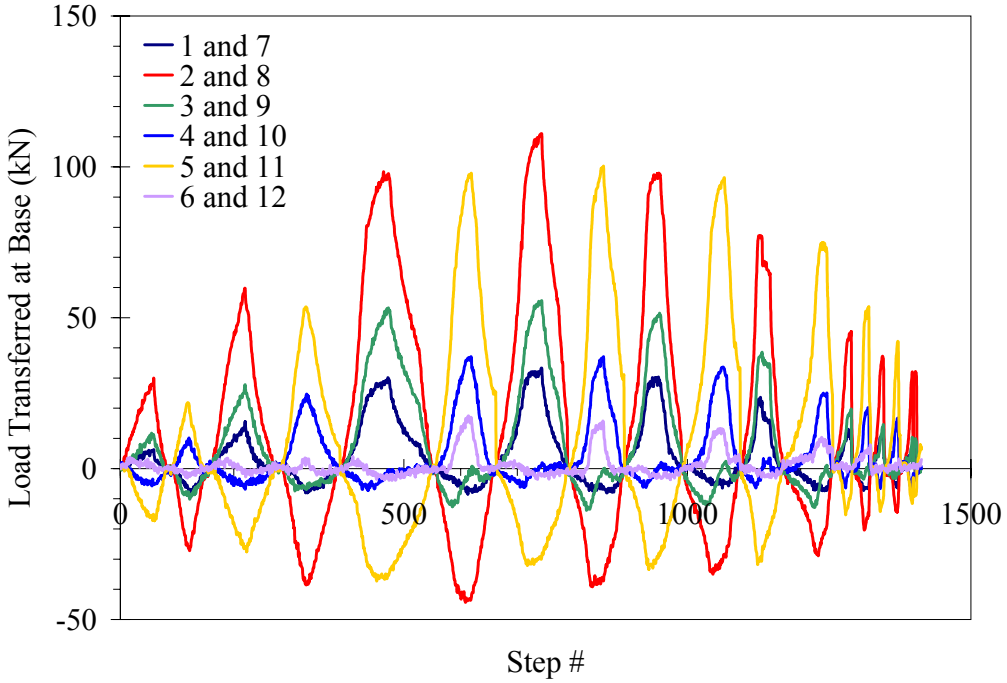

Figure 4-70. Load transferred at base of Panel 3

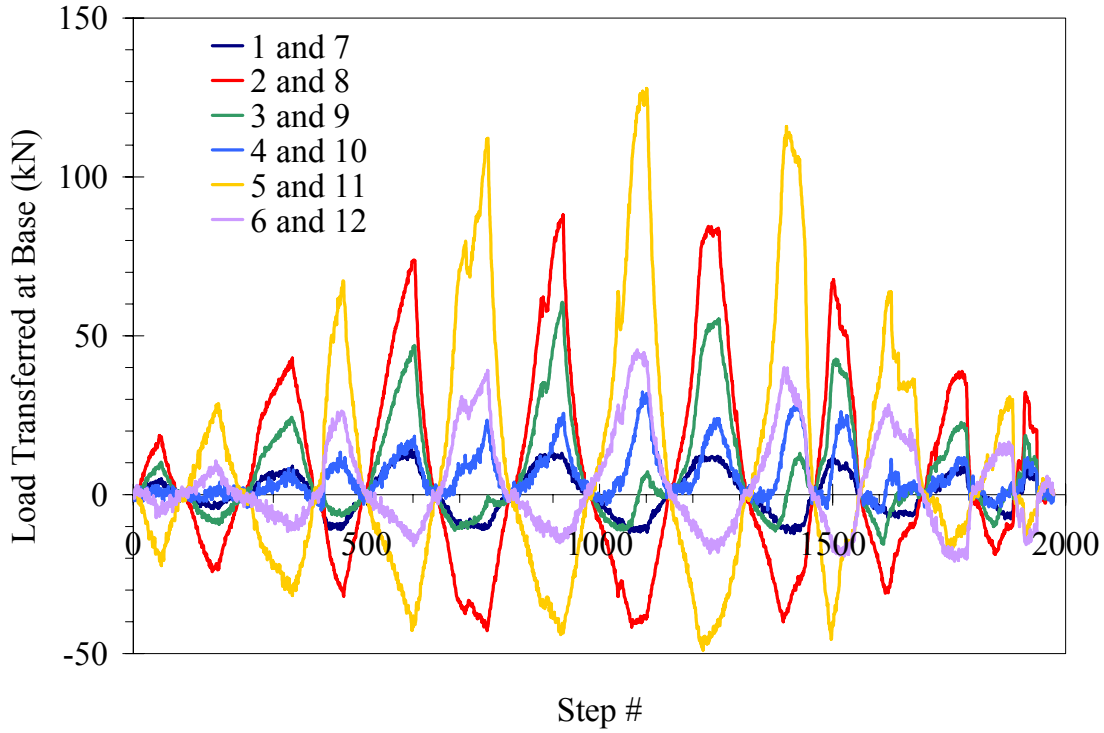

Figure 4-71. Load transferred at base of Panel 4

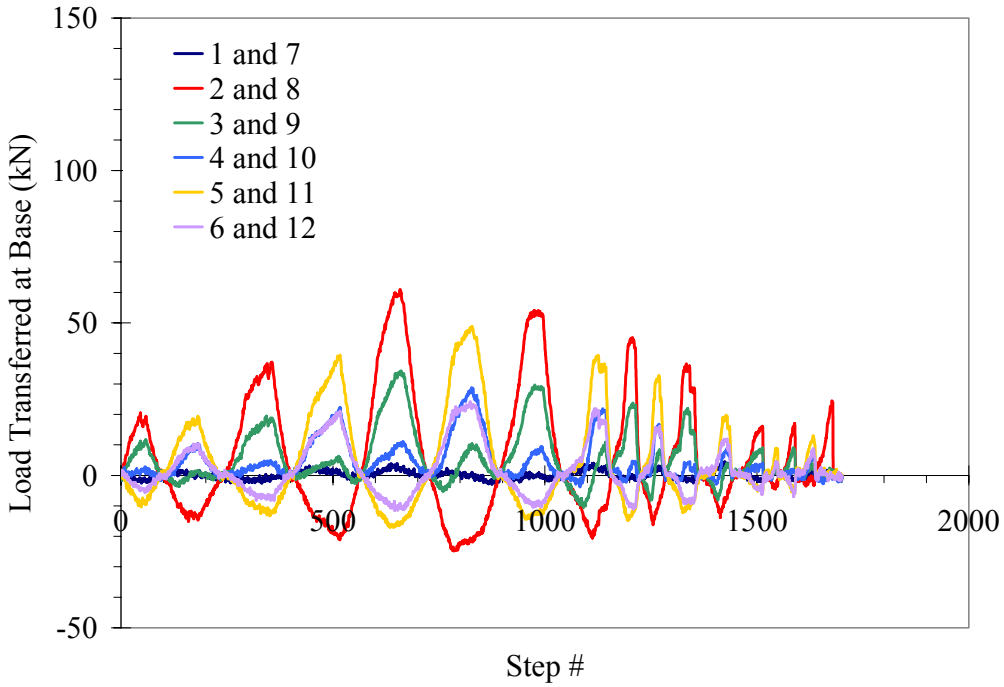

Figure 4-72. Load transferred at base of Panel 5

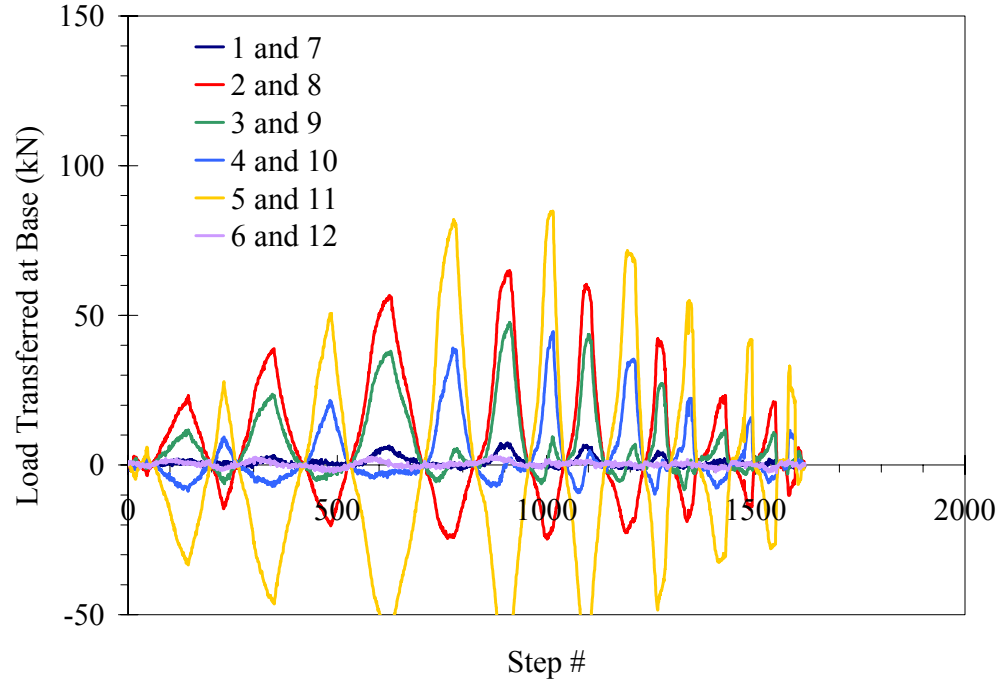

Figure 4-73. Load transferred at base of Panel 6

The tensile forces were multiplied by their moment arm at the panel base, to obtain an estimate of the bending moment at the panel base. This calculated moment was then compared to the applied bending moment (panel load multiplied by the distance from the base to the point of load application). As a simplification, the tensile forces were summed and the length of a single moment arm was determined from the approximate centroid of the tensile and compressive forces (figure 4-74) determined from the panel connection bolts. The neutral axis location was estimated from the relative values of the tensile and compressive bolt forces as seen in figure 4-74. The compressive stress block was assumed to be triangular due to the expected linear elastic behavior in the steel connections. The distance to the centroid of the tensile force was estimated from the magnitude of the bolt loads. The comparison of bending moment calculated from the panel connection bolts and the applied moment serves as an equilibrium check.

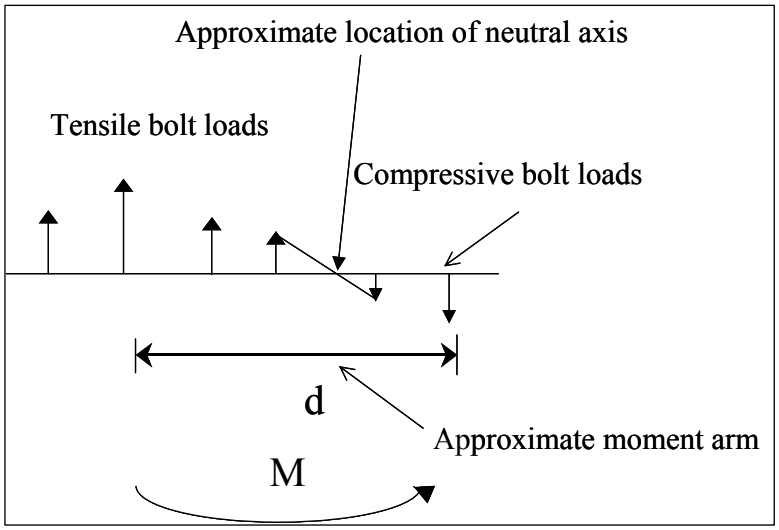

Figure 4-74. Estimation of moment arm from distribution of panel tension load

Tables 4-19 and 4-20 show a comparison between the bending moment applied to the panel and the bending moment calculated using the bolt tensile forces at drift levels of +/-0.50%, and +/-1%, respectively. The results generally show good agreement between the calculated and the measured bending moments.

Table 4-19 – Comparison of Applied and Calculated Bending Moment (kN-m) at +/-0.5% Drift

Panel	+ 0.5%			- 0.5%		
	Applied Moment (kN-m)	Calculated Moment (kN-m)	Error	Applied Moment (kN-m)	Calculated Moment (kN-m)	Error
1	43.0	46.2	7.4%	46.7	38.0	-19%
2	64.7	73.2	13%	49.6	43.9	-11%
3	64.4	73.2	14%	69.8	69.0	-1.1%
4	66.3	79.1	19%	65.0	68.1	4.8%
5	46.9	47.1	0.43%	49.5	46.2	6.7%
6	54.0	57.2	5.9%	54.2	50.8	-6.3%

Table 4-20 – Comparison of Applied and Calculated Bending Moment (kN-m) at +/-1% Drift

Panel	+ 1%			- 1%		
	Applied Moment (kN-m)	Calculated Moment (kN-m)	Error	Applied Moment (kN-m)	Calculated Moment (kN-m)	Error
1	56.8	57.3	0.88%	61.5	61.3	-0.3%
2	72.2	78.2	8.3%	59.2	56.1	-5.2%
3	60.3	62.6	3.8%	65.0	65.4	0.62%
4	62.8	70.7	13%	68.5	70.3	2.6%
5	39.7	36.8	-7.3%	33.8	33.6	0.59%
6	47.6	49.8	4.6%	56.5	53.3	-5.7%

4.3.5 Examination of Panel Base Slip and Base Confinement

The infill panels exhibited a significant loss in capacity when localization of the ECC material (a single dominant crack) occurred at the base of the panel. Prior to crack localization in the panels, slippage at the connection region caused rigid body motion, which reduced the stiffness and energy dissipation in the panels. The panel slip also led to a decrease in the confinement of the panel base. The slip in the panel was captured by the LVDTs measuring vertical displacement at the panel base, as seen in figure 4-40.

Figure 4-75 shows the panel drift versus panel slip at the base of Panel 2, up to a drift level of 0.5%. The magnitude of slip on Panel 2 was representative of the trends observed in the testing. However panel slip began at a lower drift level in Panel 2 than in other panels. In figure 4-76 the same results are shown up to 1% drift. As mentioned in Section 4.2.5, positive slip indicates upward motion of the panel. In figure 4-75, the results indicated that the West side of Panel 2 began to move in a roughly linear (up and down) manner at very low drift levels. The East side began to move downward as the panel drift approached 0.25%. At higher drift levels (figure 4-76), the measured slippage on both sides of the panel increased. The net motion of the panel was upward at increasing drift levels (e.g., after 1% drift there was a residual upward displacement of 1 mm at the west end). In particular, the motion of the west side of the panel appears to ratchet upward with increasing drift levels.

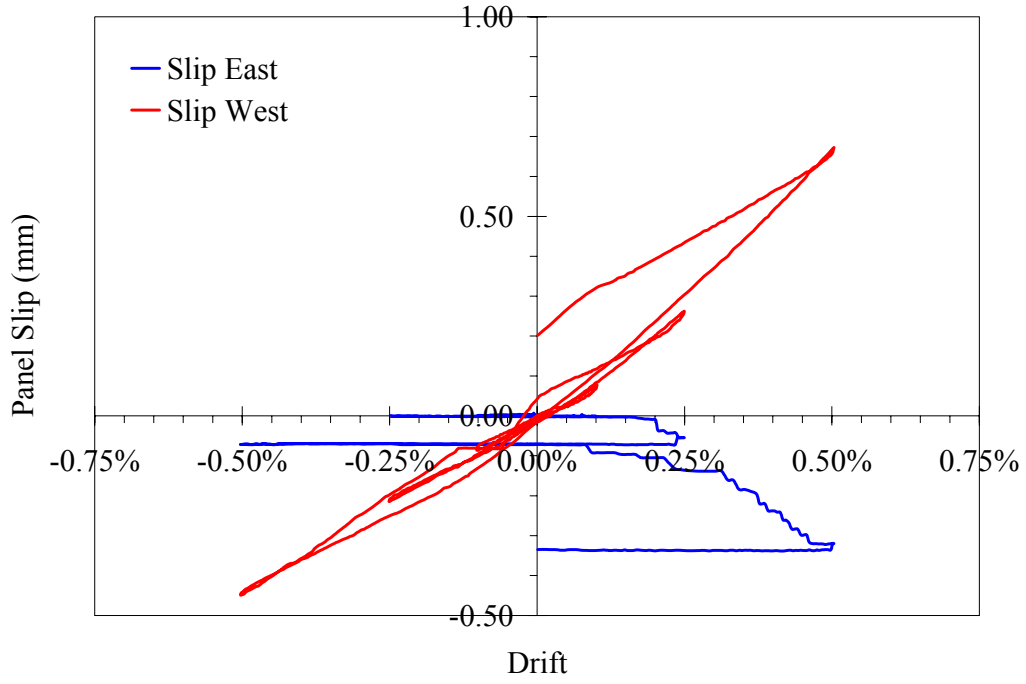

Figure 4-75. Panel base slip versus drift on Panel 2. Limited to 0.5% drift

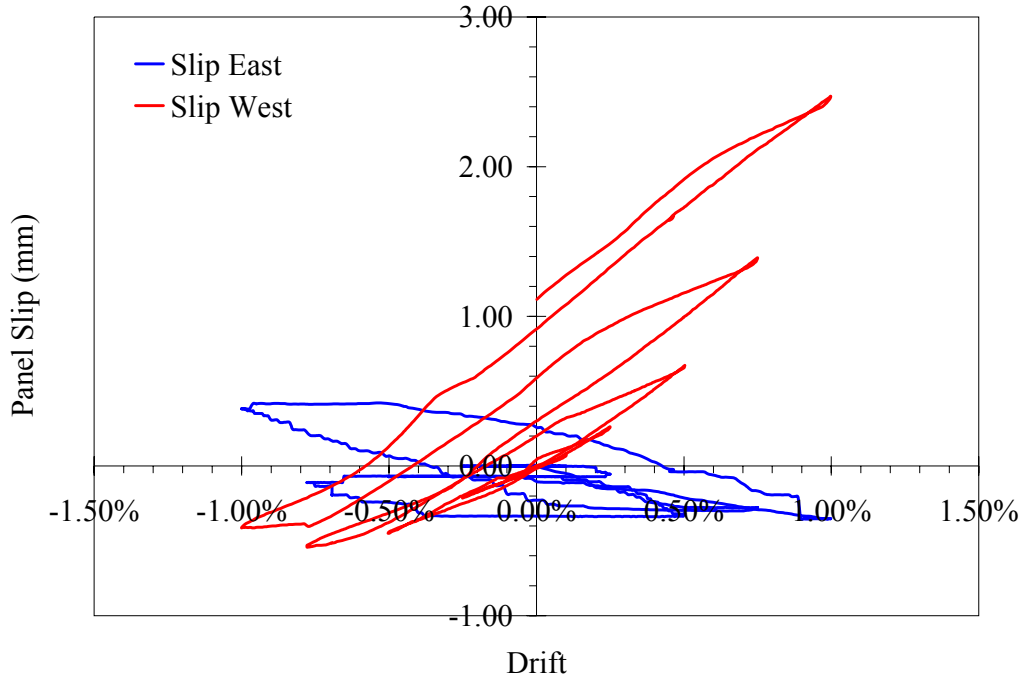

Figure 4-76. Panel base slip versus drift on Panel 2. Limited to 1% drift

The observed upward panel slip is attributed to the change in load of the panel base bolts. Figure 4-77 shows the variation in panel slippage compared to the base bolt (at the edge of the panel) load up to 0.5% drift. Figure 4-78 shows the same information with the drift limit increased to 1%. The figures show the decrease in bolt load (from the initial pretensioning force of approximately 140 kN) with the upward ratcheting of the panel slip. The decrease in bolt tension is attributed to the Poisson contraction of the panel as it was loaded in tension and subsequent damage during slippage. The decrease in panel thickness would have allowed for a decrease in pre-tensioned bolt load, which would not be recovered if the panel slip resulted in damage to the panel faces, thus precluding the panel from returning to its original position. With increasing numbers of cycles the panels base bolts exhibited a net loss of tension, decreasing the confinement of the panel base.

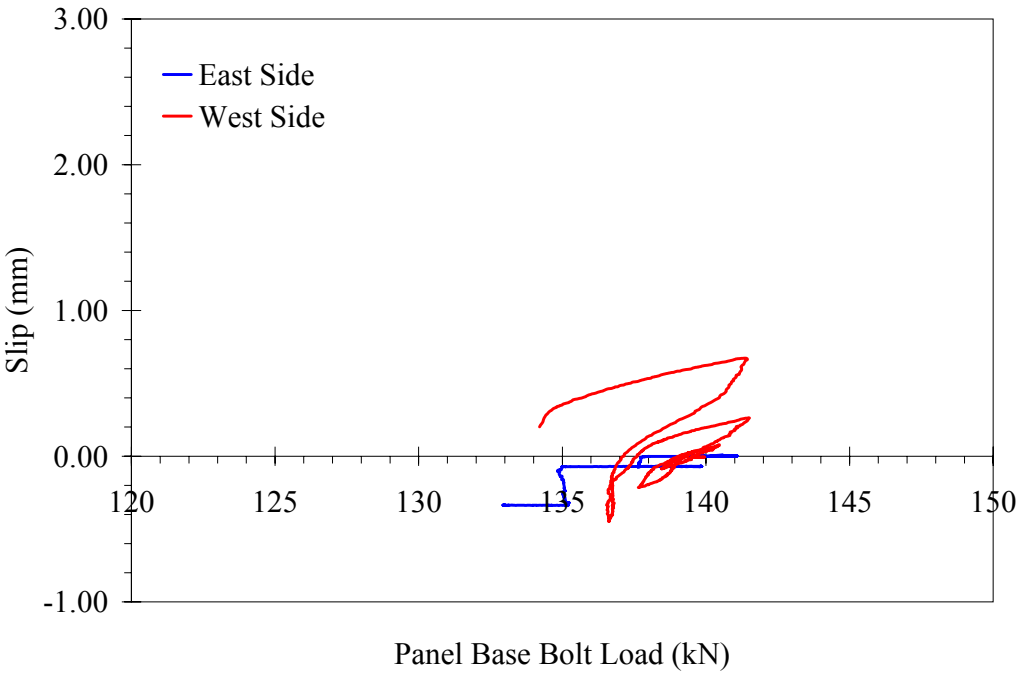

Figure 4-77. Comparison of Panel 2 base bolt load versus slip up to 0.5% drift

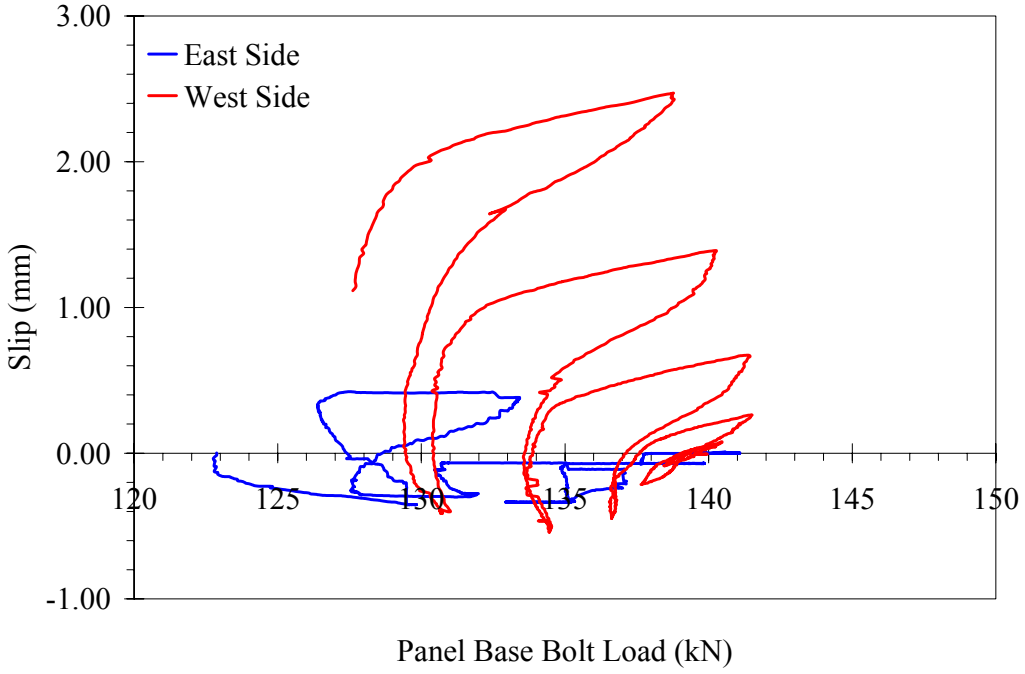

Figure 4-78. Comparison of Panel 2 base bolt load versus slip up to 1% drift

4.3.7 Testing Limitations

The infill panel testing described in this chapter was intended to examine the response of a single infill panel to quasi-statically applied cyclic loads.

One limitation of the testing was the single panel test method used. The single panel may not represent the full infill response, as vertical displacements at the top of the panel were not prevented as discussed in Section 4.2.5. Prevention of the vertical panel motion will likely increase the energy dissipation in the panels, because tensile cracks in the panels will more fully close during testing. This limitation was not expected to have a significant impact on the panel response.

An additional limitation of the testing method was the simple quasi-static cyclic displacement of the panels. The selected loading pattern, while essential for determining the cyclic strength envelope and response of the panels, represents a significant simplification when compared to a true seismic loading. To develop the infill panel concept further, more experimental testing is required. The primary areas for future testing include:

1. An assessment of loading rate sensitivity on the response of the panels, in particular the ECC.
2. Testing of full height infill sections (with a connection between panels) installed in a frame. In the current testing, the panels were attached to a rigid base beam. Testing of the full infill sections in a frame will also allow for the effect of a non-rigid base to be assessed
3. Cyclic and/or seismic testing of full frames infilled with the proposed panels.

4.3.8 Panel Improvements

The infill panel testing presented in this chapter demonstrated the viability of the panel system with pretensioned bolted connections. The primary limitation on the panel effectiveness was the slip at the panel base. To improve the panel performance, it is desirable to mitigate this slip. One approach to prevent the slip would be to fill the space between panels and the base (figure 4-11) with either a rigid shim, or non-shrink cementitious material. A cementitious material will provide the advantage of allowing for variable spacing between panels.

There are two major disadvantages to placing material between the panels. First, the addition of the shims or a cementitious material is an additional construction step. Second, a cementitious material causes difficulties when the panels need to be relocated or replaced. The use of bond breakers, which prevent bond between the cementitious material and the panel, could limit this problem. Bond breakers will allow the cementitious material to act as a shim in compression. Compression would be transferred through both the shim and the angles. The tension loads would still be transferred through the bolts in the connections.

Another way to improve the performance of the panels would be to decrease the clear cover to the reinforcing steel. In Section 4.1.1, the clear cover to the reinforcing steel was reported as 30 mm. The cover could be decreased, resulting in the perimeter reinforcing steel being further

from the neutral axis of the panel, which will increase the reinforcing steel strain. Greater strain in the reinforcing steel will increase the panel energy dissipation. The adjustment can only be made if adequate consolidation can be achieved with the decreased cover.

4.4 Summary of Infill Panel Test Results

This Section presented the results from a laboratory investigation of the response of ECC infill panels fabricated with different ECC materials, reinforcement layouts, and panel shapes. The testing was an outgrowth of the simulation results presented in Section 2, which identified promising infill systems, and the results presented in Sections 3.1 and 3.2, which demonstrated the feasibility of the connection concept proposed for the system. The goal of the testing was to establish the shape of the panel's load vs. drift response, peak load, peak drift capacity, energy dissipation, failure mechanisms, and to examine the effect of test variables.

The results of the infill panel testing showed the variation in strength, stiffness and energy dissipation that can be achieved with variations in ECC materials, reinforcement and geometry. The experimental results will be used in Section 5 to validate a constitutive model for ECC materials.

The load drift response was nonlinear as a consequence of the multi-cracking response of ECC and of steel reinforcement yielding. The nonlinear response of the panels resulted in variations in strength and stiffness of the panels. Examination of the panel's displaced shaped, as determined by LVDT data, indicated that the displacement of the panel was primarily due to flexure at low displacement levels.

The extent of cracking in the panels varied with the panel material. The greatest number of cracks was observed in the panels made with mix design SP (Panels 1 and 2), which contained no aggregate. Lesser amounts of cracking were observed in the panels made with mix designs SP-A and RECS-A (Panels 3, 4 and 6), which contained fine aggregate. The least extensive cracking was observed in Panel 5, which was made with an ordinary concrete. The panels with the most extensive cracking also had the highest drift capacity (approximately 1.5% for Panels 1 and 2) prior to strength degradation. The higher drift capacity of the panels was related to the higher strain capacity of the ECC material.

The failure of the ECC panels was predominantly flexural and occurred as the ECC materials began to soften, and form localized cracks near the panel base. The softening of the ECC was followed by failure of the WWF mesh, either by fracture or development failure. The perimeter reinforcing steel bar maintained its capacity in the ECC panels due to the precompression of the connection region by the panel bolts, which helped develop the bar. The failure of the concrete panel occurred at a lower drift level than the ECC panels, and was accompanied by extensive spalling of the concrete in the connection region, leading to reinforcement development failure.

The residual strength of the panels was a function of the type of panel reinforcing. In Panel 1, only WWF was used to reinforce the panel. The failure of the WWF resulted in a low residual strength of Panel 1 relative to the panels with both the perimeter bar and WWF. Extensive spalling of the concrete in the connection region of Panel 5 resulted in a development failure of

the perimeter reinforcing bar which reduced the residual strength of the panel. Panels 2. 3, 4 and 6, which had identical reinforcement all has similar residual strength.

The energy dissipation of the panels was observed to vary as a function of the panel material and reinforcement. The highest energy dissipation was observed in the rectangular ECC panels (2, 3, and 4) with the perimeter bar. The tapered panel (Panel 6) was found to have slightly lower amounts of energy dissipation than rectangular panels made with the same material (Panel 4). Lower amounts of energy dissipation were observed in the concrete panel (Panel 5) and the ECC panel without the perimeter bar (Panel 1). The energy dissipation in the panels was generally attributed to the yielding of the reinforcing steel with some additional contribution from multiple-cracking in the ECC material. Strain gage results verified that both the WWF and perimeter bars yielded during testing.

In the testing, the response of an ordinary concrete and ECC material were compared. The ECC panels exhibited greater strength, stiffness and energy dissipation, compared to the concrete panel. This demonstrates the improvement the ECC material provides over a conventional concrete. The ECC materials that showed the highest strain capacity in uniaxial tests also led to the highest drift capacity before the onset of softening when used in the panels.

Two different types of reinforcing were used in the panels. Using a 9.5 mm perimeter bar in addition to the WWF reinforcement was found to significantly increase the stiffness, strength (peak and residual) and energy dissipation in the panels relative to the panel with only WWF. Furthermore, two different panel shapes were examined, a rectangular panel and a tapered panel. The tapered panel was developed to represent a more optimal panel shape. Testing results indicated that the tapered panel can provide similar levels of strength, stiffness and energy dissipation, when compared to the rectangular panels.

During testing, the load in the panel connection bolts was monitored to evaluate the load distribution in the connection region. The results verified that the bending moment estimated from the tensile loads in the panel connection bolts generally matched the bending moment applied to the panel. The measured loads can be used to evaluate the impact of the retrofit on the existing structure. The panel connection bolts loads will be further examined in Section 5. The panel bolt loads at the top of the panel were not observed to vary significantly during testing. The bottom panel bolt loads decreased with increasing slip at the panel base. The decrease in load was attributed to damage in the connection region.

The primary limitation of the panels was the slip of the panel base in the connection region. The slip of the panel meant that the panels were acting partly as rigid bodies instead of flexure/shear elements, which was not desirable in terms of dissipating energy. The cause of the slip was not apparent in the test results. To address the slip, grouting of the connection regions has been suggested.

To develop the infill panel concept further, additional testing is required. Future testing should include more realistic seismic loadings and testing of full height (double panel) sections. These tests will provide a more accurate means of assessing the infill panel concept. Finally, full frame infills should be tested as well.

Section 5
Simulation of ECC Infill Performance

5.1 Introduction

In Sections 2, 3 and 4, preliminary analysis of the infill panel concept and results from laboratory tests on connection details and infill panels were presented. In this section the experimental results are integrated with additional finite element analyses to examine the effectiveness of the infill panel system further, and to examine the impact of the infill addition on an existing structure.

The results presented in this section are divided into three sections. Section 5.1 presents a material model developed by colleagues (Han, et al., 2003) for ECC materials, which was based on the cyclic material test results presented in Kesner and Billington (2004). Section 5.2 utilizes the ECC material model to simulate the response of the tested infill panels presented in Section 4. The final section, Section 5.3, examines the impact of the infill installation on the overall response of a steel frame to lateral loadings. Specifically, the impact of the retrofits is examined to determine if the retrofit installation would cause locally adverse effects such as yielding at the connection of the ECC panels to the steel structure.

5.1 Modeling of ECC Material Behavior

In Kesner and Billington (2004), the results of cyclic testing on ECC materials were presented. The goal of these tests was to determine the response of ECC to reversed cyclic (tension-compression) loadings. The results were used to develop a constitutive model for ECC materials, which incorporated the cyclic response. The model is capable of predicting the behavior of ECC materials in cyclically loaded applications (Han et al., 2003).

5.1.1 ECC Material Model

In the preliminary analysis of the infill wall system, presented in Section 2, a simplified material model was used for the 2D finite-element analyses to represent the ECC material. The primary limitation of the simplified model was the use of secant unloading and reloading for the ECC materials. The secant unloading and reloading scheme underestimates the hysteretic energy dissipation of ECC materials.

To capture the response of the ECC materials more accurately, a model has been developed (Han et al., 2003) based in part on the experiments presented in Kesner and Billington (2004). This model is for 2D finite-element analyses and uses a uniaxial, multi-linear curve to represent both the tensile and compressive strength envelopes. The unloading/reloading behavior in compression and in tension before the onset of tensile softening is modeled using power laws. Unloading in the tensile softening regime is assumed to be linear. The model uses a total strain based approach (Feenstra et al., 1998) and was implemented as a user supplied material model in the finite element program Diana (TNO, 1998a and 1998b). All of the simulations presented in this chapter were performed using this model and Diana.

Figure 5-1 shows a result from a single element test of the material model using a four noded plane-stress element. The tensile region of figure 5-1 is expanded in figure 5-2. Table 5-1 shows the ECC material properties used in the simulation. In the simulation a simple cyclic displacement of the element was performed up to +/- 4% displacement. For comparison purposes, figure 5-3 shows one of the experimental results from the balanced cyclic loading of the ECC specimens, as discussed in Kesner and Billington (2004). There is good agreement between the unloading and reloading curves in both the simulation and experimental results.

The ECC model in its current form has two limitations. The first limitation is that it cannot capture the decrease in tensile capacity in the ECC that was observed when the material was loaded in tension after the onset of softening in compression (discussed in Kesner and Billington, 2004). The second limitation is the assumption of linear softening in compression, which is slightly different from the softening curve observed in the testing (compare figure 5-1 and figure 5-3). These limitations were not addressed in the current implementation of the model.

Table 5-1 - ECC material properties used in single element simulation

ECC Property	Value
Initial Cracking Strength (MPa)	1.72
Modulus of Elasticity (GPa)	11.5
Initial Cracking Strain	0.000125
Ultimate Tensile Strength (MPa)	2.41
Ultimate Tensile Strain	0.035
Peak Compressive Strength (MPa)	55.2
Ultimate Compressive Strain	-0.05

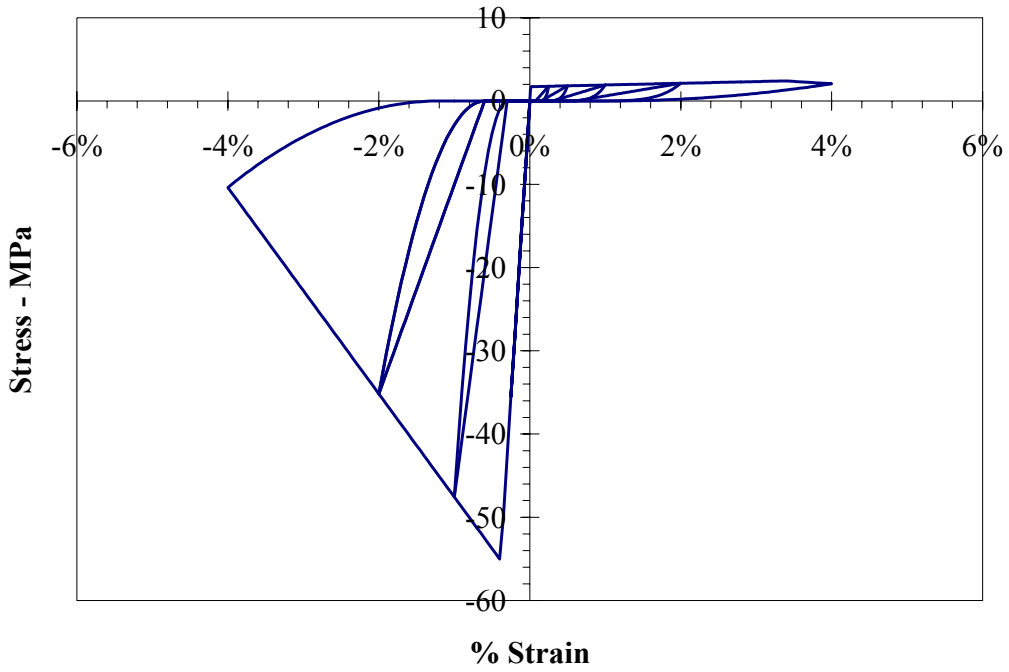

Figure 5-1. Results from single element simulation of ECC model response

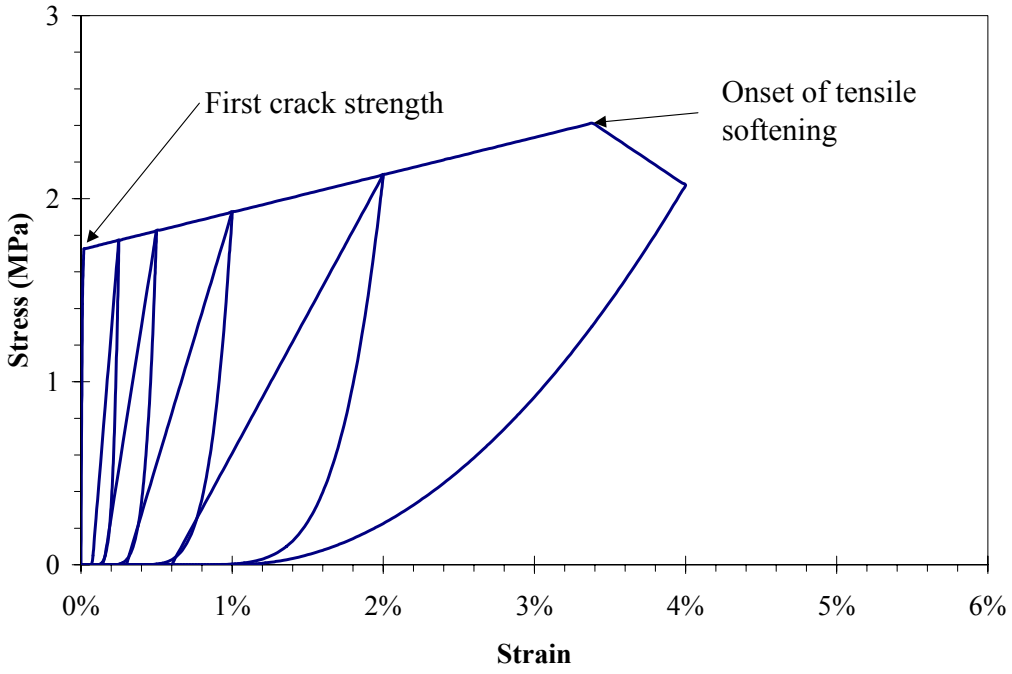

Figure 5-2. Results from tensile region of single element simulation of ECC model response

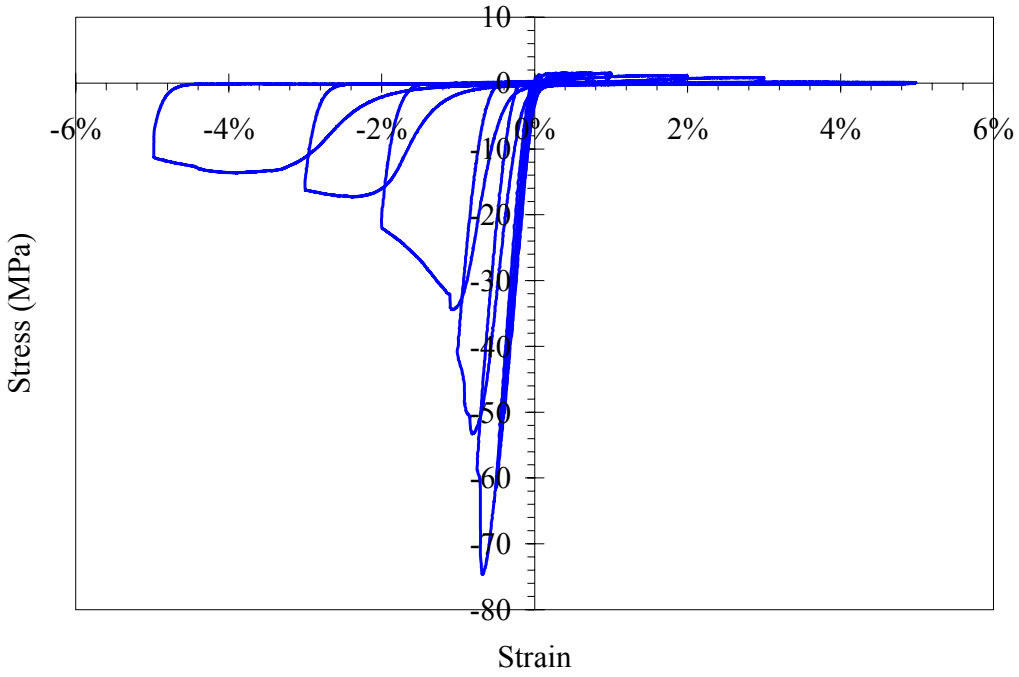

Figure 5-3. Results from balanced cyclic test on ECC material from specimen SP-2 (Kesner and Billington, 2004)

5.2 Simulation of Infill Panel Response

Simulations were performed to model the experiments on precast infill panels made with different ECC materials, reinforcing configurations and specimen geometries. The goal of the simulations was to verify the ability of the ECC material model, discussed in Section 5.1, to model the strength, stiffness, energy dissipation and residual strength in the panels.

Simulations also were performed using a more detailed model of the panel base and its connection to the stiffened reaction beam. The detailed models were used to verify the change in bolt forces observed in the panel testing (Sections 4.2.10 and 4.3.5) and to determine the stress distribution across the base connection. The inclusion of the connection to the stiffened beam in the detailed models allowed for a preliminary examination of the local impact of the retrofit installation on an existing structure.

5.2.1 Infill Panel Models

A series of finite element models of the infill panel test configuration were created. The models used the same features (discussed below) as the infill panel models discussed in Section 2. Figure 5-4 shows a typical rectangular panel model, adjacent to a finite element mesh of the panel. Figure 5-5 shows the same information for the tapered panel. Figure 5-6 shows how the connection region of the panels was idealized for the model (side view).

The two-dimensional finite element rectangular panel model was comprised of four-noded plane-stress elements with the overall physical dimensions of the model selected to match the experiments described in Section 4. In the simulation of the tapered panel, the tapered section of the panel was modeled using three-noded, triangular plane stress elements. No attempt was made to model the observed slippage (see Section 4.2.5) of the panel in the connection region. The panel bolts were also not included in the two-dimensional models.

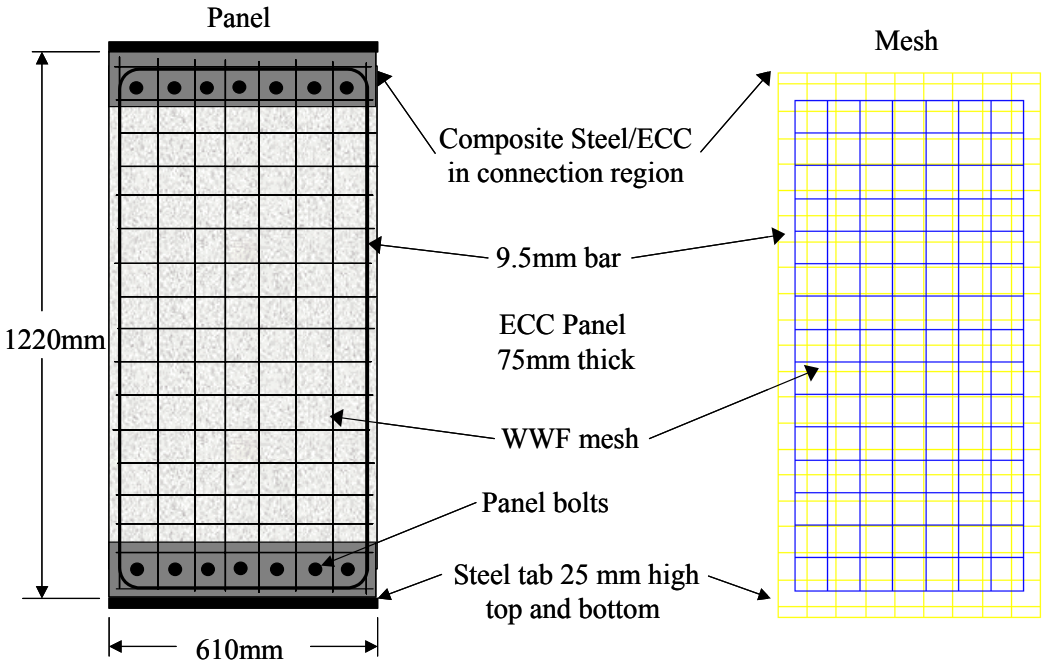

Figure 5-4. Schematic representation of rectangular panel and corresponding finite element mesh

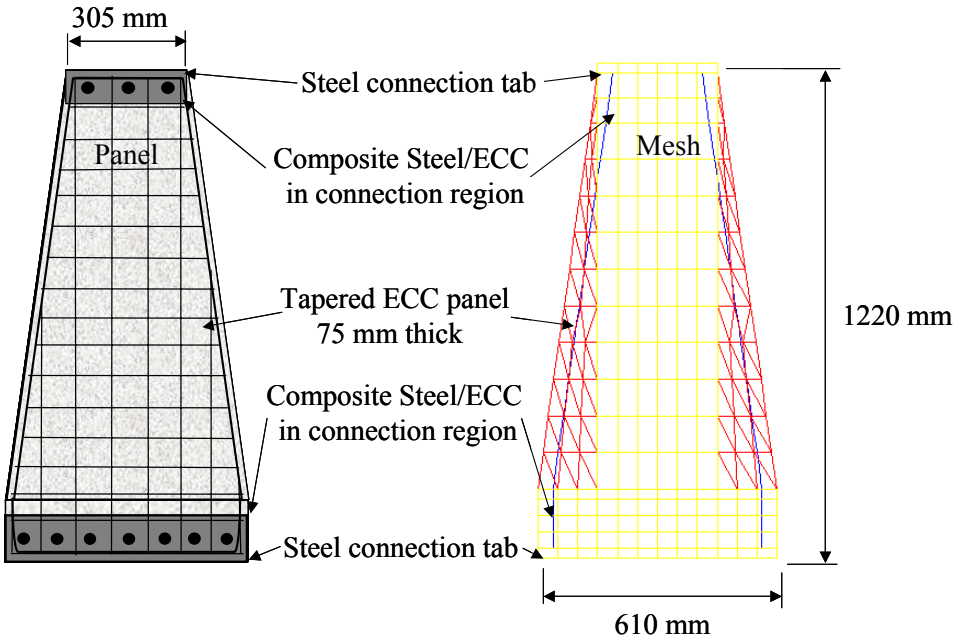

Figure 5-5. Schematic representation of tapered panel and corresponding finite element mesh

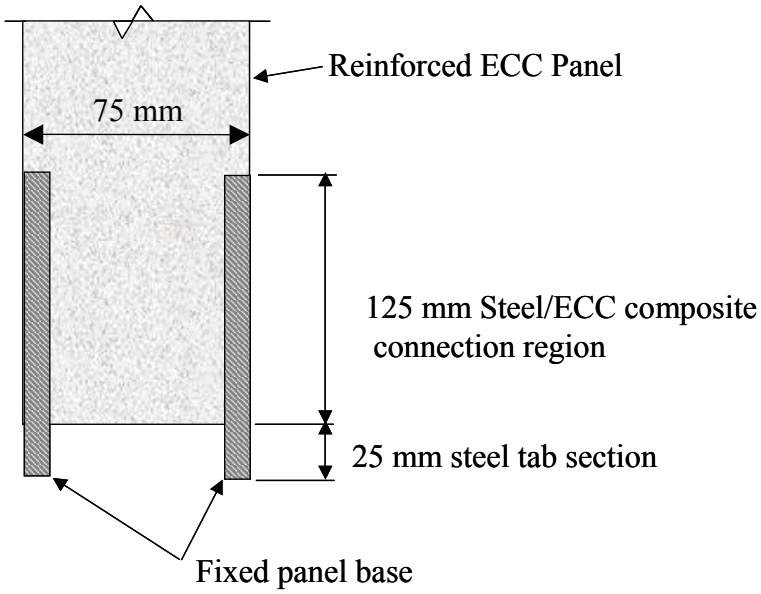

Figure 5-6. Schematic representation of connection region in panel simulations

The material properties used in the analyses are summarized in table 5-2. The material for the steel tab and reinforcing steel were elasto-plastic with a Von Mises yield criterion. The yield strength, yield strain and ultimate strength the material testing results are presented in Section 4.1.3 (Tables 4-3 and 4-4).

The reinforcement in the panels was modeled as embedded reinforcement (perfect bond), with the reinforcement area and location selected to correspond with the experiments. The reinforcement model did not include tensile fracture or the possibility of development failure of the reinforcement.

The ECC material properties were based upon results measured in the uniaxial tension testing on cylindrical specimens as discussed in Kesner and Billington, 2004. In the uniaxial tensile tests, a higher strain capacity was observed in mix SP, compared to the mixes with aggregate (SP-A and RECS-A). As discussed in Section 4, mix SP was used in casting of Panels 1 and 2, while mixes SP-A and RECS-A were used in Panels 3 (SP-A), 4 and 6 (RECS-A). To account for the differences in the strain capacity of the ECC materials used in panel testing, two different peak tensile strain capacities were used in the analyses. ECC1 corresponds to the SP mix design, and ECC2 corresponds to the SP-A and RECS-A mix design. The strain capacities in the materials were selected to correspond with the different strain capacities observed in the uniaxial tensile testing (see Section 2.4 in Kesner and Billington, 2004). The peak compressive strength of the ECC materials was not varied in the simulations. Compressive failure of the panel was not observed in any of the experimental results. The confined ECC at the base of the panels was modeled as elastic, with a composite compressive modulus determined from a strain compatibility analysis of the steel and ECC together in the connection region.

For the simulations, the modulus of elasticity of the ECC was reduced by 75% for ECC1 and by 50% for ECC2 compared to the experimental stiffness from compressive test results. These values were chosen to correlate the simulation results with the experiments. The reduction accounts for the initial cracking in the ECC due to shrinkage, as well as the decrease in panel stiffness due to slip of the panel in the connection region. The need to reduce the modulus of elasticity of cement-based materials to account for shrinkage cracking was been documented in several previous simulation studies (Han, 2001, El-Attar, et al., 1991; Bracci, et al., 1992; Shahrooz and Moehle, 1987; and D'Ambrisi and Filippou, 1997). However, based upon the amount of panel slip observed (Section 4.2.5), the majority of the decrease in modulus of elasticity represents slip of the panels. A more explicit treatment of slip in simulations of panel response is given in Douglas et al. (2004).

To simulate the experimental panel tests, the controlled cyclic displacement pattern from the experiments was used (figure 4.13) for the simulations. Displacements were stepped incrementally. The displacement step size was selected to prevent numerical divergence of the solutions. A Newton-Raphson iterative scheme was used with an energy norm for convergence criteria with a tolerance of 0.05%. A maximum of ten iterations was allowed at each displacement step. After 10 iterations, the simulations were allowed to continue, even if convergence had not occurred. During unloading from high drift levels (at low loads), the lack of convergence resulted in jumps in the load-drift response. These areas will be indicated in the discussion of the simulations.

Table 5-2 – Steel and ECC material properties used in panel simulations

Material	Elastic Modulus (GPa)	Initial (yield) Strength (MPa)	Cracking (yield) Strain	Peak Tensile Strength[1] (MPa)	Peak Tensile Strain[1]	Peak Comp. Strength[1] (MPa)	Peak Comp. Strain[1] (MPa)
Composite ECC[2]	64	-	-	-	-	-	-
Steel tab	200	345	0.0017	552	0.1	345	-0.1
Reinf. steel	200	414	0.0027	552	0.1	414	-0.1
ECC 1[3]	3.5	1.2	0.0003	2.0	0.025	55	-0.016
ECC 2[4]	6.9	1.2	0.0002	2.0	0.005	55	-0.08

1. Strength/strain at the onset of strength degradation
2. Confined material in connection region at base of panel (Section 5.3)
3. Similar to SP mix design in Chapter 3
4. Similar to SP-A or RECS-A mix design in Chapter 3

5.2.2 Infill Panel Simulation Results

Figure 5-7 shows the load-drift response from simulations of rectangular panels to +/- 3% drift using the two different ECC material models. The reinforcement in the panels in these simulations was identical to Panel 1 (0.44% WWF mesh). The results have two major differences; the initial stiffness of the model, and the peak drift capacity. The greater initial stiffness in the panel with ECC2 was a consequence of the higher modulus of elasticity of ECC2 relative to ECC1. The difference in drift at peak capacity (drift capacity after which a decrease in strength occurs) is a consequence of the difference in the ECC material's strain capacity. The panel with the ECC1 (which has a higher tensile strain capacity) had a higher drift at peak capacity, than the panel with ECC2.

The similarity in peak loads is consistent with both ECC materials having the same peak tensile strength. The slightly higher load (1 kN) in the simulation with ECC1 is due to the greater amount of reinforcing steel strain at the higher drift level. The identical reinforcement in both panels leads to the nearly identical residual strength at higher drift levels. The effect of non-converged steps can be seen in both simulations results. The non-converged steps caused the jumps during the unloading from -2 and -3% drift.

Figure 5-8 shows principle tensile strain contours at 1% drift (ECC1) and 0.5% (ECC2), which represent the drift level at the peak load in the simulations. In both figures, the peak strain at the base of the panel corresponds to the peak strain capacity of the ECC material. The softening of the simulation at a lower drift level with ECC2 resulted in less hysteretic energy dissipation relative to the simulation with ECC1.

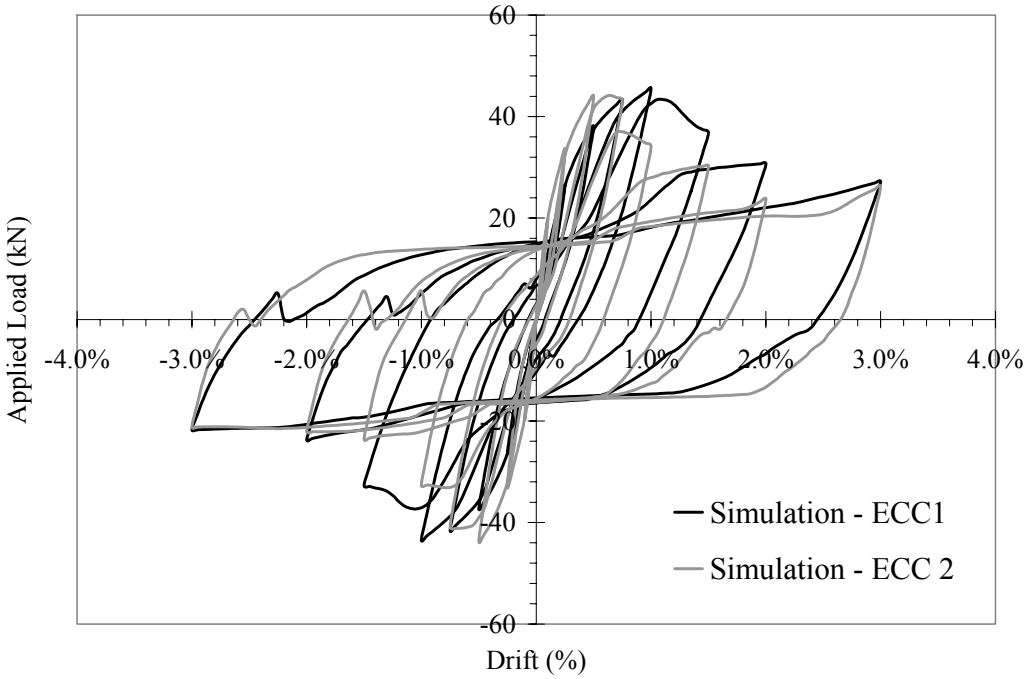

Figure 5-7. Comparison of load vs. drift response from simulations

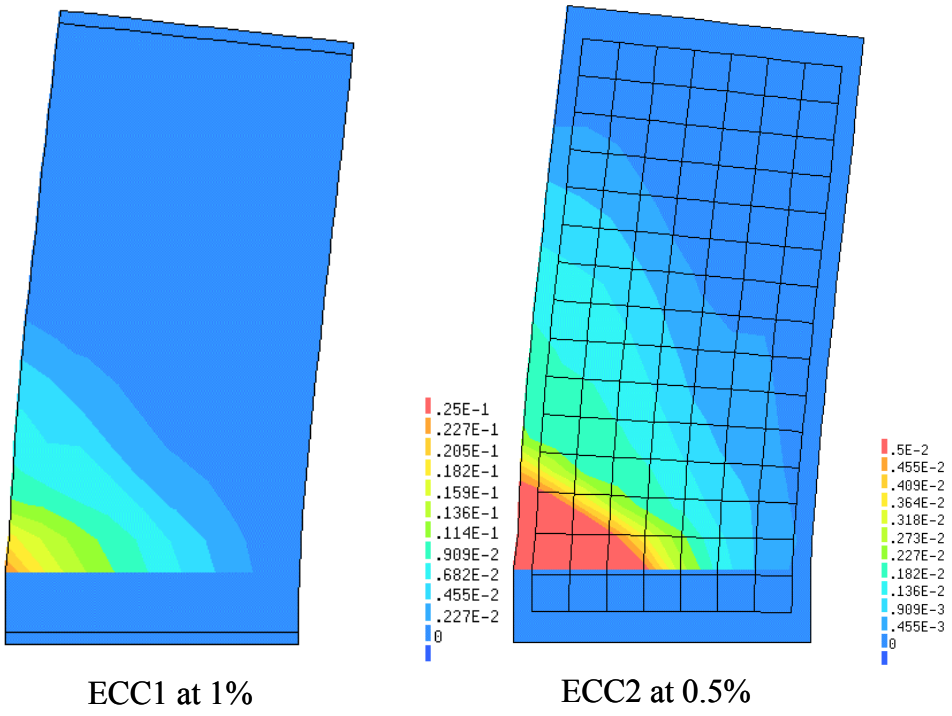

Figure 5-8. Comparison of principle tensile strain contours at peak load

5.2.3 Comparison of Simulation and Experimental Results

Figure 5-9 shows a comparison of the load-drift results from the simulation of the rectangular panel with ECC1 and the experimental results from Panel 1. In the figure, the simulation results are limited to +/- 3% drift. The simulation was able to match the load capacity approximately at various drift levels, and also capture the residual displacement of the panels, up to roughly 2% drift. At higher drift levels, the simulation overestimates the residual strength of the panel. The overestimation was due to the perfect bond modeling and the lack of modeling fracture in the reinforcing steel. Recall that in the experiment for Panel 1, both WWF fracture and development failure were observed.

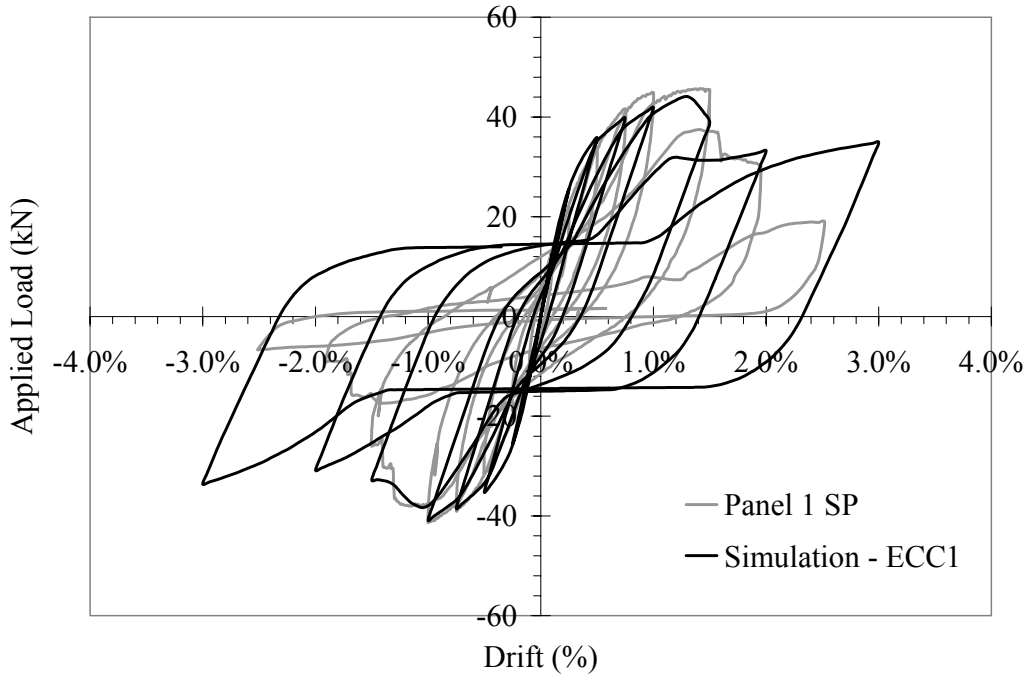

Figure 5-9. Comparison of simulation and experimental results with ECC1

Figure 5-10 compares the results of a simulation of a rectangular panel with ECC2, and the experimental results from Panels 3 and 4. Panels 3 and 4 were observed to have a very similar load-drift response, and softened at nearly identical drift levels. The ECC2 material used in the simulations represents SP-A and RECS-A. As discussed above, the simulation over estimates the residual strength. A comparison of the strength and energy dissipation between the experimental and simulation results is shown in tables 5-3 and 5-4. Prior to panel softening the simulation approximately captures the strength and energy dissipation observed in the experiments. At higher drift levels, the large jumps in the simulations results, near zero load, were caused by a lack of convergence of the solution.

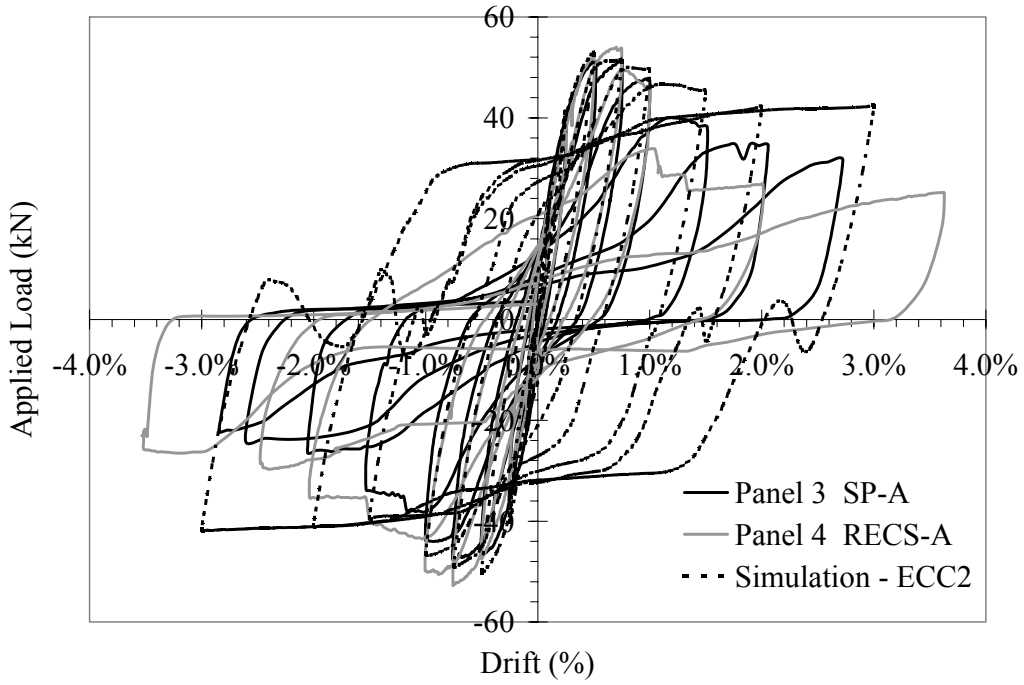

Figure 5-10. Comparison of simulation and experimental results with ECC2

Figure 5-11 shows the results of the simulation of the tapered panel compared to the experimental results. Similar to the rectangular panels, the simulations nearly matched the peak load, onset of strength degradation, and residual displacements with the experimental results. The pinching response of the panel seen in the experiment was not captured by the simulation. Similar to the previous results the simulation also overestimates the residual strength of the panel.

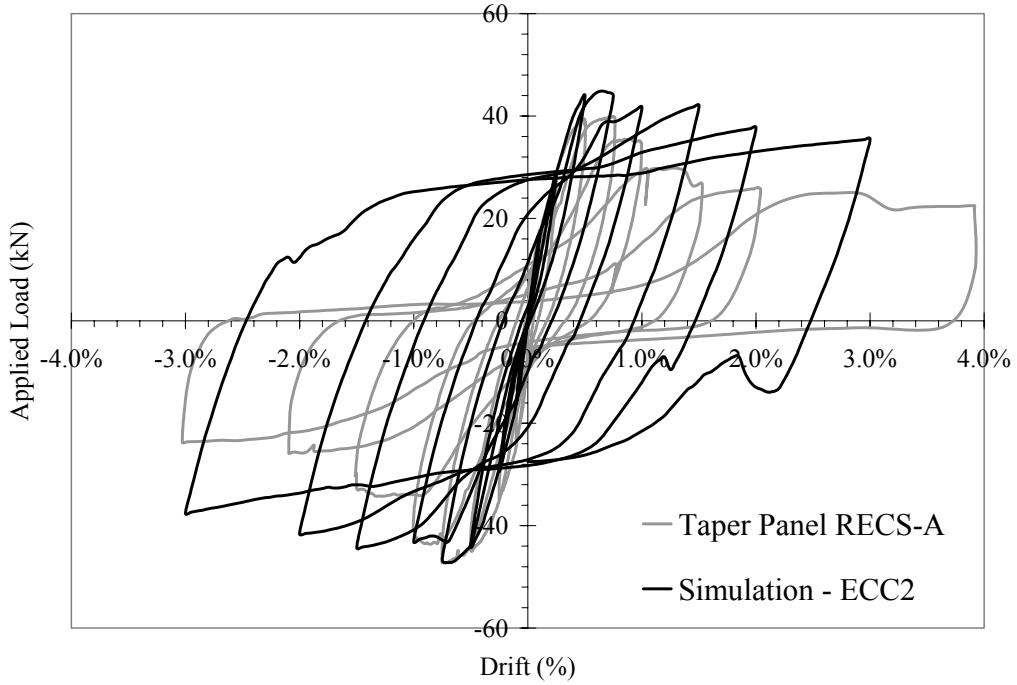

Figure 5-11. Comparison of simulation and experimental results with ECC2

Tables 5-3 and 5-4 show a comparison of the strength and energy dissipation, respectively, between the simulation and experiments at various drift levels. The energy dissipation in the simulation results was calculated using Equation 4-3. At drift levels past the onset of softening, the simulations significantly overestimated the panel's residual strength. The overestimation occurred because the reinforcing steel cannot fail in these models but rather continues to harden to high strain levels. The fracture of the reinforcing steel was not included in the models. The embedded reinforcement used in the simulations assumes perfect bond of the steel to the ECC, thus development failure and bond slip was not included in the simulations. As a result, the pinching behavior typical of bond slip, for instance, was not captured.

The simulation results were nearly symmetric, in contrast to the experimental results. As discussed in Section 4.2.5, the lack of symmetry in the experiments occurred due to slip in the connection regions, which was not considered in the models.

Table 5-3 - Comparison of Loads in Panels at Positive Drift Levels

Panel	Panel Load (kN) at various Panel Drifts						
	0.1%	**0.25%**	**0.5%**	**0.75%**	**1%**	**1.5%**	**2%**
Panel 1 (Exp.)	12.9	21.9	34.0	41.7	45.0	45.5	29.9
ECC1 (Sim.)	12.4	25.5	35.8	39.8	41.9	38.9	33.2
Panel 4 (Exp.)	22.7	35.9	46.7	47.7	44.0	33.9	26.3
ECC2 (Sim.)	22.4	41.1	52.7	51.3	49.4	45.2	42.1
Panel 6 (Exp.)	21.3	28.4	38.7	39.9	34.7	26.8	26.0
ECC2 Taper (Sim.)	16.1	28.8	43.1	44.0	41.7	42.0	37.7

Table 5-4 – Comparison of Energy Dissipation in Experimental and Simulation Results

Panel	Energy Dissipation (kN-m) at Different Panel Drift Levels						
	0.1%	**0.25%**	**0.5%**	**0.75%**	**1%**	**1.5%**	**2%**
Panel 1 (Exp.)	0.0183	0.0762	0.238	0.533	1.01	2.01	2.96
ECC1 (Sim.)	$5.4e^{-5}$	0.00946	0.102	0.335	0.717	1.71	2.45
Panel 4 (Exp.)	0.0281	0.129	0.449	0.981	1.65	2.71	3.71
ECC2 (Sim.)	0.0074	.0499	0.285	0.853	1.81	3.53	5.82
Panel 6 (Exp.)	0.0216	0.0963	0.323	0.750	1.32	2.21	3.10
ECC 2 Taper (Sim.)	0.0058	0.0365	0.147	0.479	1.12	2.50	4.10

5.2.4 Panel Connection Bolt Models

In Sections 4.2.10 and 4.3.5, the experimental results from the panel connection bolts at the panel base were presented. These pretensioned bolts connected the angles at the base of the panel to the stiffened reaction beam. No other connections were used to connect the panel to the reaction beam. During panel testing the measured force in the pretensioned connection bolts varied with the lateral load applied to the panel.

To examine the variation in panel connection bolt force, a series of simulations were performed with a more detailed model of the connection region between the base of the panel (Panel 2) and the stiffened reaction beam. A picture of the reaction beam is given in figure 4.5. Figure 5-12 shows a schematic of the panel base, with the finite element mesh shown in figure 5-13. Figure 5-14 shows a schematic side view of the connection region. The finite element model included the stiffened reaction beam, the load cells, panel connection bolts and the connection angles. The models were comprised of two-dimensional plane stress elements.

In the finite element model, a row of interface elements was used at the interface of the steel angle and the stiffened beam. The interface elements did not allow the transfer of tensile loads from the angle to the stiffened beam. Two-noded truss elements were used in the model to represent the pretensioned connection bolts. The truss elements provided a mechanism for the transfer of tensile loads from the angles to the stiffened beam. Beam elements, representing the load cells also were used in the model. The truss elements were only connected to the model at the angle and at the bottom end of the beam element. The load cell elements and bolt elements overlap in figures 5-12 to 5-14. The truss elements had the same length as the panel connection bolts in the experiment. The two panel connection bolts in the model were combined as one bolt in the two-dimensional model based upon their position along the panel base. Figure 4.10 shows a plan view of the panel base, with the bolt groupings indicated.

The model was simplified by only including the top flange of the stiffened beam, which was assumed to be continually supported in the vertical direction. The large number of vertical stiffeners along the beam length, combined with the vertical support provided by the beam web justify this assumption (figure 4-5). The remaining portions of the base connection bolt models were identical to the models described in Section 5.2.1.

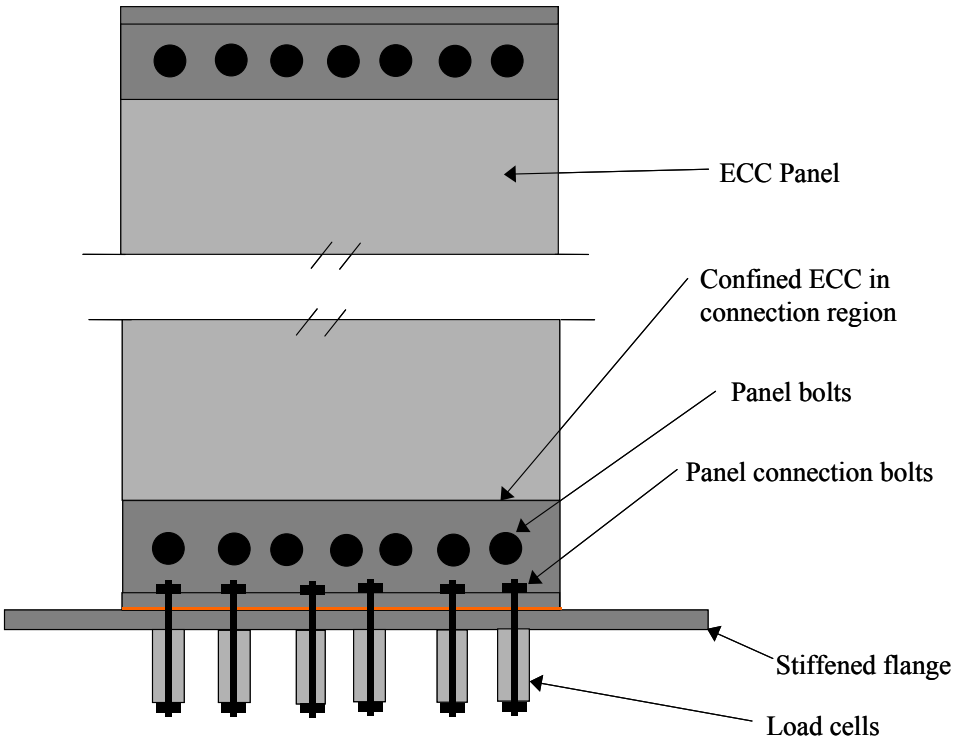

Figure 5-12. Schematic of infill panel test setup

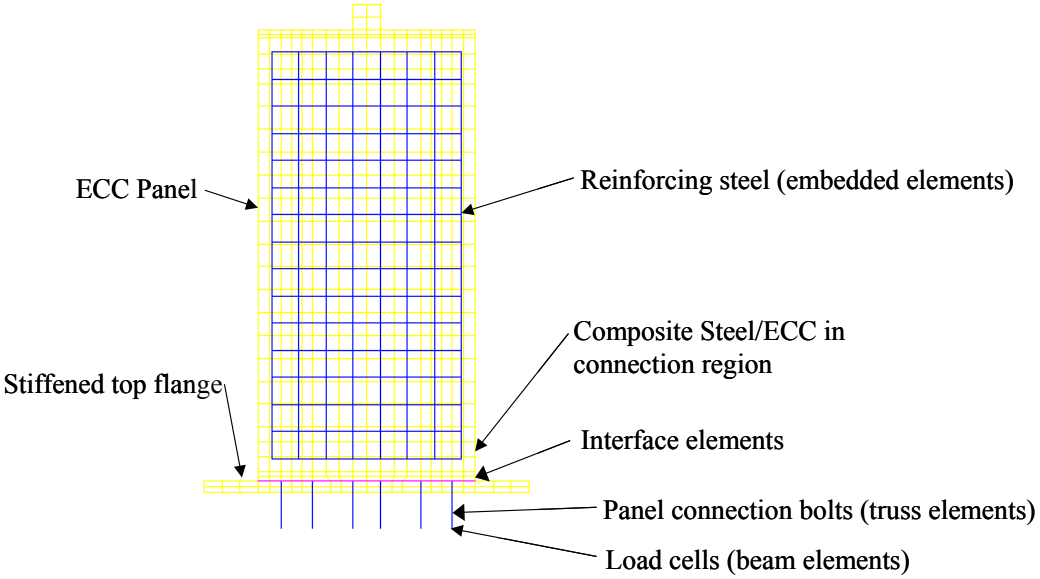

Figure 5-13. Finite element mesh from detailed simulation of panel base

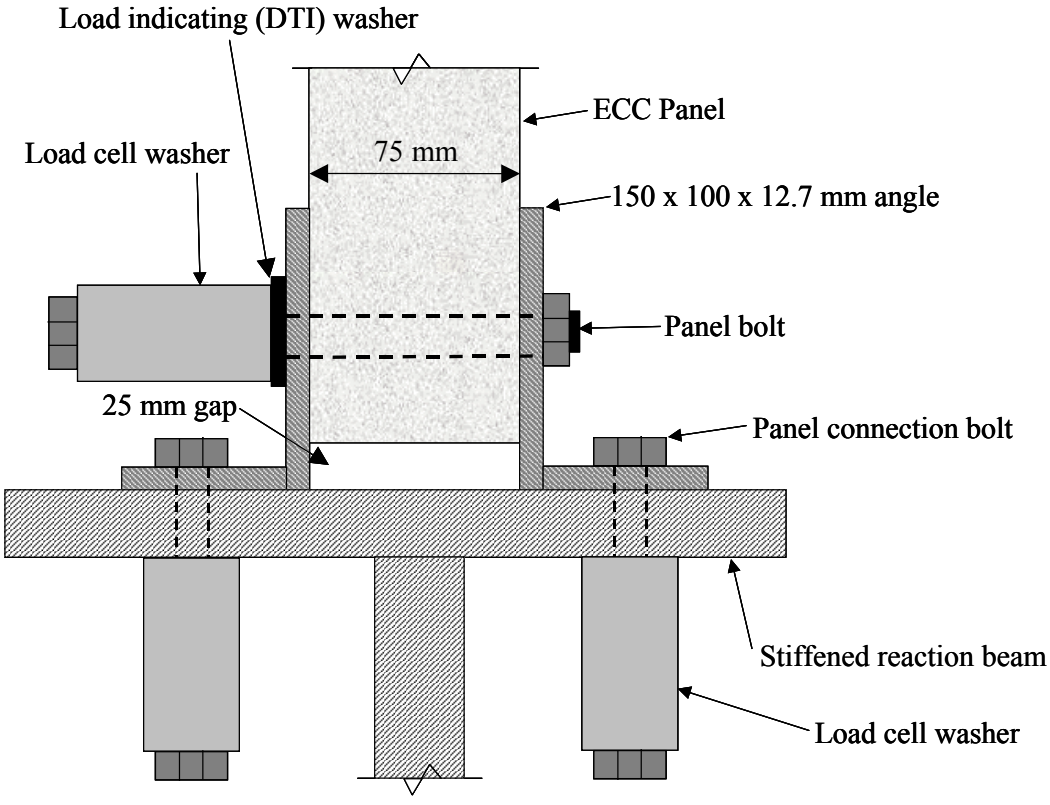

Figure 5-14. Side view of panel base

To examine the response of the pretensioned bolts, a cyclic displacement to +/- 1% drift was simulated. Two different levels of pre-tensioning in the bolts (67 kN and 111 kN) were considered in the simulations. The levels of pretensioning were selected to approximate the values used in the experiments. The principle strain contours at different drift levels were examined to determine if localized yielding occurred in either the connection members or in the top flange of the stiffened reaction beam. The load drift response of the panel was also examined to verify if the detailed base simulations matched the results of the simulations using a simplified model of the base (Section 5.2.2).

A primary goal of the simulations was to examine the variation in pretensioned connection bolts to evaluate the behavior observed in the experimental results. In the experimental results (discussed in Section 4.2.10), the second set of bolts from the panel end (bolt pairs 2 and 8 or 5 and 11) showed a higher increase in load than the bolts closest to the edge of the panel (bolts pairs 1 and 7 or 6 and 12). The simulation results were used to evaluate this observation. The results were also examined to verify the experimentally observed load distribution across the base of the panel.

5.2.5 Panel Connection Bolt Results

The initial results from the simulations, not presented here, showed a greater change in bolt force in the bolt pair at the edge of the panel connection (bolts pairs 1 and 7 or 6 and 12) than in the second set of bolt pairs, which was inconsistent with the experimental results. The reason for the lack of agreement was explained by examining the transfer of load through the connection region as follows.

In the simulations, the material in the connection region was assumed to be elastic across the length of the connection. The assumption of linear behavior in the connection region was based upon a further assumption that the pretensioned panel bolts would provide precompression that prevented damage of the confined material. However in the experimental results, cracking was observed at the exposed edges of the panel. The cracking can be seen in figures 5-15 and 5-16, which show pictures taken during testing of Panels 1 and 3, respectively. The extent of cracking damage in the connection region can be seen in figures 5-17 and 5-18, which show the connection region of Panels 2 and 4, respectively, after completion of testing.

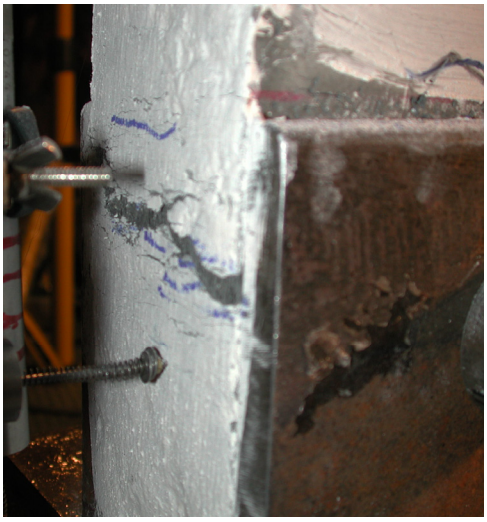

Figure 5-15. Cracking in connection region of Panel 1 during test

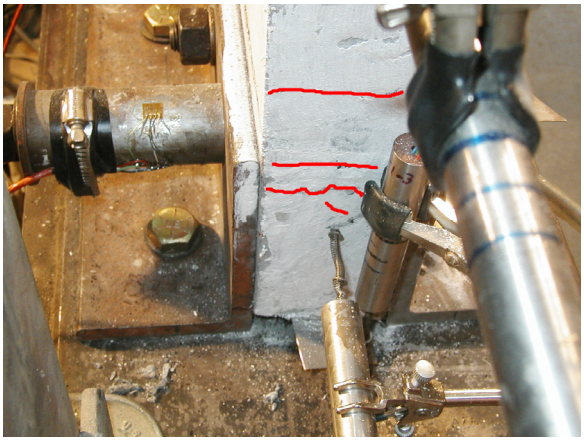

Figure 5-16. Cracking (highlighted for clarity) in connection region of Panel 3 during test

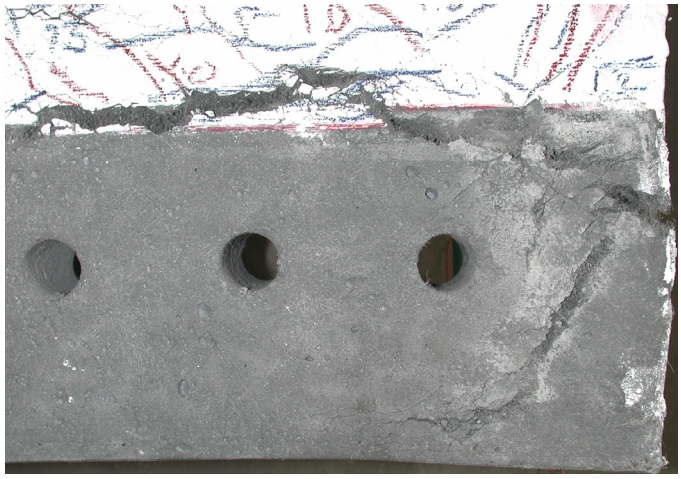

Figure 5-17. Cracking in connection region of Panel 2 after test

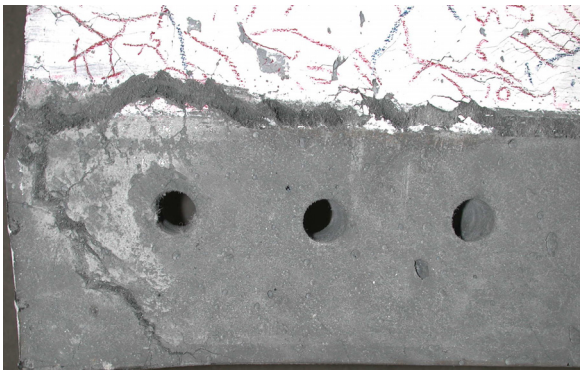

Figure 5-18. Cracking in connection region of Panel 4 after test

The cracking of the ECC at the periphery of the connection region resulted in a decrease in stiffness and strength of the cracked material relative to the uncracked material in the core of the connection region. By not allowing this damage to occur in the model, more load could be carried in the end bolt pairs in the simulations.

To account for the damage in the material at the perimeter of the connection region, the finite element model was modified. The modification consisted of changing the material model in the elements at the edge of the panel from the composite confined material to the ECC material. The modification resulted in the steel at the edge of the connections not contributing to the stiffness of the connection region, which was appropriate since the steel in the area was not physically connected to the panel as evidenced by the cracking of the ECC and measured slip in the connection region (Section 4.2.5). The reinforcing steel geometry in the connection region was also rounded to model the shape of the perimeter bar more accurately.

The simulations were repeated with modifications described above. Figure 5-19 shows a comparison of the results (up to 1% drift) from the simulations with the detailed base model compared with the experimental results obtained from Panel 2 (using ECC1) and from a simulation using the simplified base model. The results show the ability of the detailed connection model to capture the test results with similar accuracy as the simplified model.

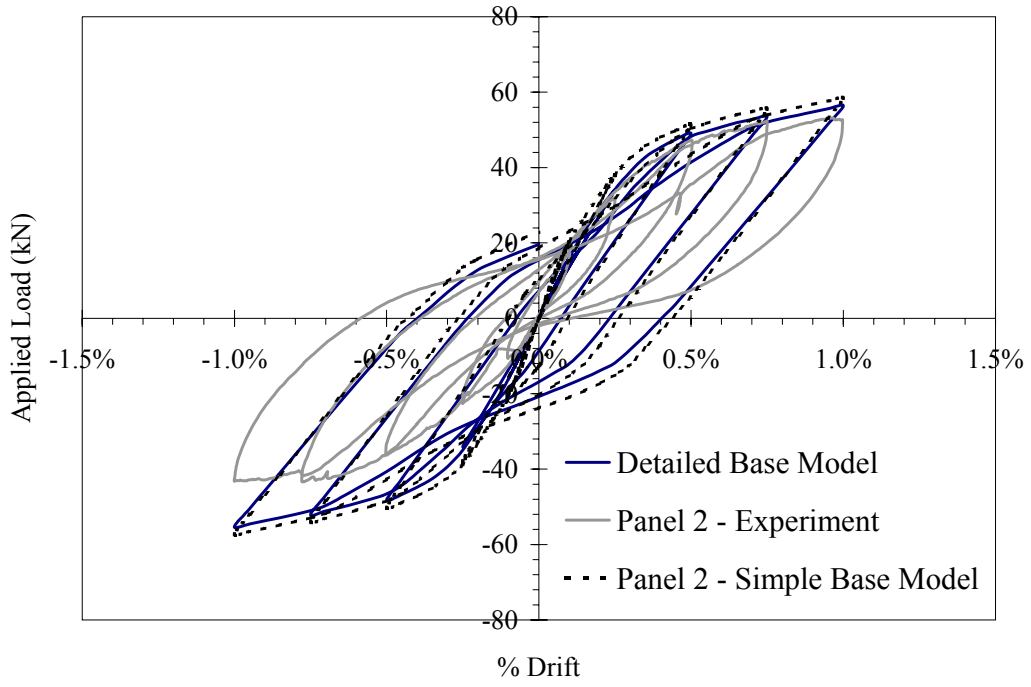

Figure 5-19. Comparison of simulation and experimental results from Panel 2

The change in bolt force results shown in this section were obtained using the procedure discussed in Section 4.3.6. Figure 5-20a and 5-20b show comparisons between the variations in panel connection bolt force obtained from the simulations and the measured experimental results from Panel 2. A pretensioning force of 67 kN was used in these simulations. To simplify the graphs, three pairs of bolts are presented in each figure.

The results indicate that the simulated bolt tension forces followed the same trends and had similar magnitudes as the experimental results from Panel 2. The difference between bolt pairs 2 and 8 in the simulations and experimental results was a consequence of the lack of symmetry in the experimental results. As seen in the experimental results in figure 4-70, the change in bolt load in bolt pairs 2 and 8 was lower than that observed in bolt pairs 5 and 11. The simulation results from the same bolt pairs were symmetric. Similar results were obtained from the simulations with a bolt pretensioning force of 111 kN (representing Panel 3, 4 and 5).

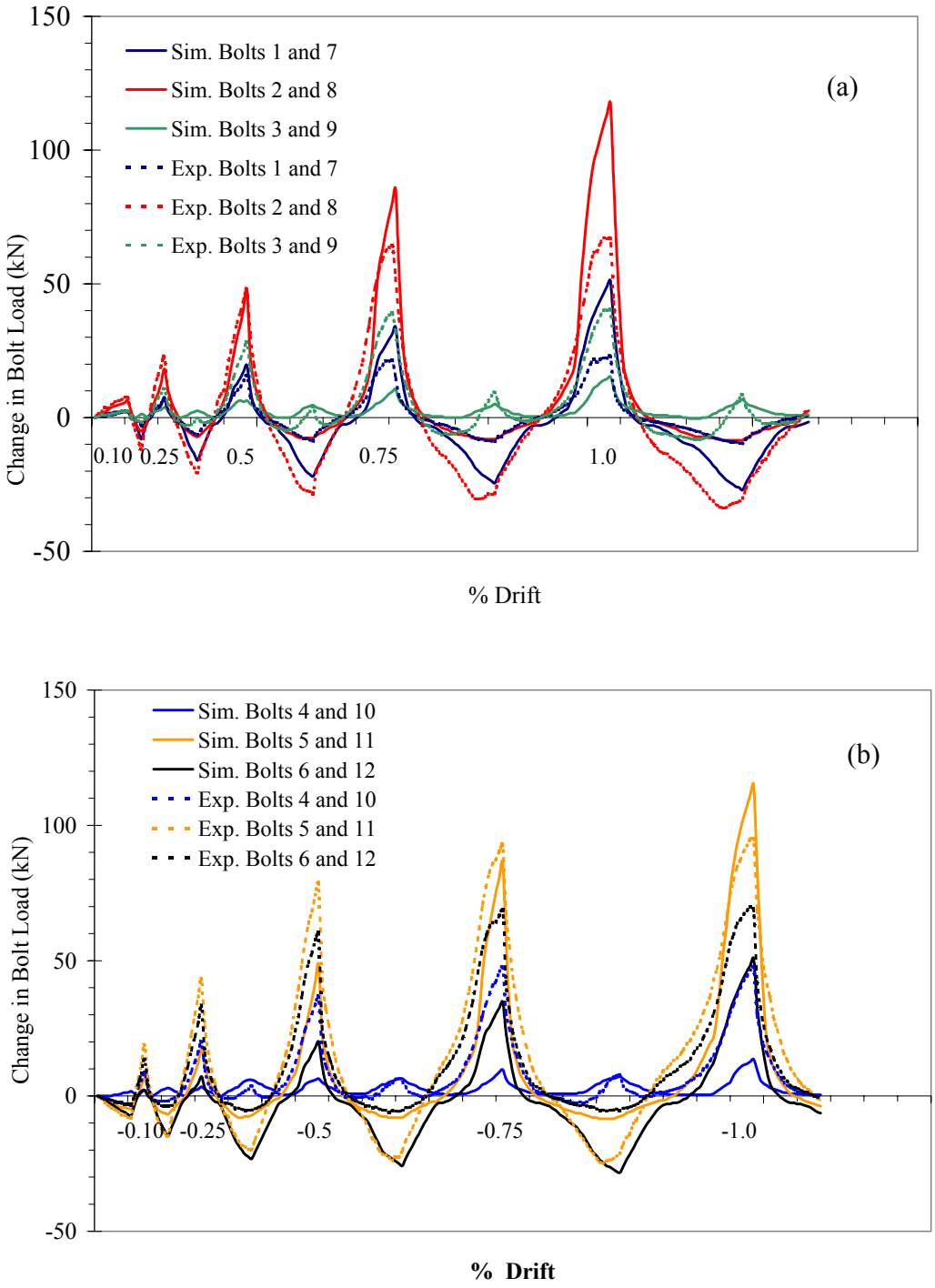

Figure 5-20. Comparison of simulation and experimental results from Panel 2 connection bolts

The greater load in the second pair of bolts (pairs 2 and 8 or 5 and 11), relative to the first pair (1 and 7 or 6 and 12); can be explained by examining the displaced shape of the model. Figure 5-

21 shows a close-up view of the displaced shape of the base of the panel at 0.75% drift. The damage in the confined ECC at the connection edge precludes the material from carrying load. The greater elongation and thus higher load of the second bolt pair, relative to the first is apparent in the figure.

To examine the impact of the retrofit installation on the connection region, the principle strains in the simulation results can be studied. Figure 5-22 and 5-23 show the principle tensile and compressive strain contours, respectively, obtained from the simulation with a 67 kN initial pretensioning force in the panel connection bolts at 1% panel drift. The upper and lower limits of the tensile strain contours were equivalent to the yield strain of the steel reaction beam and connection angles in the connection region. As seen in the figure, the strains in the steel members in the connection region were well below the yield strain. Yielding of the steel members in the connection regions was not observed in any of the simulation results (i.e. different panels and different initial pretensioning levels) up to 1% panel drift. The 1% drift limit corresponded to the maximum drift level examined in the frame analysis.

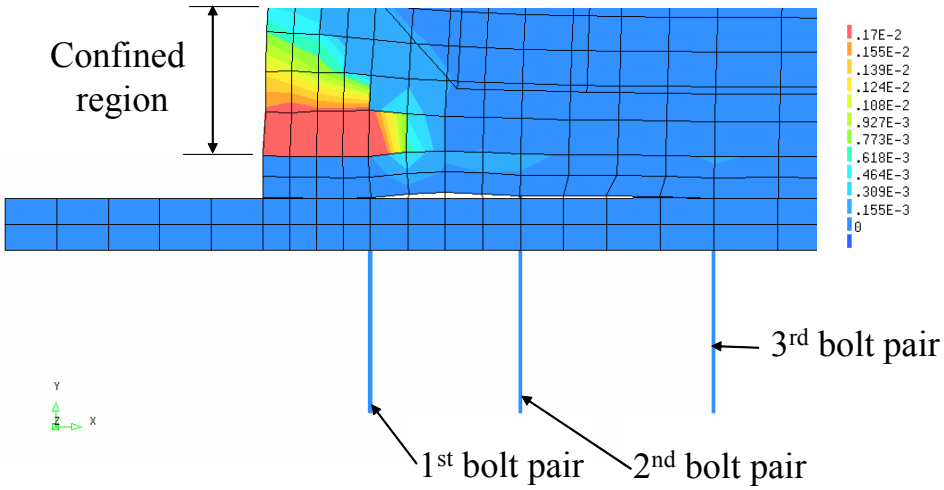

Figure 5-21. Displaced shape of connection bolt model at 0.75% drift with tensile strain limit of 0.0017

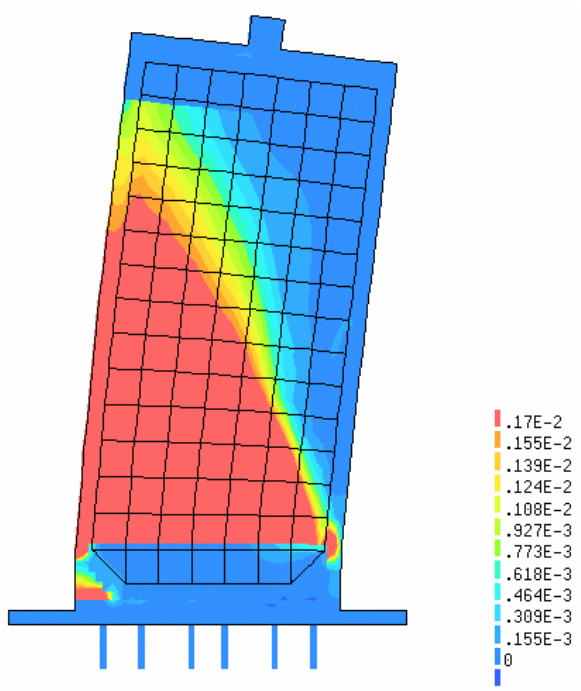

Figure 5-22. Principle tensile strain contour with strain limit of 0.0017

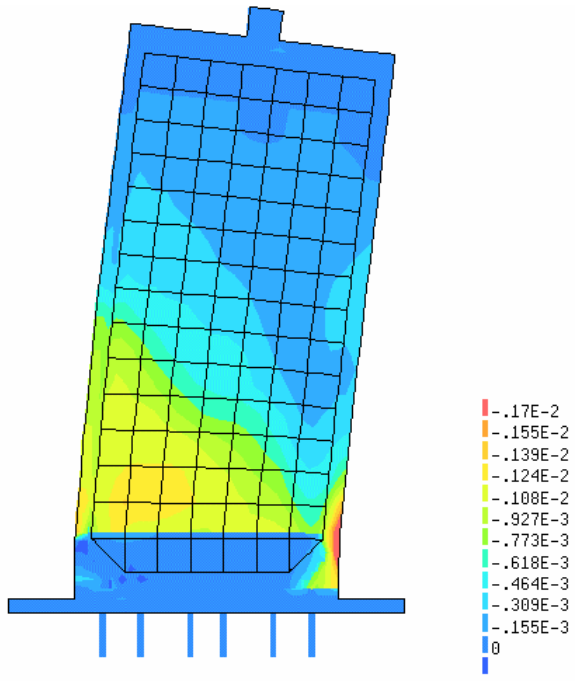

Figure 5-23. Principle compressive strain contour with strain limit of -0.0017

5.2.6 Summary of Infill Panel Simulations

In Section 4, the results from experimental tests on ECC infill panel tests were presented. In this section, finite element-based simulations were performed to model the experimental results. The material model used for the ECC material was developed based upon the material testing results presented in Sections 2.3 and 2.4 of Kesner and Billington (2004). In Section 5.1, the model was shown to capture general features of the cyclic response of ECC materials.

The infill panel simulations demonstrated the ability of the modeling approach to capture the experimental response of the infill panels. The results from uniaxial tension and compression tests on ECC and steel were used as input parameters for the material models. The simulations were able to capture the variation in stiffness, load capacity, and the onset of softening observed in the experimental results. Energy dissipation and residual strength was not captured as well due to the lack of modeling development failure (e.g. bondslip) and fracture of the reinforcement.

Detailed models of the panel connection bolt region were used to examine the transfer of load from the panel into the connection area. The variation in panel connection bolt tension in the simulations was consistent with the observed experimental results. Agreement between the results allows for the simulation results to be used in the design of ECC infill panel connections.

The results of the panel connection bolt simulations indicated that local yielding in the connection regions (e.g. the base beam) does not occur as a consequence of the infill panel installation. This an important observation within the context of using the infill panels to prevent damage in structures during seismic events. The impact of infill panel installation on the structure is further evaluated in Section 5.3.

5.3 Examination of Infill Installation in Existing Structures

In Section 2.5, the results from analyses of a one story, one bay steel frame with infill panels installed were presented. These analyses demonstrated the ability of the beam-type ECC infill sections to increase the strength, stiffness and energy dissipation capabilities of the frame without causing premature damage to the frame.

In the initial analyses, presented in Section 2.5, the frame members were modeled using two-noded beam elements, with the infill panels linked to the frame with nodal constraints. To examine further the impact of the retrofit installation on the frame, more detailed models of the connection between the beam-type infill sections and the frame members were used.

In the detailed analyses presented in this section the response of the bare frame as well as the frame with two and six beam-type infill sections are presented . These results are used to assess the impact of the beam-type infill sections on the frame.

5.3.1 Model Descriptions

To examine the impact of the retrofit installation on the frame, the initial analyses from Section 2.5 were repeated using two-dimensional continuum models comprised of four-noded plane stress elements for the frame. The infill panels and the connection of the infill panels to the frame were simulated using the approach discussed in Section 5.2.5. These detailed models provided a more realistic representation of the connection of the infill section to the frame members than the simplified methods used in Section 2.5.

Figure 5-24 shows the finite element model of the bare frame. The frame member geometries are summarized in table 5-5. Figure 5-25 shows a model with the infill panels added. Similar to the geometry used in Section 4.5, the infill panels in the models were 762 mm wide by 1549 mm tall by 100 mm thick. Two infill panels comprise a beam-type infill section. A gap of 50 mm was used between the beam-type infills. A gap of 25 mm was used between the top (or bottom) of the panels and the frame, and a 50 mm gap was used between the halves of the beam-type infill sections. The connection members were 25 mm thick (the equivalent of two 12.7 mm thick connection tabs). The bases of the column members were fixed. The beam-column joints were assumed to be full moment connections. Results from these models will be compared to results obtained from models in which the frame members are comprised of beam elements.

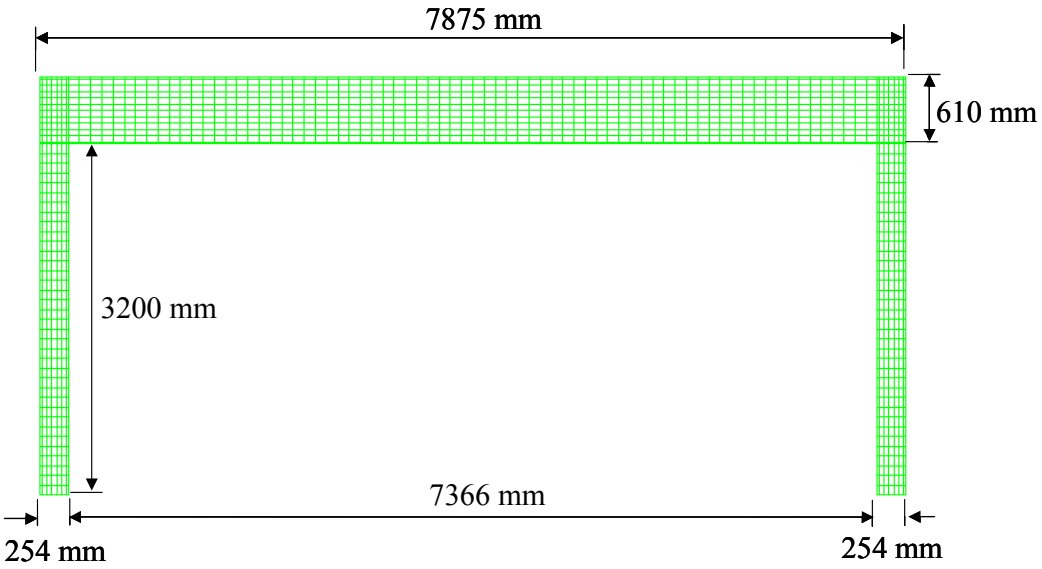

Figure 5-24. Finite element model of bare frame

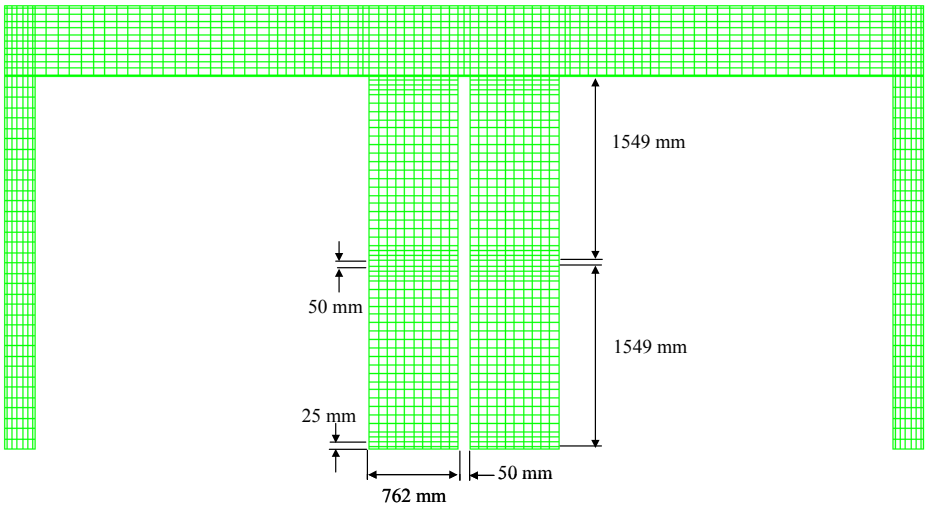

Figure 5-25. Finite element model of frame with infill sections added

Table 5-5 – Frame Member Geometric Properties (in mm)

Member	Flange width	Flange thickness	Web thickness	Member depth
Column	254	15.2	9.4	254
Beam	229	17.8	11.2	635

Two types of connections were used between the infill sections and the frame member. The connections were intended to simulate either bolted or welded connections between the bottom flange of the beam member and the beam-type infill sections. The bolted connection was simulated using interface elements between the bottom flange of the beam and the infill connection member (as described in Section 5.2.5). Six pairs of bolts, spaced 75 mm apart were simulated in the connection. In the welded connections, the bottom flange and infill connection elements were connected at common nodes.

To examine the response of the models, a cyclic displacement to varying drift levels (+/-0.1%, 0.25%, 0.50%, 0.75% and 1.0%) was simulated. The loading history was selected to correspond to the results presented in Section 2.5. The material properties used in the analysis are shown in table 5-2. The ECC1 material model was used in these analyses.

5.3.2 Bare Frame Results

Figure 5-26 shows the load-drift response of the bare frame, comparing the beam model (frame members modeled using beam elements) from Section 2.5 with the plane stress model. The results from the beam model were slightly stiffer than the results from the plane stress element model.

Figures 5-27 to 5-29 show principle strain contours at drift levels of 0.5%, 0.75% and 1.0% drift from the bare frame with plane stress elements. The upper limit on the strain contour is 0.0017, which is the yield strain of the steel in the bare frame. The load-drift results and the principle strain contours show the onset of yielding at a drift level of 0.75% in the plane stress models. The onset of yielding occurred at a similar drift level in the beam element model. Yielding of the steel members was confined to the beam-column joint region in both models. These results serve as baseline values to assess the impact of the beam-type infill sections on the frame.

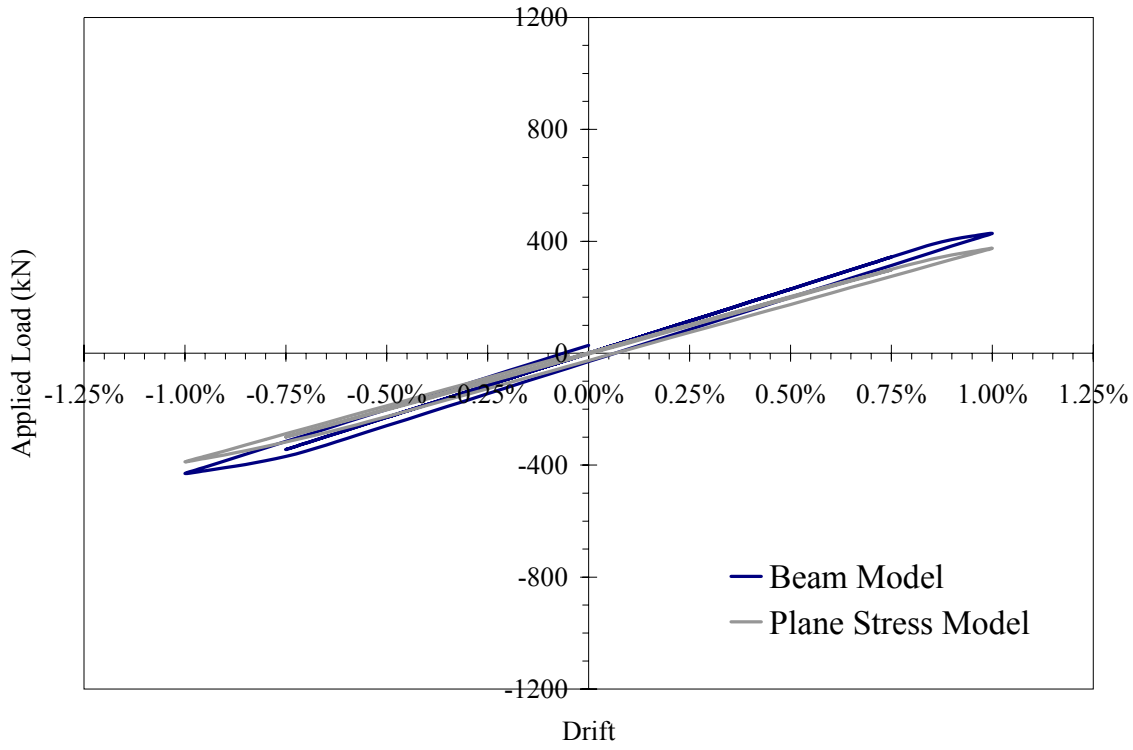

Figure 5-26. Comparison of results from simulations of bare frame

Figure 5-27. Principle strain contour from bare frame at 0.5% drift

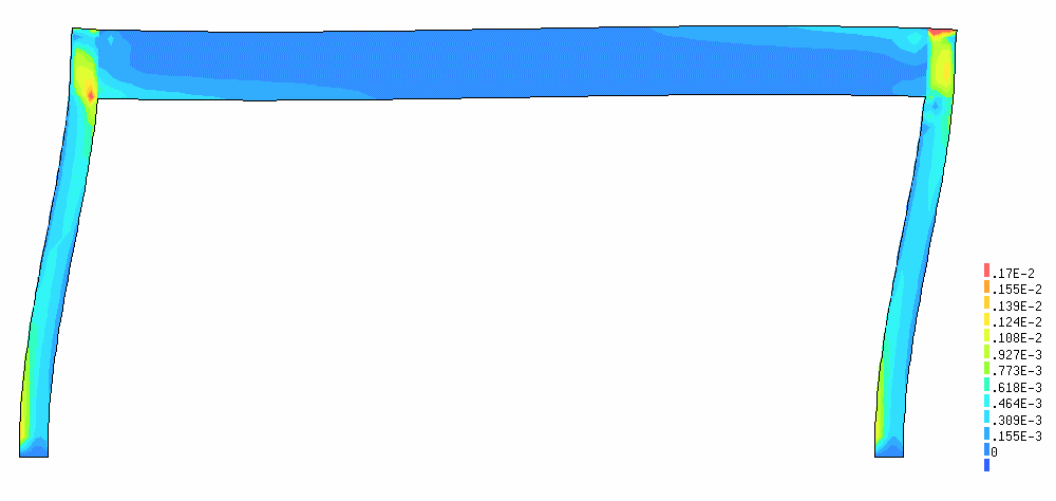

Figure 5-28. Principle strain contour from bare frame at 0.75% drift

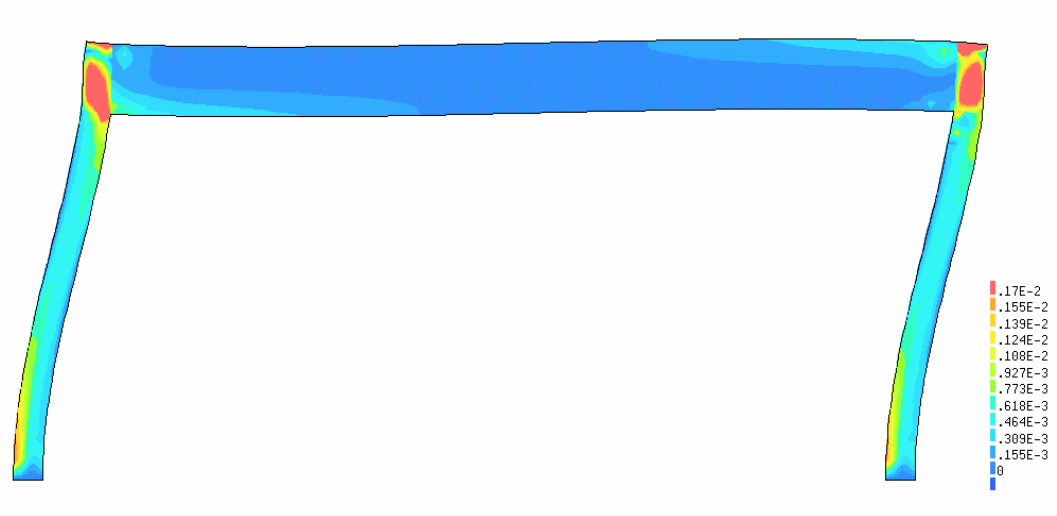

Figure 5-29. Principle strain contour from bare frame at 1.0% drift

5.3.3 Infilled Frame Results

To assess the impact of the beam-type infill on a steel frame, the installation of two and six beam-type infill sections was examined. Figures 5-30 and 5-31 show the load-drift results obtained from simulations with the two and six beam-type infill section additions, respectively. The results obtained from the simulation with the beam elements (Section 2.5) are also shown in the figures.

Only minor differences in the load-drift response were observed between the different connection types. The models made with the plane stress elements have a lower stiffness than the simulations with the beam elements, as was seen in the bare frame simulations. Consistent with the results presented in Section 2.5, the beam-type infill additions resulted in significant increases in the stiffness, strength and energy dissipation compared to the bare frame.

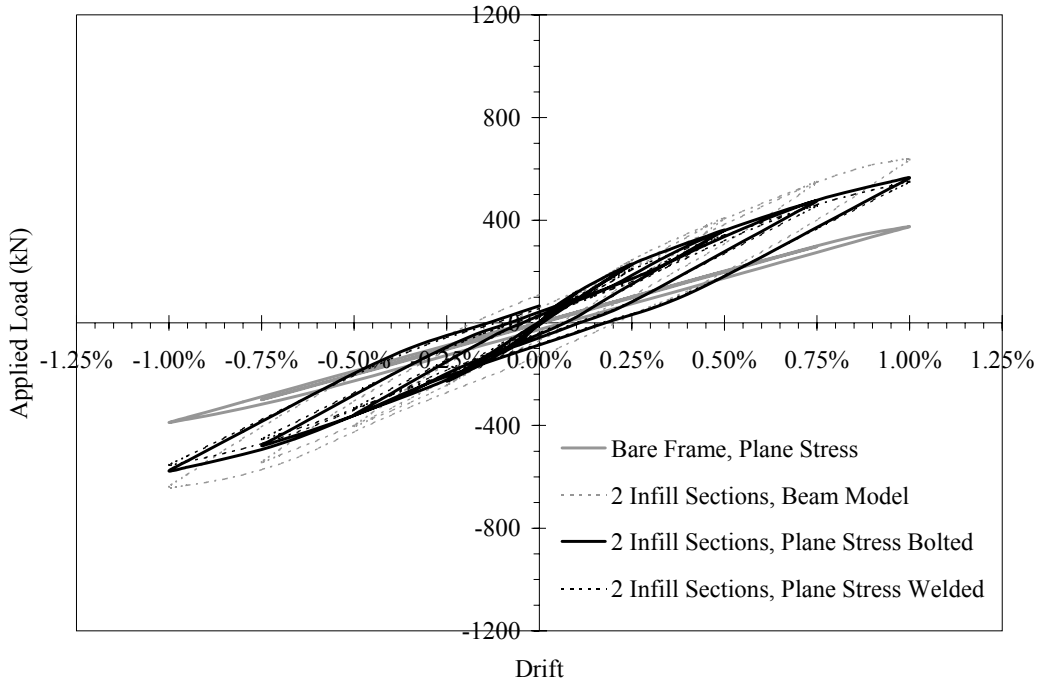

Figure 5-30. Comparison of results from simulations of frame with 2 beam-type infills added

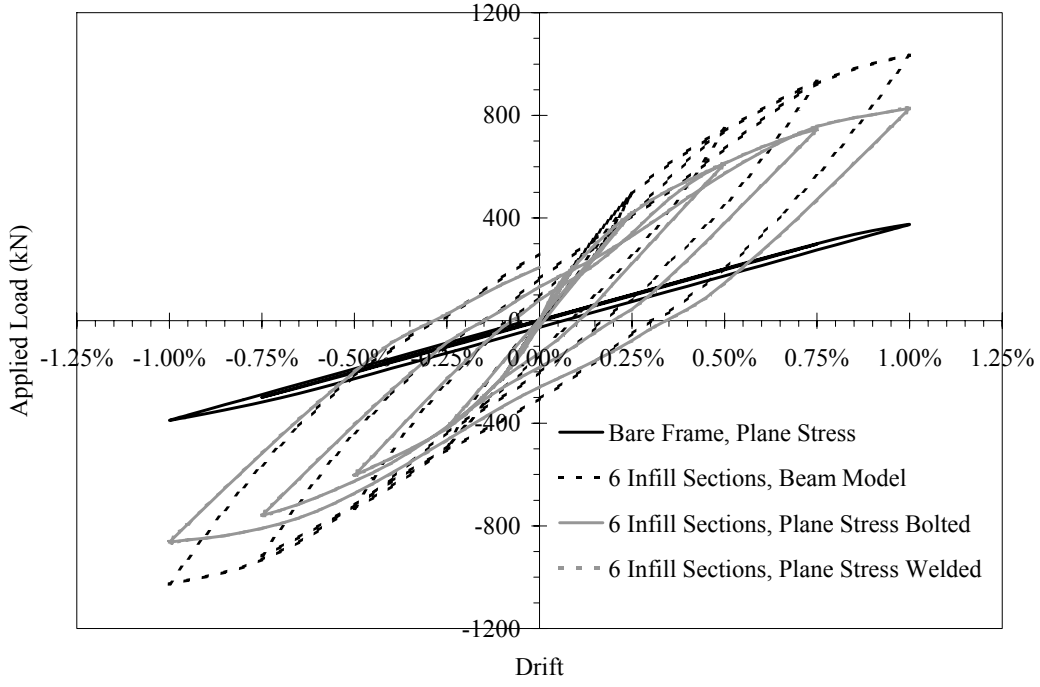

Figure 5-31. Comparison of results from simulations of frame with 6 beam-type infill sections added

A primary goal of the simulations was to examine the local impact of the beam-type infill sections on the frames. The impact of the infill installation on the existing frame can be assessed from an examination of the principle strain contours obtained in the simulations. Figure 5-32 and 5-33 show principle strain contours obtained from the two and six beam-type infill additions, respectively, with bolted connections. Figures 5-34 and 5-35 show the same results with the welded connections. All of the strain contours were taken at a drift of 1%. The upper limit in the strain contours is again 0.0017, the yield strain of the steel frame members (0.0017 is well below the 0.025 peak strain in the ECC).

In the strain contours shown, localized yielding of the frame members was not observed at the infill-to-beam connection regions. All of the yielding in the structures was confined to the beam-column joints and the column bases. Similar to the results of the bare frame simulations, yielding of the frame with the beam-type infill additions began at a drift level of approximately 0.75%. Significant differences were not observed between the modeling of bolted and welded connections. It is noted that these results are specific to the retrofit and frame modeled here and serve only as an indication of the impact of beam-type infills. The impact is expected to vary depending on the type of frame being retrofit.

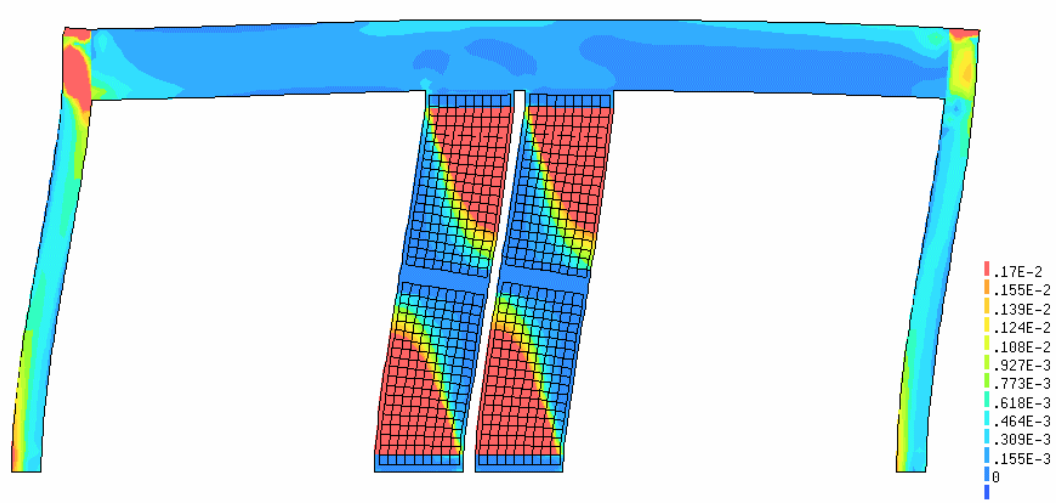

Figure 5-32. Principle strain contour from frame with 2-beam type infill sections added (bolted connections) at 1% drift

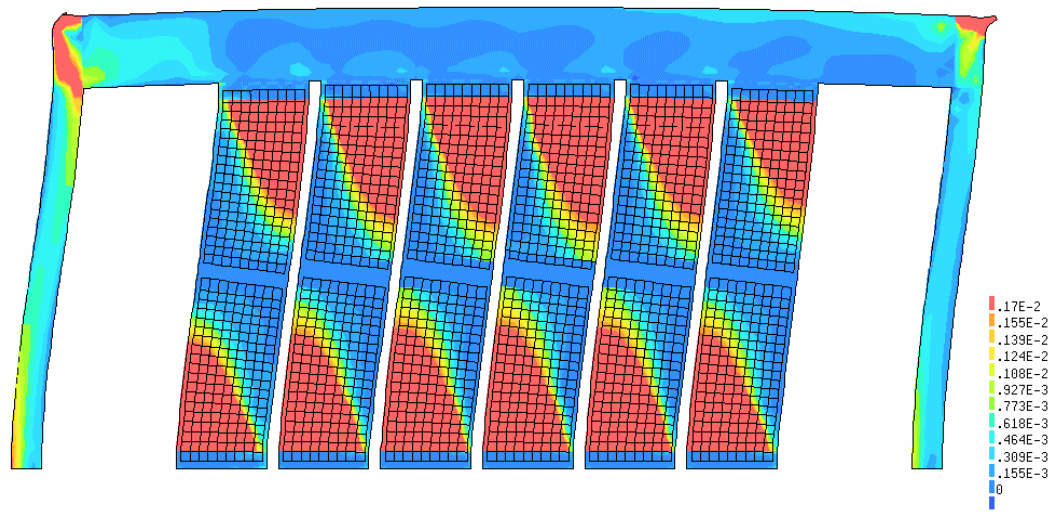

Figure 5-33. Principle strain contour from frame with 6 beam-type infill sections added (bolted connections) at 1% drift

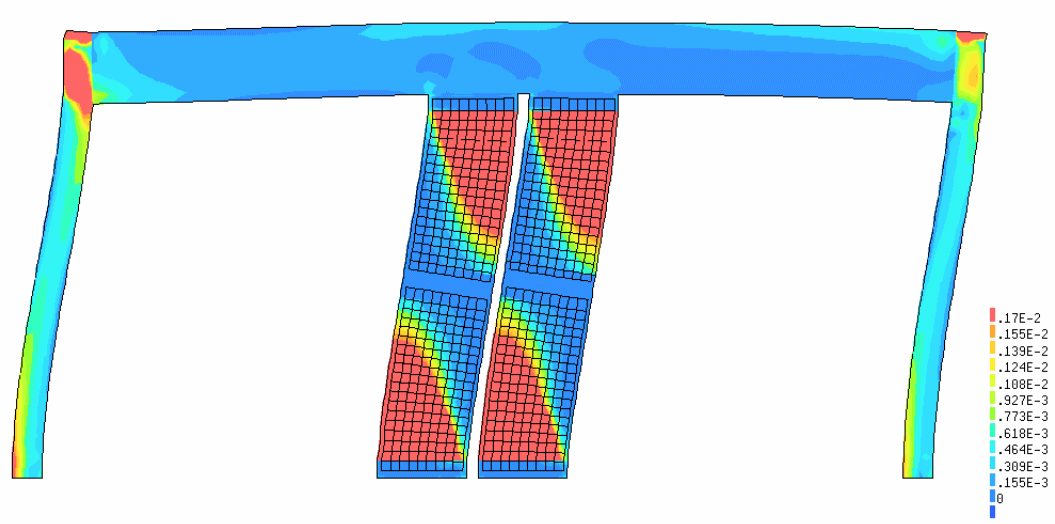

Figure 5-34. Principle strain contour from frame with 2 beam-type infill sections added (welded connections) at 1% drift

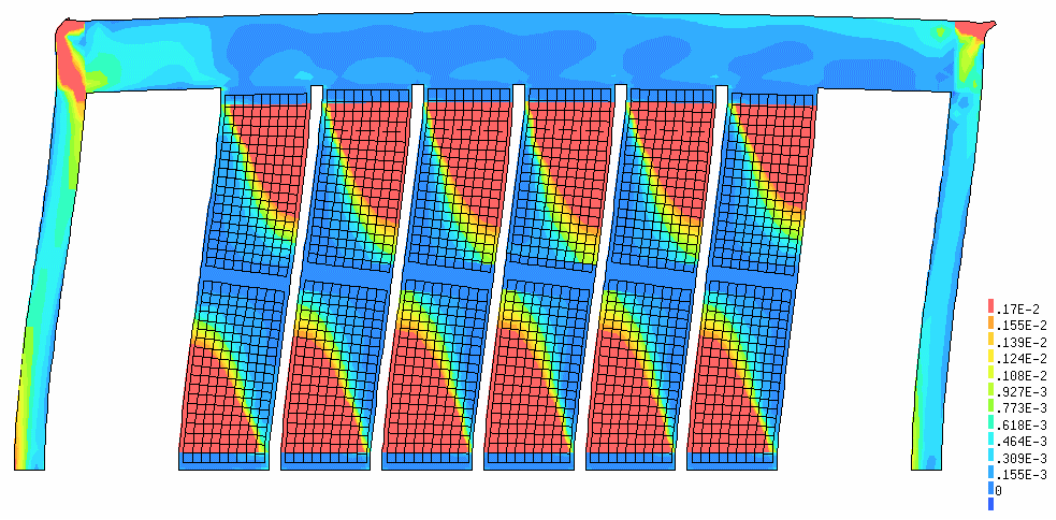

Figure 5-35. Principle strain contour from frame with 6 beam type infill sections added (welded connections) at 1% drift

5.3.4 Examination of ECC Compressive Softening

In Section 2.4 of Kesner and Billington (2004), the results of cyclic testing on ECC materials were presented. One of the key findings in the testing was a limitation on the tensile strain capacity of the ECC material when the peak compressive stress (stress at the onset of compressive softening) was exceeded. This limitation on tensile strain capacity is not included in the formulation of the ECC material model used (Section 5.1).

To determine if compressive softening occurred, the principle compressive strain contours were examined. Figure 5-36 and 5-37 show the contours for the models with 2 and 6 beam-type infill elements respectively, at 1% drift. The upper limit of the strain contours was –0.008, which represents the strain level at the onset of compressive softening. It should be noted that the value of –0.008 is lower than used in the comparisons discussed in Section 2.5. The difference occurred due to the reduction in the ECC modulus of elasticity. In both of the models the compressive strains in the infill sections were below -0.008, which indicates compressive softening has not occurred in the panels. The lack of compressive failure of the ECC was consistent with the laboratory test results presented in Section 4.

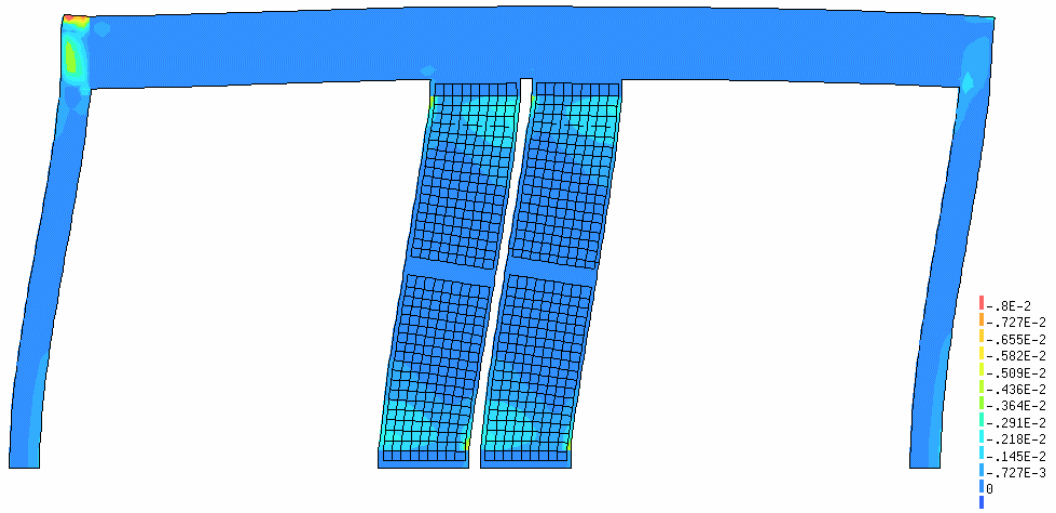

Figure 5-36. Principle strain contour from frame with 2 beam-type infill sections added (welded connections) at 1% drift

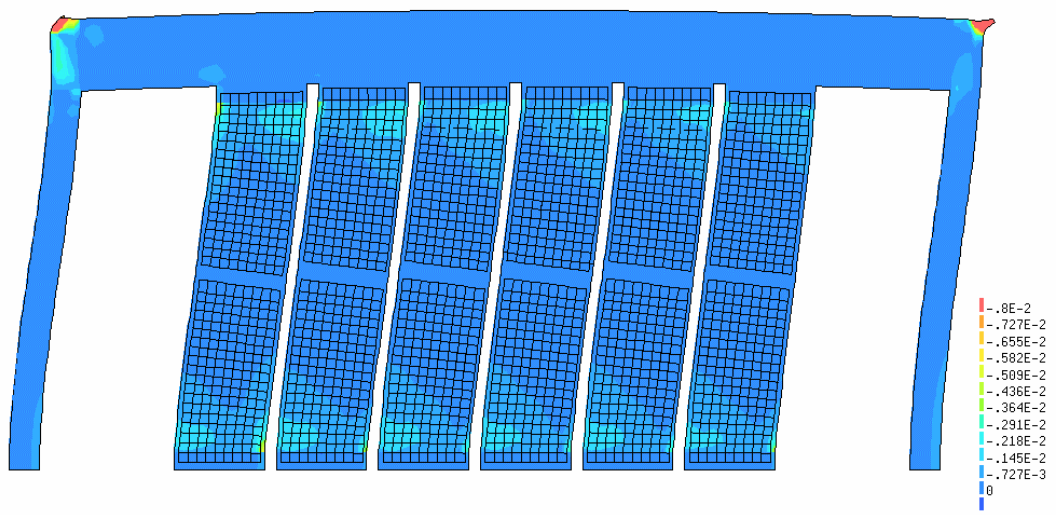

Figure 5-37. Principle strain contour from frame with 6 beam-type infill sections added (welded connections) at 1% drift

5.3.5 Summary of Installation Simulation Results

The analyses presented in this section facilitated evaluating the impact of the beam-type infills on steel frames. The 2-dimensional continuum models were comprised of plane stress elements. The models were intended to provide a more accurate representation of the connections between the ECC infill sections and the frame members than the analyses presented in Chapter 2. The simulation results were also used to determine if the peak compressive strength of the ECC in the panels would be exceeded at 1% drift. The three major findings from the simulations were:

1. The infill additions will not result in localized yielding at the connection of the infills to the frame members for the retrofit and frame system investigated here.
2. Compressive softening of the ECC infill sections was not observed at the peak drift level (1% drift) in the simulation.
3. The drift level at the onset of yielding in the infilled frame was similar to the drift level at the onset of yielding in the bare frame. This indicates the infill additions did not result in premature yielding of the frame examined here.

These findings point to the potential of an ECC infill system to retrofit structures effectively. However the ability of the ECC infill system to either delay or cause a premature onset of yielding in a frame will depend on the retrofit arrangement and the existing frame being retrofitted..

5.4 Summary of Infill Simulations

The results presented in this section focused on the use of finite element simulations to examine the behavior of the ECC infill system under investigation. The simulations utilized a material model specifically developed from the cyclic test results presented in Section 2.5 of Kesner and Billington (2004). The material model used the results from uniaxial tension and compression tests as the input parameters.

The ECC material model was used to simulate the single panel infill tests, as presented in Section 4. The simulations were able to capture the strength, stiffness, and onset of softening obtained in the panel tests with reasonable accuracy. Residual strength and energy dissipation were not captured as well due to a lack of modeling bond, development and fracture failure of the steel reinforcement. To capture accurately the strength, stiffness and onset of softening from the experimental results, the modulus of elasticity of the ECC needed to be reduced by 50-75%. The reduction accounts for the effects of shrinkage cracking and slippage in the connection regions. Based upon the experimental results presented in Section 4.3.6, slippage was the primary cause of the stiffness decrease.

Simulations were also performed to examine the transfer of load from the panels into the base structure. These simulations used a more detailed model of the connection region than was used in the panel test simulations. The simulations were able to predict approximately the variation in panel connection bolt force measured during the panel tests as well as demonstrate the reason for an interior set of bolts carrying more load than the exterior bolts. Such simulations can be used to design connections in the infill system.

The effect of the addition of ECC infill sections on an existing structure was examined by repeating some of the analyses presented in Section 2.5 with more detailed models. The new models used the detailed connection models and a more detailed representation of the steel frame. The results indicated that the ECC infill sections will not result in localized yielding at the connection of the infill section to the particular frame under investigation. Furthermore, as identified in Section 2, the infill installation did not lead to premature yielding of this frame relative to the bare (unretrofitted) frame.

The simulation results also were examined to determine if the compressive stresses in the ECC infill sections exceeded the peak compressive stress in the material, which would limit the advantageous tensile strain capacity of the ECC. The results indicated that compressive softening of the ECC does not occur up to drifts of 1%. Further simulations are needed beyond 1% drift and should include bond, development and fracture failure modes for the reinforcement to study the compressive and tensile performance of ECC at higher drifts.

The findings presented in this chapter indicate that the ECC infill system is a viable and effective approach to retrofitting steel framed structures. Further research is necessary prior to implementation, as discussed in Section 6.

Section 6
Summary and Conclusions

6.0 Introduction

The research presented herein developed an infill wall system for use as a retrofit system in critical facilities with steel frames. The proposed infill system was unique in its use of an ECC material in lieu of a traditional concrete or masonry. The focus on retrofit strategy development for critical structures addressed the needs of the MCEER research program (Program 2) that sponsored this research (MCEER, 2000).

The research was divided into two main areas. The first area developed the infill panel system to address the specific needs of critical facilities. The second area of the research used a combination of large-scale experiments and finite element simulations to evaluate the performance of the infill system.

The following sections provide a summary of the specific areas of the project and present conclusions from the work. The final section ends this report with suggestions for future research that will build upon this work and facilitate implementation of the developed retrofit system in practice.

6.1 Summary

The infill system was developed to address the specific needs of critical facilities. Aspects of previous infill research were combined with the specific needs of critical facilities. The resulting system uses precast ECC infill panels with pretensioned bolted connections between the panel sections and at the existing structure. Based upon the results of finite element simulations, a beam-type infill orientation that partially filled a structural frame was determined to be preferential over a traditional full frame infill (wall) system.

Initial simulations were used to design and conduct a series of experimental tests on connection details and full size infill sections. The connection tests verified the suitability of the pretensioned connections. The infill panel tests evaluated the response of the infill panels, made with different ECC materials, reinforcement and geometries to cyclic loadings. The results indicated that different amounts of strength, stiffness, and energy dissipation in the panels can be obtained from the panels. All of the panels tested failed in a predominantly flexural mode.

Finite element simulations were used to study further the effect of infill additions on the response of a frame to cyclic loadings. These simulations used a material model for the ECC that was developed by colleagues (Han, et al., 2003) from the cyclic testing on the materials performed described in Kesner and Billington (2004). The simulations confirmed that the beam-type infill additions will increase the strength, stiffness and energy dissipation of the structures. Adverse effects, such as localized yielding at the connection regions between the infill sections and the frame were not observed in the simulation results. Furthermore, the compressive strains in the retrofit were below the peak compressive strain level (strain level at the onset of softening),

which was important as compressive strain above the peak act to reduce the tensile strain capacity of the material.

6.2 Conclusions

The key findings and conclusions from the infill system investigations and development were:

- A beam-type infill system using precast ECC infill sections is advantageous over a traditional full wall infill. The beam-type infill was found to increase the strength, stiffness and energy dissipation in a prototype frame, while protecting the frame from yielding. The full frame (wall) infill caused premature yielding of the frame members at low drift levels. Further, the beam-type infill uses the ECC material more efficiently by allowing the tensile strain capacity of the ECC to be used in conjunction with steel reinforcement.

- Pretensioned bolted connections are a viable method to connect ECC infill sections.

- A variety of performance characteristics can be obtained with different materials, panel geometries, and reinforcement orientations in the infill panel system. Such variety makes the system an ideal choice for performance-based design.

- The infill panels are expected to fail at structural drift levels above 1%, with panel failure cause by localization of a crack at the panel base leading to ECC failure (in tension) and reinforcement fracture.

- 2D finite element simulations were able to capture the experimental response of the infill panels with reasonable accuracy using a material model based on the results of the uniaxial tension and compression tests performed in another part of this research.

- The simulation results indicated that the infilled frame studied can reach drift levels of 0.75% without damage to the existing structure. A drift of 0.75% is at the upper drift limit suggested in the building performance guidelines for critical facilities (FEMA-273, 1999)

- Detailed simulations were able to verify the ability of the proposed infill system to strengthen and stiffen existing structures without localized damage at panel locations.

6.3 Recommendations for Future Work

In the preceding sections, an ECC panel infill system was developed and investigated as a possible retrofit strategy for critical structures. To develop the system for implementation, additional research will be needed. The following sections briefly describe some of the required research.

6.3.1 Full Scale Testing and Simulation

In Section 4, the results of single panel tests on ECC infill sections were presented. These results were augmented by simulations of infill system performance in a single story, single bay frame (presented in Section 5). To develop the system for implementation, additional testing and simulation on larger scale structures are needed.

Larger scale testing of infilled frame sections is also needed to verify construction methods and performance of the larger infill sections. The testing will need to include more complicated loadings at variable strain rates than the simple cyclic displacements used in the current study, and must also include the effects of possible axial loads on the panels.

Larger scale simulations are also needed to examine the effect of infill additions on multi-story, multi-bay frames. In particular, the ability of the infilled structures to satisfy the performance limits of critical facilities needs to be evaluated (ongoing work being conducted by other MCEER researchers).

6.3.2 Cost Evaluation

The proposed retrofit system has the potential to improve the performance of critical facilities during seismic events. However, the system will not be viable as a retrofit strategy unless it provides the desired level of performance at a cost that is competitive with other retrofit strategies. Realistic assessment of the infill system cost must include both the cost of retrofit installation and an examination of the advantages of the proposed system (such as minimizing the need for utility relocation, minimizing construction time, ease of future infill relocation/replacement) over traditional retrofit systems.

Section 7
References

AISC (1988) "Specification for Structural Joints Using ASTM A325 or A490 Bolts" American Institute of Iron and Steel Construction, Chicago, IL, 52 pp.

ASTM A-490 (2002) "Standard Specification for Structural Bolts, Alloy Steel, Heat Treated, 150 ksi Minimum Tensile Strength," American Society for Testing and Materials, West Conshohocken, PA.

ASTM C39-95 (1995) "Standard Test Method for Compressive Strength of Cylindrical Concrete Specimens," American Society for Testing and Materials, West Conshohocken, PA.

ASTM C496-95 (1995) "Standard Test Method for Splitting Tensile Strength of Cylindrical Concrete Specimens," American Society for Testing and Materials, West Conshohocken, PA.

Benjamin, J.R., and William, H.A. (1957) "The behavior of one story reinforced concrete shear walls." *Proceedings of the American Society of Civil Engineers*, Vol. 83, No. ST3, Paper 1254 (49 pp).

Benjamin, J.R., and William, H.A. (1958) "The behavior of one story brick shear walls." *Proceedings of the American Society of Civil Engineers*, Vol. 84, No. ST4, Paper 1723 (30 pp).

Beres, A., White, R.N., and Gergely, P. (1992) "Seismic Behavior of Reinforced Concrete Frame Structures with Nonductile Details: Part I – Summary of Experimental Findings of Full Scale Beam-Column Joint Tests." Technical Report NCEER-9200024, National Center for Earthquake Engineering Research, State Univ. of NY at Buffalo.

Bickford, J.H., (1995) "An Introduction to the Design and Behavior of Bolted Joints," Marcel Dekker, Inc., New York, NY, pp. 951.

Billington, SL, and Yoon, JK (2004) "Cyclic Response of Precast Bridge Columns with Ductile Fiber-reinforced Concrete," *ASCE J. Bridge Engineering*, 9(4): 353-363.

Bracci, J.M., Reinhorn, A.M., and Mander, J.B. (1992) "Seismic Response of Reinforced Concrete Frame Structures Designed only for Gravity Loads: Part II – Experimental Performance of Subassemblages," Technical Report NCEER-92-0028.

Buonopane, S.G., and White, R.N. (1999) "Seismic evaluation of a masonry infilled reinforced concrete frame by pseudo-dynamic testing." Technical Report MCEER-99-0001, Multi-disciplinary Center for Earthquake Engineering Research, State University of New York at Buffalo.

D'Ambrisi, A., and Filippou, F.C. (1997) "Correlation Studies on an RC Frame Shaking-Table Specimen," Earthquake Engineering and Structural Dynamics 26, pp. 1021-1040.

Dawe, J.L., and Seah, C.K. (1989) "Behavior of masonry infilled steel frames," *Canadian Journal of Civil Engineering*, Vol. 16, pp. 877-885.

Dawe, J.L., Schriver, A.B., and Sofocleous, C. (1989) "Masonry infilled steel frames subjected to dynamic load," *Canadian Journal of Civil Engineering*, Vol. 16, pp. 865-876.

Douglas, K.S., Kesner, K.E., and Billington, S.L. (2004) "Simplified Modeling Techniques for a Proposed Retrofit System using Ductile Fiber-Reinforced Cementitious Composites," *13th World Conference on Earthquake Engineering*, Vancouver, B.C., Canada, August

El-Attar, A.G., White, R.N., and Gergely, P. (1991) "Shake Table Test of a 1/8 scale Three Story Lightly Reinforced Concrete Building," Technical Report NCEER 91-0018.

El-Borgi, S., White, R.N., Gergely, P., and Beres, A. (1993) "Evaluation and analysis of existing lightly reinforced concrete buildings," 1993 National Earthquake Conference, Memphis, TN, Vol. II, pp. 111-119.

Feenstra, P.H., Rots, J.G., Arnesen, A., Teigen, J.G., and Hoiseth, K.V. (1998) "A 3D consistitutive model for concrete based on a co-rotational concept," Computational Modeling of Concrete Structures: Proceedings of the Euro-C 1998 Conference on Computation Modelling of Concrete Structures, R. DeBorst, N. Bicanic, H. Mang, and G. Meschke (eds.), Badgastein, 31 March – 3 April 1998. Rotterdam: Balkema.

FEMA-273 (1999) "NEHRP Guidelines for Seismic Retrofit of Buildings," Federal Emergency Management Agency, Washington, D.C.

Fischer, G. and Li, V. (2002) "Influence of matrix ductility on tension-stiffening behavior of steel reinforced engineered cementitious composites (ECC)," *ACI Structures Journal*, Vol. 99, No. 1, pp.104-111.

Frosch, R., Li., W., Jirsa, J., and Kreger, M. (1996) "Retrofit of Non-Ductile Moment-Resisting Frames Using Precast Infill Wall Panels," *Earthquake Spectra*, Vol. 12, Number 4. pp. 741-760.

Gergely, P., White, R.N., Zawilinski, D., and Mosalam, K. (1993) "The interaction of masonry infill and steel or concrete frames," 1993 National Earthquake Conference, Memphis, TN, Vol. II, pp. 183-192.

Han, T.S. (2001) "Interface Modeling of Composite Material Degradation," Ph.D. Dissertation, Cornell University, Ithaca, NY, 151 pp.

Han, T.S., Feenstra, P.H., and Billington, S.L. (2003) "Simulation of Highly Ductile Fiber-Reinforced Cement-based Composites," *ACI Structures Journal,* 100(6): 749-757.

Holmes, M. (1961) "Steel frames with brickwork and concrete infilling," *Proceedings Institute of Civil Engineers*, Vol. 19, pp. 473-478.

Holmes, M. (1963) "Combined loading on infilled frames," *Proceedings Institute of Civil Engineers,* Vol. 25, pp. 31-38.

Horii, H., Kabele, P., Takeuchi, S., Li, V., Matsuoka, S., Kanda, T. (1998) "On the Prediction Method for the Structural Performance of Repaired/Retrofitted Structures" Fracture Mechanics in Concrete Structures: Proceedings FRAMCOS-3. Volume III p. 1739.

Kabele, P., Takeuchi, S., Inaba, K., and Horii, H. (1999) "Performance of Engineered Cementitious Composites in Repair and Retrofit: Analytical Estimates," High Performance Fiber Reinforced Composites (HPFRCC 3), Edited by H.W. Reinhardt, and A. Namaan, Rilem, pp. 617-627.

Kahn, L.F., and Hanson, R.D. (1979) "Infilled walls for earthquake strengthening" *Journal of the Structural Division*, ASCE, Vol. 105, No. ST 4, Feb. 1979, pp. 283-296.

Kanda, T., Watanabe, S., and Li. V.C. (1998) "Application of pseudo strain hardening cementitious composites to shear resistant structural elements," Fracture mechanics in concrete structures: Proceedings of Framcos-3, Edited by H. Mihashi and K. Rokugo. Volume III, pp. 1477-1490.

Kesner, K.E., and Billington, S.L. (2001), "Development of Ductile Cement-based Composites for Seismic Strengthening and Retrofit," Proceedings of the Fourth International Conference on Fracture Mechanics of Concrete Structures, de Borst, et al., (Eds.) 2001, A.A. Balkema Publishers, pp. 65-72.

Kesner, K.E., and Billington, S.L. (2004) *Tension, Compression and Cyclic Testing of Engineered Cementitious Composites*, Technical Report MCEER-04-0002, Multi-disciplinary Center for Earthquake Engineering Research, State University of New York at Buffalo.

Kost, G., Weaver, W. Jr. and Barber, R.B. (1974) "Nonlinear dynamic analysis of frames with filler panels," *Journal of the Structural Division*, ASCE, Vol. 100, No. ST4, April 1974, pp. 743-757.

Mallick, D.V., and Garg, R.P. (1971) "Effect of openings on the lateral stiffness of infilled frames," *Proceedings of the Institute of Civil Engineers*, Vol. 49, pp. 193-209.

Mallick, D.V., and Severn, R.T. (1967) "The behavior of infilled frames under static loading," *Proceedings of the Institute of Civil Engineers*, Vol. 38, pp. 639-656.

Mallick, D.V., and Severn, R.T. (1968) "Dynamic characterization of infilled frames," *Proceedings of the Institute of Civil Engineers*, Vol. 39, pp. 261-287.

MCEER (2000) Strategic Plan 2000, http://mceer.buffalo.edu/aboutMCEER/strategicPlan/

Mehta, P. (1986) "*Concrete Structures, Properties and Materials*," Prentice Hall Inc., Englewood Cliffs, NJ, 450 pp.

Mosalam, K. (1996) "Experimental and computational strategies for the seismic behavior evaluation of frames with infill walls," Ph.D. Dissertation, Cornell University, Ithaca, NY. 260 pp.

Mosalam, K., White, R.N., and Gergely, P. (1997) "Static response of infilled frames using quasi-static experiments" *Journal of Structural Engineering*, Vol. 123, No. 11, November 1997, pp. 1462-1469.

OSHPD (1995) "The Northridge Earthquake – A Report to the Hospital Safety Board on the Performance of Hospital," Prepared by Office of Statewide Health Planning and Development, Facilities Development Division, 63 pp.

Rouse, J.M. (2004) "Behavior of Bridge Columns with Ductile Fiber Reinforced Hinge Regions and Vertical Post-tensioning," Ph.D. Dissertation, Cornell University, Ithaca, NY, 308 pp.

Salmon, C., and Johnson, J. (1990), "Steel Structures Design and Behavior," Harper Collins, Publishers, NY, NY, 1086 pp.

Sharooz, B.M., and Moehle, J.P. (1987) "Experimental Study of Seismic Response of R.C. Setback Buildings," Earthquake Engineering Research Center, University of California at Berkeley, Report No. UCB/EERC-87/16.

Stafford Smith, B. (1962) "Lateral stiffness of infilled frames," *Journal of the Structural Division*, ASCE, Vol. 85, No. ST6, Proc. Paper 3355, pp. 183-199.

Stafford Smith, B. (1965) "Model test results of vertical and horizontal loading of infilled frames," *ACI Journal*, 65-44, pp. 618-624.

Stafford Smith, B. (1966) "Behavior of square infilled frames," *Journal of the Structural Division,* ASCE, Vol. 92, No. ST1, Proc. Paper 4690, pp. 381-403.

Taghdi, M., Bruneau, M., and Saatcioglu, M. (2000a) "Seismic retrofitting of low-rise masonry and concrete walls using steel strips" *Journal of Structural Engineering*, Vol. 126, No. 9, September 2000, pp. 1017-1025.

TNO Building and Construction Research (1998a) *DIANA Manual Release 7.2-Element Library,* Delft, the Netherlands.

TNO Building and Construction Research (1998b) *DIANA Manual Release 7.2-Nonlinear Analysis*, Delft, the Netherlands.

Yoon, J.K., (2002) "Experimental and numerical studies of precast unbonded post-tensioned bridge columns with engineered cementitious composites," Master's Thesis, Cornell University, Ithaca, NY, 167 pp.

Yuan, Y. T., and Whitaker, A. (2002) "MCEER Demonstration hospitals mathematical models and preliminary analysis results" Department of Civil, Structural and Environmental Engineering, University at Buffalo, Buffalo, NY, 29 pp.

Multidisciplinary Center for Earthquake Engineering Research
List of Technical Reports

The Multidisciplinary Center for Earthquake Engineering Research (MCEER) publishes technical reports on a variety of subjects related to earthquake engineering written by authors funded through MCEER. These reports are available from both MCEER Publications and the National Technical Information Service (NTIS). Requests for reports should be directed to MCEER Publications, Multidisciplinary Center for Earthquake Engineering Research, State University of New York at Buffalo, Red Jacket Quadrangle, Buffalo, New York 14261. Reports can also be requested through NTIS, 5285 Port Royal Road, Springfield, Virginia 22161. NTIS accession numbers are shown in parenthesis, if available.

NCEER-87-0001 "First-Year Program in Research, Education and Technology Transfer," 3/5/87, (PB88-134275, A04, MF-A01).

NCEER-87-0002 "Experimental Evaluation of Instantaneous Optimal Algorithms for Structural Control," by R.C. Lin, T.T. Soong and A.M. Reinhorn, 4/20/87, (PB88-134341, A04, MF-A01).

NCEER-87-0003 "Experimentation Using the Earthquake Simulation Facilities at University at Buffalo," by A.M. Reinhorn and R.L. Ketter, to be published.

NCEER-87-0004 "The System Characteristics and Performance of a Shaking Table," by J.S. Hwang, K.C. Chang and G.C. Lee, 6/1/87, (PB88-134259, A03, MF-A01). This report is available only through NTIS (see address given above).

NCEER-87-0005 "A Finite Element Formulation for Nonlinear Viscoplastic Material Using a Q Model," by O. Gyebi and G. Dasgupta, 11/2/87, (PB88-213764, A08, MF-A01).

NCEER-87-0006 "Symbolic Manipulation Program (SMP) - Algebraic Codes for Two and Three Dimensional Finite Element Formulations," by X. Lee and G. Dasgupta, 11/9/87, (PB88-218522, A05, MF-A01).

NCEER-87-0007 "Instantaneous Optimal Control Laws for Tall Buildings Under Seismic Excitations," by J.N. Yang, A. Akbarpour and P. Ghaemmaghami, 6/10/87, (PB88-134333, A06, MF-A01). This report is only available through NTIS (see address given above).

NCEER-87-0008 "IDARC: Inelastic Damage Analysis of Reinforced Concrete Frame - Shear-Wall Structures," by Y.J. Park, A.M. Reinhorn and S.K. Kunnath, 7/20/87, (PB88-134325, A09, MF-A01). This report is only available through NTIS (see address given above).

NCEER-87-0009 "Liquefaction Potential for New York State: A Preliminary Report on Sites in Manhattan and Buffalo," by M. Budhu, V. Vijayakumar, R.F. Giese and L. Baumgras, 8/31/87, (PB88-163704, A03, MF-A01). This report is available only through NTIS (see address given above).

NCEER-87-0010 "Vertical and Torsional Vibration of Foundations in Inhomogeneous Media," by A.S. Veletsos and K.W. Dotson, 6/1/87, (PB88-134291, A03, MF-A01). This report is only available through NTIS (see address given above).

NCEER-87-0011 "Seismic Probabilistic Risk Assessment and Seismic Margins Studies for Nuclear Power Plants," by Howard H.M. Hwang, 6/15/87, (PB88-134267, A03, MF-A01). This report is only available through NTIS (see address given above).

NCEER-87-0012 "Parametric Studies of Frequency Response of Secondary Systems Under Ground-Acceleration Excitations," by Y. Yong and Y.K. Lin, 6/10/87, (PB88-134309, A03, MF-A01). This report is only available through NTIS (see address given above).

NCEER-87-0013 "Frequency Response of Secondary Systems Under Seismic Excitation," by J.A. HoLung, J. Cai and Y.K. Lin, 7/31/87, (PB88-134317, A05, MF-A01). This report is only available through NTIS (see address given above).

NCEER-87-0014 "Modelling Earthquake Ground Motions in Seismically Active Regions Using Parametric Time Series Methods," by G.W. Ellis and A.S. Cakmak, 8/25/87, (PB88-134283, A08, MF-A01). This report is only available through NTIS (see address given above).

NCEER-87-0015 "Detection and Assessment of Seismic Structural Damage," by E. DiPasquale and A.S. Cakmak, 8/25/87, (PB88-163712, A05, MF-A01). This report is only available through NTIS (see address given above).

NCEER-87-0016 "Pipeline Experiment at Parkfield, California," by J. Isenberg and E. Richardson, 9/15/87, (PB88-163720, A03, MF-A01). This report is available only through NTIS (see address given above).

NCEER-87-0017 "Digital Simulation of Seismic Ground Motion," by M. Shinozuka, G. Deodatis and T. Harada, 8/31/87, (PB88-155197, A04, MF-A01). This report is available only through NTIS (see address given above).

NCEER-87-0018 "Practical Considerations for Structural Control: System Uncertainty, System Time Delay and Truncation of Small Control Forces," J.N. Yang and A. Akbarpour, 8/10/87, (PB88-163738, A08, MF-A01). This report is only available through NTIS (see address given above).

NCEER-87-0019 "Modal Analysis of Nonclassically Damped Structural Systems Using Canonical Transformation," by J.N. Yang, S. Sarkani and F.X. Long, 9/27/87, (PB88-187851, A04, MF-A01).

NCEER-87-0020 "A Nonstationary Solution in Random Vibration Theory," by J.R. Red-Horse and P.D. Spanos, 11/3/87, (PB88-163746, A03, MF-A01).

NCEER-87-0021 "Horizontal Impedances for Radially Inhomogeneous Viscoelastic Soil Layers," by A.S. Veletsos and K.W. Dotson, 10/15/87, (PB88-150859, A04, MF-A01).

NCEER-87-0022 "Seismic Damage Assessment of Reinforced Concrete Members," by Y.S. Chung, C. Meyer and M. Shinozuka, 10/9/87, (PB88-150867, A05, MF-A01). This report is available only through NTIS (see address given above).

NCEER-87-0023 "Active Structural Control in Civil Engineering," by T.T. Soong, 11/11/87, (PB88-187778, A03, MF-A01).

NCEER-87-0024 "Vertical and Torsional Impedances for Radially Inhomogeneous Viscoelastic Soil Layers," by K.W. Dotson and A.S. Veletsos, 12/87, (PB88-187786, A03, MF-A01).

NCEER-87-0025 "Proceedings from the Symposium on Seismic Hazards, Ground Motions, Soil-Liquefaction and Engineering Practice in Eastern North America," October 20-22, 1987, edited by K.H. Jacob, 12/87, (PB88-188115, A23, MF-A01). This report is available only through NTIS (see address given above).

NCEER-87-0026 "Report on the Whittier-Narrows, California, Earthquake of October 1, 1987," by J. Pantelic and A. Reinhorn, 11/87, (PB88-187752, A03, MF-A01). This report is available only through NTIS (see address given above).

NCEER-87-0027 "Design of a Modular Program for Transient Nonlinear Analysis of Large 3-D Building Structures," by S. Srivastav and J.F. Abel, 12/30/87, (PB88-187950, A05, MF-A01). This report is only available through NTIS (see address given above).

NCEER-87-0028 "Second-Year Program in Research, Education and Technology Transfer," 3/8/88, (PB88-219480, A04, MF-A01).

NCEER-88-0001 "Workshop on Seismic Computer Analysis and Design of Buildings With Interactive Graphics," by W. McGuire, J.F. Abel and C.H. Conley, 1/18/88, (PB88-187760, A03, MF-A01). This report is only available through NTIS (see address given above).

NCEER-88-0002 "Optimal Control of Nonlinear Flexible Structures," by J.N. Yang, F.X. Long and D. Wong, 1/22/88, (PB88-213772, A06, MF-A01).

NCEER-88-0003 "Substructuring Techniques in the Time Domain for Primary-Secondary Structural Systems," by G.D. Manolis and G. Juhn, 2/10/88, (PB88-213780, A04, MF-A01).

NCEER-88-0004 "Iterative Seismic Analysis of Primary-Secondary Systems," by A. Singhal, L.D. Lutes and P.D. Spanos, 2/23/88, (PB88-213798, A04, MF-A01).

NCEER-88-0005 "Stochastic Finite Element Expansion for Random Media," by P.D. Spanos and R. Ghanem, 3/14/88, (PB88-213806, A03, MF-A01).

NCEER-88-0006 "Combining Structural Optimization and Structural Control," by F.Y. Cheng and C.P. Pantelides, 1/10/88, (PB88-213814, A05, MF-A01).

NCEER-88-0007 "Seismic Performance Assessment of Code-Designed Structures," by H.H-M. Hwang, J-W. Jaw and H-J. Shau, 3/20/88, (PB88-219423, A04, MF-A01). This report is only available through NTIS (see address given above).

NCEER-88-0008 "Reliability Analysis of Code-Designed Structures Under Natural Hazards," by H.H-M. Hwang, H. Ushiba and M. Shinozuka, 2/29/88, (PB88-229471, A07, MF-A01). This report is only available through NTIS (see address given above).

NCEER-88-0009 "Seismic Fragility Analysis of Shear Wall Structures," by J-W Jaw and H.H-M. Hwang, 4/30/88, (PB89-102867, A04, MF-A01).

NCEER-88-0010 "Base Isolation of a Multi-Story Building Under a Harmonic Ground Motion - A Comparison of Performances of Various Systems," by F-G Fan, G. Ahmadi and I.G. Tadjbakhsh, 5/18/88, (PB89-122238, A06, MF-A01). This report is only available through NTIS (see address given above).

NCEER-88-0011 "Seismic Floor Response Spectra for a Combined System by Green's Functions," by F.M. Lavelle, L.A. Bergman and P.D. Spanos, 5/1/88, (PB89-102875, A03, MF-A01).

NCEER-88-0012 "A New Solution Technique for Randomly Excited Hysteretic Structures," by G.Q. Cai and Y.K. Lin, 5/16/88, (PB89-102883, A03, MF-A01).

NCEER-88-0013 "A Study of Radiation Damping and Soil-Structure Interaction Effects in the Centrifuge," by K. Weissman, supervised by J.H. Prevost, 5/24/88, (PB89-144703, A06, MF-A01).

NCEER-88-0014 "Parameter Identification and Implementation of a Kinematic Plasticity Model for Frictional Soils," by J.H. Prevost and D.V. Griffiths, to be published.

NCEER-88-0015 "Two- and Three- Dimensional Dynamic Finite Element Analyses of the Long Valley Dam," by D.V. Griffiths and J.H. Prevost, 6/17/88, (PB89-144711, A04, MF-A01).

NCEER-88-0016 "Damage Assessment of Reinforced Concrete Structures in Eastern United States," by A.M. Reinhorn, M.J. Seidel, S.K. Kunnath and Y.J. Park, 6/15/88, (PB89-122220, A04, MF-A01). This report is only available through NTIS (see address given above).

NCEER-88-0017 "Dynamic Compliance of Vertically Loaded Strip Foundations in Multilayered Viscoelastic Soils," by S. Ahmad and A.S.M. Israil, 6/17/88, (PB89-102891, A04, MF-A01).

NCEER-88-0018 "An Experimental Study of Seismic Structural Response With Added Viscoelastic Dampers," by R.C. Lin, Z. Liang, T.T. Soong and R.H. Zhang, 6/30/88, (PB89-122212, A05, MF-A01). This report is available only through NTIS (see address given above).

NCEER-88-0019 "Experimental Investigation of Primary - Secondary System Interaction," by G.D. Manolis, G. Juhn and A.M. Reinhorn, 5/27/88, (PB89-122204, A04, MF-A01).

NCEER-88-0020 "A Response Spectrum Approach For Analysis of Nonclassically Damped Structures," by J.N. Yang, S. Sarkani and F.X. Long, 4/22/88, (PB89-102909, A04, MF-A01).

NCEER-88-0021 "Seismic Interaction of Structures and Soils: Stochastic Approach," by A.S. Veletsos and A.M. Prasad, 7/21/88, (PB89-122196, A04, MF-A01). This report is only available through NTIS (see address given above).

NCEER-88-0022 "Identification of the Serviceability Limit State and Detection of Seismic Structural Damage," by E. DiPasquale and A.S. Cakmak, 6/15/88, (PB89-122188, A05, MF-A01). This report is available only through NTIS (see address given above).

NCEER-88-0023 "Multi-Hazard Risk Analysis: Case of a Simple Offshore Structure," by B.K. Bhartia and E.H. Vanmarcke, 7/21/88, (PB89-145213, A05, MF-A01).

NCEER-88-0024 "Automated Seismic Design of Reinforced Concrete Buildings," by Y.S. Chung, C. Meyer and M. Shinozuka, 7/5/88, (PB89-122170, A06, MF-A01). This report is available only through NTIS (see address given above).

NCEER-88-0025 "Experimental Study of Active Control of MDOF Structures Under Seismic Excitations," by L.L. Chung, R.C. Lin, T.T. Soong and A.M. Reinhorn, 7/10/88, (PB89-122600, A04, MF-A01).

NCEER-88-0026 "Earthquake Simulation Tests of a Low-Rise Metal Structure," by J.S. Hwang, K.C. Chang, G.C. Lee and R.L. Ketter, 8/1/88, (PB89-102917, A04, MF-A01).

NCEER-88-0027 "Systems Study of Urban Response and Reconstruction Due to Catastrophic Earthquakes," by F. Kozin and H.K. Zhou, 9/22/88, (PB90-162348, A04, MF-A01).

NCEER-88-0028 "Seismic Fragility Analysis of Plane Frame Structures," by H.H-M. Hwang and Y.K. Low, 7/31/88, (PB89-131445, A06, MF-A01).

NCEER-88-0029 "Response Analysis of Stochastic Structures," by A. Kardara, C. Bucher and M. Shinozuka, 9/22/88, (PB89-174429, A04, MF-A01).

NCEER-88-0030 "Nonnormal Accelerations Due to Yielding in a Primary Structure," by D.C.K. Chen and L.D. Lutes, 9/19/88, (PB89-131437, A04, MF-A01).

NCEER-88-0031 "Design Approaches for Soil-Structure Interaction," by A.S. Veletsos, A.M. Prasad and Y. Tang, 12/30/88, (PB89-174437, A03, MF-A01). This report is available only through NTIS (see address given above).

NCEER-88-0032 "A Re-evaluation of Design Spectra for Seismic Damage Control," by C.J. Turkstra and A.G. Tallin, 11/7/88, (PB89-145221, A05, MF-A01).

NCEER-88-0033 "The Behavior and Design of Noncontact Lap Splices Subjected to Repeated Inelastic Tensile Loading," by V.E. Sagan, P. Gergely and R.N. White, 12/8/88, (PB89-163737, A08, MF-A01).

NCEER-88-0034 "Seismic Response of Pile Foundations," by S.M. Mamoon, P.K. Banerjee and S. Ahmad, 11/1/88, (PB89-145239, A04, MF-A01).

NCEER-88-0035 "Modeling of R/C Building Structures With Flexible Floor Diaphragms (IDARC2)," by A.M. Reinhorn, S.K. Kunnath and N. Panahshahi, 9/7/88, (PB89-207153, A07, MF-A01).

NCEER-88-0036 "Solution of the Dam-Reservoir Interaction Problem Using a Combination of FEM, BEM with Particular Integrals, Modal Analysis, and Substructuring," by C-S. Tsai, G.C. Lee and R.L. Ketter, 12/31/88, (PB89-207146, A04, MF-A01).

NCEER-88-0037 "Optimal Placement of Actuators for Structural Control," by F.Y. Cheng and C.P. Pantelides, 8/15/88, (PB89-162846, A05, MF-A01).

NCEER-88-0038 "Teflon Bearings in Aseismic Base Isolation: Experimental Studies and Mathematical Modeling," by A. Mokha, M.C. Constantinou and A.M. Reinhorn, 12/5/88, (PB89-218457, A10, MF-A01). This report is available only through NTIS (see address given above).

NCEER-88-0039 "Seismic Behavior of Flat Slab High-Rise Buildings in the New York City Area," by P. Weidlinger and M. Ettouney, 10/15/88, (PB90-145681, A04, MF-A01).

NCEER-88-0040 "Evaluation of the Earthquake Resistance of Existing Buildings in New York City," by P. Weidlinger and M. Ettouney, 10/15/88, to be published.

NCEER-88-0041 "Small-Scale Modeling Techniques for Reinforced Concrete Structures Subjected to Seismic Loads," by W. Kim, A. El-Attar and R.N. White, 11/22/88, (PB89-189625, A05, MF-A01).

NCEER-88-0042 "Modeling Strong Ground Motion from Multiple Event Earthquakes," by G.W. Ellis and A.S. Cakmak, 10/15/88, (PB89-174445, A03, MF-A01).

NCEER-88-0043 "Nonstationary Models of Seismic Ground Acceleration," by M. Grigoriu, S.E. Ruiz and E. Rosenblueth, 7/15/88, (PB89-189617, A04, MF-A01).

NCEER-88-0044 "SARCF User's Guide: Seismic Analysis of Reinforced Concrete Frames," by Y.S. Chung, C. Meyer and M. Shinozuka, 11/9/88, (PB89-174452, A08, MF-A01).

NCEER-88-0045 "First Expert Panel Meeting on Disaster Research and Planning," edited by J. Pantelic and J. Stoyle, 9/15/88, (PB89-174460, A05, MF-A01).

NCEER-88-0046 "Preliminary Studies of the Effect of Degrading Infill Walls on the Nonlinear Seismic Response of Steel Frames," by C.Z. Chrysostomou, P. Gergely and J.F. Abel, 12/19/88, (PB89-208383, A05, MF-A01).

NCEER-88-0047 "Reinforced Concrete Frame Component Testing Facility - Design, Construction, Instrumentation and Operation," by S.P. Pessiki, C. Conley, T. Bond, P. Gergely and R.N. White, 12/16/88, (PB89-174478, A04, MF-A01).

NCEER-89-0001 "Effects of Protective Cushion and Soil Compliancy on the Response of Equipment Within a Seismically Excited Building," by J.A. HoLung, 2/16/89, (PB89-207179, A04, MF-A01).

NCEER-89-0002 "Statistical Evaluation of Response Modification Factors for Reinforced Concrete Structures," by H.H-M. Hwang and J-W. Jaw, 2/17/89, (PB89-207187, A05, MF-A01).

NCEER-89-0003 "Hysteretic Columns Under Random Excitation," by G-Q. Cai and Y.K. Lin, 1/9/89, (PB89-196513, A03, MF-A01).

NCEER-89-0004 "Experimental Study of `Elephant Foot Bulge' Instability of Thin-Walled Metal Tanks," by Z-H. Jia and R.L. Ketter, 2/22/89, (PB89-207195, A03, MF-A01).

NCEER-89-0005 "Experiment on Performance of Buried Pipelines Across San Andreas Fault," by J. Isenberg, E. Richardson and T.D. O'Rourke, 3/10/89, (PB89-218440, A04, MF-A01). This report is available only through NTIS (see address given above).

NCEER-89-0006 "A Knowledge-Based Approach to Structural Design of Earthquake-Resistant Buildings," by M. Subramani, P. Gergely, C.H. Conley, J.F. Abel and A.H. Zaghw, 1/15/89, (PB89-218465, A06, MF-A01).

NCEER-89-0007 "Liquefaction Hazards and Their Effects on Buried Pipelines," by T.D. O'Rourke and P.A. Lane, 2/1/89, (PB89-218481, A09, MF-A01).

NCEER-89-0008 "Fundamentals of System Identification in Structural Dynamics," by H. Imai, C-B. Yun, O. Maruyama and M. Shinozuka, 1/26/89, (PB89-207211, A04, MF-A01).

NCEER-89-0009 "Effects of the 1985 Michoacan Earthquake on Water Systems and Other Buried Lifelines in Mexico," by A.G. Ayala and M.J. O'Rourke, 3/8/89, (PB89-207229, A06, MF-A01).

NCEER-89-R010 "NCEER Bibliography of Earthquake Education Materials," by K.E.K. Ross, Second Revision, 9/1/89, (PB90-125352, A05, MF-A01). This report is replaced by NCEER-92-0018.

NCEER-89-0011 "Inelastic Three-Dimensional Response Analysis of Reinforced Concrete Building Structures (IDARC-3D), Part I - Modeling," by S.K. Kunnath and A.M. Reinhorn, 4/17/89, (PB90-114612, A07, MF-A01). This report is available only through NTIS (see address given above).

NCEER-89-0012 "Recommended Modifications to ATC-14," by C.D. Poland and J.O. Malley, 4/12/89, (PB90-108648, A15, MF-A01).

NCEER-89-0013 "Repair and Strengthening of Beam-to-Column Connections Subjected to Earthquake Loading," by M. Corazao and A.J. Durrani, 2/28/89, (PB90-109885, A06, MF-A01).

NCEER-89-0014 "Program EXKAL2 for Identification of Structural Dynamic Systems," by O. Maruyama, C-B. Yun, M. Hoshiya and M. Shinozuka, 5/19/89, (PB90-109877, A09, MF-A01).

NCEER-89-0015 "Response of Frames With Bolted Semi-Rigid Connections, Part I - Experimental Study and Analytical Predictions," by P.J. DiCorso, A.M. Reinhorn, J.R. Dickerson, J.B. Radziminski and W.L. Harper, 6/1/89, to be published.

NCEER-89-0016 "ARMA Monte Carlo Simulation in Probabilistic Structural Analysis," by P.D. Spanos and M.P. Mignolet, 7/10/89, (PB90-109893, A03, MF-A01).

NCEER-89-P017 "Preliminary Proceedings from the Conference on Disaster Preparedness - The Place of Earthquake Education in Our Schools," Edited by K.E.K. Ross, 6/23/89, (PB90-108606, A03, MF-A01).

NCEER-89-0017 "Proceedings from the Conference on Disaster Preparedness - The Place of Earthquake Education in Our Schools," Edited by K.E.K. Ross, 12/31/89, (PB90-207895, A012, MF-A02). This report is available only through NTIS (see address given above).

NCEER-89-0018 "Multidimensional Models of Hysteretic Material Behavior for Vibration Analysis of Shape Memory Energy Absorbing Devices, by E.J. Graesser and F.A. Cozzarelli, 6/7/89, (PB90-164146, A04, MF-A01).

NCEER-89-0019 "Nonlinear Dynamic Analysis of Three-Dimensional Base Isolated Structures (3D-BASIS)," by S. Nagarajaiah, A.M. Reinhorn and M.C. Constantinou, 8/3/89, (PB90-161936, A06, MF-A01). This report has been replaced by NCEER-93-0011.

NCEER-89-0020 "Structural Control Considering Time-Rate of Control Forces and Control Rate Constraints," by F.Y. Cheng and C.P. Pantelides, 8/3/89, (PB90-120445, A04, MF-A01).

NCEER-89-0021 "Subsurface Conditions of Memphis and Shelby County," by K.W. Ng, T-S. Chang and H-H.M. Hwang, 7/26/89, (PB90-120437, A03, MF-A01).

NCEER-89-0022 "Seismic Wave Propagation Effects on Straight Jointed Buried Pipelines," by K. Elhmadi and M.J. O'Rourke, 8/24/89, (PB90-162322, A10, MF-A02).

NCEER-89-0023 "Workshop on Serviceability Analysis of Water Delivery Systems," edited by M. Grigoriu, 3/6/89, (PB90-127424, A03, MF-A01).

NCEER-89-0024 "Shaking Table Study of a 1/5 Scale Steel Frame Composed of Tapered Members," by K.C. Chang, J.S. Hwang and G.C. Lee, 9/18/89, (PB90-160169, A04, MF-A01).

NCEER-89-0025 "DYNA1D: A Computer Program for Nonlinear Seismic Site Response Analysis - Technical Documentation," by Jean H. Prevost, 9/14/89, (PB90-161944, A07, MF-A01). This report is available only through NTIS (see address given above).

NCEER-89-0026 "1:4 Scale Model Studies of Active Tendon Systems and Active Mass Dampers for Aseismic Protection," by A.M. Reinhorn, T.T. Soong, R.C. Lin, Y.P. Yang, Y. Fukao, H. Abe and M. Nakai, 9/15/89, (PB90-173246, A10, MF-A02). This report is available only through NTIS (see address given above).

NCEER-89-0027 "Scattering of Waves by Inclusions in a Nonhomogeneous Elastic Half Space Solved by Boundary Element Methods," by P.K. Hadley, A. Askar and A.S. Cakmak, 6/15/89, (PB90-145699, A07, MF-A01).

NCEER-89-0028 "Statistical Evaluation of Deflection Amplification Factors for Reinforced Concrete Structures," by H.H.M. Hwang, J-W. Jaw and A.L. Ch'ng, 8/31/89, (PB90-164633, A05, MF-A01).

NCEER-89-0029 "Bedrock Accelerations in Memphis Area Due to Large New Madrid Earthquakes," by H.H.M. Hwang, C.H.S. Chen and G. Yu, 11/7/89, (PB90-162330, A04, MF-A01).

NCEER-89-0030 "Seismic Behavior and Response Sensitivity of Secondary Structural Systems," by Y.Q. Chen and T.T. Soong, 10/23/89, (PB90-164658, A08, MF-A01).

NCEER-89-0031 "Random Vibration and Reliability Analysis of Primary-Secondary Structural Systems," by Y. Ibrahim, M. Grigoriu and T.T. Soong, 11/10/89, (PB90-161951, A04, MF-A01).

NCEER-89-0032 "Proceedings from the Second U.S. - Japan Workshop on Liquefaction, Large Ground Deformation and Their Effects on Lifelines, September 26-29, 1989," Edited by T.D. O'Rourke and M. Hamada, 12/1/89, (PB90-209388, A22, MF-A03).

NCEER-89-0033 "Deterministic Model for Seismic Damage Evaluation of Reinforced Concrete Structures," by J.M. Bracci, A.M. Reinhorn, J.B. Mander and S.K. Kunnath, 9/27/89, (PB91-108803, A06, MF-A01).

NCEER-89-0034 "On the Relation Between Local and Global Damage Indices," by E. DiPasquale and A.S. Cakmak, 8/15/89, (PB90-173865, A05, MF-A01).

NCEER-89-0035 "Cyclic Undrained Behavior of Nonplastic and Low Plasticity Silts," by A.J. Walker and H.E. Stewart, 7/26/89, (PB90-183518, A10, MF-A01).

NCEER-89-0036 "Liquefaction Potential of Surficial Deposits in the City of Buffalo, New York," by M. Budhu, R. Giese and L. Baumgrass, 1/17/89, (PB90-208455, A04, MF-A01).

NCEER-89-0037 "A Deterministic Assessment of Effects of Ground Motion Incoherence," by A.S. Veletsos and Y. Tang, 7/15/89, (PB90-164294, A03, MF-A01).

NCEER-89-0038 "Workshop on Ground Motion Parameters for Seismic Hazard Mapping," July 17-18, 1989, edited by R.V. Whitman, 12/1/89, (PB90-173923, A04, MF-A01).

NCEER-89-0039 "Seismic Effects on Elevated Transit Lines of the New York City Transit Authority," by C.J. Costantino, C.A. Miller and E. Heymsfield, 12/26/89, (PB90-207887, A06, MF-A01).

NCEER-89-0040 "Centrifugal Modeling of Dynamic Soil-Structure Interaction," by K. Weissman, Supervised by J.H. Prevost, 5/10/89, (PB90-207879, A07, MF-A01).

NCEER-89-0041 "Linearized Identification of Buildings With Cores for Seismic Vulnerability Assessment," by I-K. Ho and A.E. Aktan, 11/1/89, (PB90-251943, A07, MF-A01).

NCEER-90-0001 "Geotechnical and Lifeline Aspects of the October 17, 1989 Loma Prieta Earthquake in San Francisco," by T.D. O'Rourke, H.E. Stewart, F.T. Blackburn and T.S. Dickerman, 1/90, (PB90-208596, A05, MF-A01).

NCEER-90-0002 "Nonnormal Secondary Response Due to Yielding in a Primary Structure," by D.C.K. Chen and L.D. Lutes, 2/28/90, (PB90-251976, A07, MF-A01).

NCEER-90-0003 "Earthquake Education Materials for Grades K-12," by K.E.K. Ross, 4/16/90, (PB91-251984, A05, MF-A05). This report has been replaced by NCEER-92-0018.

NCEER-90-0004 "Catalog of Strong Motion Stations in Eastern North America," by R.W. Busby, 4/3/90, (PB90-251984, A05, MF-A01).

NCEER-90-0005 "NCEER Strong-Motion Data Base: A User Manual for the GeoBase Release (Version 1.0 for the Sun3)," by P. Friberg and K. Jacob, 3/31/90 (PB90-258062, A04, MF-A01).

NCEER-90-0006 "Seismic Hazard Along a Crude Oil Pipeline in the Event of an 1811-1812 Type New Madrid Earthquake," by H.H.M. Hwang and C-H.S. Chen, 4/16/90, (PB90-258054, A04, MF-A01).

NCEER-90-0007 "Site-Specific Response Spectra for Memphis Sheahan Pumping Station," by H.H.M. Hwang and C.S. Lee, 5/15/90, (PB91-108811, A05, MF-A01).

NCEER-90-0008 "Pilot Study on Seismic Vulnerability of Crude Oil Transmission Systems," by T. Ariman, R. Dobry, M. Grigoriu, F. Kozin, M. O'Rourke, T. O'Rourke and M. Shinozuka, 5/25/90, (PB91-108837, A06, MF-A01).

NCEER-90-0009 "A Program to Generate Site Dependent Time Histories: EQGEN," by G.W. Ellis, M. Srinivasan and A.S. Cakmak, 1/30/90, (PB91-108829, A04, MF-A01).

NCEER-90-0010 "Active Isolation for Seismic Protection of Operating Rooms," by M.E. Talbott, Supervised by M. Shinozuka, 6/8/9, (PB91-110205, A05, MF-A01).

NCEER-90-0011 "Program LINEARID for Identification of Linear Structural Dynamic Systems," by C-B. Yun and M. Shinozuka, 6/25/90, (PB91-110312, A08, MF-A01).

NCEER-90-0012 "Two-Dimensional Two-Phase Elasto-Plastic Seismic Response of Earth Dams," by A.N. Yiagos, Supervised by J.H. Prevost, 6/20/90, (PB91-110197, A13, MF-A02).

NCEER-90-0013 "Secondary Systems in Base-Isolated Structures: Experimental Investigation, Stochastic Response and Stochastic Sensitivity," by G.D. Manolis, G. Juhn, M.C. Constantinou and A.M. Reinhorn, 7/1/90, (PB91-110320, A08, MF-A01).

NCEER-90-0014 "Seismic Behavior of Lightly-Reinforced Concrete Column and Beam-Column Joint Details," by S.P. Pessiki, C.H. Conley, P. Gergely and R.N. White, 8/22/90, (PB91-108795, A11, MF-A02).

NCEER-90-0015 "Two Hybrid Control Systems for Building Structures Under Strong Earthquakes," by J.N. Yang and A. Danielians, 6/29/90, (PB91-125393, A04, MF-A01).

NCEER-90-0016 "Instantaneous Optimal Control with Acceleration and Velocity Feedback," by J.N. Yang and Z. Li, 6/29/90, (PB91-125401, A03, MF-A01).

NCEER-90-0017 "Reconnaissance Report on the Northern Iran Earthquake of June 21, 1990," by M. Mehrain, 10/4/90, (PB91-125377, A03, MF-A01).

NCEER-90-0018 "Evaluation of Liquefaction Potential in Memphis and Shelby County," by T.S. Chang, P.S. Tang, C.S. Lee and H. Hwang, 8/10/90, (PB91-125427, A09, MF-A01).

NCEER-90-0019 "Experimental and Analytical Study of a Combined Sliding Disc Bearing and Helical Steel Spring Isolation System," by M.C. Constantinou, A.S. Mokha and A.M. Reinhorn, 10/4/90, (PB91-125385, A06, MF-A01). This report is available only through NTIS (see address given above).

NCEER-90-0020 "Experimental Study and Analytical Prediction of Earthquake Response of a Sliding Isolation System with a Spherical Surface," by A.S. Mokha, M.C. Constantinou and A.M. Reinhorn, 10/11/90, (PB91-125419, A05, MF-A01).

NCEER-90-0021 "Dynamic Interaction Factors for Floating Pile Groups," by G. Gazetas, K. Fan, A. Kaynia and E. Kausel, 9/10/90, (PB91-170381, A05, MF-A01).

NCEER-90-0022 "Evaluation of Seismic Damage Indices for Reinforced Concrete Structures," by S. Rodriguez-Gomez and A.S. Cakmak, 9/30/90, PB91-171322, A06, MF-A01).

NCEER-90-0023 "Study of Site Response at a Selected Memphis Site," by H. Desai, S. Ahmad, E.S. Gazetas and M.R. Oh, 10/11/90, (PB91-196857, A03, MF-A01).

NCEER-90-0024 "A User's Guide to Strongmo: Version 1.0 of NCEER's Strong-Motion Data Access Tool for PCs and Terminals," by P.A. Friberg and C.A.T. Susch, 11/15/90, (PB91-171272, A03, MF-A01).

NCEER-90-0025 "A Three-Dimensional Analytical Study of Spatial Variability of Seismic Ground Motions," by L-L. Hong and A.H.-S. Ang, 10/30/90, (PB91-170399, A09, MF-A01).

NCEER-90-0026 "MUMOID User's Guide - A Program for the Identification of Modal Parameters," by S. Rodriguez-Gomez and E. DiPasquale, 9/30/90, (PB91-171298, A04, MF-A01).

NCEER-90-0027 "SARCF-II User's Guide - Seismic Analysis of Reinforced Concrete Frames," by S. Rodriguez-Gomez, Y.S. Chung and C. Meyer, 9/30/90, (PB91-171280, A05, MF-A01).

NCEER-90-0028 "Viscous Dampers: Testing, Modeling and Application in Vibration and Seismic Isolation," by N. Makris and M.C. Constantinou, 12/20/90 (PB91-190561, A06, MF-A01).

NCEER-90-0029 "Soil Effects on Earthquake Ground Motions in the Memphis Area," by H. Hwang, C.S. Lee, K.W. Ng and T.S. Chang, 8/2/90, (PB91-190751, A05, MF-A01).

NCEER-91-0001 "Proceedings from the Third Japan-U.S. Workshop on Earthquake Resistant Design of Lifeline Facilities and Countermeasures for Soil Liquefaction, December 17-19, 1990," edited by T.D. O'Rourke and M. Hamada, 2/1/91, (PB91-179259, A99, MF-A04).

NCEER-91-0002 "Physical Space Solutions of Non-Proportionally Damped Systems," by M. Tong, Z. Liang and G.C. Lee, 1/15/91, (PB91-179242, A04, MF-A01).

NCEER-91-0003 "Seismic Response of Single Piles and Pile Groups," by K. Fan and G. Gazetas, 1/10/91, (PB92-174994, A04, MF-A01).

NCEER-91-0004 "Damping of Structures: Part 1 - Theory of Complex Damping," by Z. Liang and G. Lee, 10/10/91, (PB92-197235, A12, MF-A03).

NCEER-91-0005 "3D-BASIS - Nonlinear Dynamic Analysis of Three Dimensional Base Isolated Structures: Part II," by S. Nagarajaiah, A.M. Reinhorn and M.C. Constantinou, 2/28/91, (PB91-190553, A07, MF-A01). This report has been replaced by NCEER-93-0011.

NCEER-91-0006 "A Multidimensional Hysteretic Model for Plasticity Deforming Metals in Energy Absorbing Devices," by E.J. Graesser and F.A. Cozzarelli, 4/9/91, (PB92-108364, A04, MF-A01).

NCEER-91-0007 "A Framework for Customizable Knowledge-Based Expert Systems with an Application to a KBES for Evaluating the Seismic Resistance of Existing Buildings," by E.G. Ibarra-Anaya and S.J. Fenves, 4/9/91, (PB91-210930, A08, MF-A01).

NCEER-91-0008 "Nonlinear Analysis of Steel Frames with Semi-Rigid Connections Using the Capacity Spectrum Method," by G.G. Deierlein, S-H. Hsieh, Y-J. Shen and J.F. Abel, 7/2/91, (PB92-113828, A05, MF-A01).

NCEER-91-0009 "Earthquake Education Materials for Grades K-12," by K.E.K. Ross, 4/30/91, (PB91-212142, A06, MF-A01). This report has been replaced by NCEER-92-0018.

NCEER-91-0010 "Phase Wave Velocities and Displacement Phase Differences in a Harmonically Oscillating Pile," by N. Makris and G. Gazetas, 7/8/91, (PB92-108356, A04, MF-A01).

NCEER-91-0011 "Dynamic Characteristics of a Full-Size Five-Story Steel Structure and a 2/5 Scale Model," by K.C. Chang, G.C. Yao, G.C. Lee, D.S. Hao and Y.C. Yeh," 7/2/91, (PB93-116648, A06, MF-A02).

NCEER-91-0012 "Seismic Response of a 2/5 Scale Steel Structure with Added Viscoelastic Dampers," by K.C. Chang, T.T. Soong, S-T. Oh and M.L. Lai, 5/17/91, (PB92-110816, A05, MF-A01).

NCEER-91-0013 "Earthquake Response of Retaining Walls; Full-Scale Testing and Computational Modeling," by S. Alampalli and A-W.M. Elgamal, 6/20/91, to be published.

NCEER-91-0014 "3D-BASIS-M: Nonlinear Dynamic Analysis of Multiple Building Base Isolated Structures," by P.C. Tsopelas, S. Nagarajaiah, M.C. Constantinou and A.M. Reinhorn, 5/28/91, (PB92-113885, A09, MF-A02).

NCEER-91-0015 "Evaluation of SEAOC Design Requirements for Sliding Isolated Structures," by D. Theodossiou and M.C. Constantinou, 6/10/91, (PB92-114602, A11, MF-A03).

NCEER-91-0016 "Closed-Loop Modal Testing of a 27-Story Reinforced Concrete Flat Plate-Core Building," by H.R. Somaprasad, T. Toksoy, H. Yoshiyuki and A.E. Aktan, 7/15/91, (PB92-129980, A07, MF-A02).

NCEER-91-0017 "Shake Table Test of a 1/6 Scale Two-Story Lightly Reinforced Concrete Building," by A.G. El-Attar, R.N. White and P. Gergely, 2/28/91, (PB92-222447, A06, MF-A02).

NCEER-91-0018 "Shake Table Test of a 1/8 Scale Three-Story Lightly Reinforced Concrete Building," by A.G. El-Attar, R.N. White and P. Gergely, 2/28/91, (PB93-116630, A08, MF-A02).

NCEER-91-0019 "Transfer Functions for Rigid Rectangular Foundations," by A.S. Veletsos, A.M. Prasad and W.H. Wu, 7/31/91, to be published.

NCEER-91-0020 "Hybrid Control of Seismic-Excited Nonlinear and Inelastic Structural Systems," by J.N. Yang, Z. Li and A. Danielians, 8/1/91, (PB92-143171, A06, MF-A02).

NCEER-91-0021 "The NCEER-91 Earthquake Catalog: Improved Intensity-Based Magnitudes and Recurrence Relations for U.S. Earthquakes East of New Madrid," by L. Seeber and J.G. Armbruster, 8/28/91, (PB92-176742, A06, MF-A02).

NCEER-91-0022 "Proceedings from the Implementation of Earthquake Planning and Education in Schools: The Need for Change - The Roles of the Changemakers," by K.E.K. Ross and F. Winslow, 7/23/91, (PB92-129998, A12, MF-A03).

NCEER-91-0023 "A Study of Reliability-Based Criteria for Seismic Design of Reinforced Concrete Frame Buildings," by H.H.M. Hwang and H-M. Hsu, 8/10/91, (PB92-140235, A09, MF-A02).

NCEER-91-0024 "Experimental Verification of a Number of Structural System Identification Algorithms," by R.G. Ghanem, H. Gavin and M. Shinozuka, 9/18/91, (PB92-176577, A18, MF-A04).

NCEER-91-0025 "Probabilistic Evaluation of Liquefaction Potential," by H.H.M. Hwang and C.S. Lee," 11/25/91, (PB92-143429, A05, MF-A01).

NCEER-91-0026 "Instantaneous Optimal Control for Linear, Nonlinear and Hysteretic Structures - Stable Controllers," by J.N. Yang and Z. Li, 11/15/91, (PB92-163807, A04, MF-A01).

NCEER-91-0027 "Experimental and Theoretical Study of a Sliding Isolation System for Bridges," by M.C. Constantinou, A. Kartoum, A.M. Reinhorn and P. Bradford, 11/15/91, (PB92-176973, A10, MF-A03).

NCEER-92-0001 "Case Studies of Liquefaction and Lifeline Performance During Past Earthquakes, Volume 1: Japanese Case Studies," Edited by M. Hamada and T. O'Rourke, 2/17/92, (PB92-197243, A18, MF-A04).

NCEER-92-0002 "Case Studies of Liquefaction and Lifeline Performance During Past Earthquakes, Volume 2: United States Case Studies," Edited by T. O'Rourke and M. Hamada, 2/17/92, (PB92-197250, A20, MF-A04).

NCEER-92-0003 "Issues in Earthquake Education," Edited by K. Ross, 2/3/92, (PB92-222389, A07, MF-A02).

NCEER-92-0004 "Proceedings from the First U.S. - Japan Workshop on Earthquake Protective Systems for Bridges," Edited by I.G. Buckle, 2/4/92, (PB94-142239, A99, MF-A06).

NCEER-92-0005 "Seismic Ground Motion from a Haskell-Type Source in a Multiple-Layered Half-Space," A.P. Theoharis, G. Deodatis and M. Shinozuka, 1/2/92, to be published.

NCEER-92-0006 "Proceedings from the Site Effects Workshop," Edited by R. Whitman, 2/29/92, (PB92-197201, A04, MF-A01).

NCEER-92-0007 "Engineering Evaluation of Permanent Ground Deformations Due to Seismically-Induced Liquefaction," by M.H. Baziar, R. Dobry and A-W.M. Elgamal, 3/24/92, (PB92-222421, A13, MF-A03).

NCEER-92-0008 "A Procedure for the Seismic Evaluation of Buildings in the Central and Eastern United States," by C.D. Poland and J.O. Malley, 4/2/92, (PB92-222439, A20, MF-A04).

NCEER-92-0009 "Experimental and Analytical Study of a Hybrid Isolation System Using Friction Controllable Sliding Bearings," by M.Q. Feng, S. Fujii and M. Shinozuka, 5/15/92, (PB93-150282, A06, MF-A02).

NCEER-92-0010 "Seismic Resistance of Slab-Column Connections in Existing Non-Ductile Flat-Plate Buildings," by A.J. Durrani and Y. Du, 5/18/92, (PB93-116812, A06, MF-A02).

NCEER-92-0011 "The Hysteretic and Dynamic Behavior of Brick Masonry Walls Upgraded by Ferrocement Coatings Under Cyclic Loading and Strong Simulated Ground Motion," by H. Lee and S.P. Prawel, 5/11/92, to be published.

NCEER-92-0012 "Study of Wire Rope Systems for Seismic Protection of Equipment in Buildings," by G.F. Demetriades, M.C. Constantinou and A.M. Reinhorn, 5/20/92, (PB93-116655, A08, MF-A02).

NCEER-92-0013 "Shape Memory Structural Dampers: Material Properties, Design and Seismic Testing," by P.R. Witting and F.A. Cozzarelli, 5/26/92, (PB93-116663, A05, MF-A01).

NCEER-92-0014 "Longitudinal Permanent Ground Deformation Effects on Buried Continuous Pipelines," by M.J. O'Rourke, and C. Nordberg, 6/15/92, (PB93-116671, A08, MF-A02).

NCEER-92-0015 "A Simulation Method for Stationary Gaussian Random Functions Based on the Sampling Theorem," by M. Grigoriu and S. Balopoulou, 6/11/92, (PB93-127496, A05, MF-A01).

NCEER-92-0016 "Gravity-Load-Designed Reinforced Concrete Buildings: Seismic Evaluation of Existing Construction and Detailing Strategies for Improved Seismic Resistance," by G.W. Hoffmann, S.K. Kunnath, A.M. Reinhorn and J.B. Mander, 7/15/92, (PB94-142007, A08, MF-A02).

NCEER-92-0017 "Observations on Water System and Pipeline Performance in the Limón Area of Costa Rica Due to the April 22, 1991 Earthquake," by M. O'Rourke and D. Ballantyne, 6/30/92, (PB93-126811, A06, MF-A02).

NCEER-92-0018 "Fourth Edition of Earthquake Education Materials for Grades K-12," Edited by K.E.K. Ross, 8/10/92, (PB93-114023, A07, MF-A02).

NCEER-92-0019 "Proceedings from the Fourth Japan-U.S. Workshop on Earthquake Resistant Design of Lifeline Facilities and Countermeasures for Soil Liquefaction," Edited by M. Hamada and T.D. O'Rourke, 8/12/92, (PB93-163939, A99, MF-E11).

NCEER-92-0020 "Active Bracing System: A Full Scale Implementation of Active Control," by A.M. Reinhorn, T.T. Soong, R.C. Lin, M.A. Riley, Y.P. Wang, S. Aizawa and M. Higashino, 8/14/92, (PB93-127512, A06, MF-A02).

NCEER-92-0021 "Empirical Analysis of Horizontal Ground Displacement Generated by Liquefaction-Induced Lateral Spreads," by S.F. Bartlett and T.L. Youd, 8/17/92, (PB93-188241, A06, MF-A02).

NCEER-92-0022 "IDARC Version 3.0: Inelastic Damage Analysis of Reinforced Concrete Structures," by S.K. Kunnath, A.M. Reinhorn and R.F. Lobo, 8/31/92, (PB93-227502, A07, MF-A02).

NCEER-92-0023 "A Semi-Empirical Analysis of Strong-Motion Peaks in Terms of Seismic Source, Propagation Path and Local Site Conditions, by M. Kamiyama, M.J. O'Rourke and R. Flores-Berrones, 9/9/92, (PB93-150266, A08, MF-A02).

NCEER-92-0024 "Seismic Behavior of Reinforced Concrete Frame Structures with Nonductile Details, Part I: Summary of Experimental Findings of Full Scale Beam-Column Joint Tests," by A. Beres, R.N. White and P. Gergely, 9/30/92, (PB93-227783, A05, MF-A01).

NCEER-92-0025 "Experimental Results of Repaired and Retrofitted Beam-Column Joint Tests in Lightly Reinforced Concrete Frame Buildings," by A. Beres, S. El-Borgi, R.N. White and P. Gergely, 10/29/92, (PB93-227791, A05, MF-A01).

NCEER-92-0026 "A Generalization of Optimal Control Theory: Linear and Nonlinear Structures," by J.N. Yang, Z. Li and S. Vongchavalitkul, 11/2/92, (PB93-188621, A05, MF-A01).

NCEER-92-0027 "Seismic Resistance of Reinforced Concrete Frame Structures Designed Only for Gravity Loads: Part I - Design and Properties of a One-Third Scale Model Structure," by J.M. Bracci, A.M. Reinhorn and J.B. Mander, 12/1/92, (PB94-104502, A08, MF-A02).

NCEER-92-0028 "Seismic Resistance of Reinforced Concrete Frame Structures Designed Only for Gravity Loads: Part II - Experimental Performance of Subassemblages," by L.E. Aycardi, J.B. Mander and A.M. Reinhorn, 12/1/92, (PB94-104510, A08, MF-A02).

NCEER-92-0029 "Seismic Resistance of Reinforced Concrete Frame Structures Designed Only for Gravity Loads: Part III - Experimental Performance and Analytical Study of a Structural Model," by J.M. Bracci, A.M. Reinhorn and J.B. Mander, 12/1/92, (PB93-227528, A09, MF-A01).

NCEER-92-0030 "Evaluation of Seismic Retrofit of Reinforced Concrete Frame Structures: Part I - Experimental Performance of Retrofitted Subassemblages," by D. Choudhuri, J.B. Mander and A.M. Reinhorn, 12/8/92, (PB93-198307, A07, MF-A02).

NCEER-92-0031 "Evaluation of Seismic Retrofit of Reinforced Concrete Frame Structures: Part II - Experimental Performance and Analytical Study of a Retrofitted Structural Model," by J.M. Bracci, A.M. Reinhorn and J.B. Mander, 12/8/92, (PB93-198315, A09, MF-A03).

NCEER-92-0032 "Experimental and Analytical Investigation of Seismic Response of Structures with Supplemental Fluid Viscous Dampers," by M.C. Constantinou and M.D. Symans, 12/21/92, (PB93-191435, A10, MF-A03). This report is available only through NTIS (see address given above).

NCEER-92-0033 "Reconnaissance Report on the Cairo, Egypt Earthquake of October 12, 1992," by M. Khater, 12/23/92, (PB93-188621, A03, MF-A01).

NCEER-92-0034 "Low-Level Dynamic Characteristics of Four Tall Flat-Plate Buildings in New York City," by H. Gavin, S. Yuan, J. Grossman, E. Pekelis and K. Jacob, 12/28/92, (PB93-188217, A07, MF-A02).

NCEER-93-0001 "An Experimental Study on the Seismic Performance of Brick-Infilled Steel Frames With and Without Retrofit," by J.B. Mander, B. Nair, K. Wojtkowski and J. Ma, 1/29/93, (PB93-227510, A07, MF-A02).

NCEER-93-0002 "Social Accounting for Disaster Preparedness and Recovery Planning," by S. Cole, E. Pantoja and V. Razak, 2/22/93, (PB94-142114, A12, MF-A03).

NCEER-93-0003 "Assessment of 1991 NEHRP Provisions for Nonstructural Components and Recommended Revisions," by T.T. Soong, G. Chen, Z. Wu, R-H. Zhang and M. Grigoriu, 3/1/93, (PB93-188639, A06, MF-A02).

NCEER-93-0004 "Evaluation of Static and Response Spectrum Analysis Procedures of SEAOC/UBC for Seismic Isolated Structures," by C.W. Winters and M.C. Constantinou, 3/23/93, (PB93-198299, A10, MF-A03).

NCEER-93-0005 "Earthquakes in the Northeast - Are We Ignoring the Hazard? A Workshop on Earthquake Science and Safety for Educators," edited by K.E.K. Ross, 4/2/93, (PB94-103066, A09, MF-A02).

NCEER-93-0006 "Inelastic Response of Reinforced Concrete Structures with Viscoelastic Braces," by R.F. Lobo, J.M. Bracci, K.L. Shen, A.M. Reinhorn and T.T. Soong, 4/5/93, (PB93-227486, A05, MF-A02).

NCEER-93-0007 "Seismic Testing of Installation Methods for Computers and Data Processing Equipment," by K. Kosar, T.T. Soong, K.L. Shen, J.A. HoLung and Y.K. Lin, 4/12/93, (PB93-198299, A07, MF-A02).

NCEER-93-0008 "Retrofit of Reinforced Concrete Frames Using Added Dampers," by A. Reinhorn, M. Constantinou and C. Li, to be published.

NCEER-93-0009 "Seismic Behavior and Design Guidelines for Steel Frame Structures with Added Viscoelastic Dampers," by K.C. Chang, M.L. Lai, T.T. Soong, D.S. Hao and Y.C. Yeh, 5/1/93, (PB94-141959, A07, MF-A02).

NCEER-93-0010 "Seismic Performance of Shear-Critical Reinforced Concrete Bridge Piers," by J.B. Mander, S.M. Waheed, M.T.A. Chaudhary and S.S. Chen, 5/12/93, (PB93-227494, A08, MF-A02).

NCEER-93-0011 "3D-BASIS-TABS: Computer Program for Nonlinear Dynamic Analysis of Three Dimensional Base Isolated Structures," by S. Nagarajaiah, C. Li, A.M. Reinhorn and M.C. Constantinou, 8/2/93, (PB94-141819, A09, MF-A02).

NCEER-93-0012 "Effects of Hydrocarbon Spills from an Oil Pipeline Break on Ground Water," by O.J. Helweg and H.H.M. Hwang, 8/3/93, (PB94-141942, A06, MF-A02).

NCEER-93-0013 "Simplified Procedures for Seismic Design of Nonstructural Components and Assessment of Current Code Provisions," by M.P. Singh, L.E. Suarez, E.E. Matheu and G.O. Maldonado, 8/4/93, (PB94-141827, A09, MF-A02).

NCEER-93-0014 "An Energy Approach to Seismic Analysis and Design of Secondary Systems," by G. Chen and T.T. Soong, 8/6/93, (PB94-142767, A11, MF-A03).

NCEER-93-0015 "Proceedings from School Sites: Becoming Prepared for Earthquakes - Commemorating the Third Anniversary of the Loma Prieta Earthquake," Edited by F.E. Winslow and K.E.K. Ross, 8/16/93, (PB94-154275, A16, MF-A02).

NCEER-93-0016 "Reconnaissance Report of Damage to Historic Monuments in Cairo, Egypt Following the October 12, 1992 Dahshur Earthquake," by D. Sykora, D. Look, G. Croci, E. Karaesmen and E. Karaesmen, 8/19/93, (PB94-142221, A08, MF-A02).

NCEER-93-0017 "The Island of Guam Earthquake of August 8, 1993," by S.W. Swan and S.K. Harris, 9/30/93, (PB94-141843, A04, MF-A01).

NCEER-93-0018 "Engineering Aspects of the October 12, 1992 Egyptian Earthquake," by A.W. Elgamal, M. Amer, K. Adalier and A. Abul-Fadl, 10/7/93, (PB94-141983, A05, MF-A01).

NCEER-93-0019 "Development of an Earthquake Motion Simulator and its Application in Dynamic Centrifuge Testing," by I. Krstelj, Supervised by J.H. Prevost, 10/23/93, (PB94-181773, A-10, MF-A03).

NCEER-93-0020 "NCEER-Taisei Corporation Research Program on Sliding Seismic Isolation Systems for Bridges: Experimental and Analytical Study of a Friction Pendulum System (FPS)," by M.C. Constantinou, P. Tsopelas, Y-S. Kim and S. Okamoto, 11/1/93, (PB94-142775, A08, MF-A02).

NCEER-93-0021 "Finite Element Modeling of Elastomeric Seismic Isolation Bearings," by L.J. Billings, Supervised by R. Shepherd, 11/8/93, to be published.

NCEER-93-0022 "Seismic Vulnerability of Equipment in Critical Facilities: Life-Safety and Operational Consequences," by K. Porter, G.S. Johnson, M.M. Zadeh, C. Scawthorn and S. Eder, 11/24/93, (PB94-181765, A16, MF-A03).

NCEER-93-0023 "Hokkaido Nansei-oki, Japan Earthquake of July 12, 1993, by P.I. Yanev and C.R. Scawthorn, 12/23/93, (PB94-181500, A07, MF-A01).

NCEER-94-0001 "An Evaluation of Seismic Serviceability of Water Supply Networks with Application to the San Francisco Auxiliary Water Supply System," by I. Markov, Supervised by M. Grigoriu and T. O'Rourke, 1/21/94, (PB94-204013, A07, MF-A02).

NCEER-94-0002 "NCEER-Taisei Corporation Research Program on Sliding Seismic Isolation Systems for Bridges: Experimental and Analytical Study of Systems Consisting of Sliding Bearings, Rubber Restoring Force Devices and Fluid Dampers," Volumes I and II, by P. Tsopelas, S. Okamoto, M.C. Constantinou, D. Ozaki and S. Fujii, 2/4/94, (PB94-181740, A09, MF-A02 and PB94-181757, A12, MF-A03).

NCEER-94-0003 "A Markov Model for Local and Global Damage Indices in Seismic Analysis," by S. Rahman and M. Grigoriu, 2/18/94, (PB94-206000, A12, MF-A03).

NCEER-94-0004 "Proceedings from the NCEER Workshop on Seismic Response of Masonry Infills," edited by D.P. Abrams, 3/1/94, (PB94-180783, A07, MF-A02).

NCEER-94-0005 "The Northridge, California Earthquake of January 17, 1994: General Reconnaissance Report," edited by J.D. Goltz, 3/11/94, (PB94-193943, A10, MF-A03).

NCEER-94-0006 "Seismic Energy Based Fatigue Damage Analysis of Bridge Columns: Part I - Evaluation of Seismic Capacity," by G.A. Chang and J.B. Mander, 3/14/94, (PB94-219185, A11, MF-A03).

NCEER-94-0007 "Seismic Isolation of Multi-Story Frame Structures Using Spherical Sliding Isolation Systems," by T.M. Al-Hussaini, V.A. Zayas and M.C. Constantinou, 3/17/94, (PB94-193745, A09, MF-A02).

NCEER-94-0008 "The Northridge, California Earthquake of January 17, 1994: Performance of Highway Bridges," edited by I.G. Buckle, 3/24/94, (PB94-193851, A06, MF-A02).

NCEER-94-0009 "Proceedings of the Third U.S.-Japan Workshop on Earthquake Protective Systems for Bridges," edited by I.G. Buckle and I. Friedland, 3/31/94, (PB94-195815, A99, MF-A06).

NCEER-94-0010 "3D-BASIS-ME: Computer Program for Nonlinear Dynamic Analysis of Seismically Isolated Single and Multiple Structures and Liquid Storage Tanks," by P.C. Tsopelas, M.C. Constantinou and A.M. Reinhorn, 4/12/94, (PB94-204922, A09, MF-A02).

NCEER-94-0011 "The Northridge, California Earthquake of January 17, 1994: Performance of Gas Transmission Pipelines," by T.D. O'Rourke and M.C. Palmer, 5/16/94, (PB94-204989, A05, MF-A01).

NCEER-94-0012 "Feasibility Study of Replacement Procedures and Earthquake Performance Related to Gas Transmission Pipelines," by T.D. O'Rourke and M.C. Palmer, 5/25/94, (PB94-206638, A09, MF-A02).

NCEER-94-0013 "Seismic Energy Based Fatigue Damage Analysis of Bridge Columns: Part II - Evaluation of Seismic Demand," by G.A. Chang and J.B. Mander, 6/1/94, (PB95-18106, A08, MF-A02).

NCEER-94-0014 "NCEER-Taisei Corporation Research Program on Sliding Seismic Isolation Systems for Bridges: Experimental and Analytical Study of a System Consisting of Sliding Bearings and Fluid Restoring Force/Damping Devices," by P. Tsopelas and M.C. Constantinou, 6/13/94, (PB94-219144, A10, MF-A03).

NCEER-94-0015 "Generation of Hazard-Consistent Fragility Curves for Seismic Loss Estimation Studies," by H. Hwang and J-R. Huo, 6/14/94, (PB95-181996, A09, MF-A02).

NCEER-94-0016 "Seismic Study of Building Frames with Added Energy-Absorbing Devices," by W.S. Pong, C.S. Tsai and G.C. Lee, 6/20/94, (PB94-219136, A10, A03).

NCEER-94-0017 "Sliding Mode Control for Seismic-Excited Linear and Nonlinear Civil Engineering Structures," by J. Yang, J. Wu, A. Agrawal and Z. Li, 6/21/94, (PB95-138483, A06, MF-A02).

NCEER-94-0018 "3D-BASIS-TABS Version 2.0: Computer Program for Nonlinear Dynamic Analysis of Three Dimensional Base Isolated Structures," by A.M. Reinhorn, S. Nagarajaiah, M.C. Constantinou, P. Tsopelas and R. Li, 6/22/94, (PB95-182176, A08, MF-A02).

NCEER-94-0019 "Proceedings of the International Workshop on Civil Infrastructure Systems: Application of Intelligent Systems and Advanced Materials on Bridge Systems," Edited by G.C. Lee and K.C. Chang, 7/18/94, (PB95-252474, A20, MF-A04).

NCEER-94-0020 "Study of Seismic Isolation Systems for Computer Floors," by V. Lambrou and M.C. Constantinou, 7/19/94, (PB95-138533, A10, MF-A03).

NCEER-94-0021 "Proceedings of the U.S.-Italian Workshop on Guidelines for Seismic Evaluation and Rehabilitation of Unreinforced Masonry Buildings," Edited by D.P. Abrams and G.M. Calvi, 7/20/94, (PB95-138749, A13, MF-A03).

NCEER-94-0022 "NCEER-Taisei Corporation Research Program on Sliding Seismic Isolation Systems for Bridges: Experimental and Analytical Study of a System Consisting of Lubricated PTFE Sliding Bearings and Mild Steel Dampers," by P. Tsopelas and M.C. Constantinou, 7/22/94, (PB95-182184, A08, MF-A02).

NCEER-94-0023 “Development of Reliability-Based Design Criteria for Buildings Under Seismic Load,” by Y.K. Wen, H. Hwang and M. Shinozuka, 8/1/94, (PB95-211934, A08, MF-A02).

NCEER-94-0024 “Experimental Verification of Acceleration Feedback Control Strategies for an Active Tendon System,” by S.J. Dyke, B.F. Spencer, Jr., P. Quast, M.K. Sain, D.C. Kaspari, Jr. and T.T. Soong, 8/29/94, (PB95-212320, A05, MF-A01).

NCEER-94-0025 “Seismic Retrofitting Manual for Highway Bridges,” Edited by I.G. Buckle and I.F. Friedland, published by the Federal Highway Administration (PB95-212676, A15, MF-A03).

NCEER-94-0026 “Proceedings from the Fifth U.S.-Japan Workshop on Earthquake Resistant Design of Lifeline Facilities and Countermeasures Against Soil Liquefaction,” Edited by T.D. O’Rourke and M. Hamada, 11/7/94, (PB95-220802, A99, MF-E08).

NCEER-95-0001 “Experimental and Analytical Investigation of Seismic Retrofit of Structures with Supplemental Damping: Part 1 - Fluid Viscous Damping Devices,” by A.M. Reinhorn, C. Li and M.C. Constantinou, 1/3/95, (PB95-266599, A09, MF-A02).

NCEER-95-0002 “Experimental and Analytical Study of Low-Cycle Fatigue Behavior of Semi-Rigid Top-And-Seat Angle Connections,” by G. Pekcan, J.B. Mander and S.S. Chen, 1/5/95, (PB95-220042, A07, MF-A02).

NCEER-95-0003 “NCEER-ATC Joint Study on Fragility of Buildings,” by T. Anagnos, C. Rojahn and A.S. Kiremidjian, 1/20/95, (PB95-220026, A06, MF-A02).

NCEER-95-0004 “Nonlinear Control Algorithms for Peak Response Reduction,” by Z. Wu, T.T. Soong, V. Gattulli and R.C. Lin, 2/16/95, (PB95-220349, A05, MF-A01).

NCEER-95-0005 “Pipeline Replacement Feasibility Study: A Methodology for Minimizing Seismic and Corrosion Risks to Underground Natural Gas Pipelines,” by R.T. Eguchi, H.A. Seligson and D.G. Honegger, 3/2/95, (PB95-252326, A06, MF-A02).

NCEER-95-0006 “Evaluation of Seismic Performance of an 11-Story Frame Building During the 1994 Northridge Earthquake,” by F. Naeim, R. DiSulio, K. Benuska, A. Reinhorn and C. Li, to be published.

NCEER-95-0007 “Prioritization of Bridges for Seismic Retrofitting,” by N. Basöz and A.S. Kiremidjian, 4/24/95, (PB95-252300, A08, MF-A02).

NCEER-95-0008 “Method for Developing Motion Damage Relationships for Reinforced Concrete Frames,” by A. Singhal and A.S. Kiremidjian, 5/11/95, (PB95-266607, A06, MF-A02).

NCEER-95-0009 “Experimental and Analytical Investigation of Seismic Retrofit of Structures with Supplemental Damping: Part II - Friction Devices,” by C. Li and A.M. Reinhorn, 7/6/95, (PB96-128087, A11, MF-A03).

NCEER-95-0010 “Experimental Performance and Analytical Study of a Non-Ductile Reinforced Concrete Frame Structure Retrofitted with Elastomeric Spring Dampers,” by G. Pekcan, J.B. Mander and S.S. Chen, 7/14/95, (PB96-137161, A08, MF-A02).

NCEER-95-0011 “Development and Experimental Study of Semi-Active Fluid Damping Devices for Seismic Protection of Structures,” by M.D. Symans and M.C. Constantinou, 8/3/95, (PB96-136940, A23, MF-A04).

NCEER-95-0012 “Real-Time Structural Parameter Modification (RSPM): Development of Innervated Structures,” by Z. Liang, M. Tong and G.C. Lee, 4/11/95, (PB96-137153, A06, MF-A01).

NCEER-95-0013 “Experimental and Analytical Investigation of Seismic Retrofit of Structures with Supplemental Damping: Part III - Viscous Damping Walls,” by A.M. Reinhorn and C. Li, 10/1/95, (PB96-176409, A11, MF-A03).

NCEER-95-0014 “Seismic Fragility Analysis of Equipment and Structures in a Memphis Electric Substation,” by J-R. Huo and H.H.M. Hwang, 8/10/95, (PB96-128087, A09, MF-A02).

NCEER-95-0015 “The Hanshin-Awaji Earthquake of January 17, 1995: Performance of Lifelines,” Edited by M. Shinozuka, 11/3/95, (PB96-176383, A15, MF-A03).

NCEER-95-0016 “Highway Culvert Performance During Earthquakes,” by T.L. Youd and C.J. Beckman, available as NCEER-96-0015.

NCEER-95-0017 “The Hanshin-Awaji Earthquake of January 17, 1995: Performance of Highway Bridges,” Edited by I.G. Buckle, 12/1/95, to be published.

NCEER-95-0018 “Modeling of Masonry Infill Panels for Structural Analysis,” by A.M. Reinhorn, A. Madan, R.E. Valles, Y. Reichmann and J.B. Mander, 12/8/95, (PB97-110886, MF-A01, A06).

NCEER-95-0019 “Optimal Polynomial Control for Linear and Nonlinear Structures,” by A.K. Agrawal and J.N. Yang, 12/11/95, (PB96-168737, A07, MF-A02).

NCEER-95-0020 "Retrofit of Non-Ductile Reinforced Concrete Frames Using Friction Dampers," by R.S. Rao, P. Gergely and R.N. White, 12/22/95, (PB97-133508, A10, MF-A02).

NCEER-95-0021 "Parametric Results for Seismic Response of Pile-Supported Bridge Bents," by G. Mylonakis, A. Nikolaou and G. Gazetas, 12/22/95, (PB97-100242, A12, MF-A03).

NCEER-95-0022 "Kinematic Bending Moments in Seismically Stressed Piles," by A. Nikolaou, G. Mylonakis and G. Gazetas, 12/23/95, (PB97-113914, MF-A03, A13).

NCEER-96-0001 "Dynamic Response of Unreinforced Masonry Buildings with Flexible Diaphragms," by A.C. Costley and D.P. Abrams," 10/10/96, (PB97-133573, MF-A03, A15).

NCEER-96-0002 "State of the Art Review: Foundations and Retaining Structures," by I. Po Lam, to be published.

NCEER-96-0003 "Ductility of Rectangular Reinforced Concrete Bridge Columns with Moderate Confinement," by N. Wehbe, M. Saiidi, D. Sanders and B. Douglas, 11/7/96, (PB97-133557, A06, MF-A02).

NCEER-96-0004 "Proceedings of the Long-Span Bridge Seismic Research Workshop," edited by I.G. Buckle and I.M. Friedland, to be published.

NCEER-96-0005 "Establish Representative Pier Types for Comprehensive Study: Eastern United States," by J. Kulicki and Z. Prucz, 5/28/96, (PB98-119217, A07, MF-A02).

NCEER-96-0006 "Establish Representative Pier Types for Comprehensive Study: Western United States," by R. Imbsen, R.A. Schamber and T.A. Osterkamp, 5/28/96, (PB98-118607, A07, MF-A02).

NCEER-96-0007 "Nonlinear Control Techniques for Dynamical Systems with Uncertain Parameters," by R.G. Ghanem and M.I. Bujakov, 5/27/96, (PB97-100259, A17, MF-A03).

NCEER-96-0008 "Seismic Evaluation of a 30-Year Old Non-Ductile Highway Bridge Pier and Its Retrofit," by J.B. Mander, B. Mahmoodzadegan, S. Bhadra and S.S. Chen, 5/31/96, (PB97-110902, MF-A03, A10).

NCEER-96-0009 "Seismic Performance of a Model Reinforced Concrete Bridge Pier Before and After Retrofit," by J.B. Mander, J.H. Kim and C.A. Ligozio, 5/31/96, (PB97-110910, MF-A02, A10).

NCEER-96-0010 "IDARC2D Version 4.0: A Computer Program for the Inelastic Damage Analysis of Buildings," by R.E. Valles, A.M. Reinhorn, S.K. Kunnath, C. Li and A. Madan, 6/3/96, (PB97-100234, A17, MF-A03).

NCEER-96-0011 "Estimation of the Economic Impact of Multiple Lifeline Disruption: Memphis Light, Gas and Water Division Case Study," by S.E. Chang, H.A. Seligson and R.T. Eguchi, 8/16/96, (PB97-133490, A11, MF-A03).

NCEER-96-0012 "Proceedings from the Sixth Japan-U.S. Workshop on Earthquake Resistant Design of Lifeline Facilities and Countermeasures Against Soil Liquefaction, Edited by M. Hamada and T. O'Rourke, 9/11/96, (PB97-133581, A99, MF-A06).

NCEER-96-0013 "Chemical Hazards, Mitigation and Preparedness in Areas of High Seismic Risk: A Methodology for Estimating the Risk of Post-Earthquake Hazardous Materials Release," by H.A. Seligson, R.T. Eguchi, K.J. Tierney and K. Richmond, 11/7/96, (PB97-133565, MF-A02, A08).

NCEER-96-0014 "Response of Steel Bridge Bearings to Reversed Cyclic Loading," by J.B. Mander, D-K. Kim, S.S. Chen and G.J. Premus, 11/13/96, (PB97-140735, A12, MF-A03).

NCEER-96-0015 "Highway Culvert Performance During Past Earthquakes," by T.L. Youd and C.J. Beckman, 11/25/96, (PB97-133532, A06, MF-A01).

NCEER-97-0001 "Evaluation, Prevention and Mitigation of Pounding Effects in Building Structures," by R.E. Valles and A.M. Reinhorn, 2/20/97, (PB97-159552, A14, MF-A03).

NCEER-97-0002 "Seismic Design Criteria for Bridges and Other Highway Structures," by C. Rojahn, R. Mayes, D.G. Anderson, J. Clark, J.H. Hom, R.V. Nutt and M.J. O'Rourke, 4/30/97, (PB97-194658, A06, MF-A03).

NCEER-97-0003 “Proceedings of the U.S.-Italian Workshop on Seismic Evaluation and Retrofit,” Edited by D.P. Abrams and G.M. Calvi, 3/19/97, (PB97-194666, A13, MF-A03).

NCEER-97-0004 "Investigation of Seismic Response of Buildings with Linear and Nonlinear Fluid Viscous Dampers," by A.A. Seleemah and M.C. Constantinou, 5/21/97, (PB98-109002, A15, MF-A03).

NCEER-97-0005 "Proceedings of the Workshop on Earthquake Engineering Frontiers in Transportation Facilities," edited by G.C. Lee and I.M. Friedland, 8/29/97, (PB98-128911, A25, MR-A04).

NCEER-97-0006 "Cumulative Seismic Damage of Reinforced Concrete Bridge Piers," by S.K. Kunnath, A. El-Bahy, A. Taylor and W. Stone, 9/2/97, (PB98-108814, A11, MF-A03).

NCEER-97-0007 "Structural Details to Accommodate Seismic Movements of Highway Bridges and Retaining Walls," by R.A. Imbsen, R.A. Schamber, E. Thorkildsen, A. Kartoum, B.T. Martin, T.N. Rosser and J.M. Kulicki, 9/3/97, (PB98-108996, A09, MF-A02).

NCEER-97-0008 "A Method for Earthquake Motion-Damage Relationships with Application to Reinforced Concrete Frames," by A. Singhal and A.S. Kiremidjian, 9/10/97, (PB98-108988, A13, MF-A03).

NCEER-97-0009 "Seismic Analysis and Design of Bridge Abutments Considering Sliding and Rotation," by K. Fishman and R. Richards, Jr., 9/15/97, (PB98-108897, A06, MF-A02).

NCEER-97-0010 "Proceedings of the FHWA/NCEER Workshop on the National Representation of Seismic Ground Motion for New and Existing Highway Facilities," edited by I.M. Friedland, M.S. Power and R.L. Mayes, 9/22/97, (PB98-128903, A21, MF-A04).

NCEER-97-0011 "Seismic Analysis for Design or Retrofit of Gravity Bridge Abutments," by K.L. Fishman, R. Richards, Jr. and R.C. Divito, 10/2/97, (PB98-128937, A08, MF-A02).

NCEER-97-0012 "Evaluation of Simplified Methods of Analysis for Yielding Structures," by P. Tsopelas, M.C. Constantinou, C.A. Kircher and A.S. Whittaker, 10/31/97, (PB98-128929, A10, MF-A03).

NCEER-97-0013 "Seismic Design of Bridge Columns Based on Control and Repairability of Damage," by C-T. Cheng and J.B. Mander, 12/8/97, (PB98-144249, A11, MF-A03).

NCEER-97-0014 "Seismic Resistance of Bridge Piers Based on Damage Avoidance Design," by J.B. Mander and C-T. Cheng, 12/10/97, (PB98-144223, A09, MF-A02).

NCEER-97-0015 “Seismic Response of Nominally Symmetric Systems with Strength Uncertainty,” by S. Balopoulou and M. Grigoriu, 12/23/97, (PB98-153422, A11, MF-A03).

NCEER-97-0016 “Evaluation of Seismic Retrofit Methods for Reinforced Concrete Bridge Columns,” by T.J. Wipf, F.W. Klaiber and F.M. Russo, 12/28/97, (PB98-144215, A12, MF-A03).

NCEER-97-0017 “Seismic Fragility of Existing Conventional Reinforced Concrete Highway Bridges,” by C.L. Mullen and A.S. Cakmak, 12/30/97, (PB98-153406, A08, MF-A02).

NCEER-97-0018 “Loss Asssessment of Memphis Buildings,” edited by D.P. Abrams and M. Shinozuka, 12/31/97, (PB98-144231, A13, MF-A03).

NCEER-97-0019 “Seismic Evaluation of Frames with Infill Walls Using Quasi-static Experiments,” by K.M. Mosalam, R.N. White and P. Gergely, 12/31/97, (PB98-153455, A07, MF-A02).

NCEER-97-0020 “Seismic Evaluation of Frames with Infill Walls Using Pseudo-dynamic Experiments,” by K.M. Mosalam, R.N. White and P. Gergely, 12/31/97, (PB98-153430, A07, MF-A02).

NCEER-97-0021 “Computational Strategies for Frames with Infill Walls: Discrete and Smeared Crack Analyses and Seismic Fragility,” by K.M. Mosalam, R.N. White and P. Gergely, 12/31/97, (PB98-153414, A10, MF-A02).

NCEER-97-0022 "Proceedings of the NCEER Workshop on Evaluation of Liquefaction Resistance of Soils," edited by T.L. Youd and I.M. Idriss, 12/31/97, (PB98-155617, A15, MF-A03).

MCEER-98-0001 "Extraction of Nonlinear Hysteretic Properties of Seismically Isolated Bridges from Quick-Release Field Tests," by Q. Chen, B.M. Douglas, E.M. Maragakis and I.G. Buckle, 5/26/98, (PB99-118838, A06, MF-A01).

MCEER-98-0002 "Methodologies for Evaluating the Importance of Highway Bridges," by A. Thomas, S. Eshenaur and J. Kulicki, 5/29/98, (PB99-118846, A10, MF-A02).

MCEER-98-0003 "Capacity Design of Bridge Piers and the Analysis of Overstrength," by J.B. Mander, A. Dutta and P. Goel, 6/1/98, (PB99-118853, A09, MF-A02).

MCEER-98-0004 "Evaluation of Bridge Damage Data from the Loma Prieta and Northridge, California Earthquakes," by N. Basoz and A. Kiremidjian, 6/2/98, (PB99-118861, A15, MF-A03).

MCEER-98-0005 "Screening Guide for Rapid Assessment of Liquefaction Hazard at Highway Bridge Sites," by T. L. Youd, 6/16/98, (PB99-118879, A06, not available on microfiche).

MCEER-98-0006 "Structural Steel and Steel/Concrete Interface Details for Bridges," by P. Ritchie, N. Kauhl and J. Kulicki, 7/13/98, (PB99-118945, A06, MF-A01).

MCEER-98-0007 "Capacity Design and Fatigue Analysis of Confined Concrete Columns," by A. Dutta and J.B. Mander, 7/14/98, (PB99-118960, A14, MF-A03).

MCEER-98-0008 "Proceedings of the Workshop on Performance Criteria for Telecommunication Services Under Earthquake Conditions," edited by A.J. Schiff, 7/15/98, (PB99-118952, A08, MF-A02).

MCEER-98-0009 "Fatigue Analysis of Unconfined Concrete Columns," by J.B. Mander, A. Dutta and J.H. Kim, 9/12/98, (PB99-123655, A10, MF-A02).

MCEER-98-0010 "Centrifuge Modeling of Cyclic Lateral Response of Pile-Cap Systems and Seat-Type Abutments in Dry Sands," by A.D. Gadre and R. Dobry, 10/2/98, (PB99-123606, A13, MF-A03).

MCEER-98-0011 "IDARC-BRIDGE: A Computational Platform for Seismic Damage Assessment of Bridge Structures," by A.M. Reinhorn, V. Simeonov, G. Mylonakis and Y. Reichman, 10/2/98, (PB99-162919, A15, MF-A03).

MCEER-98-0012 "Experimental Investigation of the Dynamic Response of Two Bridges Before and After Retrofitting with Elastomeric Bearings," by D.A. Wendichansky, S.S. Chen and J.B. Mander, 10/2/98, (PB99-162927, A15, MF-A03).

MCEER-98-0013 "Design Procedures for Hinge Restrainers and Hinge Sear Width for Multiple-Frame Bridges," by R. Des Roches and G.L. Fenves, 11/3/98, (PB99-140477, A13, MF-A03).

MCEER-98-0014 "Response Modification Factors for Seismically Isolated Bridges," by M.C. Constantinou and J.K. Quarshie, 11/3/98, (PB99-140485, A14, MF-A03).

MCEER-98-0015 "Proceedings of the U.S.-Italy Workshop on Seismic Protective Systems for Bridges," edited by I.M. Friedland and M.C. Constantinou, 11/3/98, (PB2000-101711, A22, MF-A04).

MCEER-98-0016 "Appropriate Seismic Reliability for Critical Equipment Systems: Recommendations Based on Regional Analysis of Financial and Life Loss," by K. Porter, C. Scawthorn, C. Taylor and N. Blais, 11/10/98, (PB99-157265, A08, MF-A02).

MCEER-98-0017 "Proceedings of the U.S. Japan Joint Seminar on Civil Infrastructure Systems Research," edited by M. Shinozuka and A. Rose, 11/12/98, (PB99-156713, A16, MF-A03).

MCEER-98-0018 "Modeling of Pile Footings and Drilled Shafts for Seismic Design," by I. PoLam, M. Kapuskar and D. Chaudhuri, 12/21/98, (PB99-157257, A09, MF-A02).

MCEER-99-0001 "Seismic Evaluation of a Masonry Infilled Reinforced Concrete Frame by Pseudodynamic Testing," by S.G. Buonopane and R.N. White, 2/16/99, (PB99-162851, A09, MF-A02).

MCEER-99-0002 "Response History Analysis of Structures with Seismic Isolation and Energy Dissipation Systems: Verification Examples for Program SAP2000," by J. Scheller and M.C. Constantinou, 2/22/99, (PB99-162869, A08, MF-A02).

MCEER-99-0003 "Experimental Study on the Seismic Design and Retrofit of Bridge Columns Including Axial Load Effects," by A. Dutta, T. Kokorina and J.B. Mander, 2/22/99, (PB99-162877, A09, MF-A02).

MCEER-99-0004 "Experimental Study of Bridge Elastomeric and Other Isolation and Energy Dissipation Systems with Emphasis on Uplift Prevention and High Velocity Near-source Seismic Excitation," by A. Kasalanati and M. C. Constantinou, 2/26/99, (PB99-162885, A12, MF-A03).

MCEER-99-0005 "Truss Modeling of Reinforced Concrete Shear-flexure Behavior," by J.H. Kim and J.B. Mander, 3/8/99, (PB99-163693, A12, MF-A03).

MCEER-99-0006 "Experimental Investigation and Computational Modeling of Seismic Response of a 1:4 Scale Model Steel Structure with a Load Balancing Supplemental Damping System," by G. Pekcan, J.B. Mander and S.S. Chen, 4/2/99, (PB99-162893, A11, MF-A03).

MCEER-99-0007 "Effect of Vertical Ground Motions on the Structural Response of Highway Bridges," by M.R. Button, C.J. Cronin and R.L. Mayes, 4/10/99, (PB2000-101411, A10, MF-A03).

MCEER-99-0008 "Seismic Reliability Assessment of Critical Facilities: A Handbook, Supporting Documentation, and Model Code Provisions," by G.S. Johnson, R.E. Sheppard, M.D. Quilici, S.J. Eder and C.R. Scawthorn, 4/12/99, (PB2000-101701, A18, MF-A04).

MCEER-99-0009 "Impact Assessment of Selected MCEER Highway Project Research on the Seismic Design of Highway Structures," by C. Rojahn, R. Mayes, D.G. Anderson, J.H. Clark, D'Appolonia Engineering, S. Gloyd and R.V. Nutt, 4/14/99, (PB99-162901, A10, MF-A02).

MCEER-99-0010 "Site Factors and Site Categories in Seismic Codes," by R. Dobry, R. Ramos and M.S. Power, 7/19/99, (PB2000-101705, A08, MF-A02).

MCEER-99-0011 "Restrainer Design Procedures for Multi-Span Simply-Supported Bridges," by M.J. Randall, M. Saiidi, E. Maragakis and T. Isakovic, 7/20/99, (PB2000-101702, A10, MF-A02).

MCEER-99-0012 "Property Modification Factors for Seismic Isolation Bearings," by M.C. Constantinou, P. Tsopelas, A. Kasalanati and E. Wolff, 7/20/99, (PB2000-103387, A11, MF-A03).

MCEER-99-0013 "Critical Seismic Issues for Existing Steel Bridges," by P. Ritchie, N. Kauhl and J. Kulicki, 7/20/99, (PB2000-101697, A09, MF-A02).

MCEER-99-0014 "Nonstructural Damage Database," by A. Kao, T.T. Soong and A. Vender, 7/24/99, (PB2000-101407, A06, MF-A01).

MCEER-99-0015 "Guide to Remedial Measures for Liquefaction Mitigation at Existing Highway Bridge Sites," by H.G. Cooke and J. K. Mitchell, 7/26/99, (PB2000-101703, A11, MF-A03).

MCEER-99-0016 "Proceedings of the MCEER Workshop on Ground Motion Methodologies for the Eastern United States," edited by N. Abrahamson and A. Becker, 8/11/99, (PB2000-103385, A07, MF-A02).

MCEER-99-0017 "Quindío, Colombia Earthquake of January 25, 1999: Reconnaissance Report," by A.P. Asfura and P.J. Flores, 10/4/99, (PB2000-106893, A06, MF-A01).

MCEER-99-0018 "Hysteretic Models for Cyclic Behavior of Deteriorating Inelastic Structures," by M.V. Sivaselvan and A.M. Reinhorn, 11/5/99, (PB2000-103386, A08, MF-A02).

MCEER-99-0019 "Proceedings of the 7th U.S.- Japan Workshop on Earthquake Resistant Design of Lifeline Facilities and Countermeasures Against Soil Liquefaction," edited by T.D. O'Rourke, J.P. Bardet and M. Hamada, 11/19/99, (PB2000-103354, A99, MF-A06).

MCEER-99-0020 "Development of Measurement Capability for Micro-Vibration Evaluations with Application to Chip Fabrication Facilities," by G.C. Lee, Z. Liang, J.W. Song, J.D. Shen and W.C. Liu, 12/1/99, (PB2000-105993, A08, MF-A02).

MCEER-99-0021 "Design and Retrofit Methodology for Building Structures with Supplemental Energy Dissipating Systems," by G. Pekcan, J.B. Mander and S.S. Chen, 12/31/99, (PB2000-105994, A11, MF-A03).

MCEER-00-0001 "The Marmara, Turkey Earthquake of August 17, 1999: Reconnaissance Report," edited by C. Scawthorn; with major contributions by M. Bruneau, R. Eguchi, T. Holzer, G. Johnson, J. Mander, J. Mitchell, W. Mitchell, A. Papageorgiou, C. Scaethorn, and G. Webb, 3/23/00, (PB2000-106200, A11, MF-A03).

MCEER-00-0002 "Proceedings of the MCEER Workshop for Seismic Hazard Mitigation of Health Care Facilities," edited by G.C. Lee, M. Ettouney, M. Grigoriu, J. Hauer and J. Nigg, 3/29/00, (PB2000-106892, A08, MF-A02).

MCEER-00-0003 "The Chi-Chi, Taiwan Earthquake of September 21, 1999: Reconnaissance Report," edited by G.C. Lee and C.H. Loh, with major contributions by G.C. Lee, M. Bruneau, I.G. Buckle, S.E. Chang, P.J. Flores, T.D. O'Rourke, M. Shinozuka, T.T. Soong, C-H. Loh, K-C. Chang, Z-J. Chen, J-S. Hwang, M-L. Lin, G-Y. Liu, K-C. Tsai, G.C. Yao and C-L. Yen, 4/30/00, (PB2001-100980, A10, MF-A02).

MCEER-00-0004 "Seismic Retrofit of End-Sway Frames of Steel Deck-Truss Bridges with a Supplemental Tendon System: Experimental and Analytical Investigation," by G. Pekcan, J.B. Mander and S.S. Chen, 7/1/00, (PB2001-100982, A10, MF-A02).

MCEER-00-0005 "Sliding Fragility of Unrestrained Equipment in Critical Facilities," by W.H. Chong and T.T. Soong, 7/5/00, (PB2001-100983, A08, MF-A02).

MCEER-00-0006 "Seismic Response of Reinforced Concrete Bridge Pier Walls in the Weak Direction," by N. Abo-Shadi, M. Saiidi and D. Sanders, 7/17/00, (PB2001-100981, A17, MF-A03).

MCEER-00-0007 "Low-Cycle Fatigue Behavior of Longitudinal Reinforcement in Reinforced Concrete Bridge Columns," by J. Brown and S.K. Kunnath, 7/23/00, (PB2001-104392, A08, MF-A02).

MCEER-00-0008 "Soil Structure Interaction of Bridges for Seismic Analysis," I. PoLam and H. Law, 9/25/00, (PB2001-105397, A08, MF-A02).

MCEER-00-0009 "Proceedings of the First MCEER Workshop on Mitigation of Earthquake Disaster by Advanced Technologies (MEDAT-1), edited by M. Shinozuka, D.J. Inman and T.D. O'Rourke, 11/10/00, (PB2001-105399, A14, MF-A03).

MCEER-00-0010 "Development and Evaluation of Simplified Procedures for Analysis and Design of Buildings with Passive Energy Dissipation Systems," by O.M. Ramirez, M.C. Constantinou, C.A. Kircher, A.S. Whittaker, M.W. Johnson, J.D. Gomez and C. Chrysostomou, 11/16/01, (PB2001-105523, A23, MF-A04).

MCEER-00-0011 "Dynamic Soil-Foundation-Structure Interaction Analyses of Large Caissons," by C-Y. Chang, C-M. Mok, Z-L. Wang, R. Settgast, F. Waggoner, M.A. Ketchum, H.M. Gonnermann and C-C. Chin, 12/30/00, (PB2001-104373, A07, MF-A02).

MCEER-00-0012 "Experimental Evaluation of Seismic Performance of Bridge Restrainers," by A.G. Vlassis, E.M. Maragakis and M. Saiid Saiidi, 12/30/00, (PB2001-104354, A09, MF-A02).

MCEER-00-0013 "Effect of Spatial Variation of Ground Motion on Highway Structures," by M. Shinozuka, V. Saxena and G. Deodatis, 12/31/00, (PB2001-108755, A13, MF-A03).

MCEER-00-0014 "A Risk-Based Methodology for Assessing the Seismic Performance of Highway Systems," by S.D. Werner, C.E. Taylor, J.E. Moore, II, J.S. Walton and S. Cho, 12/31/00, (PB2001-108756, A14, MF-A03).

MCEER-01-0001 "Experimental Investigation of P-Delta Effects to Collapse During Earthquakes," by D. Vian and M. Bruneau, 6/25/01, (PB2002-100534, A17, MF-A03).

MCEER-01-0002 "Proceedings of the Second MCEER Workshop on Mitigation of Earthquake Disaster by Advanced Technologies (MEDAT-2)," edited by M. Bruneau and D.J. Inman, 7/23/01, (PB2002-100434, A16, MF-A03).

MCEER-01-0003 "Sensitivity Analysis of Dynamic Systems Subjected to Seismic Loads," by C. Roth and M. Grigoriu, 9/18/01, (PB2003-100884, A12, MF-A03).

MCEER-01-0004 "Overcoming Obstacles to Implementing Earthquake Hazard Mitigation Policies: Stage 1 Report," by D.J. Alesch and W.J. Petak, 12/17/01, (PB2002-107949, A07, MF-A02).

MCEER-01-0005 "Updating Real-Time Earthquake Loss Estimates: Methods, Problems and Insights," by C.E. Taylor, S.E. Chang and R.T. Eguchi, 12/17/01, (PB2002-107948, A05, MF-A01).

MCEER-01-0006 "Experimental Investigation and Retrofit of Steel Pile Foundations and Pile Bents Under Cyclic Lateral Loadings," by A. Shama, J. Mander, B. Blabac and S. Chen, 12/31/01, (PB2002-107950, A13, MF-A03).

MCEER-02-0001 "Assessment of Performance of Bolu Viaduct in the 1999 Duzce Earthquake in Turkey" by P.C. Roussis, M.C. Constantinou, M. Erdik, E. Durukal and M. Dicleli, 5/8/02, (PB2003-100883, A08, MF-A02).

MCEER-02-0002 "Seismic Behavior of Rail Counterweight Systems of Elevators in Buildings," by M.P. Singh, Rildova and L.E. Suarez, 5/27/02. (PB2003-100882, A11, MF-A03).

MCEER-02-0003 "Development of Analysis and Design Procedures for Spread Footings," by G. Mylonakis, G. Gazetas, S. Nikolaou and A. Chauncey, 10/02/02, (PB2004-101636, A13, MF-A03, CD-A13).

MCEER-02-0004 "Bare-Earth Algorithms for Use with SAR and LIDAR Digital Elevation Models," by C.K. Huyck, R.T. Eguchi and B. Houshmand, 10/16/02, (PB2004-101637, A07, CD-A07).

MCEER-02-0005 "Review of Energy Dissipation of Compression Members in Concentrically Braced Frames," by K.Lee and M. Bruneau, 10/18/02, (PB2004-101638, A10, CD-A10).

MCEER-03-0001 "Experimental Investigation of Light-Gauge Steel Plate Shear Walls for the Seismic Retrofit of Buildings" by J. Berman and M. Bruneau, 5/2/03, (PB2004-101622, A10, MF-A03, CD-A10).

MCEER-03-0002 "Statistical Analysis of Fragility Curves," by M. Shinozuka, M.Q. Feng, H. Kim, T. Uzawa and T. Ueda, 6/16/03, (PB2004-101849, A09, CD-A09).

MCEER-03-0003 "Proceedings of the Eighth U.S.-Japan Workshop on Earthquake Resistant Design f Lifeline Facilities and Countermeasures Against Liquefaction," edited by M. Hamada, J.P. Bardet and T.D. O'Rourke, 6/30/03, (PB2004-104386, A99, CD-A99).

MCEER-03-0004 "Proceedings of the PRC-US Workshop on Seismic Analysis and Design of Special Bridges," edited by L.C. Fan and G.C. Lee, 7/15/03, (PB2004-104387, A14, CD-A14).

MCEER-03-0005 "Urban Disaster Recovery: A Framework and Simulation Model," by S.B. Miles and S.E. Chang, 7/25/03, (PB2004-104388, A07, CD-A07).

MCEER-03-0006 "Behavior of Underground Piping Joints Due to Static and Dynamic Loading," by R.D. Meis, M. Maragakis and R. Siddharthan, 11/17/03, (PB2005-102194, A13, MF-A03, CD-A00).

MCEER-03-0007 "Seismic Vulnerability of Timber Bridges and Timber Substructures," by A.A. Shama, J.B. Mander, I.M. Friedland and D.R. Allicock, 12/15/03.

MCEER-04-0001 "Experimental Study of Seismic Isolation Systems with Emphasis on Secondary System Response and Verification of Accuracy of Dynamic Response History Analysis Methods," by E. Wolff and M. Constantinou, 1/16/04 (PB2005-102195, A99, MF-E08, CD-A00).

MCEER-04-0002 "Tension, Compression and Cyclic Testing of Engineered Cementitious Composite Materials," by K. Kesner and S.L. Billington, 3/1/04, (PB2005-102196, A08, CD-A08).

MCEER-04-0003 "Cyclic Testing of Braces Laterally Restrained by Steel Studs to Enhance Performance During Earthquakes," by O.C. Celik, J.W. Berman and M. Bruneau, 3/16/04, (PB2005-102197, A13, MF-A03, CD-A00).

MCEER-04-0004 "Methodologies for Post Earthquake Building Damage Detection Using SAR and Optical Remote Sensing: Application to the August 17, 1999 Marmara, Turkey Earthquake," by C.K. Huyck, B.J. Adams, S. Cho, R.T. Eguchi, B. Mansouri and B. Houshmand, 6/15/04, (PB2005-104888, A10, CD-A00).

MCEER-04-0005 "Nonlinear Structural Analysis Towards Collapse Simulation: A Dynamical Systems Approach," by M.V. Sivaselvan and A.M. Reinhorn, 6/16/04, (PB2005-104889, A11, MF-A03, CD-A00).

MCEER-04-0006 "Proceedings of the Second PRC-US Workshop on Seismic Analysis and Design of Special Bridges," edited by G.C. Lee and L.C. Fan, 6/25/04, (PB2005-104890, A16, CD-A00).

MCEER-04-0007 "Seismic Vulnerability Evaluation of Axially Loaded Steel Built-up Laced Members," by K. Lee and M. Bruneau, 6/30/04, (PB2005-104891, A16, CD-A00).

MCEER-04-0008 "Evaluation of Accuracy of Simplified Methods of Analysis and Design of Buildings with Damping Systems for Near-Fault and for Soft-Soil Seismic Motions," by E.A. Pavlou and M.C. Constantinou, 8/16/04, (PB2005-104892, A08, MF-A02, CD-A00).

MCEER-04-0009 "Assessment of Geotechnical Issues in Acute Care Facilities in California," by M. Lew, T.D. O'Rourke, R. Dobry and M. Koch, 9/15/04, (PB2005-104893, A08, CD-A00).

MCEER-04-0010 "Scissor-Jack-Damper Energy Dissipation System," by A.N. Sigaher-Boyle and M.C. Constantinou, 12/1/04.

MCEER-04-0011 "Seismic Retrofit of Bridge Steel Truss Piers Using a Controlled Rocking Approach," by M. Pollino and M. Bruneau, 12/20/04.

MCEER-05-0001 "Experimental and Analytical Studies of Structures Seismically Isolated with an Uplift-Restraint Isolation System," by P.C. Roussis and M.C. Constantinou, 1/10/05.

MCEER-05-0002 "A Versatile Experimentation Model for Study of Structures Near Collapse Applied to Seismic Evaluation of Irregular Structures," by D. Kusumastuti, A.M. Reinhorn and A. Rutenberg, 3/31/05.

MCEER-05-0003 "Proceedings of the Third PRC-US Workshop on Seismic Analysis and Design of Special Bridges," edited by L.C. Fan and G.C. Lee, 4/20/05.

MCEER-05-0004 "Approaches for the Seismic Retrofit of Braced Steel Bridge Piers and Proof-of-Concept Testing of an Eccentrically Braced Frame with Tubular Link," by J.W. Berman and M. Bruneau, 4/21/05.

MCEER-05-0005 "Simulation of Strong Ground Motions for Seismic Fragility Evaluation of Nonstructural Components in Hospitals," by A. Wanitkorkul and A. Filiatrault, 5/26/05.

MCEER-05-0006 "Seismic Safety in California Hospitals: Assessing an Attempt to Accelerate the Replacement or Seismic Retrofit of Older Hospital Facilities," by D.J. Alesch, L.A. Arendt and W.J. Petak, 6/6/05.

MCEER-05-0007 "Development of Seismic Strengthening and Retrofit Strategies for Critical Facilities Using Engineered Cementitious Composite Materials," by K. Kesner and S.L. Billington, 8/29/05.

MULTIDISCIPLINARY CENTER FOR EARTHQUAKE ENGINEERING RESEARCH

A National Center of Excellence in Advanced Technology Applications

University at Buffalo, State University of New York
Red Jacket Quadrangle ▪ Buffalo, New York 14261
Phone: (716) 645-3391 ▪ Fax: (716) 645-3399
E-mail: *mceer@mceermail.buffalo.edu* ▪ WWW Site *http://mceer.buffalo.edu*

University at Buffalo *The State University of New York*

ISSN 1520-295X